UNIVERSITY OF OKLAHOMA

GRADUATE COLLEGE

ATMOSPHERIC MOISTURE TRANSPORT ASSOCIATED WITH THE WEST AFRICAN MONSOON SYSTEM: AN OBSERVATIONAL STUDY AND EVALUATION OF A WRF DYNAMICAL DOWNSCALING SIMULATION

A DISSERTATION

SUBMITTED TO THE GRADUATE FACULTY

in partial fulfillment of the requirements for the

Degree of

DOCTOR OF PHILOSOPHY

By

MOUHAMADOU ISSA LÉLÉ
Norman, Oklahoma
2014

ATMOSPHERIC MOISTURE TRANSPORT ASSOCIATED WITH THE WEST AFRICAN MONSOON SYSTEM: AN OBSERVATIONAL STUDY AND EVALUATION OF A WRF DYNAMICAL DOWNSCALING SIMULATION

A DISSERTATION APPROVED FOR THE
SCHOOL OF METEOROLOGY

BY

_____
Dr. Peter J. Lamb, Co-Chair

_____
Dr. Lance Leslie, Co-Chair

_____
Dr. Michael Richman

_____
Dr. John Kain

_____
Dr. Aondover Tarhule

Dedication

In the memory of my beloved parents,

Issa Lélé and Zéinabou Biga,

My brothers, Adamou I. Lélé and Hamidou I. Lélé,

May Allah (SWT) make them among the guided ones.

To Djegga Demmon, my mentor who instilled in me the love of learning, and

Without whom none of my success would be possible

This dissertation is also dedicated to the nameless tens of thousands of

innocent children, women, and men victims of the Sahelian droughts.

Acknowledgements

I would like to express my deepest appreciation to my advisors, Professor Peter J. Lamb and Professor Lance Leslie. They have been a model of scientific excellence and generous mentorship. I deeply appreciate their guidance, support, patience and understanding, as a teacher, and a researcher. I admire their incommensurable knowledge, they real keenness for science and unmatched modesty. Most of all, I am grateful that Professor Peter J. Lamb gave me the opportunity to come and study with him, in one of the most prestigious Atmospheric Science departments in the world. For everything you've done for me and my wife Prof. Lamb, I sincerely thank you.

Thank you to my committee, Professor Michael Richman, Dr. John Kain and Dr. Aondover Tarhule, for the useful contributions to this work. I would also like to acknowledge Dr. Michael Douglas, for reading my dissertation and providing me with very useful comments and suggestions. He and his wife Rosario Douglas have always encouraged and supported my wife and myself throughout our graduate school years. My thanks to Mr. Also Idrissa, who, unfortunately, is no longer with us, Professor Abdelkrim Ben Mohamed, and Mohamed Sadeck Boulahya for making everything possible for me to pursue my education dream.

Special thanks to Luwanda Byrd, for listening to my complaints and providing me continuous moral support, and Tracy Reinke, and Melanie Norris who made my school life easier. I am particularly grateful for the assistance given by the OU Supercomputing Center for Education and Research (OSCER) team, in particular Dr. Henry Neeman. I would like to thank the School of Meteorology staff, especially

Marcia Pallutto. I also enjoyed very much my interaction and friendship with Dr. Zewdu Tessama, Reed Timmer, Esther White, Ashton Robinson Cook, and Irenea Lodangco.

I owe my deepest gratitude to many people who encouraged and supported me morally; I want to name Dr. Boureima Sambo, Dr. Wato Nsa, Cheick Abdurahman Basir, Dr. Mamoudou Djingarey, Dr. Ousmane Ndiaye, Dr. Bala Saho, Dr. Samir Wazzi, Mme Ouseini Tinni, Mme Mariama Sambo, Mme Amy Nsa, Hama Hamidou, Idrissa Hassan, Moussa Mouhaimouni, Boukari Zacari, Abdourahman Kelani, Judith Henry, Celia Jones, Erman Ouedrago.

This dissertation would never have been completed without the continuous moral support, unconditional love and total devotion of my family in Niger and Benin. I want to thank my brothers and sisters, my late brothers Adamou and Hamidou Lélé for always encouraging me and building up my confidence. I would like to show my greatest appreciation to my wife Rahama, for the love, encouragement, and support you have surrounded me with all this time, for making me happy and bringing joy into my everyday life, and to our children Abdoul-Madjid, Ismael, and Adam for being Honor Roll students.

My time at the Sooner State was also made enjoyable in large part due to my young brothers and nephews from Niger, especially Ali Tinni, and Moustafa Ari, our Saturday night gathering and their frequent visits to my house keep me from being homesick.

Table of Contents

List of Tables

List of Figures

Abstract

The intraseasonal variability of the low-level atmospheric moisture transport and its divergence associated with the West African monsoon (WAM) has been investigated for the 1960-2008 period using the NCEP-NCAR reanalysis data. The climatology of the moisture flux integrated from the surface to 850 hPa, shows moderate southerly moisture transport prior to the WAM onset (March-April), associated with cross-equatorial flow in the South Atlantic Ocean and southwesterly flux exceeding 200 kg m^{-1} s^{-1} over the Guinea coast just after the WAM onset (May-June). On the intraseasonal time-scale, the study indicates that besides the transport/divergence by the mean flow, the transport/divergence by the intraseasonal climate (timescale >10 day) anomalies dominates the total atmospheric moisture transport over West Africa. There is also a relatively strong and uniform moisture transport by the synoptic (timescale <10 day) anomalies over the Guinean coast but its associated moisture divergence was relatively small. It is also shown that the zonal component is the largest contributor to the mean moisture transport into the Sahel while over the Guinean coast, the meridional transport contributes the most, and the prevailing strong westerly transport extends polward to 20^{o}N. Large scale moisture flux convergence is suggested to be the primary source of water vapor needed to support enhanced convection over West Africa.

In the second part of the study, the active and break monsoon periods have been analyzed. Results showed that intraseasonal wet (dry) spells in the Sudan-Sahel region are the manifestations of the superposition of the 2-9, 10-25, and 30-90 day intraseasonal oscillation associated with enhanced (suppressed) moisture transport and convection. In general, wet (dry) spells over the Sudan-Sahel region are associated with dry (wet) spells over the Guinean coast. Lag regression between the intraseasonal

wet/dry spell anomalies and 30-90 day filtered moisture transport/divergence anomalies shows that the 30-90 day timescale has a very large zonal scale encompassing both the Sudan and the Sahelian zone. The suppressed convection over West Africa leads to an increased surface temperature and surface pressure gradient. These effects act to further strengthen the monsoon winds and moisture transport towards the ITF, and increased convection in the continental Intertropical convergence zone. Strong and significant positive linear correlations (+0.59 to +0.89) are found between Sudan-Sahel July-September precipitation and moisture flux convergence of the intraseasonal moisture flux anomalies, while moderate positive correlations (+0.32 to +0.63) are found with that of the mean flow. These relationships indicate potential short term monsoon predictability which will be useful for agriculture.

Lastly, an attempt was made to evaluate the performance of convective parameterization scheme options for the Weather Research and Forecasting (WRF) model in simulating WAM features that occurred during August 2006. Skill score measures for six configurations indicated that no scheme was obviously best at all times in simulating WAM variability. The greatest variability in forecasts is found to come from changes in the choice of convective scheme, although notable impacts also occurred from changes in the microphysics schemes. Specifically, changes in convective schemes had the largest impact on the simulated rain rate, while simulations of total domain rainfall were influenced by choices of both the microphysics and convective schemes. However, the WRF model has been able to simulate reasonably well the gross pattern of many regional features, such as the magnitudes of the monthly accumulated precipitation, the low- and upper-level winds including the location of the AEJ, the monsoon depth, and the time and passage of westward propagating storms crossing the West African domain.

Chapter 1

1. Introduction

1.1 Background

Monsoons are a key aspect of both the regional and general circulation of the atmosphere. For this reason, the major monsoon systems throughout the world have been extensively studied in recent decades. It has been recognized that the major forcing of monsoons is the thermal contrast between the continent and the ocean, with moist processes and the earth's rotation being important factors (Trewartha and Horn 1980; Webster 1987; Rodwell and Hoskins 1996; Zheng 1997; Loschnigg and Webster 2000). Although some progress has been made in understanding the causes of large-scale monsoon variability, many aspects of their circulation as well as their influences on rainfall are still not fully understood, and much remains to be done in the modeling and quantitative prediction of monsoon rainfall events. Africa spans a variety of tropical climatic zones (i.e., tropical rainforest, monsoon, savanna, semi-arid, and desert), along with northern and southern temperate extremities, and rain-producing systems differ from one region to the other. Among these climatic regions, the West African monsoon (hereafter, "WAM") variability has received much attention due to

the sequence of extremely dry years that have been experienced in the region since the mid-twentieth century.

As with other monsoonal regimes, the WAM is characterized by a seasonal reversal of the prevailing low tropospheric wind (e.g., Ramage 1971). In the northern hemisphere summer, this wind has a southwesterly, onshore orientation and, as a result, the monsoon transports abundant water vapor from the Atlantic Ocean to inland, and helps initiate and sustain rainfall and water the budget in the region between May and October (e.g., Thorncroft et al. 2011), which is crucial to the agricultural production and the economy of the respective countries. Further inland this southwesterly flow meets the dry northeasterly harmattan wind to form a discontinuity referred to as the ITF (e.g., Hagos and Zhang 2009; Lélé and Lamb 2010).

Since the early 20st century, the continent of Africa has seen an increasing number of natural disasters (i.e., droughts, floods, disaster-related epidemics …) associated mainly to extreme weather events and climate variability. These repetitive climate driven natural disasters have undermined the hard-fought gains in the economic development of many countries in Africa. The low capacity for State-initiated interventions to these disasters have prompted the IPCC to consider the continent as the most vulnerable to climate change in its Fourth Assessment Report (AR4, 2007). This vulnerability is due to the widespread poverty and to the fact that a large portion of its economy is based on rainfed agriculture. Increased global warming is expected to result in more rainfall variability over Africa which will severely impact livelihoods,

especially over heavily populated areas along the coastal zones. A potential sea level rise associated with climate change could be a direct threat to many of the coastal communities and the low-lying deltas (e.g., the Niger, Nile, Moulouya, and Volta among others) of Africa (IPCC, AR4 2007). A gradual multidecadal regional climate change has already been observed in part of the continent since the 1950s, and it has been associated with the observed below average Sahelian rainfall (e.g., Fig. 1.1) and with the persistent and often severe droughts that the West African Sudan-Sahel zone (10^{o}-18^{o}N) has experienced (Dai et al. 2004; Bell and Lamb 2006). This climate variability and change, in combination with the weak levels of agricultural investments, contributed to a significant erosion of agricultural performance in West Africa. The food security threat in this region is great, particularly in countries where agricultural yields and *per capita* food production have been progressively declining as the population growth considerably increases and the demand for food and water high. Figure 1.2 illustrates the relationship between food production and climate variability. The figure compared the food production index in Africa to that of the world for the period 1961-2001. As expected, food production over Africa has declined considerably in the early 1980s and that declining period coincides with the Sahelian drought period.

Past studies of monsoon variability over West Africa have identified a number of mechanisms that govern rainfall climatology over the region (e.g., Asplinden and Adefolalu 1976; Pedgley and Krishnamurti 1976; Lamb 1978a, b; Nicholson 1981; Opoku-Ankomah and Cordery 1994; Wagner and Da Silva 1994; Ward 1998; Nicholson and Grist 2001; Vizy and Cook 2001; Gu and Adler 2004; Bell and Lamb

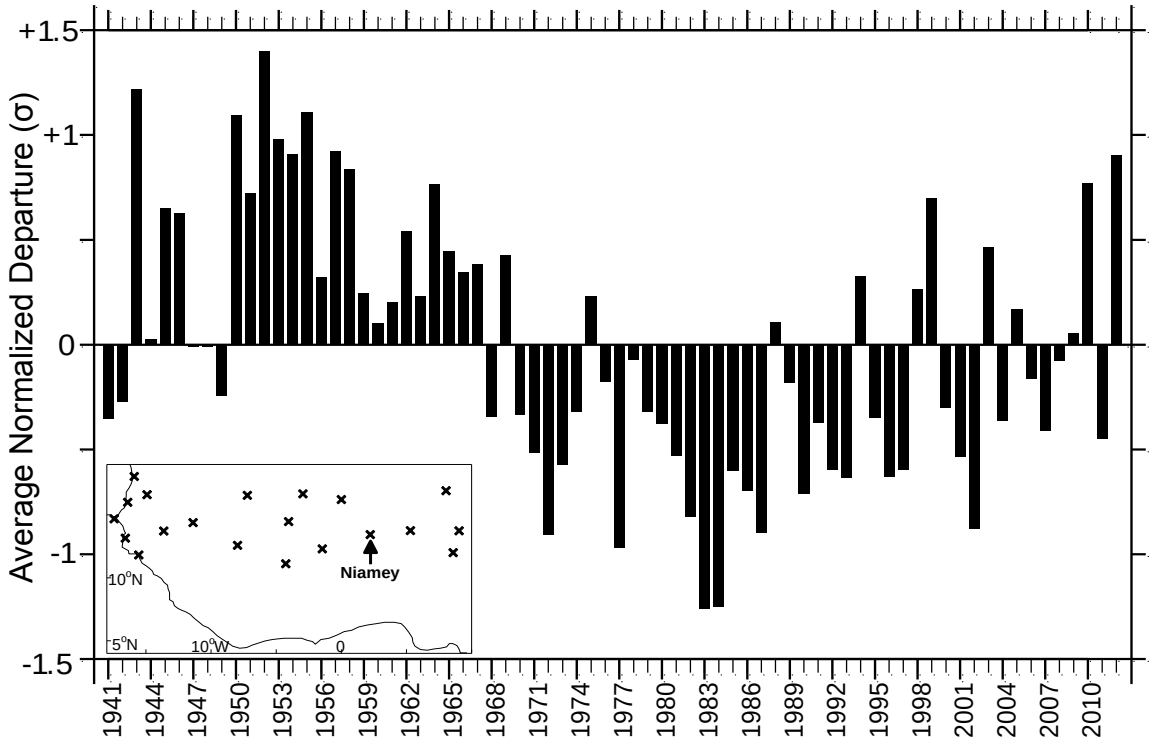

Figure 1.1: Time series (1941–2012) of average normalized April–October rainfall departure (σ) for 20 stations in the West African Sudan-Sahel zone (11°-18°N) west of 10°E. Normalization is with respect to 1941-2000. Station locations are shown in inset map. Extended from previous documentation of index in Lamb (1978a, b, 1981, 1985), and Lamb and Peppler (1991, 1992), where further details can be found. This index correlates strongly (> +0.90) with other zone-wide rainfall indices based on many more stations (Dai et al. 2004, +0.95; Fall et al. 2006, +0.91) (from Boyd et al. 2013).

2006; Lélé and Lamb 2010; Laurent et al. 2011). Such mechanisms have included the land-biosphere-atmosphere system (i.e. surface albedo, soil moisture, and savanna grassland and forest cover), the basin wide meridional SST gradient in the tropical Atlantic, and the changes in atmospheric circulation and weather system behavior over and around West Africa during wet and dry rainy season. However, the spatial distributions of the mean water vapor flux and low frequency variations in this moisture

transport have received comparatively little attention. Earlier investigations of water vapor transport over West Africa focused mostly on seasonal-to-interannual variability (e.g., Lamb 1983b; Cadet and Nnoli 1987; Long et al 2000) and to a lesser extent on intraseasonal variability (e.g., Sultan et al. 2003; Mathiews 2004). While these studies have focused mostly on the Sahel zone, study of the full spectrum of water vapor transport over the rest of the continent associated with the large-scale circulation, as well as its relationship to the geographical distribution of precipitation, was left for further investigations. The present study attempts to address this deficiency through observational analysis and modeling experiments, using state-of-the-science analysis products and modeling tools, including the Weather Research and Forecasting (WRF) model.

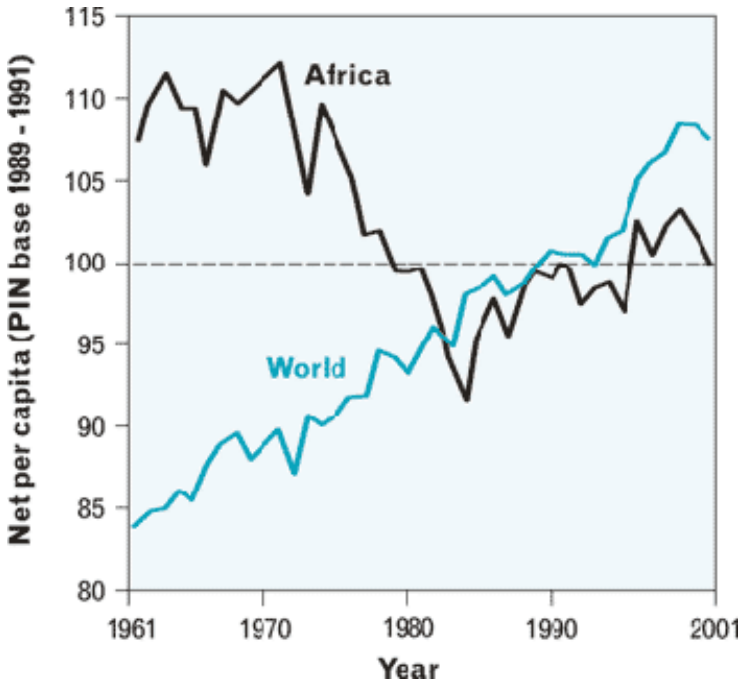

Figure 1.2: Food production index *per capita* in Africa compared to the world for the period 1961-2001. Source: Food and Agriculture Organization (FAO)

1.2 Overview of West African Rainfall Variability

The Sahelian countries of West Africa (hereafter "WA") are known for their devastating and widespread droughts that began several years after achieving their independence in the 1960s. These countries were forced to deal not only with nation building, but also with the socioeconomic impact of the world's largest regional climate change of the latter half of the twentieth century (e.g., Glantz 1977, Dai et al. 2004, Bell and Lamb 2006, Henson 2008). Analyses such as those of Hastenrath (1991); Nicholson (1993), and Lélé and Lamb (2010) found that rainfall has been markedly below normal over the semi-arid region of WA, with a dramatic change from wet conditions in the 1950s (especially) and 1960s to much drier conditions in the 1970s, 1980s, and 1990s (Fig. 1.1). A consequence of this persistent drought over several decades has been widespread famine, mass human migration, conflicts, and political instability in the region (Findley 1994; Koohafkan 1996; Benson and Clay 1998; Miguel et al. 2004; Burke et al. 2009; Barrios et al. 2010; Couttenier and Soubeyran 2012). For example, Burki (1986) reported that during the 1983-84 droughts, cereal production in Mauritania fell to two-thirds its normal level, and 40% of Niger's population was considered affected with as many as 400,000 people displaced.

Rainfall in WA plays a major role in determining agricultural production and hence the economic and social wellbeing of the rural communities. According to the 2011 United Nations Department of Economic and Social Affairs Population Division, 60% of West Africans live in rural areas, while 75% of the Sudan-Sahel labor force

works in agriculture (World Bank 2008). Livestock and crop production represent 30 to 40% of the Gross Domestic Product (GDP, World Bank 2008) and provide many of the opportunities for employment in WA. Unfortunately, in the Sahel and Sudan zones (10^{o}-18^{o}N) the annual rainfall cycle features a pronounced summer monsoon rainfall peak, with most (80%) of the annual rainfall occurring each year in June-September (Lamb 1978a, 1980). In contrast, the annual cycle of rainfall over the Gulf of Guinean region is bimodal, and features the first rainfall peak during May-June, and the second during September-October (Fig. 1.3). The rainfall pattern in the region is also influenced by large-scale interannual climate variability, including occasional El-Niño events in the tropical Pacific. These large-scale climate events are the summation of frequent extreme weather events, such as dry spells and floods, which reduce agricultural output and can result in severe food shortages. Because of the high global visibility of these impacts, and soon after the devastating 1972-1973 drought, the causes of West African rainfall variability and the notable persistence of the Sudan-Sahel drought have received much attention from climatologists (e.g., Lamb 1978a, b; Nicholson 1981; Folland et al. 1986; Lamb and Peppler 1992; Hastenrath 2000; Long et al. 2000; Nicholson et al. 2000; Hulme et al. 2001; Giannini et al. 2003; Hoerling et al. 2006). Less often noted is the fact that the 1970's drought also affected the more humid coastal zone and was therefore not simply limited to the northern reaches of the monsoon (e.g., Lamb 1978; Nicholson 1981; Moron 1994; Paeth and Friederichs 2004).

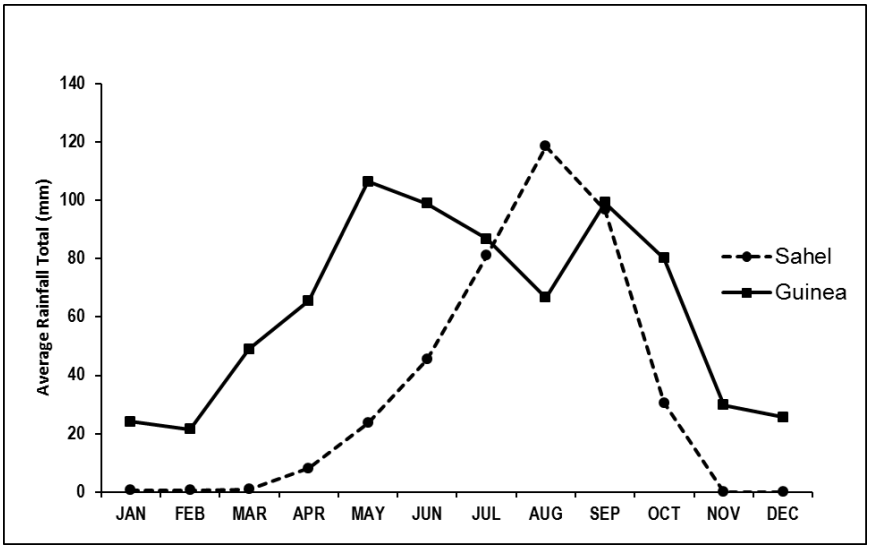

Figure 1.3: Annual cycle of rainfall over West Africa.

1.3 Atmospheric Features Associated to West African Rainfall Variability

The source of rainfall variability over WA can be linked to changes in different atmospheric features since precipitation is produced through a set of complex interactions between diverse circulation systems. Some of the earliest studies on interannual rainfall variability in the Sudan-Sahel region related these changes to anomalous sea surface temperature (SST) patterns in the equatorial and subtropical Atlantic (Lamb 1978a, b), and the inter-hemispheric SST gradients (Folland et al. 1986). Although SST has been widely recognized as a major forcing of tropical rainfall variability, it only explained a fraction (~ 5 to 20%; Diatta and Fink 2014, and 25% to 50%; Biasutti et al. 2003) of the Sudan-Sahel rainfall variability. Accordingly, it is now accepted that WAM rainfall is modulated and associated with a range of phenomena,

including the meridional movement of the Intertropical Front (ITF), the intensity of the Saharan Heat Low (SHL), the strength of the African Easterly Jet (AEJ) and the Tropical Easterly Jet (TEJ), and synoptic disturbances traversing from east to west across the continent (e.g., Burpee 1972; Thorncroft and Hodges 2001; Mekonnen et al. 2006). The circulation features depicted in Figure 1.4 are described in the next subsections. On the largest spatial scales, the WAM seasonality reflects the annual movement of the quasi-permanent subtropical high pressure systems centered over the Azores (North Atlantic) and St. Helena (South Atlantic), and the intervening near-equatorial trough (Hastenrath 1991, pp. 169-173). Even these hemispheric-scale features are modulated to varying degrees by the global scale Hadley and Walker-type circulations.

1.3.1 The Intertropical Front

The Intertropical Front (ITF) or Intertropical Discontinuity (ITD) (Figure 1.3) is one of the fundamental features of the atmospheric circulation over WA. The studies by Hamilton and Archbold (1954), Eldridge (1957), and Hare (1977), based on the initial study by Hamilton and Archbold (1945) presented the first evidence of the ITF. The ITF is a west-east oriented quasi-stationary discontinuity that separates the warm and moist southwesterly monsoon flow from the tropical Atlantic from the much hotter, very dry, and frequently dust laden northeasterly air (regionally termed the Harmattan) from the Sahara. At the surface, the discontinuity is characterized by pronounced

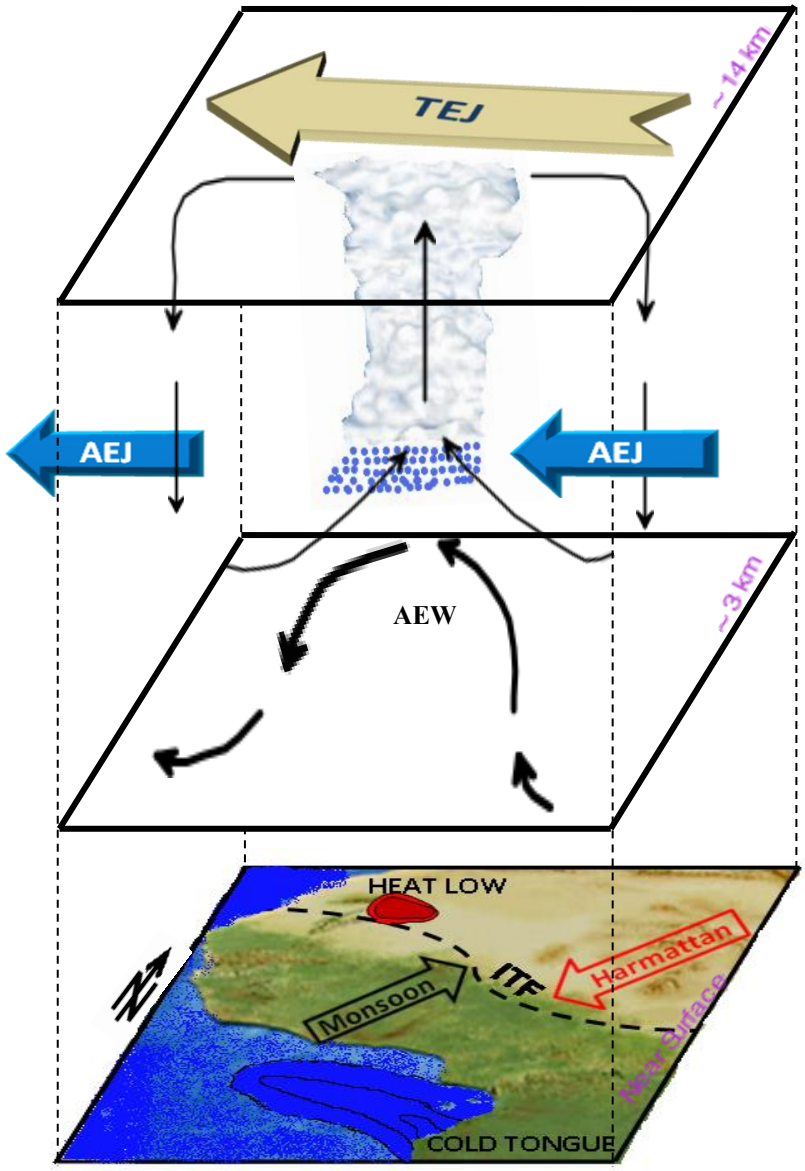

Figure 1.4: Idealized average spatial patterns of complex interplay elements of WAM circulation system. The dash line in the lower panel indicates the InterTropical Front (ITF), which is the transition zone between the southwesterly monsoon flow (black arrow) and the northeasterly Harmattan wind (red arrow). The red circle represents the location of the heat low. The arrows in the middle panel indicate the African easterly wave (AEW). The heavy blue arrows indicate the position of the African Easterly Jet (AEJ; ~600 hPa), top by the tropical easterly jet (TEJ; brown arrow) in the upper troposphere (~200 hPa).

temperature and humidity gradients that migrate seasonally northward then southward, somewhat lagging the zenith angle of the sun in the northern tropics. The monsoon surface winds can penetrate to approximately 20^{o}N and the associated zones of maximum horizontal velocity, moisture convergence and rainfall that are the West African manifestations of the ITCZ occur a few hundred kilometers south of the ITF, where the southwesterly monsoon air is deeper. The onset, length, and annual march of rainfall in West African countries depend primarily on the seasonal excursion of the ITF.

The importance of the ITF has been recognized under the African Monsoon Multidisciplinary Analysis (AMMA) framework, as advocated by Redelsperger et al. (2006) among others. The seasonal cycle of precipitation is accompanied by a southerly boundary-layer flow across the coast of the Gulf of Guinea which, turns southwesterly farther inland. This flow transports moisture into the continent throughout the monsoon season, and is associated with both surface sensible heating and atmospheric latent heating (Hagos and Zhang 2009). Hagos and Cook (2007) and Ramel et al. (2006) showed that the abrupt northward shift of precipitation maximum follows enhanced moisture convergence and condensation over land, which in turn follow the intensification and northward movement of the Africa heat low. But a quantitative assessment of the role of the ITF in moisture transport and precipitation feedback has yet to be made. This would provide a clearer insight into the dynamics of WAM since the SST anomaly patterns in the tropical Atlantic (e.g., Lamb 1978a,b; Lamb and Peppler 1992; Gu and Adler 2004; Biasutti et al. 2008; Okumura and Xie 2004) and the

anticyclonic circulation on the windward side of the Atlas-Ahaggar mountains (Sultan and Janicot 2003) have already been shown to play important roles in the WAM seasonal cycle. In the present study, and based on Lélé and Lamb (2010), the relationship between the ITF latitude displacement and moisture transport associated with the seasonal cycle of WAM precipitation is examined, and the regional control features on the moisture supply for the WAM were identified.

1.3.2 The Saharan Heat Low

The Saharan Heat Low (SHL, Fig. 1.4) is another major feature of the atmospheric circulation over WA. It represents a thermal low pressure system (high surface temperature, low surface pressure) centered over the northwestern Sahara near 20^{o}N. It forms over regions of high solar insolation and very low-to-zero rates of evaporation (i.e., desert areas). Like the ITF, the SHL shows a pronounced seasonal migration. Located south of the Darfur Mountains (~ 8^{o}N, 20^{o}E) in the boreal winter (November-March), it migrates northwestward to the western Sahara (~ 22^{o}N, 2^{o}W) by June. It remains centered in the location between the Hoggar and the Atlas Mountains prior to the WA rainfall onset and persists between June and September (e.g., Lavaysse et al. 2009).

While the SHL has been identified in recent studies as a key deep, dry convection feature of the WAM (e.g., Thorncroft and Blackburn 1999; Thorncroft et al. 2003; Parker et al. 2005; Lavaysse et al. 2009; Grams et al. 2010; Chauvin et al. 2010),

its role on the monsoon seasonal variability remains to be clarified, in particular its relationship to the ITF seasonal latitude migration. Lavaysse et al. (2010) found that on the intraseasonal time scale, the weakening of SHL is accompanied by enhanced convection over WA and the northernmost displacement of the ITF. This suggests that the strength of the SHL may influence rainfall variability over WA and, if so, needs to be understood. Accordingly, an effort was made during the 2006 AMMA Special Observing Period (SOP) to make aircraft observations in the ITF-SHL region with the objective of measuring the dynamical processes around both the SHL and the ITF.

1.3.3 The African Easterly Jet

The WAM circulation includes two approximately zonal flows: the African Easterly Jet (AEJ) in the mid-troposphere, and the Tropospheric Easterly Jet stream (TEJ) in the upper troposphere (Fig. 1.4). The AEJ has attracted the interest of scientists for over four decades because of its role in generating the African Easterly Waves (AEW). It is considered the most complex and intriguing dynamical feature in tropical meteorology (Wu et al. 2009), and flows over North Africa in the summer, with a predominately easterly component of 15-20 m s^{-1}, at 600-700 hPa. Questions, including its formation mechanism, maintenance and causes of its intensity fluctuations to its role in generating synoptic scale weather systems were first addressed by Burpee (1972). He suggested that the AEJ was a response of the mid-tropospheric flow to the lower tropospheric temperature gradient and the reversal of temperature gradients in the mid-troposphere. With some minor differences, most of the recent theoretical and

observational studies (e.g., Reed et al. 1977; Cook 1999; Thorncroft and Blackburn 1999; Dickison and Molinari 2000) have agreed with earlier results of Burpee (1972).

The role of the AEJ in the initiation of regional synoptic-scale weather events has also been a key focus for scientists in recent decades because the major weather systems over the WAM region can intensify after reaching the Atlantic and evolve into tropical cyclones. Instability of the AEJ has been shown to explain the genesis of AEW disturbances that characterize the rainy season (Burpee 1972, 1974; Nicholson and Grist 2001). Cook (1999) considered the AEJ a prominent feature of the WAM system because of its strong influence on the occurrence, intensity, and frequency of WA weather systems. Its vertical shear has been recognized to favor organized long-lived mesoscale convective systems responsible for most of the daily rainfall events in WA (e.g., Houze and Betts 1981; Cook 1999; Thorncroft et al. 2003). Burpee (1972) suggested that the associated potential vorticity of the AEJ and the low level temperature gradient are the necessary instability conditions for the genesis of the African easterly waves.

1.3.4 The Tropical Easterly Jet

Besides the ITCZ and the AEJ, the other inter-regional circulation feature that prominently controls WAM summer weather systems is the TEJ. This strong easterly current is maintained by the thermal gradient present in the upper troposphere between the heated Asian land masses, and the elevated heat source of the Tibetan plateau, and the relatively cooler Indian Ocean during the northern hemisphere summer

(Koteswaram 1958). Hence, the TEJ provides an example of an inter-regional scale interaction between WAM and Southeast Asian monsoon systems (Hulme and Tosdevin 1989). The TEJ lies in the upper troposphere between 200-100 hPa, stretching from Southeast Asia across the Indian Ocean and over Africa, reaching core speeds of about 40 m s^{-1} at 150 hPa over southern Indian, and decreasing to about 10 m s^{-1} over Africa. It remains, however, a well-defined jet above eastern and western Africa between 10^{o} – 15^{o}N during July-August core monsoon (e.g., Osman and Hastenrath 1969; Hulme and Tosdevin 1989; Camberlin 1997; Roja Raman et al. 2011).

The role of the TEJ in WAM dynamics has received relatively little attention until recently. The significant results of TEJ-Sudan-Sahel monsoon variability studies all are in general agreement -- in drier years the TEJ is weaker and further south compare to wetter years (e.g., Newell and Kidson 1984; Hulme and Tosdevin 1989; Fontaine and Janicot 1992). Osman and Hastenrath (1969) found that when the ITF/ITD juxtaposition with the TEJ failed to occur, Sudan experienced a dry season, suggesting a link between the core latitude of the TEJ and the ITF. This noteworthy result that applies to Sudan needs to be evaluated over the WAM region.

1.3.5 Mesoscale Convective Systems

Several types of precipitation systems characterize the West African summer monsoon season. Perhaps best known are Mesoscale Convective Systems (MCSs) or Disturbance Lines (DLs), also known as squall lines, or Lignes de Grains (LDGs) in French (Fig. 1.4). Most of the WA summer water cycle is linked to these westward

propagating linear, DLs that typically have a much longer north-south extent (of about 100 km) than their east-west extent which vary from 10 to over 100 km (Bell and Lamb 2006). These cloud clusters have typical lifetimes of hours to a day, but tend to be embedded within the African easterly waves, and move westward at the speed of the AEJ (~12 m s^{-1}). Since the GATE program in 1974, the scientific community has a better understanding of the dynamics of DLs and their role in shaping the monsoon seasonal cycle. For example, Mathon et al. (2002) found that about 90% of the WA seasonal rainfall is associated with organized convective systems, while Bell and Lamb (2006) found that the size/organization of convective systems is greater during the peak monsoon season.

1.4 Objectives

The cited studies on the WA rainfall variability in Section 1.2 have focused on the interannual variability at seasonal to decadal scales while the intraseasonal scale has not been well documented. Also, current global climate models (GCM) have great difficulty in correctly simulating the rainfall variability in WA. For example, Hoerling et al. (2006) have shown large discrepancies between simulated and observed rainfall in the African region. These discrepancies could be due to many factors among other the uncertainties in the moisture budget in these models. A better understanding of the physical processes governing the rainfall distribution and variability in WAM region would contribute to the efforts at improving GCMs performance. Furthermore, moisture transport over the WAM region, including the dual role it plays in the global energy

cycle, and as the source of water for WA, is poorly understood. So, the aim of this study is to investigate the variability of moisture transport associated with WA low-level wind regimes and its relationship to the boreal summer rainfall on the intraseasonal to interannual time-scales. This is because an analysis of the atmospheric water cycle in WAM regions will contributes to the understanding of the processes responsible for the low frequency of precipitation and therefore the occurrence of multiyear drought periods in the Sahelian zone. Such investigation also can contribute to an explanation of the reduction in rainfall totals that the region has experienced during the last decades.

Very few systematic studies exist concerning the variability of moisture transport and associated moisture convergence and its relationship to rainfall variations over WAM region. However, the WA climate is part of a larger climate system that includes the surrounding oceanic basin and, so, components of this system include phenomena ranging from smaller-scale mesoscale convective systems (MCSs) through synoptic-scale waves. All of these features are modulated by the diurnal cycle. The trade winds in particular and the associated seasonal displacement of the ITF play an important role in modulating precipitation over WA during the monsoon season. As the southerly trade wind enters the WA landmass, it intensifies, veers southwesterly and forms two low-level westerly regimes. The first is the southwesterly cross equatorial onshore flow across the Gulf of Guinean coast known as the WAM flow, and the second is the westerly flow between 5^{o} to 10^{o}N which is directed from the West Atlantic Ocean onto the west coast of WA (Grodsky et al. 2003; Pu and Cook 2010, 2012). These low-level wind regimes are very important for the transport of moisture

needed to sustain convective precipitation development into WA. Therefore, atmospheric moisture transport plays an essential role in the hydrological cycle in WA and is characterized, like WAM, by complex interactions across time and space scales.

The present effort at understanding the intraseasonal moisture flux variability and potential predictability of the WAM precipitation variability is motivated by the fact that the associated weather (e.g., heavy rain, drought, strong surface winds) poses a serious threat to the lives of the citizens, and impacts the economies of the countries of the region. Previous moisture transport studies over Africa have used short observational records mainly because of the limited sounding observations. And so, it has been long suspected that the South Atlantic Ocean serves as the major source of water vapor for rainfall in both the Guinean, and Sahelian land regions.This study advances our understanding of the sources of moisture for rainfall in WA. In addition, it obtains quantitative estimates of the separate contributions of the transport by synoptic and climate anomalies, defined as time-varying departures from the seasonally mean state and split into high-frequency (periods < 10 days) and low-frequency (periods > 10 days) components (e.g., Newman et al. 2012). This analysis allows us to investigate (i) the role of changing major regional circulation systems and their relationships to moisture flux associated with rainfall on intraseasonal time-scales; and (ii) the identification of potential predictors for monsoon onset and withdrawal over WA.

Furthermore, while observational analyses have been employed in many studies, RCM studies constitute a potentially complementary way to investigate the impact of

climate variability and change in WA because of their ability to capture some details of mesoscale systems and their representation of orographic features is better than in GCMs. Hence, motivated by the improved results of the current regional climate model simulations for the United States, the other objective of this study is to investigate the extent to which the Weather Research and Forecasting (WRF) model can capture the variability of WAM features in high resolution nested regional model simulations. But, it is well known that adequate representation of microphysics and convective processes are very important in regional climate models because of their scale dependence. Also, several different Convective Parameterization Schemes (CPS) exist with contrasting subgrid changes of mass, heat, and moisture, and to date there is no comprehensive assessment of CPS performance in simulating convection over WA. Therefore, this investigation of WRF ability to simulate WAM features will be carried out through a comparison of CPS and microphysics schemes in order to propose the WRF model setup the most appropriate in simulating WAM.

The data, model, and methods used in this study are described in Chapter 2. Chapter 3 focuses on the mechanisms and interannual variability of the lower troposphere atmospheric moisture transport into West Africa and associated large-scale circulation patterns that influence rainfall variability. The scale decomposition and the nature of the intraseasonal variability of moisture transport into WA as well as the relative contribution of the large scale and small scale transport of moisture are investigated in Chapter 4. The ability of the WRF model in simulating various aspects of WAM including its diurnal cycle is investigated in Chapter 5 through sensitivity

experiments involving different combinations of cumulus and microphysics processes. Chapter 5 further documents the predictability of the large scale monsoon onset and withdrawal dates. A summary of the key findings and conclusions that can be drawn from these findings are presented in Chapter 6.

Chapter 2

2. Data and Analysis Techniques

2.1 Datasets

2.1.1 Rainfall Data

Various observationally based datasets have been used in this study to evaluate the model performance, to identify the key systematic errors and to provide a description of monsoon variability and its teleconnections with large scale atmospheric features. The monthly and daily surface observation rainfall records covering 1979-2008, have provided the principal source of data for evaluating the model performance and describing monsoon variability over West Africa. The station rainfall totals were provided by both the National Weather Services of countries across the region and the Centre Régional de Formation et d'Application en Agroméorologie et Hydrologie Opérationelle (AGRYMET) based in Niamey (Niger). These countries include: Senegal, Mali, Gambia, Guinea, Guinea-Bissau, Mauritania, Chad, Niger, Benin, Nigeria, Togo, Ghana, Burkina Faso, and Côte d'Ivoire. Figure 2.1 shows the location of the stations. The majority of the station records in the original dataset were incomplete, with considerable variation in the length of continuous data as well as in the

distribution of gaps existing within the records. The data were quality controlled, and values exceeding physically reasonable limits were excluded. Since no attempt was made to estimate the missing values, the stations with least complete records were excluded. The final dataset contained 180 stations distributed throughout the region (Fig. 2.1). In addition, a regional scale time series of average normalized April-October (1941-2012) rainfall departure known as Lamb index (Fig. 1.1) is also used in this study. The Lamb index results from an average normalized departure for 20 stations in the West African Sudan-Sahelian zone (11^{o}-18^{o}N) west of 10°E.

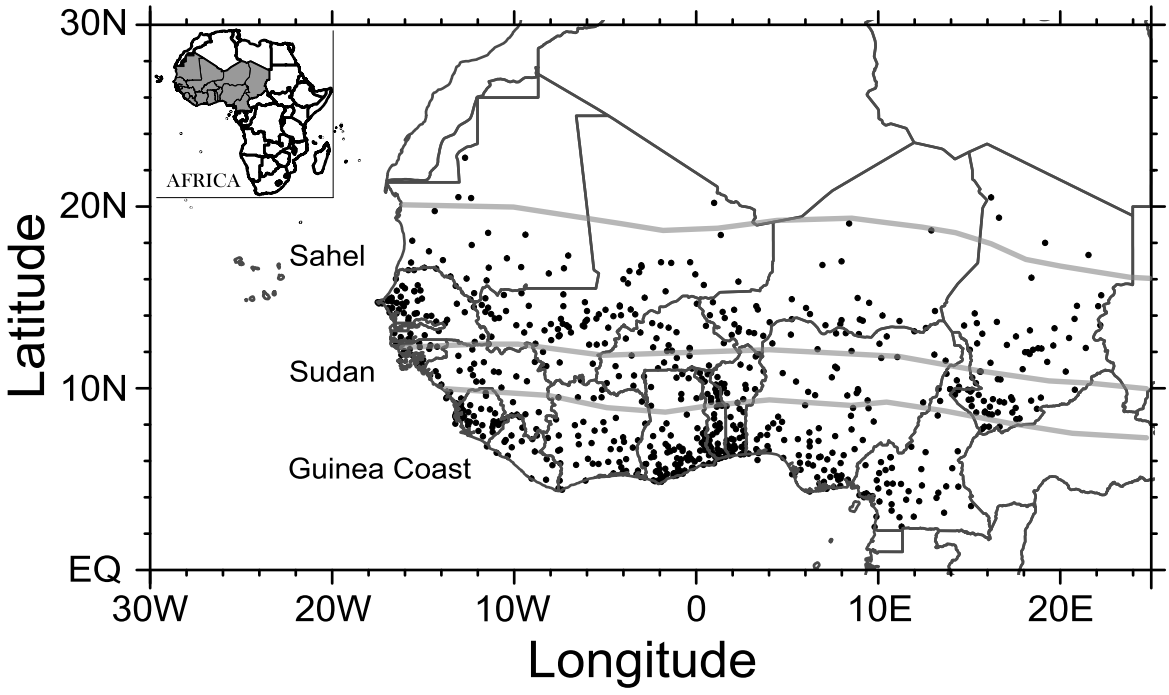

Figure 2.1: Location of stations of sixteen countries in West Africa, Cameroon and Chad for which daily and monthly rainfall data were analyzed. The gray lines delineate from top to bottom -- the Sahelian zone (single annual rainfall peak), the Guinean coast (bimodal annual rainfall peaks), and the Sudan zone which represents the transition zone between the Sahel and the Guinea coast zones.

While rain gauge measurements have the advantage of providing -- for their point locations -- better temporal resolution and are good candidates for model evaluation, they are limited by their spatial coverage. Remote sensing techniques using space borne sensors provide an excellent complement for filling gaps in ground-based data networks. So, the Climate Prediction Center (CPC) Merged Analysis of Precipitation (CMAP; Xie and Arkin 1997), the Global Precipitation Climatology Project (GPCP; Xie et al. 2003), and the Tropical Rainfall Measuring Mission (TRMM; Huffman et al. 2007) satellite datasets were also used in this study to assess the large scale patterns of rainfall variations and the model mean climate. Both the CMAP and the GPCP dataset blend rain gauge observations and satellite estimations. They are gridded on 2.5^{o} latitude x 2.5^{o} longitude boxes and are freely available from 1979 to present at both pentad (5 day) and monthly time scales. Over land areas, the CMAP and the GPCP datasets were shown to have similar major precipitation patterns (e.g., Xie and Arkin 1997; Yin, et al. 2004). The TRMM dataset used is the 3B43 algorithm which provides the best estimate of total monthly rainfall. This dataset is the result of the combination of precipitation data provided by multiple satellites in addition to TRMM as well as rain gauge data provided by the GPCP. Each record is 0.25^{o} x 0.25^{o} spatial resolution.

2.1.2 NCEP-NCAR Reanalysis Data

The present study also uses the National Center for Environmental Prediction-National Center for Atmospheric Research (NCEP-NCAR) reanalysis (Kalnay et al.

1996) dataset. These data were freely provided by the National Oceanic and Atmospheric Administration (NOAA) Climate Diagnostics Center (CDC). The NCEP-NCAR reanalysis were produced with a fixed assimilation system consisting of the NCEP Medium Range Forecast Spectral model and the operational NCEP Spectral Statistical Interpolation scheme to represent a dynamical interpolation of global observational network of meteorological variables. The data are recorded on a 2.5^{o} x 2.5^{o} grid resolution every 6 hours.

2.1.3 ECMWF/AMMA Reanalysis Data

The European Centre for Medium-Range Weather Forecasts (ECMWF) has performed a reanalysis specifically for the AMMA observational campaign (Agustí-Panareda, et al. 2010) using an improved version of the ECWMF Spectral model. The ECMWF/AMMA reanalysis assimilation system incorporates the largest number of sounding data recorded in West Africa during the SOP, and is available from May to September 2006 in its original 8 time daily format, 0.5^{o} x 0.5^{o} resolution, and 25 pressure levels.

2.1.4 NCEP FNL Data

The NCEP FNL (Final) Operational Global Analysis data is on the 1^{o} x 1^{o} degree grids prepared operationally every six hours and provided by the Global Data Assimilation System (GDAS). The analyses are freely available at http://rda.ucar.edu/datasets/ds083.2/ on the surface, at 26 mandatory (and other

pressure) levels, in the surface boundary layer and at some sigma layers, and the tropopause. FNL data are used in model initialization and lateral boundary conditions which are updated every 6 hours.

2.1.5 Sea Surface Temperature

The daily, high-resolution, Real-Time Global sea surface temperature (RTG_SST) analysis provided by NCEP/ Marine Modeling and Analysis Branch (NCEP/MMAB) is used in this study. The SST data are produced on a 0.5 degree grid resolution, with a 2-D variational interpolation analysis of the most recent 24-hours buoy and ship data, satellite-retrieved SST data, and SST's derived from satellite-observed sea-ice coverage. Also used in the study is the most recent version of the Extended Reconstructed Sea Surface Temperature (ERSST) analysis (Smith et al. 2008), provided by the NOAA Earth System Research Laboratory (ESRL) and has a 2^{o} x 2^{o} grid resolution.

2.1.6 Outgoing Long Wave Radiation

Outgoing longwave radiation (OLR) data (Liebmann and Smith 1996) of the NOAA polar-orbiting satellites is employed as a proxy for large-scale tropical convective activity. Low OLR values correspond to cold cloud tops associated with deep convective activity and high precipitation in the Tropics. The data are mapped onto a 2.5^{o}x 2.5^{o}grid and represents the average of twice daily satellite passes. Pentads of OLR non-overlapping averages (73 pentads $year^{-1}$) were used in this study.

2.2 Analysis Techniques

2.2.1 Statistical Techniques

A broad range of statistical techniques which will facilitate the exploration of the dataset used and their relationships to WAM variability are employed. The details of each statistical technique are provided within the body of the dissertation at the point of first use, except for the correlation and linear regression method which is described in the following section.

2.2.1.1 Correlation Coefficient

Correlation, lagged cross-correlation, and regression analyses are used to investigate the dependence of the spatial and temporal monsoon variability on large-scale atmospheric circulation fields. Concurrent and lag relationship between Sudan-Sahel monsoon index and area-averaged index of circulation fields are analyzed in this manner for the study period, on intraseasonal to interannual time-scales. The statistical significance of the correlation coefficients are assessed using the Student's *t*-test (Wilks 2006 pp. 131-135). However, it is known that a standard *t*-test rests on the assumption that the underlying data are composed of independent samples from their parent populations, which is not always true for atmospheric and other geophysical data (Wilks, 1997). Moreover, Mason and Mimmack (1992) point out that the Neyman-Pearson method of hypothesis testing yields only the probability of achieving the observed result purely by chance, and does not give any indication of the reliability of the sample statistic as an estimator of the population parameter. Hence, null hypothesis

statistical significance testing in general tells us relatively little of what we need to know and inherently can be misleading (i.e., Nicholls, 2001).

An alternate method to assess the reliability of the correlation coefficient is to give the estimate in the form of a confidence interval. In response to this situation, this study used the bootstrap techniques (Efron and Tibshirani 1993) to estimate confidence intervals for correlation coefficients. In view that the bootstrap-*t* method estimates the confidence limits in exactly the same way as the standard normal *t*-distribution, that is without making the assumption of normality (e.g., Efron and Tibshirani, 1993, pp. 160-162), the study make use of the more robust method, which is the bias-corrected (BCa) method. According to Efron and Tibshirani 1993, pp. 178-188 the BCa produces good confidence intervals than the bootstrap percentile and the bootstrap-*t* methods.

2.2.1.2 Compositing Analysis

Composite analyses that compare monsoon rainfall patterns for sets of extremely deficient and abundant rainy seasons, and place the results in the context of large scale atmospheric circulation variability over West Africa is employed. Evaluation of the temporal and spatial evolution of circulation and precipitation patterns associated with the Atlantic moisture transport is performed by forming composites based on the meridional and zonal components of the low-level moisture flux crossing the southern and western boundaries of the study region. This procedure highlights the difference

patterns between each of the dry and wet composite and the long term average, as well as between the dry and wet composites themselves.

2.2.1.3 Empirical Orthogonal Function (EOF) Analysis

Monsoon phenomena are usually the combination of various parameters difficult to dissociate, and interacting at many different time and space scales (e.g., Redelsperger et al. 2002, Nicholson and Grist 2003, Redelsperger et al. 2006). Hence, monsoon rainfall such as that observed over WA are organized into large scale patterns which suggest that rainfall over the region is more the result of larger climate fluctuation occurring in summer over the whole of WA than a single feature of regional extent. It is therefore important to objectively delineate the extent of the monsoon and describe its variability at any time scale by proposing a rational monsoon index. An EOF technique (Richman 1981; Jolliffe 1986) is of extreme importance in this matter.

Time series derived from EOF analysis of fields of meteorological variables have long been used in statistical prediction models, but many of these studies have considered the representation of fields of individual meteorological variables. The eigenvector representation can be extended to include the combined representation of fields of several variables (Wilks 2006, pp. 477-508) that is a field with observations of more than one variable at each location or grid point. This is known as the simultaneous principal component analysis for multiple fields or combined empirical orthogonal functions (Combined-EOF). As in the EOF analysis, the matrix for extraction can be a correlation matrix or a covariance matrix. For this study, a correlation matrix was used

as a matrix for extraction in the Combined-EOF analysis. The decomposition into EOFs is advantageous because it is built on modes calculated from the data themselves. Hence, it can summarize multivariate variation in data. Accordingly, the Combined-EOF method, allows the simultaneous consideration of the possible modes of variation of different fields. For example, let assume two meteorological fields **K** and **L**. **K** consists of time series of length N at locations m = 1 …M_s, and field **L** consists of time series of length N at locations m = 1…M_L. A new data matrix **R** can be written in such a way to keep the time correspondence between the fields, so that fields at the same time are put in the same column. The new combined data matrix is:

$$\mathbf{R} = \begin{bmatrix} K_1(1) & K_1(2) & \dots. & K_1(N) \\ K_2(1) & K_2(2) & \dots. & K_2(N) \\ & & \dots. & \\ K_{M_S}(1) & K_{M_S}(2) & \dots. & K_{M_S}(N) \\ L_1(1) & L_1(2) & \dots. & L_1(N) \\ L_2(1) & L_2(2) & \dots. & L_2(N) \\ & & \dots. & \\ L_{M_L}(1) & L_{M_L}(2) & \dots. & L_{M_L}(N) \end{bmatrix}$$

Assuming a zero mean, the covariance matrix for the combined field is given by:

$$\mathbf{RR}^* = \begin{bmatrix} \mathbf{K} \\ \mathbf{L} \end{bmatrix} [\mathbf{K}^*, \quad \mathbf{L}^*] = \begin{bmatrix} \mathbf{KK}^* & \mathbf{KL}^* \\ \mathbf{LK}^* & \mathbf{LL}^* \end{bmatrix}, \tag{2.1}$$

where $\mathbf{R}^*$, $\mathbf{K}^*$, and $\mathbf{L}^*$ are the complex conjugates of the transposed **R**, **K**, and **L** matrices respectively. Equation 2.1 shows that the total variance of the combined field is the sum of the variance of the composing fields. The advantage of the Combined-

EOF is that the fields can have different geographical extensions, but they must have the same time period. Also, there is no limitation in the number of fields to be used.

2.2.2 Vertically Integrated Moisture Flux

The vertically integrated moisture transport (VIMT) $\vec{Q}$, is obtained by integrating over the depth of the atmosphere. The moisture budget indicates that precipitation, evaporation, and net moisture transport into and out of an atmospheric column through its lateral boundary are in balance at the seasonal time-scale (Brubaker et al. 1993). Following Peixoto and Oort (1992), the atmospheric water budget in pressure coordinates is expressed as follows:

$$\frac{\partial \overline{W}}{\partial t} + \overline{\nabla \bullet Q} = \overline{E} - \overline{P} \tag{2.2}$$

In Eq. (2.1), *W* is precipitable water, *E* is evaporation, *P* precipitation, and $\nabla \bullet \boldsymbol{Q}$ is the divergence field of moisture flux, which represents the net moisture transport. The overbars denote the seasonally varying climatological mean. From a climatological perspective, the long-term accumulation of precipitable water in the atmosphere is negligible ($\frac{\partial \overline{W}}{\partial t}$ = 0). Therefore, the mean moisture budget is a balance between moisture flux divergence and the water source/sink. Thus, Eq. (2.2) can be written as:

$$\nabla \bullet \overline{Q} = \overline{E} - \overline{P}, \tag{2.3}$$

and

$$\vec{Q} = \frac{1}{g} \int_{p_t}^{p_s} \vec{V} q \, dp, \tag{2.4}$$

where $\vec{V}$ is the horizontal wind vector, q the specific humidity, g the gravitational acceleration, p_t the pressure at the top of the atmosphere, and p_s the surface pressure. Using the zonal (u) and meridional (v) components of the horizontal wind, the zonal and meridional transport of $\vec{Q}$ can be separately obtained by the following equations.

$$qu = \frac{1}{g} \int_{p_t}^{p_s} uq \, dp \, , \tag{2.5}$$

$$qv = \frac{1}{g} \int_{p_t}^{p_s} vq \, dp. \tag{2.6}$$

The integration limit p_t is the pressure above which the flux and flux divergence become negligible. Since in the NCEP/NCAR reanalysis, the specific humidity is set to zero above 300 hPa level, moisture flux calculation using these dataset usually set the p_t = 300 hPa. Neglecting the moisture flux above that level does not greatly impact the overall water budget because most of water vapor is concentrated in the lower troposphere. In this study, the VIMT computation was limited to the layer from the surface to 850 hPa. The choice of this layer is motivated by previous moisture flux studies which results show that over West Africa, moisture flux divergence activity is confined below 800 hPa, where the low-level monsoon flow is confined (Lamb 1983; Cadet and Nnoli 1987; Bielli and Roca 2009; Pu and Cook 2012). The monsoon flow

over WAM region occurs primarily below 700 hPa and confined mainly in the lower-troposphere and therefor makes the surface-850 hPa layer decomposition well suited to study the moisture fluxes over the region. Also, Mo and Higgins 1996, and Schneider et al. 2010 have noted that, more than 40% of the zonally averaged atmospheric column moisture in the tropics is located below 850 hPa. The monthly and seasonal values of moisture transport are obtained by averaging over the given month and over 3 months of the season. The value used for gravity is 9.81 m s^{-2}, so that the units of *qu* and *qv* are kg m^{-1} s^{-1}.

2.2.3 Numerical Simulation

The version 3.1 of the Weather Research and Forecasting (WRF; Skamarock et al. 2008) model was utilized in this study. WRF is a next-generation mesoscale numerical weather prediction system designed to serve both operational forecasting and atmospheric research needs. It features multiple dynamical cores, a 3-dimensional variational (3DVAR) data assimilation system, and a software architecture allowing for computational parallelism and system extensibility. Moreover, it is suitable for use in a broad spectrum of applications across space scales ranging from meters (large-eddy) to thousands of kilometers. The Advanced Research WRF (ARW) dynamic core is a fully compressible, three-dimensional non-hydrostatic model with the terrain following eta-coordinate mesoscale modeling system, and the horizontal grid is an Arakawa C-grid. The latter uses a third order Rang-Kutta split-explicit time integration, a fifth order horizontal advection, and third order vertical advection. The governing equations are

written in flux form, and the WRF dynamics solver conserves mass, momentum, entropy, and scalar. The ARW is designed to be a flexible, state-of-the-science atmospheric simulation system with portable code that is efficient in available computing environment ranging from massively-parallel supercomputers to laptops. The WRF modeling system software is in the public domain and it is maintained and supported as a community model to facilitate wide use internationally, for research, operations, and teaching.

Chapter 3

3. Mechanisms and Interannual Variability of Low-Level Moisture Transport Associated to the Inter-Tropical Front and Rainfall during West African Monsoon Season

3.1 Background

The WAM is an integral component of the Earth's climate system, involving complex interactions between the atmosphere, the hydrosphere and the biosphere, and between many time scales during the boreal summer (e.g., Redelsperger et al. 2002; Nicholson and Grist 2003; Redelsperger et al. 2006). It encompasses many developing countries that are particularly vulnerable to climate variability and climate change.

The variability of water is one of the most limiting parameters for sustaining life, agriculture, and economic development in WA Sudan-Sahel region. So, the role played by the atmospheric moisture transfer and its phase transitions through evaporation, latent heat release and associated energy transports and exchanges are of central importance for WAM dynamics and its variability. This because the hydrological processes play an important role in determining the scale of the major circulation patterns (e.g., Webster 1994), and the natural variability of weather and

climate at both regional and global scales is regulated by the water cycle (e.g., Eltahir and Bras 1996). Therefore, research on the moisture transport has both scientific and societal value.

Over 80% of annual mean precipitation for WA falls during the June-September interval when the ITF extends further north to permits convection over the region, yet the overall amount of precipitation has large year-to-year variations (Nicholson et al. 2000; Le Barbé et al. 2002). The WAM region frequently suffers from droughts, which may cause water shortages and disrupt agriculture and economic activities (e.g., Nicholson 1981; Le Barbé et al. 2002). Considerable effort has been devoted in understanding how the strength of the WAM could be influenced by the latitude position of the ITF including the tropical Atlantic SST anomalies and the El-Niño-Southern Oscillation (ENSO) phenomenon and regional scale atmospheric features (Chapter 1). The northward excursion of the ITF may act to redistribute preferred low-level moisture convergence and deep convection in the Sahelian region, while it southward latitude position may act to maintain this low-level moisture convergence and deep convection south in the Gulf of Guinea region.

Giving the proximity of the extent of monsoon layer, the ITF latitude, and rainfall over WA, the concept of an interaction between the three has an intuitive appeal. Nevertheless, atmospheric moisture transport over the WAM region, including the dual role it plays in the global energy cycle and as the source of water over the African continent is poorly understood. So, and in view of its importance in the

maintenance of monsoons, and how its distribution at low-levels varies so greatly during the ITF phases, a study of moisture flux variability during WAM season is timely. This because an analysis of the atmospheric water cycle in WAM regions will contribute to the understanding of the processes responsible for the low frequency of precipitation and therefore the occurrence of multiyear drought periods in the Sahelian zone. Such investigation also, can contribute to an explanation of the reduction in rainfall total that the region has experienced during the last decades.

3.2 Review of Early Work

Atmospheric moisture transport variability has been poorly studied over WA, and few of the studies that exist have been focused on extreme hydrologic events over the Sahelian zone. Lamb (1978b) presented a comparative analysis of moisture availability during wet and dry events over sub-Saharan zone. The study found a southward (northward) displacement of the tropical Atlantic SSTa and WAM trough during dry (wet) years. Similarly, Lamb (1983) found that during the extremely dry 1972 Sahelian rainy season, the northward moisture flux across the Gulf of Guinea was shallower compared with the much extent monsoon depth found during the less severe 1968 droughts. This suggests that the location of the monsoon trough and associated moisture flux convergence influence the rainfall pattern over the Guinean, and central Sahelian region.

Cadet and Nnoli (1987) have also examined the transport of water vapor over WA and the Atlantic Ocean during the 1979 summer season. They estimated the water

budgets and roles of evaporation over the Gulf of Guinea and evapotranspiration over land. Their study shows that the Gulf of Guinea supplies most of the moisture needed for rainfall over WA while also emphasizing the importance of moisture recycling. Gong and Eltahir (1996) used a short period of data (3-years) to quantify the contribution from the Atlantic Ocean (23%) and continental recycling (27%) over a large area of ~3.10^6 km^2. Druyan and Koster (1989) studied the source of Sub-Saharan precipitation using a climate model with the focus on July precipitation in the Sahel. They found that the tropical North Atlantic Ocean contributes the most to rainfall over western Sahel while the Gulf of Guinea and the South Atlantic Ocean, contributes the most over the central Sahel. The second largest contributor to rainfall for both regions according to their study is the local evaporation. Long et al. (2000) showed that the easterly flow dominates water vapor transport pattern over WA, and that the meridional transport in June-July is larger than that in August-September. Fontaine et al. (2003) found that a portion of West African low-level moisture originated from the Mediterranean, and that the zonal moisture flux is most important for the Sahel. Their results are in agreement with those of Rowell (2003), Cadet and Nnoli (1987) and Gong and Eltahir (1996).

Studies by Brubaker et al. (1993), Gong and Eltahir (1996), and Nieto et al. (2006) did not support the above moisture transport mechanisms and its contribution to West African precipitation. They however, support the idea that the recycling represents a significant contribution to the annual and interannual mean variability of total water budget rather than the transport from surrounding Oceans. For example, Brubaker et al.

(1993) used aerological and precipitation data to quantify the contribution of the moisture cycling to local precipitation. They found that WA is a source of moisture in July-September, and estimated continental recycling as about 40%, which is greater than Gong and Eltahir's (1996) estimation.

The lack of consensus among the above studies may be due to the differences in data sources, period of study, or the regions studied. Most studies also pointed out the deficiencies of the atmospheric station data that limit the validity of the results obtained. The limitations of station network over the region involve not only insufficient spatial sampling, but also insufficient resolution in time. The primary purpose of this chapter is to develop a phenomenological description of the seasonal mode of moisture transport anomalies over WAM region that will help lead to the investigation of hypotheses regarding their causal mechanisms. We will focus on the interannual variations, in particular the phases of WAM life-cycle, from build-up and onset to maturity and withdrawal in order to better understand the relation between large-scale atmospheric circulation, moisture flux, and precipitation. This is now possible owing to the availability of NCEP/NCAR global gridded atmospheric analyses with a significant length of record and to the unprecedented observation and modeling effort conducted over WA during the AMMA field campaign.

3.3 Mechanism of Rainfall Variability over West Africa

That rainfall variability over the Sudan-Sahel region is characterized by the northward migration of the ITF, the rain band, and associated surface and low level

circulations features has long been recognized. In this section we present the mean circulation over WA and adjacent oceans, and the associated rainfall climatology.

3.3.1 Seasonal Cycle

The origins of the seasonal cycle in WA are linked to the annual cycle of solar declination. Figure 3.1 illustrates the long term seasonal cycle of the mean wind field at 925 hPa superimpose by the surface skin temperature, the mean SLP, and the ITF. During January-March (Fig. 3.1a), strong northeasterly winds (Harmattan) dominate much of the region, a warm pool develops over the Gulf of Guinea, and the ITF lies at its southernmost position at about 5^{o}N, limiting the southwesterly monsoon flow over the coast. During the boreal spring (AMJ), temperatures are higher over the Sahel where the highest surface temperature coincide with the lowest surface pressure and form the SHL located between 10-12^{o}N, and 5^{o}W-5^{o}E (Fig. 3.1b). A cold tongue also develops over the equatorial Atlantic, and the southeasterly trades associated with the Saint Helena high intensifies. The low pressure system create in the SHL creates a steady wind that blows toward the land currying the near-surface moist air from the Atlantic Ocean. This act to shifts the ITF further north and permits the onset of WAM to be initiated.

During the boreal summer (JAS, Fig.3.1c), the HL becomes strongest, it is displaced northwestward and centered approximately at 5^{o}W-22^{o}N, consistent with its positions describe by Ramel et al. (2006), and the cold tongue over the Atlantic

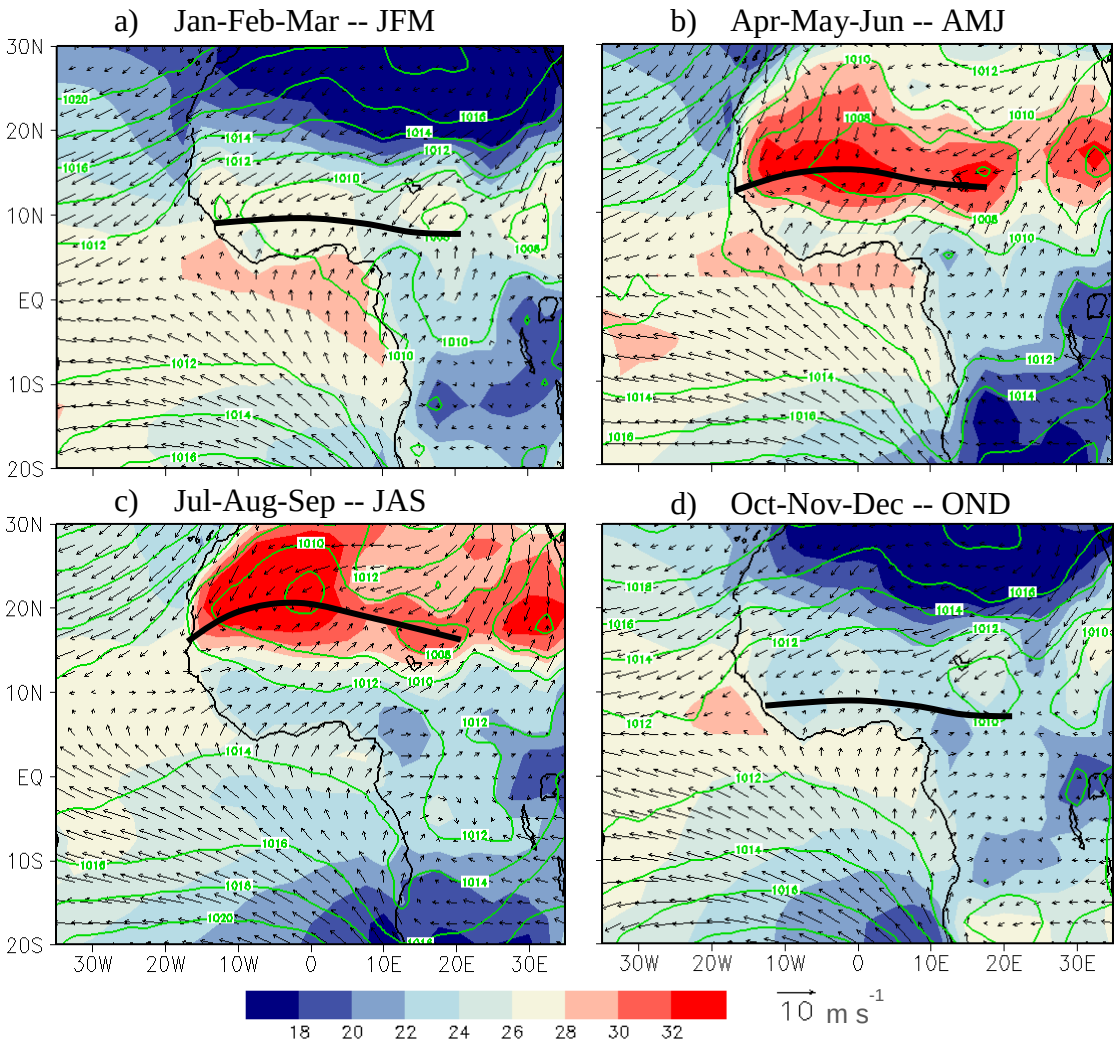

Figure 3.1: Long term seasonal average (1960-2008) of surface skin temperature (shading, ^{o}C), 925 hPa wind field (vectors, m s^{-1}), and mean sea level pressure (contour, hPa) from NCEP-NCAR. Heavy solid lines indicate the boundary between the dry northerly and moist southerly wind (an indication of the ITF).

becomes coldest and spread on shore. This pronounced temperature difference between West African land masses and the ocean enhanced the existent meridional gradient of temperature and thereby, enhanced the southerly boundary layer monsoon flows. These flows become stronger and extends further north in association to the northward shift of

the ITF which, reaches its northernmost latitude position at about 20^{o}N in August. The timing of the development of the cold tongue suggests its significant contribution to WAM onset as well as to the northward advance of the ITF. October-December (OND) season (Fig. 3.1d) is characterized by a very weak southwesterly flow in response to increasing insolation in the southern Hemisphere. The northeasterly winds that prevailed during JFM season recur. They intensify and influence the Sahelian region in conjuction with the southward withdrawal of the ITF back to its JFM position.

Both the monthly mean precipitation climatology (Fig. 3.2) from rain gauges for the period 1960-2008 and the daily precipitation climatology for selected latitude bands (Fig. 3.3) indicate that there are two precipitation regimes over the WAM region: the Gulf of Guinea regime and the summer continental Sahelian regime. Over the Guinea coast, rainfall begins in March (~5^{o}N) and peaks in June (Fig. 3.2a-d). As the season progresses, precipitation extends northward over the Sudan zone (~5^{o}-10^{o}N), but the most significant rainfall during April to May occurred in the Guinea region (Fig. 3.2b, c). In July, the precipitation band suddenly moves northward over the Sahel (Fig. 3.1e) and peaks in August (Fig. 3.1f). At that time, precipitation decreases over the Guinea coast; it is “the little dry season”. In September however, precipitation progressively retreats back to the south (Fig. 3.2g), and then peaks again over the Guinea coast in October (Fig. 3.2h). This results in a bimodal distribution of rainfall over the Gulf of Guinea (Fig. 1.2). The first maximum is in June and the second maximum is in late October. The Sahel region however, has only one maximum, in August.

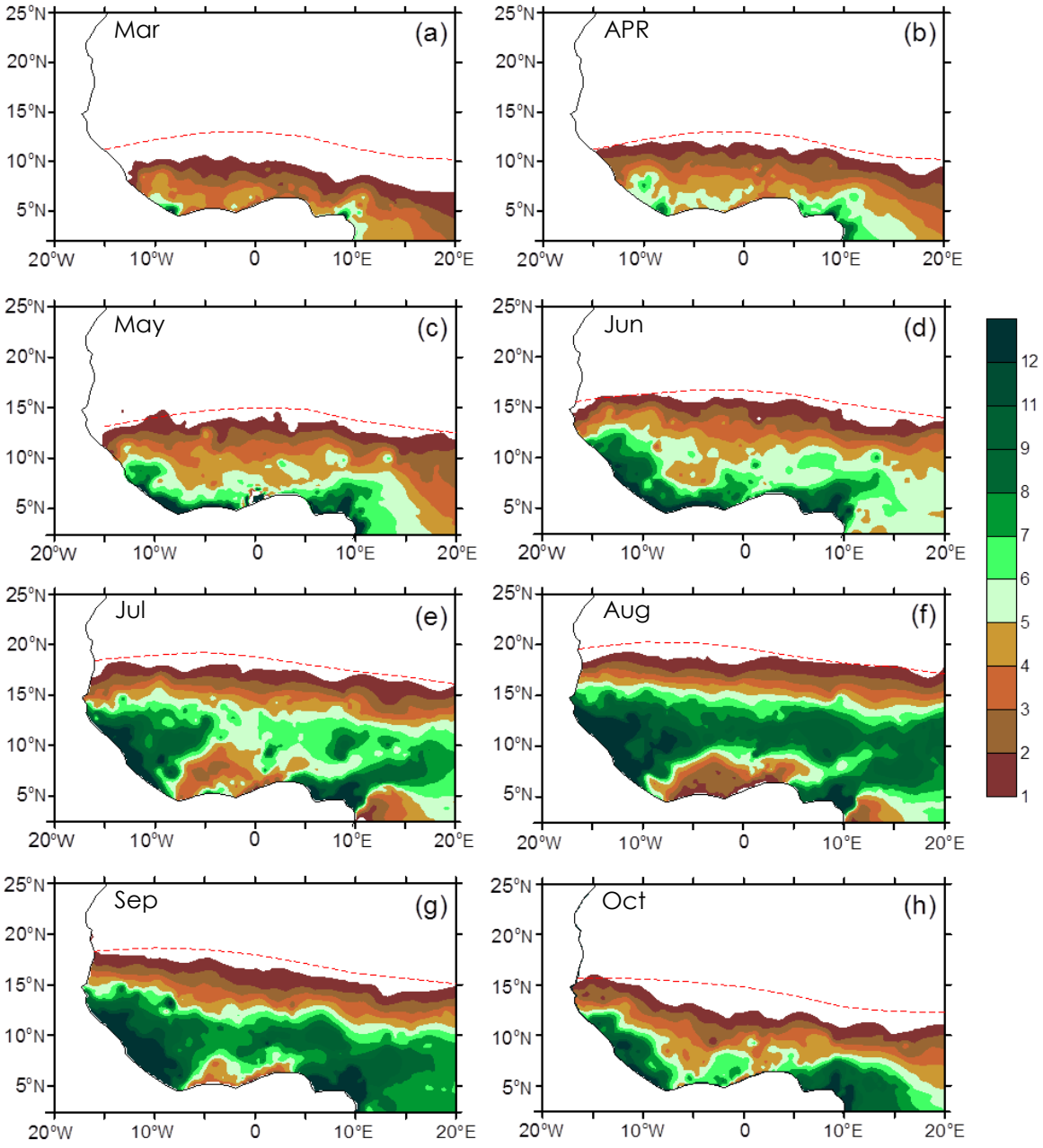

Figure 3.2: Monthly mean precipitation climatology from rain gauge observations for the period from 1960 to 2008 for (a) March, (b) April, (c) May, (d) June, (e) July, (f), August, (g) September, and (h) October in relation to the long-term average (1974-2008) monthly ITF position (red broken line). Contour intervals are 1 mm day^{-1}.

3.3.2 Annual Cycle

Figure 3.3 summarizes the gross features of the annual cycle of precipitation across WA as a time-latitude cross-section averaged between 10^{o}W and 10^{o}E. The mean precipitation shows a zonal band with two regional precipitation maxima (Hastenrath 1984). The northward migration of precipitation is characterized by a succession of active and break phases. First, rain events start to increase along the Equator and progresses northward at about 2^{o} $month^{-1}$ before reaching the first peak in June south of 8^{o}N over the Gulf of Guinea. The monthly migration of the rain band is in tandem with that of the ITF which experience a short period of stagnation after the first rainfall peak in June. This corresponds to the first pause of the monsoon season often termed to the "little dry season" over the Guinea coast. Then, the ITF migrates further north and reaches its maximum position in August followed by the second monsoon phase in July-September. This second monsoon phase is characterized by a systematic and almost ceaseless northward migration of rainfall from about 7.5^{o}N to 18°N over the Sahel. The peak rainfall for this phase is reached in August and then moves back abruptly toward the coast as does the ITF. These two monsoon phases suggest that the onset of the rainy season over the Sahelian zone is not in phase with the onset over the Guinean coast and, so, two dynamics systems seem to interplay in the annual rainfall cycle. One initiates the onset of the Guinea coast rainfall season in February, and the other initiates an abrupt surge in mid-June and concerning the Sahelian zone. This space-time cell of rainfall occurrences is clearly connected with the space-time positions of the ITF.

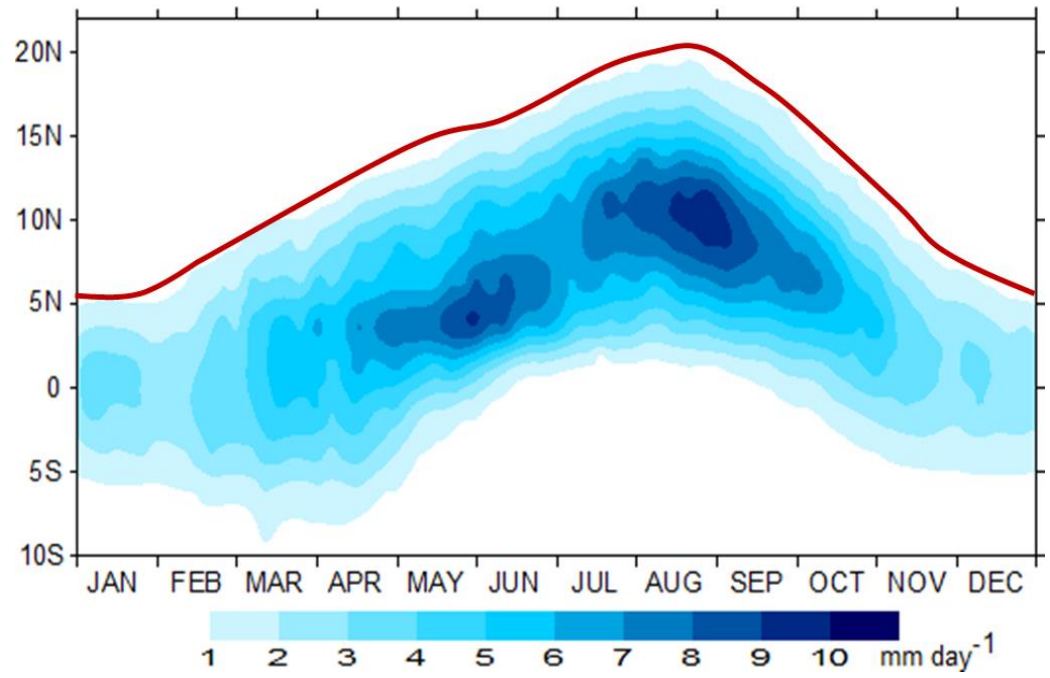

Figure 3.3: Time-latitude cross-section of GPCP long-term average precipitation (shading) in interval of 1 mm day^{-1}. The solid red line indicates the mean latitude position of the ITF average across 10^{o}W-10^{o}E.

3.4 Lower-Tropospheric Moisture Transport and Moisture Convergence

3.4.1 Seasonal Mean Climatology of Moisture flux

Figure 3.4 and 3.5 shows the climatological vertically integrated moisture flux between the surface and 850 hPa for eight months of monsoon cycle. The contours in these Figures represent the moisture flux vector magnitude. The shading represents the absolute values of moisture flux magnitude equal or greater than 100 kg m^{-1} s^{-1} with 40

kg m^{-1} s^{-1} interval. The solid dashed line represents the latitude of the ITF that is the 15^{o}C dew point temperature calculated at each 5^{o} longitude strip.

During March-April (Fig. 3.4a, b), the ITF is centered near the Gulf of Guinea coast, between the southern coast of WA and south of 10^{o}N. On average its reaches 10^{o}N in April in the western portion of the region, but is slightly south in the eastern portion. Even in those pre-monsoonal months, a degree of cross-equatorial southwesterly moisture flow is observed, much of which is redirected onto the Gulf of Guinea coast under the influence of the St. Helena anticyclone circulation centered south of 10^{o}S. Although the actual monthly mean vectors are relatively small off the south Guinea coast, there is a substantial mean transport of approximately 120 to 160 kg m^{-1} s^{-1} onto the coast of the Gulf of Guinea region. This enhanced magnitude of moisture flux is associated with the northward shift of the ITF from its winter position near the Guinea coast to around 10^{o}N in April. It is also associated to the local sea-breeze/land-breeze regime and the onset of the first rainy season which occurred over the Guinean coast during the spring season (e.g., Sultan and Janicot 2003).

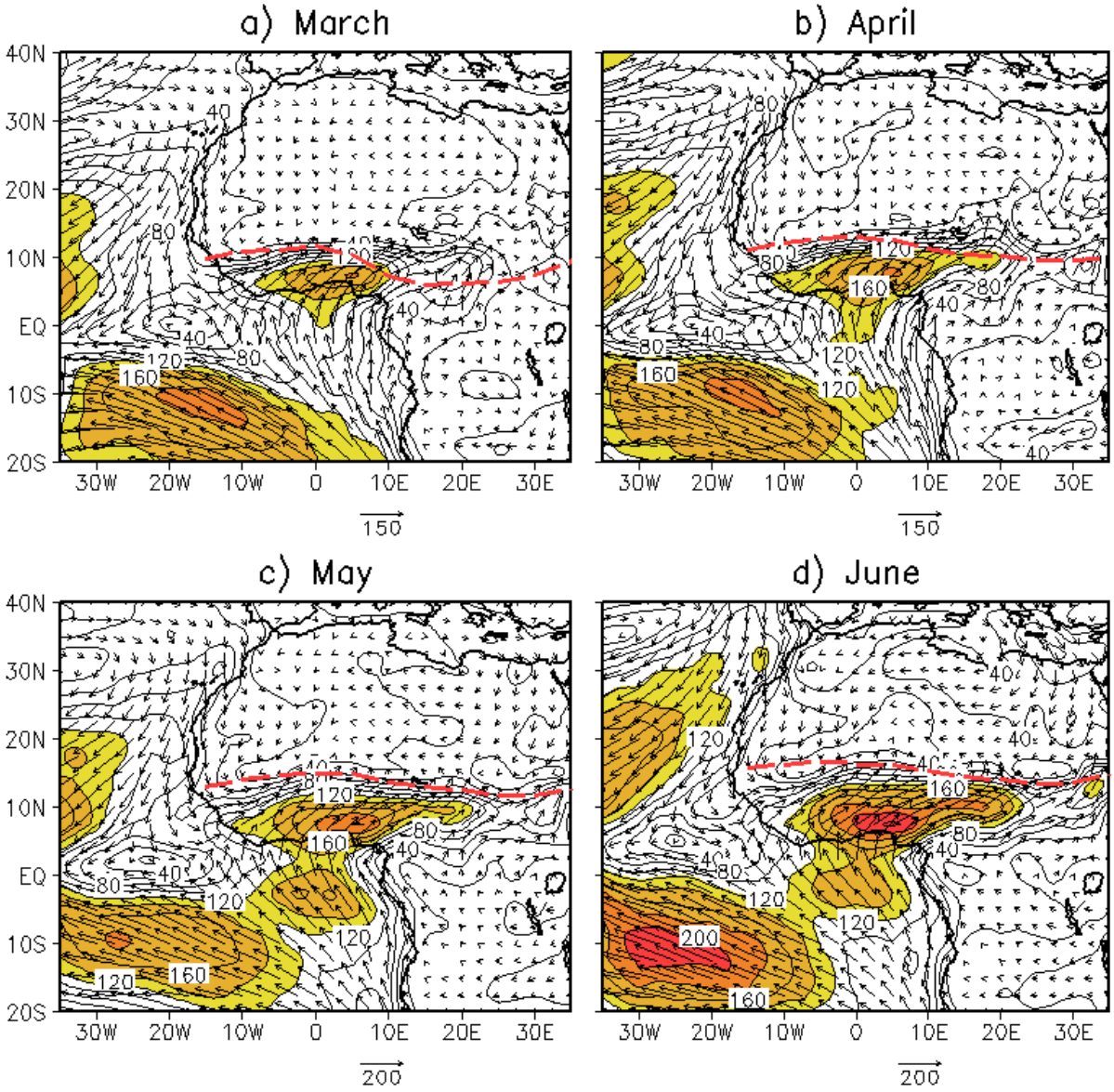

Figure 3.4: Mean surface-850 hPa seasonal distribution of vertically integrated mean moisture flux (vectors, kg m^{-1} s^{-1}) over WAM region, overlaid by moisture flux magnitude (contour) in (a) April, (b) May, (c) May and (d) June averaged from 1960 to 2010. The unit vector is displaced at the bottom of each graph and the contour interval for flux magnitude is 20 kg m^{-1} s^{-1}. Value of moisture flux magnitude ≥ 100 kg m^{-1} s^{-1} is shaded. Heavy dashed line indicates the ITF latitude defines as the 15°C dew point temperature.

Another notable feature in March-April is the prominent east-west inter-hemispheric northeastward moisture transport off the west coast of WA between 20^{o}N and 30^{o}N. Although this zone of moisture transport has a weaker flow pattern at this period of time, it however merges with the cross-equatorial southwesterly flow south of the ITF, in the region centered between the equator - 5^{o}N and 10^{o}W over the coast of Liberia and Sierra Leon. This inter-hemispheric moisture transport increases considerably in April (Fig. 3.4b), and feeds into the dramatic rise in zonal moisture flux over the Guinea coast region as the ITF slightly moves northward. Meanwhile, neither the cross-equatorial southwesterly monsoon flow nor the northwesterly monsoonal flow affects the northern region of WA (i.e., north of 10^{o}N), instead northeasterly trade winds emanating from the Libyan anticyclone essentially dominate over this period.

The most salient features in May and June (Fig. 3.4c, and 3.4d) are the sudden northward latitude shift of the ITF from its position around 12^{o}N in April to 15^{o}N in May then, to 18^{o}N in June and the associated, enhanced southerly and westerly monsoon flows. Two branches of moisture fluxes transport from the Atlantic Ocean bring needed moisture for rainfall over the Sudan, a region extending from ~7.5^{o}N to 12^{o}N. The first branch is the cross-equatorial southwesterly moisture transport belt previously described but, has now a well demarcated region of strong flow that can be referred to as a "Moisture River" and feeds the WA. This strong flow originates from the equatorial south Atlantic in the southern hemisphere, moves across the equator along the Gulf region, down to the Guinea coast, and supplies moisture to south Sub-Sahara and extending eastward to central African regions. The enhanced southwesterly

transport is associated to both the strengthening and poleward shift of the St. Helena high pressure circulation system, and to the rainfall pick observed during the high-sun rainy season in June over the Sudan region (Fig. 3.2d). In June, the moisture river becomes stronger and thereby increases the moisture build-up along the Guinea coast where the transport exceeds 200 kg m^{-1} s^{-1}. This strengthening of the southerly flux south of the Equator during April- June and its associated moisture build-up over the Gulf of Guinea, have previously been documented (e.g., Omotosho 1990; Omotosho et al. 2000; Thorncroft et al. 2011), and suggested to be linked to the development of a cold-tongue over the tropical Atlantic Ocean.

A northwestern branch of moisture flux originates from the northeast Atlantic, turns eastward and form jet-like structure to supply moisture to the coast of Guinea Bissau, Guinea, Liberia, and Sierra Leon. This westerly moisture transport could have been linked to the low-level westerly jet over the Atlantic, describe by Grodsky et al. (2003). The authors argued that it appears as a near-surface wind maximum at over the equatorial Atlantic and is evident from May through September. The jet was recently termed the West African Westerly Jet (WAWJ) by Pu and Cook (2012) who suggested that it is most developed around 10^{o}N in June (e.g., Fig. 3.4d) and lies in the region where trade winds converge, and appears to be the surface manifestation of the mid-tropospheric westerly wind maximum. Pu and Cook (2012) have also linked the interannual variability of WAWJ to rainfall over the Sahelian region.

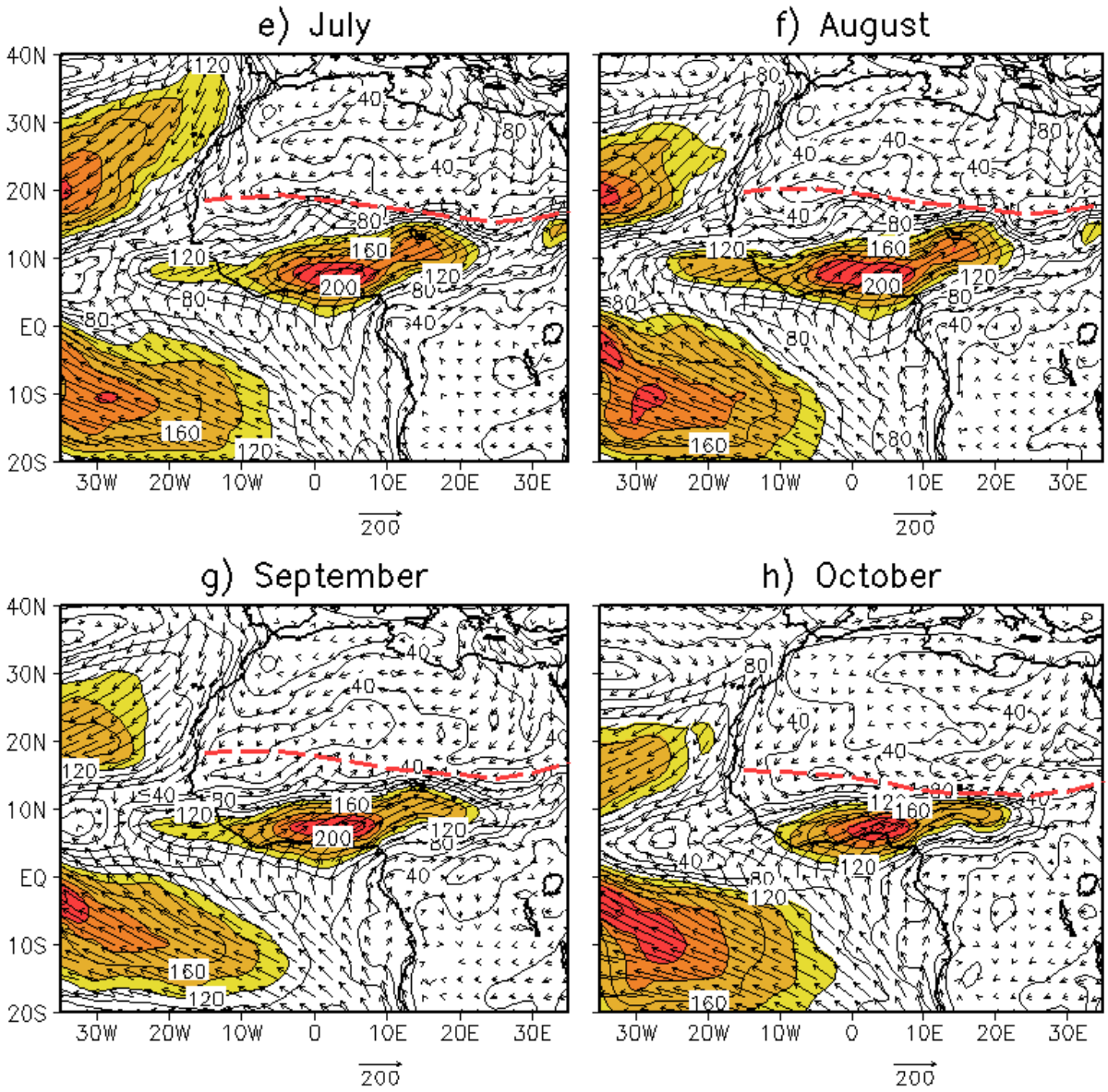

Figure 3.5: Same as Fig. 3.4, but for (e) July, (f) August, (g) September, and (h) October.

As the monsoon extends into July, August, and September months (Figs. 3.5e-g), and the gradually shifting northward, the southwesterly transport in the South Atlantic Ocean progressively weaken but becomes more extensive. The center of moisture flux maximum initially centered inland over the immediate coast of the Gulf of Guinea between 5-12.5^{o}N and 10^{o}W-10^{o}E undergoes a considerable intensification and extend north, east, and westward to influence the Sahelian and central African regions. The westerly flux transport over the west coast also increases in July-August due to an enhanced WAWJ. Both the expansion of the southerly moisture flux maxima and the enhanced of the westerly transport bring moisture onto the central Sahelian region during the peak monsoon season in July-September with magnitude over 160 kg m^{-1} s^{-1} (Figs. 3.5e-g). September constitute a transition period with marked southward shift of the ITF. Southerly and westerly transport progressively weakens and becomes less extensive, which indicates that the moisture transport commences its seasonal withdrawal process from the Sahelian region. In October both the monsoon southwesterly and westerly VIMT retreat more southward. The pattern for October resembles the pre-monsoon month (March), in terms of vector moisture transport, although moisture magnitudes are over 40 kg m^{-1} s^{-1} higher in the Guinea coast (Fig. 3.5h). This is the final phase of the WAM which, is also characterized by the equatorward withdrawal of the ITF and the reestablishment of the prevailing ground level stream of dry, hot, and dust laden northeasterly winds which is part of the continental trade wind system over WA.

3.4.2 Annual Cycle of Moisture Flux Convergence

Figure 3.6 shows a Hovmöeller diagram of the annual cycle of the pentad mean moisture flux convergence averaged over 10^{o}W-10^{o}E. Also shown is the latitude position of the ITF. The figure demonstrates that the convergence of water vapor over WA undergoes a relatively small meridional variation with a sudden northward movement and a notable increase during the boreal spring. From March to October there are two regions of moisture convergence located respectively over the Guinean coast and the Sahelian zone. Convergence of water vapor generally prevails north of the Equator and the center of the maximum flux convergence is located south of the ITF latitude. This is consistent with the observation that appreciable rainfall over WA generally occurs more than 400 km south of the ITF (Hastenrath 1991, pp 169; Lélé and Lamb 2010). In the period from March to May the peak of moisture convergence is over 8 mm day^{-1} over the Gulf of Guinea region (5^{o}-10^{o}N), but only 0-2 mm day^{-1} over the Sahelian zone. Hence, this amount of the vertically integrated moisture flux convergence in the Guinean region is sufficient to support the first rainfall season there.

Moisture flux convergence progressively migrates northward between June and August and reaches its maximum latitude extent around 20^{o}N in August, as does the ITF position during the same period. Moisture flux convergence is about 4-8 mm day^{-1} in the Sahel, and these values agree with the observed rainfall amounts over the Sahelian zone. In September, convergence gradually weakens and retreats southward in

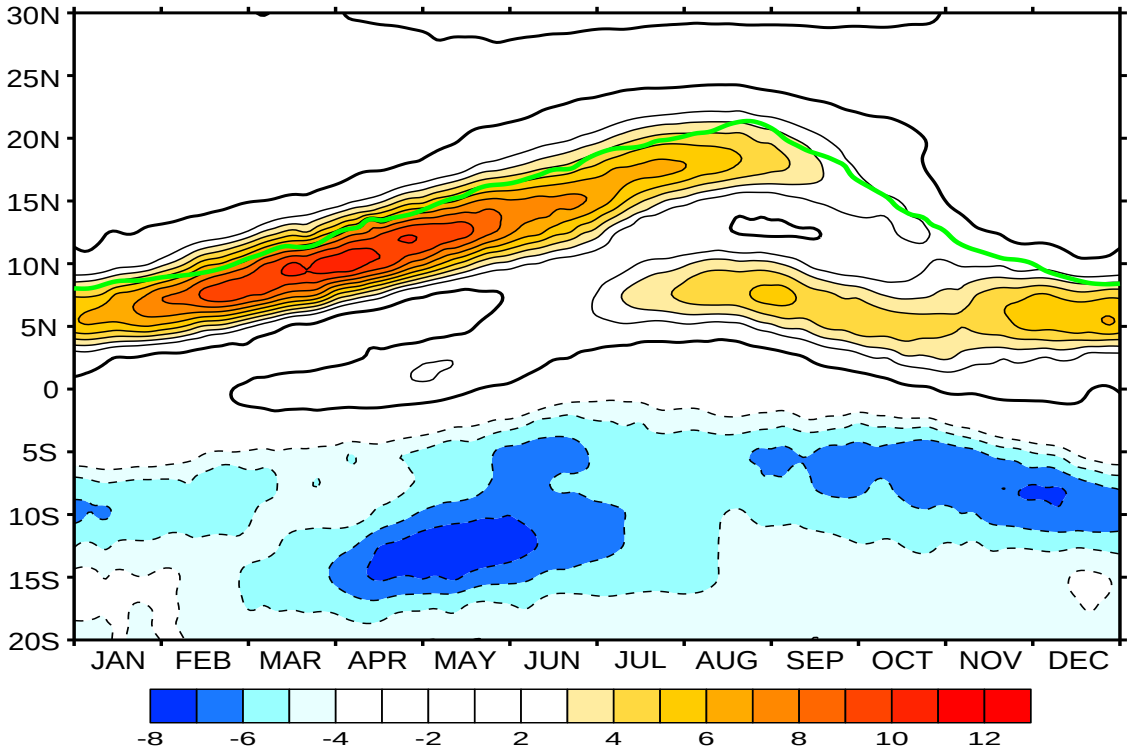

Figure 3.6: Hovmöeller diagrams of pentad mean annual cycles of total moisture flux convergence averaged over 10°W-10°E in mm day^{-1}. The latitude position of the ITF from 15° dew point temperature (green line) is superimposed. The contour/shading interval is ±1 mm day^{-1}.

parallel with the ITF retreat. The latitudinal belt of the migrating moisture flux convergence maximum is always between the Equator and 20°N, as shown in Fig. 3.6. Interestingly, the center of the observed maximum rainfall band, for each month of the monsoon seasons (Figs. 3.2a-h, and Fig. 3.3), is nearly co-located with the center of moisture convergence zone. This is an indication that the vertically integrated moisture flux convergence is one of the largest contributors to WAM seasonal precipitation.

Local evaporation resulting from the interaction between local groundwater and climate constitutes the second largest contributor to precipitation in WA, as suggested in other studies (e.g., Druyan and Koster 1989; Gong and Eltahir 1996). It is also evident from Figs. 3.4 and 3.6 that enhanced moisture buildup and strong moisture flux convergence over WA occurs during the April-June spring season rather than during the peak summer monsoon season in July-September, suggesting that the moistening of the atmospheric column in WA occurs during the pre-monsoon season.

Another latitudinal band of moisture flux convergence exists over the Guinea coast around 10^{o}N. Although relatively weaker than the first band of convergence zone, it prevails however from late July to December and peaks around 2.5^{o}N in late August early September. The peak of the secondary zone of moisture convergence is roughly coincident with the time that rainfall starts to decrease over the Sahelian zone and increases over the Guinea coast. It therefore constitutes the main contributor to the second rainfall season observed over the Guinea coast (Fig. 3.2e-h).

The observed convergence zones over land are accompanied by a large zone of moisture flux divergence over the equatorial South Atlantic Ocean. The seasonal cycle of the flux divergence over the Ocean matches that of the flux convergence over land. It has two centers of maximum flux divergent, one in April-June and centered below the first maximum flux convergence zone observed inland, and a second that occurs from the beginning of September, extending to late winter, and located below the secondary inland convergence zone. The two centers were separated by a period of weak flux

divergence between July-August, coincident with the rainfall peak over the Sahelian region. This juxtaposition of flux divergence over the Ocean and convergence inland suggests that the summer moisture transport over WA is partially regulated by an enhanced evaporation over the tropical Atlantic Ocean, thereby confirming the Atlantic Ocean as the main source of water vapor suppliers to the WAM (Lamb 1983b; Cadet and Nnoli 1987; Fontaine et al. 2003; Thorncroft et al. 2011), and that the transport is essentially poleward.

3.5 Northward Flux of Moisture Transport into West Africa and Associated Circulations

Characterization of flow associated with enhanced northward moisture flux into WA is important in understanding the seasonal cycle of rainfall associated to WAM variability. To evaluate the temporal and spatial evolution of circulation and precipitation associated with moisture surges, composites based on the meridional component of moisture flux ($q\nu$) were formed. The first composite consists of the flow during periods when the moisture flux across the southern border of the Guinean coast (5^oN, 15^oW-15^oE) in April to June exceed one standard deviation ($q\nu_{850} > 1\sigma$) of the long-term meridional moisture transport climatology. This composite of moisture transport is particularly important to rainfall occurrences over the Guinea coast in the early stages of the monsoon season. The second composite is similar to the first but, consists of fluxes crossing the southern border of the Sahelian zone (10^oN, 15^oW-15^oE) in July to September. These two boundaries of moisture flux are close to the regions of

interest, that is, the Gulf of Guinea region which experiences a bimodal rainfall season, and the Sahelian region which experience a single rainfall peak.

The robustness of our composite is tested at each grid point using the student *t*-test to see whether the composite anomaly fields are significantly different from zero (e.g., Wu et al. 2009). But for the wind field, the vectors winds are plotted if any of the components is significant at the 5% level of the student *t*-test. As in Janicot et al. (2011), daily outgoing longwave radiation (OLR) was used as a proxy for tropical convection, with low OLR values representing cold cloud tops associated with deep convective activity and high precipitation in the tropics.

3.5.1 Moisture Transport and Hydrological Cycle

Figure 3.7a and 3.7b show the temporal and spatial northward migration of the vertically integrated moisture Transport (VIMT; vectors) over WA and associated rainfall pattern (shading) during April-May-June (AMJ) and July-August-September (JAS) respectively. The enhanced moisture flux into the region is clearly associated with a low-level southwesterly circulation flow and a large region of enhanced precipitation across the coastal areas in the spring season and further inland in the summer season. Northward moisture flux originates from the eastern Atlantic and penetrates through the location of the rain-band. The largest southerly moisture transport magnitude occurs in AMJ season rather than JAS, which is consistent with discussions in section 3.4 (Fig. 3.4c, d). This suggests that moistening of WA occurs

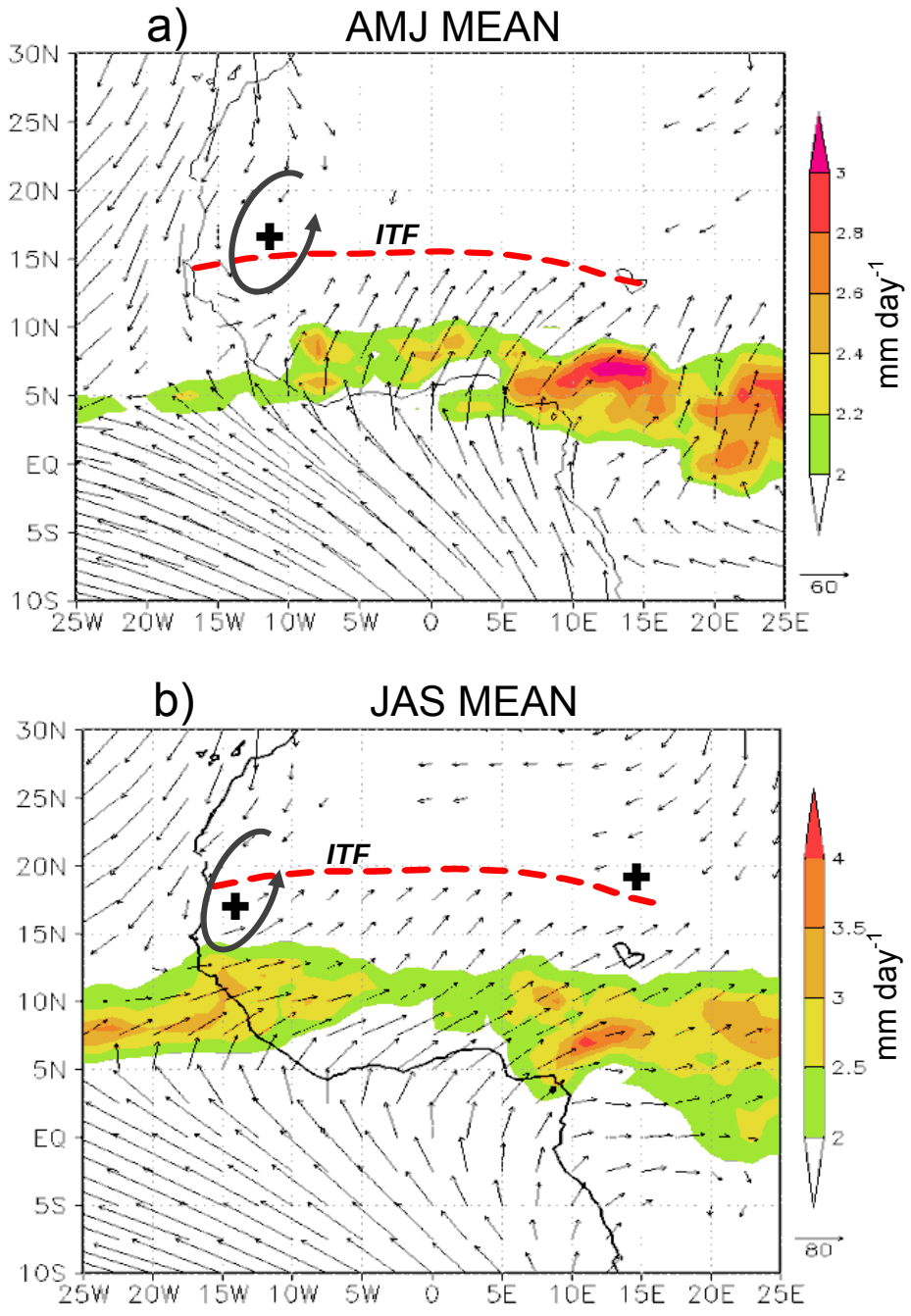

Figure 3.7: Composites based on qv_{850} >1σ across (a) 5°N for AMJ, and (b) across 10°N for JAS and 15°W-15°E. Shading is the GPCP precipitation climatology with plotting interval of 0.2 mm day^{-1} for (a) and 0.5 mm day^{-1} for (b). The unit moisture transport is kg m^{-1} s^{-1}. Only 5% significant levels using the Student *t*-test are plotted for both precipitation and moisture vectors. Red dash lines are the 15°C isodrosotherm indicating the ITF seasonal mean latitude position.

during the spring season prior to the Sudan-Sahel rainfall onset. Omotosho (1990) and Omotosho et al. (2007) also found a very high correlation between the boundary layer moisture anomalies from April to June and annual rainfall over Kano and argued that a necessary condition for abundant Sahelian rainfall in any year is a pre-rainy season (April-May) moisture build-up. When the monsoon rainfall starts in the Sahelian region, rainfall over the Gulf of Guinea and the south coast diminishes.

The mean composite of moisture transport over the Guinean region exhibits a strong southwesterly branch of moisture inflow during the AMJ season (Fig. 3.7a). This southwesterly monsoon flow is regulated by the semi-permanent high pressure system over the South Atlantic which has intensified and moved equatoward from its JFM position allowing the southwesterly flows to become stronger and penetrate inland to the Guinea coast (Fig. 3.1b). These southwesterly winds carry sufficient amount of moisture to sustain rainfall over the region. Along the west coast between 10^{o} and 30^{o}N, a northeasterly flux transports moisture off the coast, some of which is redirected onto the Guinean territory under the influence of a cyclonic circulation centered inland at about 15^{o}N-12.5^{o}W. AMJ seasonal rainfall cycle over WA is therefore accompanied by a boundary layer southerly flow across the coast of Guinea and the northern limit of this flux coincides with the mean latitude position of the ITF.

During JAS, the extent of the moisture inflow moved northward together with the rain-band (Fig.3.7b). This northward shift of rain producing system from the Guinea coast to the Sahelian region is associated to the northward migration of the high

pressure system and the development of a cold tongue in the Atlantic (Fig. 3.1c). Note that the isobar 1014 hPa, initially located along10^{o}S between 10^{o}W-0^{o} in AMJ, has moved northward and is now located just south off the coast of Africa in JAS. This results in the development of the cold tongue which becomes colder during the season. It then contributes to the enhancement of the southerly flow across the Guinea coast which eventually reached the Sahelian region.

Over the west coast, a branch of westerly transport by the mean flow develops and is enhanced during JAS. This eastward moisture transport is regulated by the WAWJ and by the enhanced westerly moisture flux located between 15^{o} and 25^{o}W over the eastern Atlantic Ocean. The cyclonic cell previously centered at 15^{o}N-12.5^{o}W, moves northwestward and is located at 18^{o}N – 15^{o}W, allowing the northeasterly flux to be redirected into the Sahelian region. Over the northwest, the low-level moisture transport into the Sahelian region is rather weak, and consists of a southward transport from the Mediterranean Sea. This source of moisture has been subject of a recent investigation by Fontaine et al. (2003) who suggested that, in addition to the Gulf of Guinea, the low-level moisture into the Sahelian region originates from the Mediterranean Sea.

3.5.2 Interannual Variability of Moisture Transport into West Africa

3.5.2.1 Case Studies of Two Contrasting Years

The infamous 1984 drought year and the 1988 wet year (which is the first wet year after the 1984 drought) are selected to examine the relationship between moisture transport and convection in individual extreme years. Also utilized is the outgoing longwave radiation (OLR), considered as an index of tropical convective activity. The use of OLR is motivated by the fact that it is controlled not only by the temperature of the earth, but likewise by the presence of water vapor in the atmosphere and cloud cover as well. OLR therefore reveals some information on the temperature, humidity, and cloudiness of the atmosphere. In the tropics, low values of OLR are symptomatic of a large amount of seasonal or recurrent cold clouds (i.e., thunderstorm anvils), and high OLR values imply a lack of atmospheric water vapor. The July-August seasonal average for VIMT and OLR anomalies for the 1984 (dry) and 1988 (wet) are displayed in Figures 3.8a, and 3.8b, respectively. It is apparent for both years that the areas of enhanced convective activities coincide with the regions of strong moisture transport convergence.

During the 1984 drought season (Fig.3.8a), large decreases in moisture content between the surface and 850 hPa are associated primarily with a weak southwesterly monsoon flow, a much further southward extent of moisture depth across WA, and a much further southward ITF latitude position compared to its long-term average latitude position.

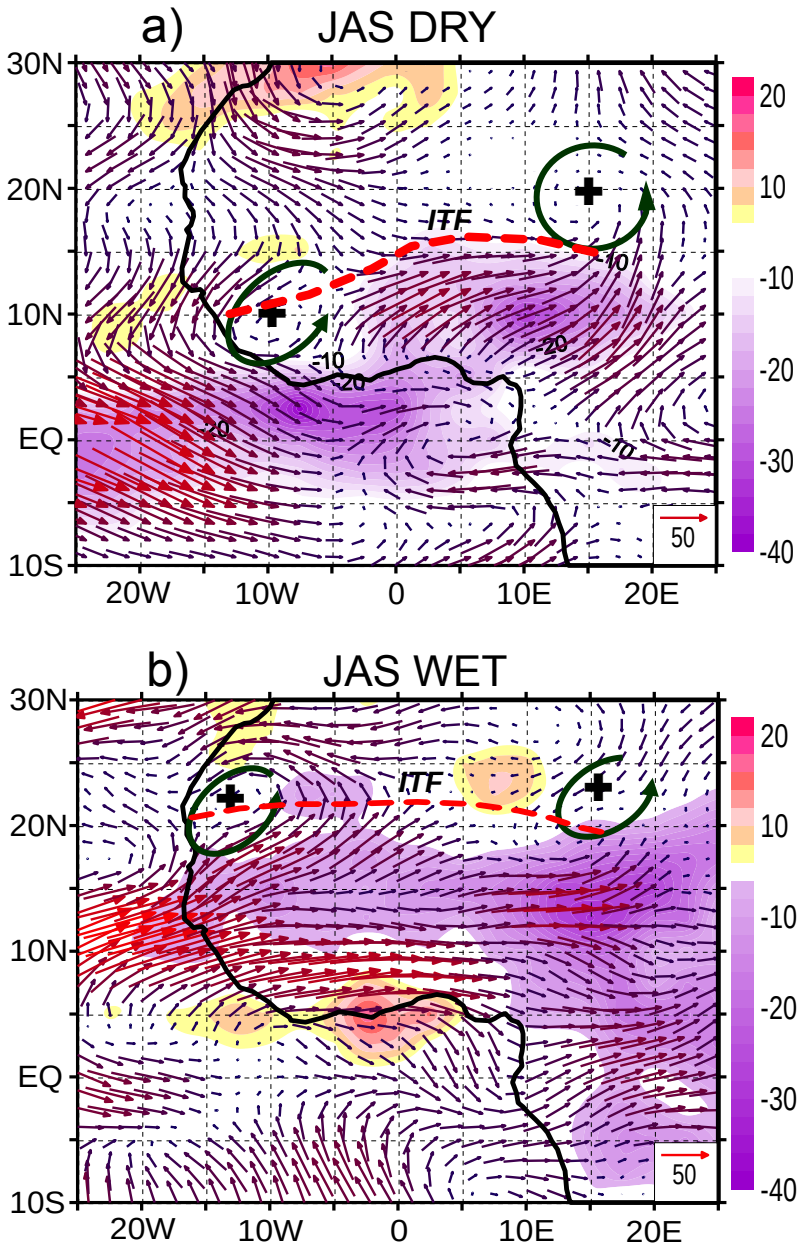

Figure 3.8: July-September moisture transport (vectors, kg m^{-1} s^{-1}) and NOAA OLR anomalies (shading, W m^{-2}) during contrasting years. (a) Infamous 1984 drought year and (b) 1988 wet year. Fluxes less than 1 kg m^{-1} s^{-1} are omitted. OLR anomaly is used as a proxy for deep convection, where negative (positive) values denote regions of enhanced (suppression) of convection. Red dash lines are the 15°C isodrosotherms indicating the ITF seasonal mean latitude position.

Significant convective activity occurred during that year but, the areas of occurrence of this convection are away from the Sahel zone and are located over the Gulf of Guinean. Two centers of deep convection are noted, one inland over the southwestern part of the Guinea region and another over the Atlantic Ocean. The cyclonic cell along the western coast, climatologically centered at 18^{o}N-15^{o}W (Fig. 3.7b), has shifted southward and is located at 10^{o}N-10^{o}W thereby suppressing the westerly moisture transport into the Sahel. As a consequence, a widespread and severe drought occurred across Sub-Saharan region and caused large-scale water and food deficits, famine, human fatalities, and mega economic problems and the exodus of people and animals.

In the 1988 wet season, the transport of moisture flux extends further north, due to the strengthening of the westerly and southwesterly inflow. The ITF migrates northward and reaches its northernmost latitude position. The cyclonic cell along the western coast also migrates northwestward and centered at 22^{o}N-12.5^{o}W. The WAWJ becomes stronger and extend from the eastern Atlantic to the west coast of Africa. Consequently, the zone of moisture convergence and the areas of convective activity migrate further northward and are centered over the Sahelian region (Fig. 3.8b). A widespread and abundant monsoon rainfall then occurs over the Sahel while, at the same time, a relatively dry condition is observed over the Guinean coast.

The widespread of convective activity over the Sahelian zone during wet years, and their suppression during dry years, suggests that large-scale moisture flux transport (moisture convergence) is the source of water vapor needed to support enhanced

precipitation. The weakening of the meridional flux circulation during the dry year and its strengthening during the wet year suggests that the seasonal characteristics of the low level westerly flow across the equator into the Northern Hemisphere are very important in determining the behavior of the monsoon precipitation over WA (e.g., Kidson 1977; Newell and Kidson 1984; Fontain and Janicot 1992; Long et al. 2000).

3.5.2.2 Ocean-to-Land Moisture Transport Variations During Dry and Wet Years

This section examines the importance of ocean-to-land moisture transport and the seasonal time-scale of the zonal and meridional components of the transport across WAM borders for four very wet years (1988, 1994, 1998, and 1999) and four very dry years (1982, 1983, 1984, and 1987). The selection of wet and dry years are based exclusively on the Lamb index time series (Fig. 1.1) where these years appear as pronounced wet and dry years. The selected years include the driest years (1983, 1984) and the wettest years (1994, 1999) since 1983-84 experiencing the most devastating drought, while flooding occurred during 1994 and 1999 all across the Sudan-Sahel region (Tarhule, 2005). Although the computation of Lamb index only involves stations north of 11^{o} for April-October, it does give an overall June-September area-average rainfall character of the entire WAM region. Table 3.1 quantifies the rainfall departures for those years.

Table 3.1 Documentation of extreme seasons used in composite (Fig. 3.9) analyses. West African mean April–October departures (from Fig. 1.1) are relative to 1941–2000 averages. Seasons shown were driest/wettest in the study region during 1960–2008.

	Dry seasons		Wet seasons	
	Years	West African Apr–Oct rainfall departure in Fig. 1.1 (σ)	Years	West African Apr–Oct rainfall departure in Fig. 1.1 (σ)
Most extreme	1983	-1.26	1999	+0.70
↓	1984	-1.25	1994	+0.32
	1987	-0.89	1998	+0.26
Less extreme	1982	-0.82	1988	+0.11

The meridional component of moisture transport is evaluated along the southern lateral boundary of the Guinea region (5^oN) and southern lateral boundary of the Sahelian zone (10^oN), and along the northern lateral boundary of the Sahel (20^oN), while its zonal component is evaluated along the western (15^oW) and easterly (15^oE) lateral boundaries of the whole region. These boundaries were chosen according to WA climatic airflow pattern shown earlier in this chapter. They were designed to account, as much as possible, for the impact of moisture influxes from the two main moisture sources onto the Sudan-Sahel zone. Figure 3.9 displays the seasonal average inflow of moisture into WA along the lateral boundaries of the Guinean and Sahelian regions, for the two composites of wet and dry years. Each bar indicates the magnitude and direction of water vapor flux at region boundaries at each 2.5^o latitude and longitude.

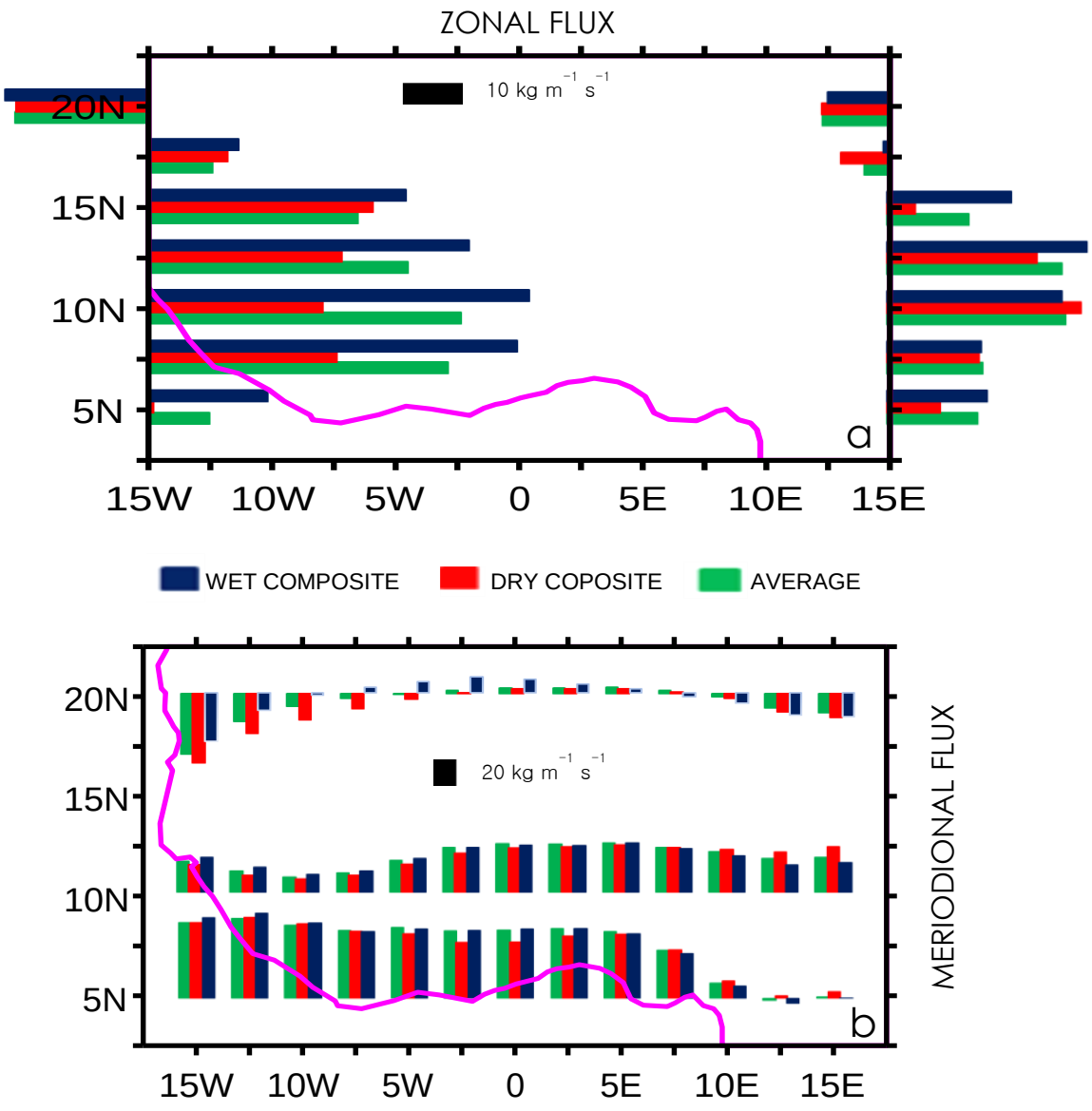

Figure 3.9: June-September (JAS) vertically integrated moisture fluxes cross the lateral boundaries for a sets of wet years (blue bars), dry years (red bars) and the 1960-2008 long term average (green bars). (a) Zonal moisture transport cross 15°W and 15°E. (b) Meridional moisture transport cross 5°N, 10°N, and 20°N. The bars indicate the magnitude in unit of kg m^{-1} s^{-1} and direction of water vapor flux at region boundaries.

The inflow and outflow generally reflect the anomalies shown in Fig. 3.8. During the Sahelian wet conditions in July-August-September (blue bars), both the zonal (Fig. 3.9a) and meridional (Fig. 3.9b) components of moisture transport show anomalous inflow from the southern and western boundaries, and outflow across the eastern and northern boundaries. In comparison to the long-term average inflow and outflow (green bars), the inflow magnitudes during wet periods are much stronger especially for the zonal component (Fig. 3.9a). The southern boundaries show relatively strong inflow compare to the long-term average, but weaker than the western inflow. The southerly flux sustained from the Guinean boundary to the Sahelian boundary with a slightly decreasing intensity as one goes north regardless of the season. The eastern boundary shows relatively weak outflow compare to average during the wet periods, while that of the northern boundary is negligible. During dry years, the western and southern boundaries show relatively weak fluxes compare to average. The western boundary, however, shows a relatively large outflow which is of almost the same order of magnitude as the climatological outflow.

The differences in moisture transport crossing the lateral boundaries (Figs 3.9a, b) reflect the differences in the patterns described in section 3.5.2a for contrasting individual years. It supports the argument that the Atlantic Ocean is the major source of moisture for WAM, and shows that during extremely wet monsoon season, the zonal moisture transport crossing the western boundary of West African domain is larger than the meridional moisture transport crossing it southern boundary. However, the zonal

and meridional outflow is always a magnitude smaller than the stronger inflow of the zonal and meridional moisture flux components, regardless of the season.

The analysis also shows that the summer moisture transport over WA is regulated by two meridional low-level jets from the South Atlantic and from the Mediterranean Sea, and one zonal jet from the eastern Atlantic. The major branch of transport during near-normal monsoon years is carried by the anomalous southeasterly flow at 10^{o}E-10^{o}W from the tropical Atlantic to the Gulf of Guinea and then is transported from the Gulf of Guinea to the West African landmass. The path turns southwesterly under the influence of the Coriolis Effect and the jet brings moisture to the Sahelian region. Over the northwest, the moisture comes from the Mediterranean but that branch is weak. Both jets can be represented by the meridional component of the VIMT. During wet years however, the major branch of transport is carried by the WAWJ directly from the eastern Atlantic onto the continent. The WAWJ can be represented by the zonal component of the moisture flux (e.g., Gu and Adler 2004; Pu and Cook 2010).

3.5.3 Relationship Between Moisture Transport and Sahelian Precipitation

To investigate the strength of the relationship between moisture transport and Sahelian rainfall, a moisture transport index is defined as area average of zonal and the meridional moisture transport along lateral boundaries defined in section 3.5.2b. As previously stated, these boundaries were chosen to capture the maximum moisture

inflow into the region. There were also characterized by low level wind fluctuations tied to changing in large-scale circulation. Lag correlations were calculated between the zonal and meridional components of moisture transport index and precipitation over the Sahel (Fig. 3.10).

Figure 3.10a and 3.10b display the lagged correlations between the GPCP pentad precipitation and the zonal and meridional component of the moisture flux respectively. Only correlation coefficients exceeding the 95% confidence interval are displayed. In general, significant positive correlations extend across the Sahel but they are considerably lower at zero lead time, and continue to be stronger as the lead time increases. For example, when the zonal moisture transport leads by one to four pentads, significant positive correlations extend across the Sahel region, suggesting that the zonal component of moisture transport has a significant control on rainfall. Significant correlations coefficients also are depicted between the GPCP precipitation and the meridional component of the moisture transport. However, these correlation coefficients appear to be significant only from lag 3 and lag 4, and they are not as strong as the correlation coefficients between the zonal moisture transport and rainfall counterpart. These two correlation patterns between components of moisture transport and rainfall over the Sahelian zone suggests that more so than the southwesterly moisture transport from the Gulf of Guinea, the zonal transport of moisture from the eastern Atlantic during July-August-September monsoon season is the major contributor to the July-August-September Sahelian rainfall variability, in agreement to the weakening of the southwesterly flow mentioned in section 3.4.1 (Fig.3.5).

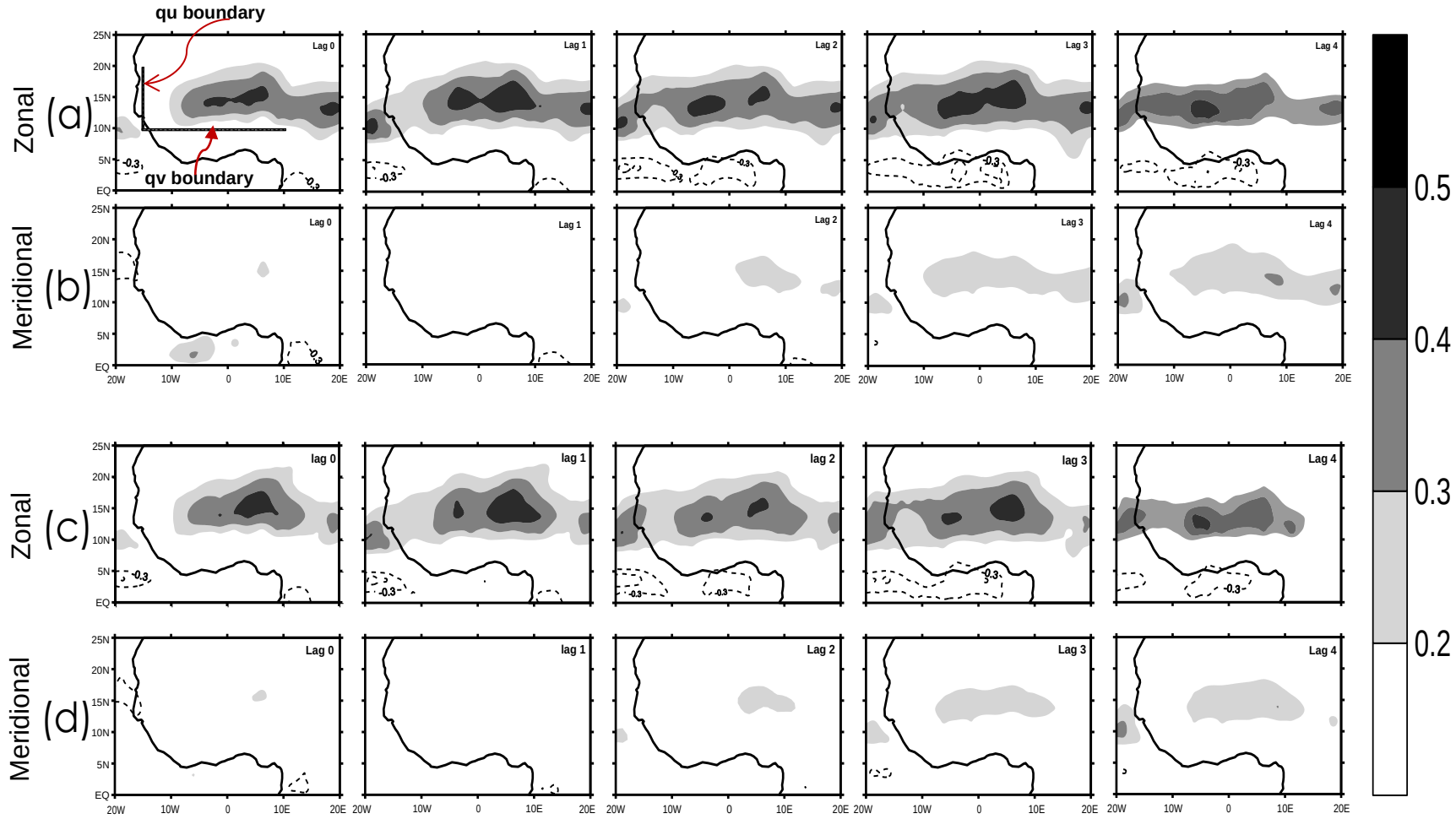

Figure 3.10: Lag (in pentad) correlations between (a) the zonal and (b) the meridional components of moisture flux and the GPCP precipitation for 1979-2008 periods. Shading denotes positive correlations while dash contours denote negative correlations. Only positive correlation coefficients exceeding the 95% confidence levels are shown. (c), and (d) Similar to (a) and (b) respectively but, the correlations were with the CMAP precipitation. The thick lines in the first map in (a) are the boundaries used to construct moisture flux time series.

A similar correlation analysis is performed using the components of moisture transport time series at the western and southern boundaries of Sahelian zone and CMAP precipitation (Figs 3.10c, d). Remarkably, similar correlations patterns as those where the GPCP precipitation was used emerge indicating that the relationship between moisture transport anomalies and Sahelian rainfall is robust and consistent across the data used. Although the simultaneous correlation between the zonal component of moisture transport and precipitation (lag 0) is positive, it is weak and localized compared with the other lag correlations. This suggests that the precipitation occurrences over the Sahelian region lag the moisture inflow into the region, which is in agreement to the fact that most of the moistening of the atmospheric column over WA occurs during the pre-monsoon season. The extent and magnitude of the correlation between Sahelian precipitation, and the zonal component of moisture transport for other lags, supports our previous claim that the eastern Atlantic Ocean is a valuable source of moisture for the Sahelian region. This source of moisture for the Sahelian region is also noted by Cadet and Nnoli (1987), and more recently by Long et al. (2000), who found that the westerly flow dominates water vapor transport patterns over Sub-Saharan Africa.

Chapter 4

4. Scale Decomposition and the Intraseasonal Variability of Tropical Atlantic Moisture Transport Associated with West African Monsoon Rainfall Variability

4.1 Background

Understanding the mechanisms and associated predictability of seasonal-scale rainfall variability over the WAM region requires accurate estimates of the various components of the hydrological cycle. In the previous chapter, it is proven that the WAM is characterized by a seasonal reversal of the prevailing lower tropospheric wind, which in the boreal summer has a southwesterly (onshore) orientation. The resulting transport of moist air across the Gulf of Guinea coast helps initiate and sustain deep convection over the region between June and September. It is likewise also shown that the interannual variation of boreal rainfall in the West African Sudan-Sahel region is reflected in the movement of the ITF which, in turn, is associated with low-level moisture transport from the tropical Atlantic. Moisture flux variations over WA and their associated precipitation are particularly important for the population of the region due to their impact on socio-economic activities (e.g., agriculture, health, transport). For example, the semi-arid region of WA is particularly sensitive to the intraseasonal variation in the monsoon system, because it is only during one part of the year (June-

September) that the ITF extends far enough north for this region to experience its short, single rainfall season. Despite advances in our understanding of the physical processes and predictability of monsoon systems, and despite the increased capabilities of high-resolution global modeling, the accuracy of intraseasonal-to-decadal climate predictions over WAM region remains limited.

Although numerical weather forecasting has improved tremendously in recent years, we must recognize the limits of deterministic weather forecasting -- about 2 weeks. This is of limited help for people of regions where the economies are very sensitive to any deficit or abundance of the total summer rainfall. Consequently, longer timescale (seasonal-to-decadal) prediction models have been developed and used experimentally during the last few decades. Lamb (1978a, b) demonstrating the dependence of Sahelian rainfall on SST anomalies in the tropical Atlantic, allowed for the development of statistical models that used SST anomalies as predictors in a form of indices. These predictors averaged over selected domains or EOF time series have now been widely used for seasonal prediction and, in particular, at the African Center of Meteorological Application for Development (ACMAD), to make probabilistic seasonal forecasts of July-September monsoon rainfall patterns over Africa. Although these seasonal rainfall predictions have contributed to the early warning system over Sahelian countries, the skill of the SST-based statistical models remains poor over the WAM region, suggesting that only a fraction of WAM rainfall variability is explained by the SST anomalies. Because the lead time for accurate deterministic forecasts varies from a few days to less than a week, and that of climate prediction is typically seasonal, yearly,

or at much longer timescales, it is now becoming important to address prediction at the 10-90 day timescale to bridge the gap between weather forecasts and climate prediction. Understanding the existence of atmosphere-ocean phenomena within these timescales, and how they influence rainfall predictability over a given region, is vital for skillful intraseasonal prediction.

The understanding of multiscale regional climate variations, and the extraction of subregional dominant modes of circulations and associated links to particular climate modes, is an essential step in improving seasonal rainfall prediction, especially during drought and wet seasons. This chapter focuses on the role of the large-scale anomalies in moisture transport variability over West Africa. The physical processes, intraseasonal interactions, and predictability associated with the 30-90 days mode of variability in moisture transport associated with convective activities is also described. Our goal is to understand how water vapor transport at this timescale (a typical MJO timescale) is related to the prediction of total seasonal rainfall variability. Moisture transport during active (wet spell) and break (dry spell) phases of monsoon rainfall events are described.

4.2 Scale Decomposition and Contributions of Synoptic and Climate Anomalies to Moisture Transport Variability over West Africa

4.2.1 Method for Scale Separation

The atmospheric moisture balance equation (Eq. (2.3)) implies that the changes in both evaporation and moisture transport can contribute to the variation of summer

monsoon precipitation. The scale analysis adopted in this study is based on methodology from Newman et al (2012), where moisture transport is partitioned into three terms:

$$X = \bar{X} + X^C + X^S \tag{4.1}$$

In Equation (4.1), the overbar indicates the seasonally varying climatological mean, the superscript C indicates the climatic-timescale or low-frequency anomalies, and S indicates the high frequency (synoptic-scale) anomalies. Application of (4.1) to the mean moisture transport equation yield:

$$\overline{\boldsymbol{Q}} = \overline{\boldsymbol{Q}}^m + \overline{\boldsymbol{Q}}^C + \overline{\boldsymbol{Q}}^S \tag{4.2}$$

Where

$$\overline{\boldsymbol{Q}}^m = \langle \overline{P_s \boldsymbol{V}\, q} \rangle \tag{4.2a}$$

$$\overline{\boldsymbol{Q}}^C \cong \langle \overline{P}_s \overline{\boldsymbol{V}^C q^C} \rangle \tag{4.2b}$$

$$\overline{\boldsymbol{Q}}^S \cong \langle \overline{P}_s \overline{\boldsymbol{V}^S q^S} \rangle \tag{4.2c}$$

and where P_s is the surface pressure, $\boldsymbol{V}$ is the horizontal wind vector, and q the specific humidity. Eq. (4.2a) represents the moisture transport by the mean flow, (4.2b) is the transport by climate-scale anomalies with a period greater than 10 days, and (4.2c) indicates the transport by synoptic-scale anomalies with period less than 10 days. The brackets in Eqs (4.2a-c) indicate the vertical integral in pressure coordinates.

Calculating each term of Eq. (4.2) permits the quantification of the contribution from the high and low frequency moisture flux variations that characterize the WAM. Our objective in this section is to highlight the importance of local evaporation and remote moisture transport in regulating the interannual variation of West African summer rainfall. The separation of moisture transport into scales <10 day (synoptic scales) to those >10 day (large scales) is well suited for the climate of the region. This is because the West African mesoscale convective systems, as well as the local circulation effects such as mountain circulation and or sea breezes, is manifested at synoptic scales, whereas circulations associated with the AEJ correspond to the large scale.

4.2.2 Time Series Analysis and Filtering

4.2.2.1 Wavelet Analysis

Wavelet analysis has attracted much attention in recent years and has been successfully applied in many applications such as transient signal analysis, image analysis, and other signal processing applications. They have also been used for numerous studies in geophysics (Torrence and Compo 1998), and they have become popular since they allow the decomposition of data into different frequencies or scale components. Each component can then be studied with a resolution that matches its scales. This makes the wavelet transform more efficient in isolating either the high or low frequency variations than the Fourier transforms although, the approach is similar to that of an adjustable window Fourier-type spectral analysis. The wavelet analysis methodology is described in Kaiser (1994) and the algorithm used in this study is the

continuous wavelet transform (Morlet wavelet), defined as Gaussian enveloped sine and cosine wave groups. The Morlet wavelet methodology is described in detail in Torrence and Compo (1998), and to some degree in Segele et al. (2009).

Wavelet analysis was applied in this study to characterize the temporal and spatial evolution of moisture transport associated with WAM rainfall patterns, and determine the optimal frequency bands to study the strength of the relationship. The time series were then bandpass filtered to isolate the high and low frequency transport.

The wavelet transform of a non-stationary climate data x_n, used to extract time and frequency domain information from x_n with a mother wavelet ψ, is a convolution integral given as:

$$W_n(s) = \sum_{n'}^{N-1} x_{n'}\, \psi^* \left[\frac{(n'-n)\delta t}{s}\right] \tag{4.3}$$

where ψ* is the complex conjugate of ψ, δt is the time spacing, n is the total length of the time series, s is the scale, and $W_n(s)$ is a wavelet spectrum, a matrix of energy coefficients of the decomposed time series. The advantage of using a complex wavelet is that it can present both the amplitude and phase to better capture the oscillatory behavior of a time series. One of the tools in characterizing the time series x_n in a time–frequency domain is the wavelet power spectrum $|W_n(s)|^2$ describes as the energy contained in the wavenumber bandwidth (e.g., Yang et al. 2007).

The global wavelet spectrum (Torrence and Compo 1998) can also be used in the characterization of x_n. It is simply the measure of the time-averaged wavelet spectrum over all local wavelet spectra and expressed by the equation below.

$$\overline{W}^2(s) = \frac{1}{N}\sum_{n=0}^{N-1}|W_n(s)|^2 \tag{4.4}$$

In this equation, *N* is the total number of the data points in the time domain that are involved in the wavelet spectrum. Based on the Monte Carlo realizations, the 5% significance level of the normalized global wavelet spectrum (normalization is done by the variance (σ^2) of the time series) against a certain mean background spectrum (white noise or red noise) can be empirically fitted by a chi-square curve $\chi^2_\nu/_\nu$, where the degree-of-freedom ν can be estimated through the relation:

$$\nu = \sqrt[2]{1 + \left(\frac{n_{a\delta t}}{\gamma_a}\right)^2} \tag{4.5}$$

4.2.2.2 Dominant Modes of Variability

In the frequency domain, the strong seasonal variability of West African summer precipitation documented in many studies (e.g., Nicholson 1980; Janowiak 1988; Janicot 1992a, b, Rodwell and Hoskins 1996) could be interpreted as an amplification of variability at seasonal scales during recent decades. Wavelet analysis was performed herein to characterize the evolutionary behavior of periodicity for the interval 1960-2008. Figure 4.1a, c shows the wavelet power spectrum for the moisture flux across the western (15^{o}W) and southern boundaries (10^{o}N) of the Sahelian region.

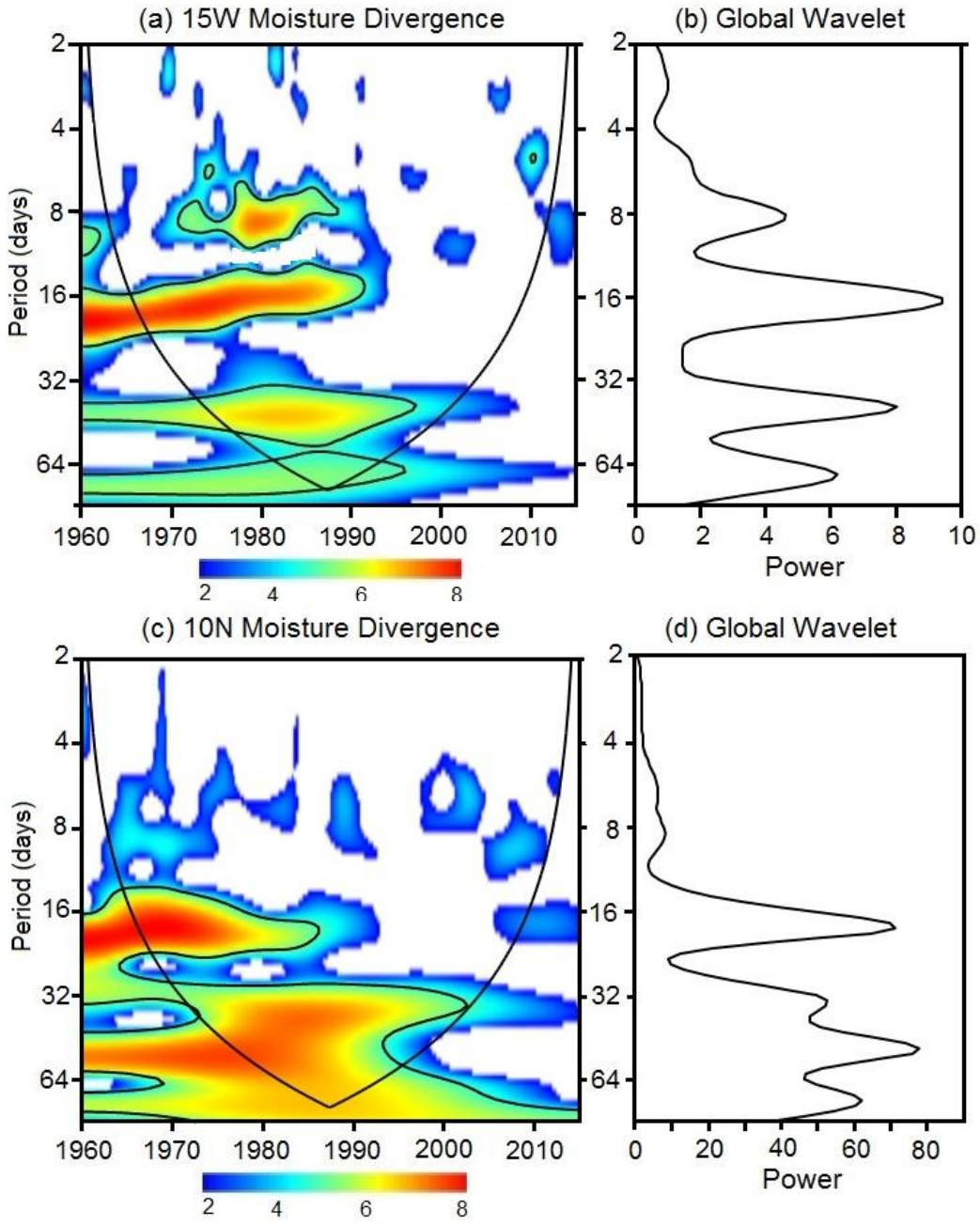

Figure 4.1: The local wavelet power spectrum (shaded, Units: mm^2 day^{-2}) of moisture flux divergence across the (a) western and (c) southern lateral boundaries of the Sahel during the 1960-2010 period using the "Morlet" wavelet. The areas below the thick solid curve indicate the "cone-of-influence", where edge effects become important. The thick black contours in the wavelet spectrum indicate that the power is statistically significant at the 95% confidence level using the white noise background spectrum. (b) and (d) are the global wavelet which is the time averaged wavelet spectrum over the local wavelet spectra.

The wavelet power spectra represents the changes of wavelet power in terms of scale with respect to time. The results show a rich spectrum of variability ranging from seasonal to sub-seasonal with substantial variability on synoptic, weekly, and monthly timescales. For example, in Fig. 4.1a, three significant spectral peaks for moisture divergence exist at the intraseasonal timescale. One spectral peak shows periods of enhanced subweekly (2-9 day) variability associated with AEW (Burpee 1975). Recent studies have also indicated the existence of periodicity between 6 and 9 days in the mid-tropospheric circulation over WA (Viltard et al. 1998; Diedhiou et al. 1999). Another spectral peak is centered near 15-day and may be related to the 10-25 day variability in WAM highlighted in other studies (e.g., Janicot and Sultan 2001; Grodsky and Carton 2001; Sultan et al. 2003; Lavaysse et al. 2006; Maloney and Shaman 2008). Significant power also emerges in the flux time series of the western and southern boundaries of Sahelian zone, with the 30-60 day band being its characteristic periodicity (Fig 4.1a, c). The 30-60 day power spectrum attains its maximum during the mid-1960s, which corresponds to a period of declining Sahelian rainfall (Fig.1.1).

To ensure that these diagnosed periodicities are robust, and independent of the choice of statistical techniques, and to find out whether other frequency bands that might not be evident in wavelet transform method can be identify, results from a similar analysis using the Fourier transform are shown separately in Fig. 4.2. The red-noise spectra (REDFIT) method describes in Schulz and Mudelsee (2002) was used. The REDFIT procedure carries out a spectral analysis using the Lomb periodogram algorithm (Hammer, 2010), but includes more analysis options and also statistical

testing using the more realistic null hypothesis of red-noise which tests if peaks in the spectrum of a time series are significant against the red-noise background via a first-order autoregressive (AR1) process. Both the spectrums of moisture flux divergence across the western (Fig. 4.2a) and across the southern (Fig. 4.2b) boundaries reveal evidence for spectral peaks centered near 50, 13, and (to a lesser extent) 3 days. The periodicity depicted in both Figs. 4.2a-b closely resembles that from the wavelet analysis (Fig. 4.1) and the discrepancies between these two techniques are minor.

Based on these results, and for the remainder of this section, all waves with periods greater than 10 day will be considered long period, while all waves with periods less than 10 day will be considered short period.

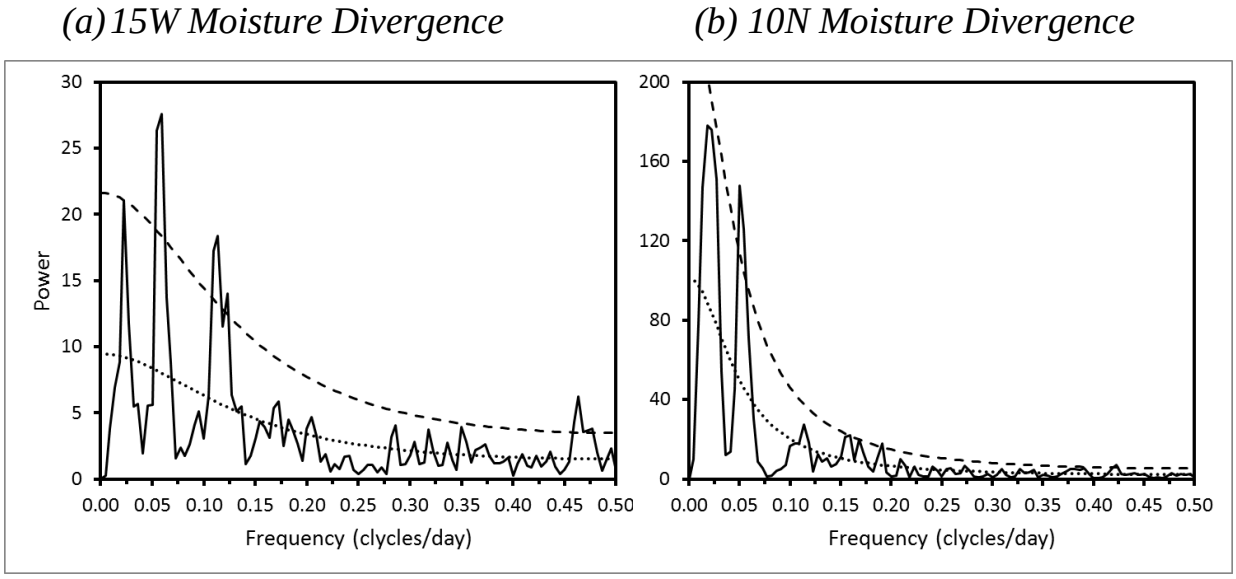

Figure 4.2: Power spectra of April-May moisture flux divergence average across (a) the western and (b) southern lateral boundaries of Sahelian zone (see text). The seasonal cycle was removed prior to the computation of the spectrum. The lower dotted line indicates the red noise background spectrum and the upper dash line is the 95% confidence limit on the red noise background based on lag-1 autocorrelation.

4.3 Seasonal Mean Moisture Budget

Figure 4.3 shows the mean moisture transport (vectors) and its divergence (shading) obtained from Eq. 7 for June-September (JJAS). Fig. 4.3a represents the total mean atmospheric moisture transport $\overline{Q}$ (vectors) and its divergence $\nabla \bullet \overline{Q}$ (shading). This is the sum of the moisture transport and divergence by the mean flow (Fig. 4.3b), the transport and divergence by climate anomalies (Fig. 4.3c), and the transport and divergence by synoptic anomalies (Fig. 4.3d). The main balance of the atmospheric water budget is between the moisture flux divergence and precipitation because, for a sufficiently long period, the precipitable water is negligible. So, in Figs. 4.3a-d $\nabla \bullet \overline{Q}$ is nearly equal to $\overline{E}$ - $\overline{P}$, and the main moisture flux divergence displays a pattern similar to that of precipitation.

Large moisture sources are found over the South Atlantic Ocean and to some extent over the northeast Atlantic, whereas moisture sinks are found over the continent with two maxima (Fig. 4.3a) centered over the Guinean coast and the Sahel respectively. Moisture transport by the mean flow is southwesterly and stronger along the southwestern coast of the continent. There is also a strong northeastward transport by the synoptic and climate anomalies over the Gulf of Guinea region whereas over the western coast, it is mostly eastward and somewhat poleward from the western to the central Sahel. The magnitude and extent of these moisture sources once again demonstrates that the Atlantic Ocean is the main provider of moisture for West African summer rainfall.

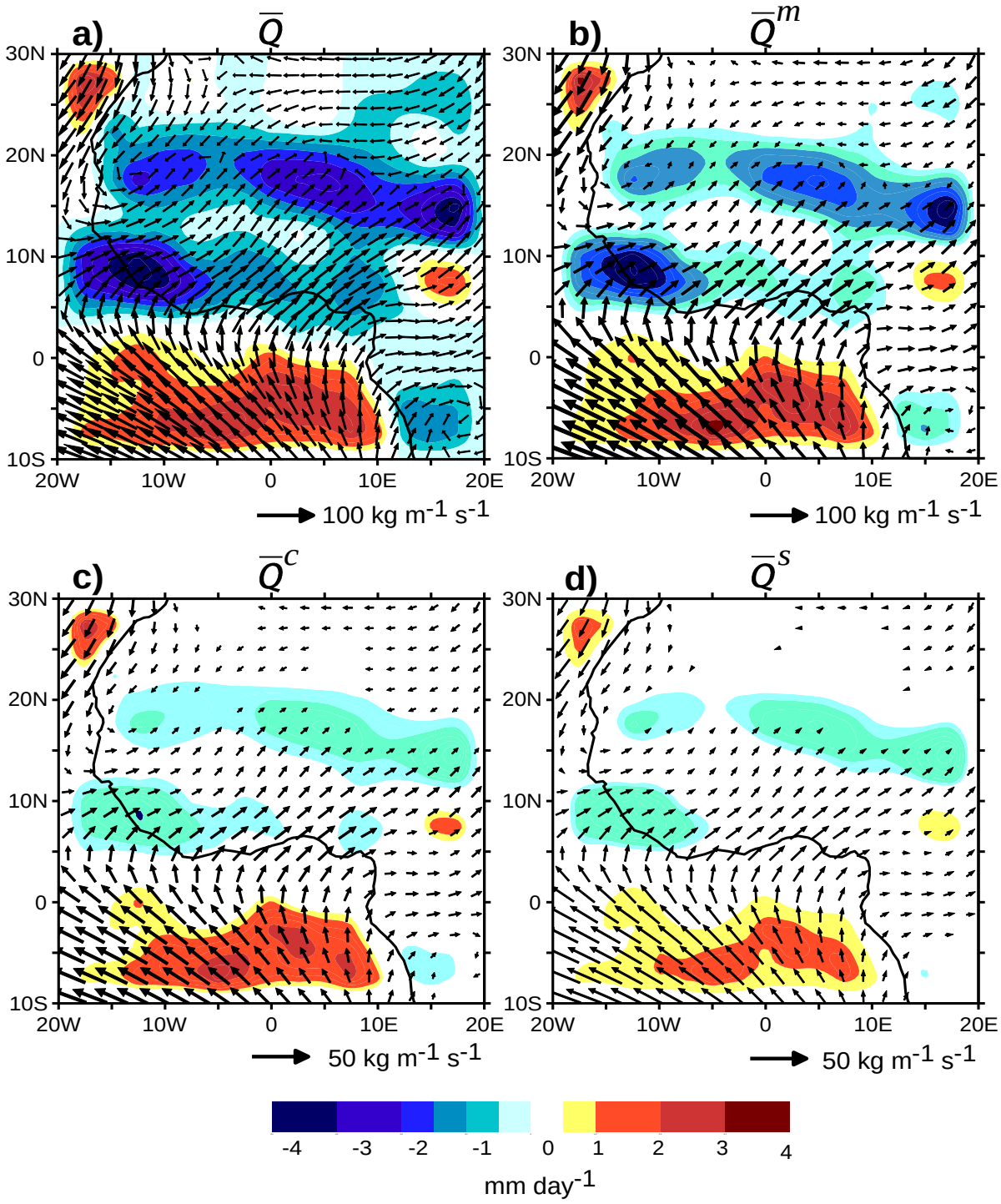

Figure 4.3: Moisture transport (vectors) and its divergence (shading) for June-September of 1979-2008 for (a) the total flow, (b) by the mean flow, (c) by climate anomalies, and (d) by synoptic anomalies. Moisture transport vectors are in unit of kg m^{-1} s^{-1}, and moisture divergence is in mm day^{-1}.

Moisture transport and divergence by the mean flow (Fig. 4.3b) is an order of magnitude higher than that of the other two components and therefore dominates the total mean moisture transport and divergence. The moisture transport and its divergence by climate anomalies (Fig. 4.3c) are larger than that of the transport and its divergence by the synoptic anomalies (Fig. 4.3d). There is considerable evidence that synoptic-timescales (<10 day) easterly waves play an important role in moisture transport over WA, although the exact mechanisms by which they influence the moisture surges into the continent is not clear. Nevertheless, disturbances with timescales of about 2-8 days, which develop over WA and the tropical Atlantic and between the AEJ and the ITCZ latitudes, have been noted for a long time. Burpee (1972, 1975) showed the existence of AEW with period of 2-8 days and wavelengths ranging from 2000-4000 km and propagation speeds of about 15 m s^{-1} in connection to organized mesoscale convective systems which are the major contributors to of rainfall generation over WA. Norquist et al. (1977) investigated the wave energetics and revealed two centers of energy conversion – one characterized by a predominance of moist convective processed to the south of the AEJ, and the other characterized by a drier conversion to the north, and dominated by baroclinic processes. Similar results were obtained by Thompson et al. (1979) and Albignat and Reed (1980) who emphasized the baroclinic tilt of the waves produced to the north of the AEJ, and the dominance of latent heat release for the waves produced south of the AEJ. Duvel (1990) investigated the AEW modulation of cloudiness using ECMWF analyses and found two centers of consistent cloudiness-wave phase relationships. One was centered at about 7.5^{o}N over the ocean, where convective activity was concentrated at or ahead of the wave trough and the other was

found at about 17.5^{o}N over the Sahelian region and characterized by a convective maximum east of the trough.

4.3.1 Meridional Transport

The important role of transient eddies in driving a large fraction of the meridional transport of water vapor was highlighted by Peixoto and Oort (1992, pp. 287-291). Evidence of this transport is presented in Figure 4.4, which shows the zonal average of each term contributing to the mean meridional moisture transport as a function of the time of year. The latitude of the ITF characterizes the extent of the southwesterly monsoon flow over West Africa and therefore constitutes an important parameter to describe the WAM variability. Fig. 4.4 reveals some details regarding the intensities and directions of the meridional moisture transport. The meridional transport patterns are well defined, with predominantly poleward transport throughout the season, and the shape of the ITF seasonal cycle tracking the direction of the transport. The transport by the mean circulation (Fig. 4.4b) dominates the meridional moisture transport, primarily northward from the southern hemisphere but with a cross-equatorial component toward the African continent near the equator with a southwest direction (e.g., Peixoto and Oort 1992; Newman et al 2012). Two centers of maximum meridional flux are noted. The first, centered near the equator, occurs during May-June and contributes certainly to the enhanced of precipitation over the Guinean coast at that time. The second center of maximum meridional flux occurs in July and is centered along latitude 5^{o}N and probably is associated with the enhancement of precipitation over the Sahelian region during the July-August-September period. The influence of the

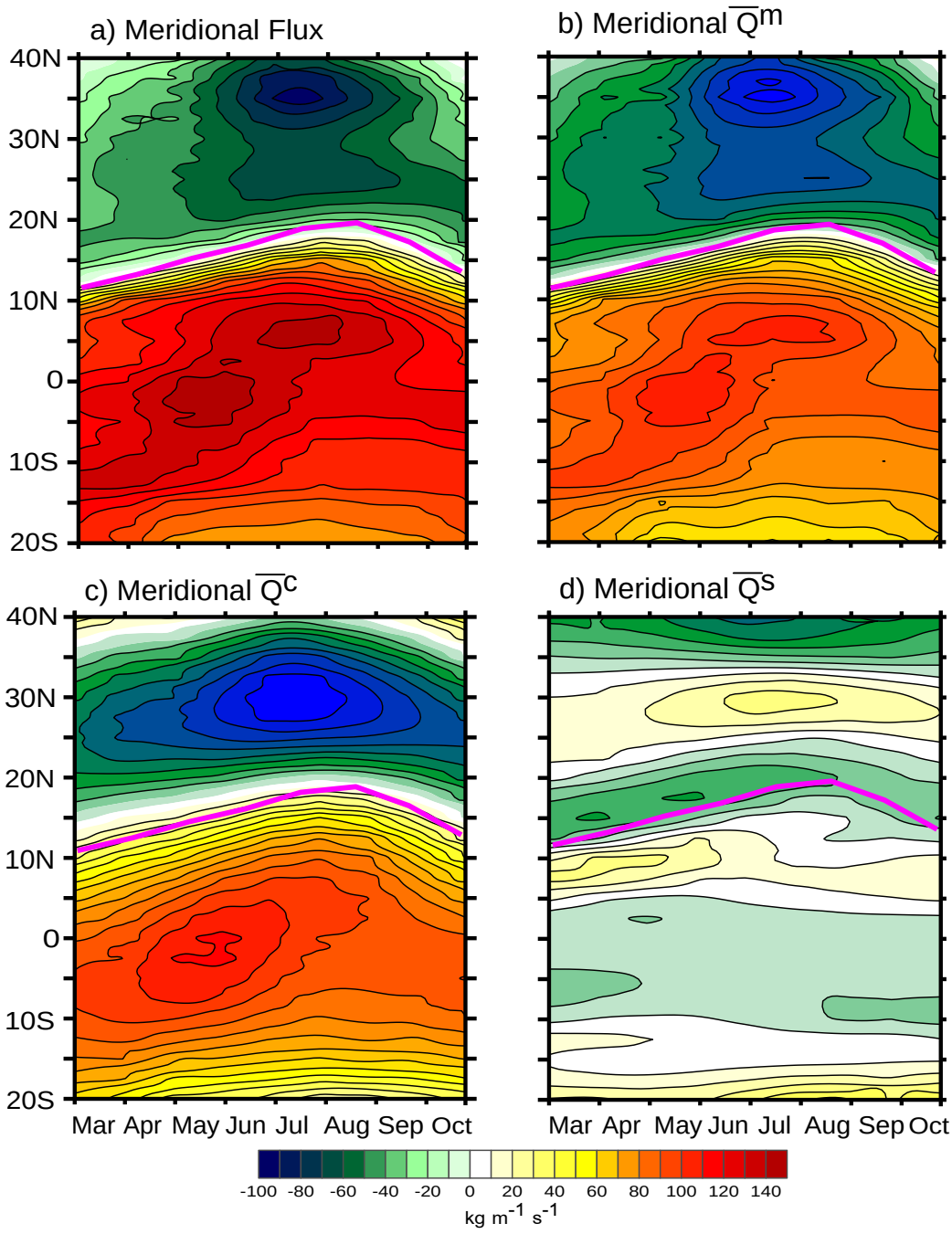

Figure 4.4: Seasonal cycle of terms contributing to the vertically integrated mean meridional moisture transport (shading and contours), zonally averaged across 20°W-10°E. (a) Total mean transport, (b) transport by the mean flow, (c) transport by the climate anomalies, and (d) transport by synoptic anomalies. Moisture transport is in units of kg m^{-1} s^{-1}. Intervals for contour and shading are 10 kg m^{-1} s^{-1}, and heavy magenta line indicates the ITF latitude.

ITF is evident in the location of these maxima, due to the strong (weak) equatorward flow of dry air during March-May (June-July) and the poleward flux of moist air.

The large-scale (low frequency) meridional moisture transport (Fig. 4.4c) contributes more than the high frequency meridional transport (Fig. 4.4d), which is very weak during April-June, and almost vanishing north of 5^{o}N during July-August-September period. The largest meridional transport by the large scale anomalies occurs generally between 5^{o}S in the Atlantic Ocean to 8^{o}N in the Guinean coast. In general, the meridional moisture transport is weak over the Sahelian zone, which is also reflected in the components contributing to the total meridional transport. The largest seasonal variability during the spring and summer seasons is associated with the seasonal advance of the ITF, which has its position almost at the same latitude as the zero meridional moisture transport. This suggests a positive relationship between the variability of the ITF latitude and the moisture availability and rainfall over the continent in agreement to Lamb (1983), Hastenrath (1984), Janicot (1992a, b), and Lélé and Lamb (2010). Another region of meridional moisture transport is observed over the Mediterranean Sea with a strong maxima centered along 35^{o}N during June-July-August (JAS). Hence, a relatively weak southward transport of moisture from the Mediterranean Sea to the Sahelian zone by the synoptic anomalies is noticeable during the JAS season. Note that during this period the ITF lies in the belt of the northerly flux of moisture transport by the synoptic anomalies (Fig. 4.4d), indicating the existence of northerly moist air south of the ITF over the Sahelian zone. The existence of the southward moisture transport over the Sahel by the synoptic anomalies supports

previous studies that have mentioned the Mediterranean as a potential source of moisture for Sahelian rainfall (e.g., Fontaine et al. 2010a; Gaetani et al. 2010b). However, Figure 4.4 shows that most of the southward moisture flux between 30-40^{o}N is over the eastern Atlantic, around the Canary Islands, and not over the Mediterranean Sea, suggesting that the mean flow (Fig. 4.4b) transports moisture southward, followed by the intraseasonal fluctuations (Fig. 4.4c), and lastly by the synoptic fluctuations (Fig. 4.4c).

4.3.2 Zonal Transport

As with the meridional moisture transport, the terms contributing to the zonal moisture transport over WA are presented in Fig. 4.5. The mean zonal moisture transport is characterized by 1) a band of westward moisture transport over WA between 0^{o}-15^{o}N and 2) two bands of eastward moisture transport surrounding the westward band. The seasonal cycle of the zonal moisture transport presents a moisture flux maximum in August centered at about 5^{o}N (Fig. 4.5a-c). This center of maximum zonal flux is also reported in Cadet and Nnoli (1987) who identified a strong westerly moisture flux from the eastern Atlantic below 850 hPa. The seasonal cycle of the meridional extent of these westerlies again mirrors the seasonal cycle of the ITF latitude, suggesting that clear sky conditions always prevail north of the ITF while convection followed by significant rain events occurs south of it. The pattern of the zonal transport by the mean flow also dominates the total transport (Fig. 4.5b). Next, the other major contributor to the zonal moisture transport is the large-scale anomalies. In fact, this contribution is almost the same magnitude as the transport by the mean flow

(Fig. 4.5c). The zonal transport by small-scale anomalies (Fig. 4.5d), although weaker than the other component of the zonal transport, shows a consistent westerly transport across the 5°-10°N latitude band.

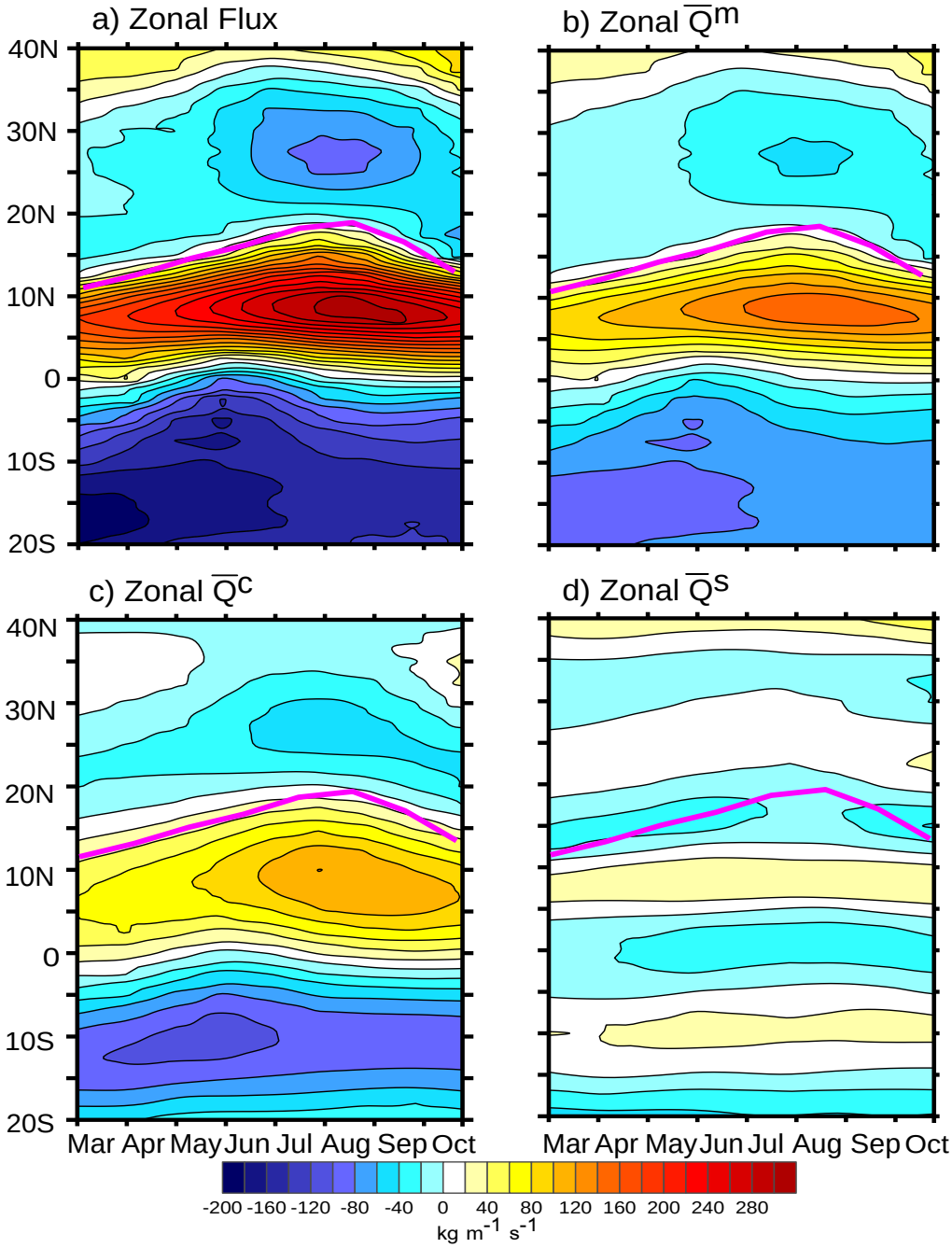

Figure 4.5: Same as Fig. 4.4, but for the vertically integrated zonal moisture transport averaged across 20°W-10°E.

A feature apparent from Figure 4.5 is that the westerly moisture transport is largest during the JAS peak of the monsoon season when the Sahelian region experiences its only rainfall season, suggesting its association with regional scale rainfall variability. This is consistent with previous discussion in Chapter 3, Sections 3.5.2 and 3.5.3 that relates the zonal moisture transport from the eastern Atlantic and Sahelian rainfall variability during JAS. The role of the so-called WAWJ in bringing moisture onto the west coast of Africa has been recently described by Pu and Cook (2012). They demonstrated that during the Sahelian drought period (1972-1987), the anomalous moisture transport from the eastern Atlantic was negative and related to a weak WAWJ whereas during the wet period (1958-1971), an enhanced eastward moisture transport toward the African land mass was present. Figure 4.5 suggests that the interannual variations of Sahel precipitation are related to not only to the variations of the low-level meridional moisture transport from the south Atlantic, but also to the variations of the low-level moisture transport from the eastern Atlantic.

Figure 4.6 shows the meridional profiles of the zonal- and meridional moisture transport by all motions for March-October. These profiles summarize the main characteristics of the sub-scales meridional and zonal transport of moisture in WA and surrounding ocean. The synthesize behavior of the zonal profile indicates that the flow is from the east across the WAM domain (yellow shaded), with a unimodal configuration and a maxima near 7.5^{o} latitude north (Fig. 4.6b). Both the northward and eastward transport of moisture change sign near 20^{o}N, which also coincide with the northernmost latitude position of the ITF. Thereafter, the northerly and northeasterly

fluxes manifest over the region and marked the end of the WAM summer rainfall season.

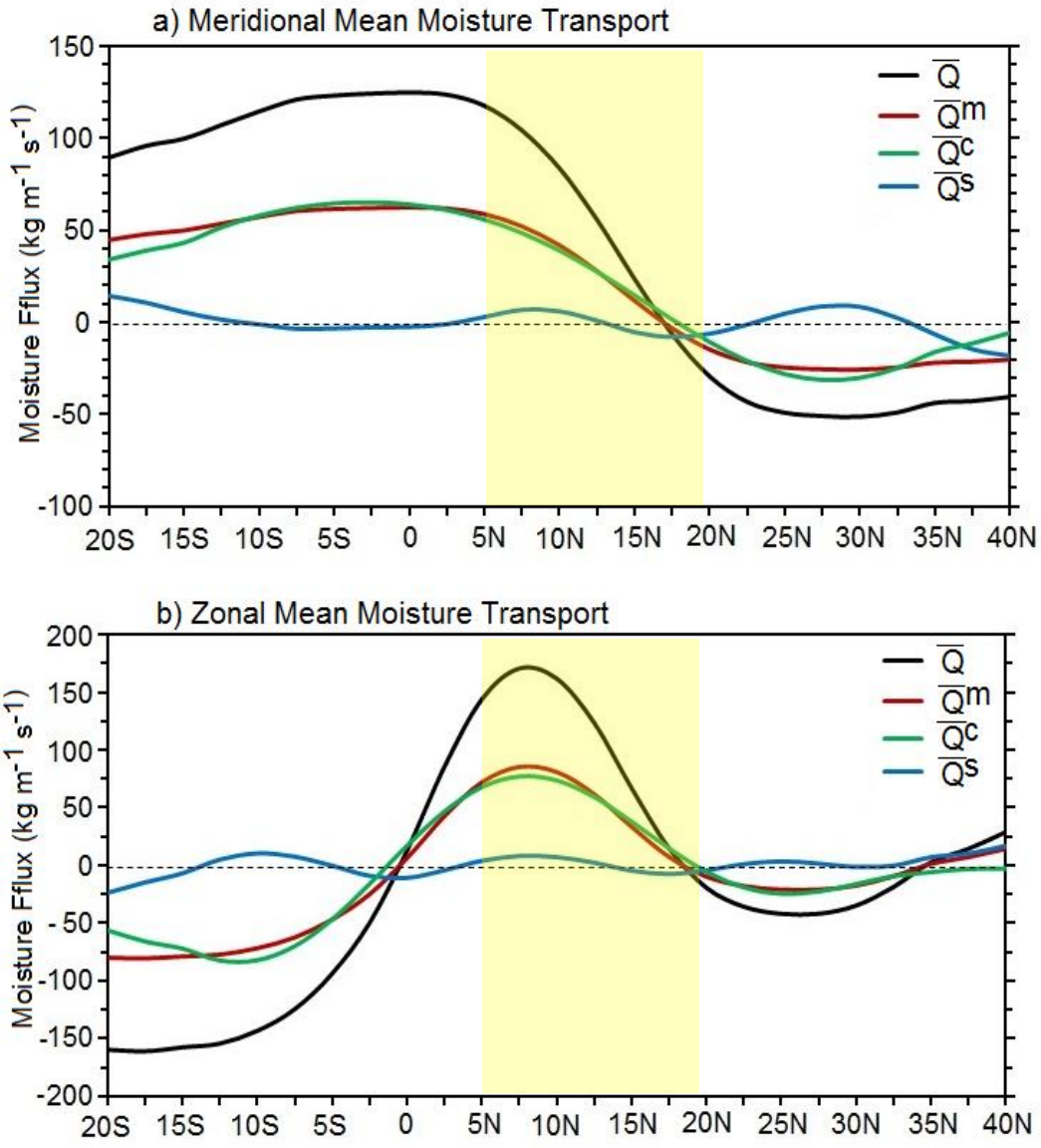

Figure 4.6: Meridional profiles of the zonal average (20°W-20°E) of the (a) meridional and (b) zonal moisture fluxes and terms contributing to the their total transport during March-October. Moisture flux is in kg m^{-1} s^{-1}. The dashed horizontal lines indicate the zero meridional and zonal flux, and shading indicates the latitude extent of the West African monsoon domain. A 3-point smoother is applied to the curves.

4.3.3 Case Study of Summertime Atmospheric Moisture Budget and its Regulation of Precipitation in West Africa

The relations between the summertime atmospheric moisture transport terms and seasonal rainfall over WA also were investigated for the 2005 and 2006 monsoon seasons. During 2005, the monsoon season over the Sahelian zone was relatively wet while in 2006 it was relatively dry (Fig. 1.1). The choice of these years, though not the wettest nor the driest in the study period, was based on the recent AMMA field experiments which provided more reliable observational data for these years.

Precipitation rates for AMJ and JAS of 2005-6 are displayed in Figs. 4.7a-b, and Figs. 4.8a-b respectively. During AMJ, precipitation is characterized by a south-north gradient, with higher precipitation (13 mm day^{-1}) near the coastal regions and lower precipitation (1-4 mm day^{-1}) inland over the Sudan zone. It extends across the Guinean region, with less precipitation in the Sahelian regions, in both 2005 and 2006 (Figs. 4.7a-b). This precipitation pattern may result from a thermally driven circulation induced by localized land-sea heating contrast along the subtropical coastal areas and by the cold tongue that develops in late spring (e. g., Gu and Adler 2004; Joly and Voldoire 2010; Thorncroft et al. 2011). As a manifestation of the first phase of the ITF seasonal cycle, the precipitation belts during the boreal summer abruptly shift northward to the latitudes of about 10^{o}N, with intense convection across the Sudan-Sahel zone and its diminution over the Guinean regions.

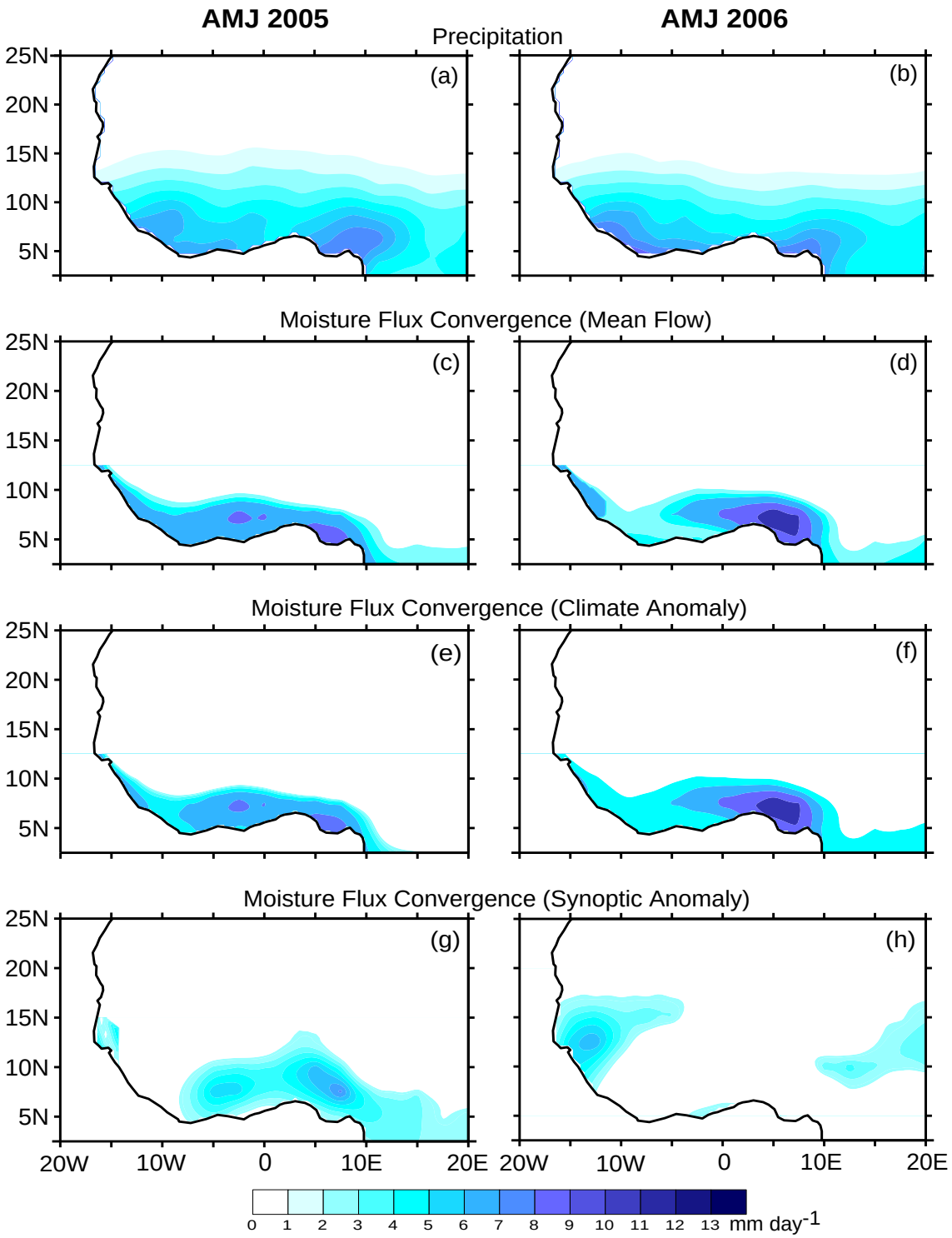

Figure 4.7: Seasonal mean precipitation and moisture flux convergence terms over the Gulf of Guinea regions during 2005 (left panel) and 2006 (right panel) April-May monsoon seasons. a) and b) Precipitation, c) and d), e) and f), and g) and h) are moisture flux convergence by the mean flow, the large scale eddies, and the small scale eddies respectively. Precipitation and flux convergence units are in mm day^{-1}.

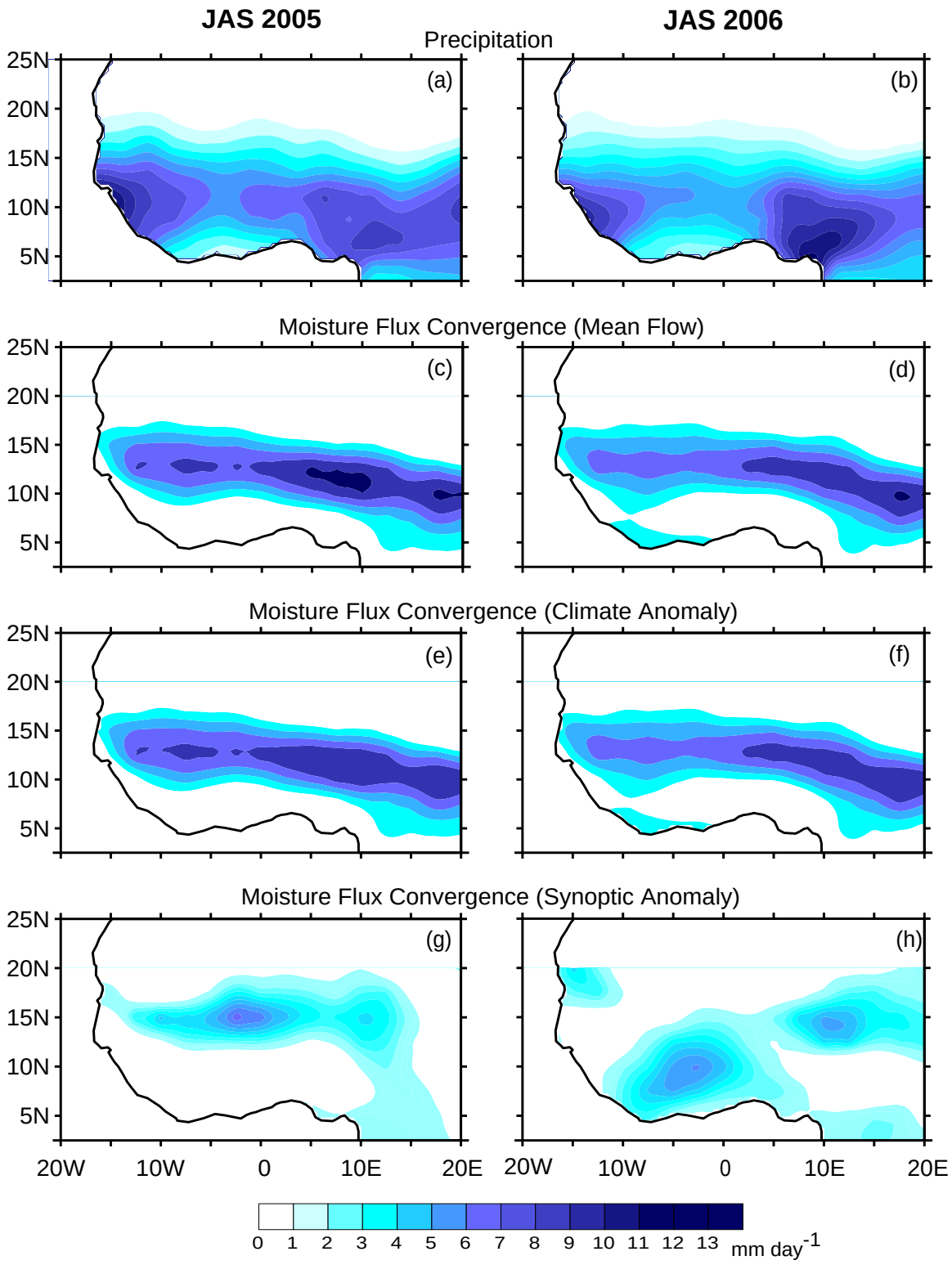

Figure 4.8: Same as Figs. 4.7, but for period July-August-September over West Africa.

In 2005, precipitation anomalies near the Guinean coast are characterized by lower precipitation rates (5-7 mm day^{-1}) compared to the 2006 season (7-10 mm day^{-1}). However, the 2005 precipitation rate over the Sahelian zone (Fig. 4.8a) is significantly higher than in 2006 (Fig. 4.8b), suggesting that a dry (wet) Guinean region rainfall is accompanied by a wet (dry) Sahelian summer rainfall. Such spatial features in precipitation during the spring and summer are also reflected in the field of moisture flux convergence by the mean flow, which is higher over the coastal regions than inland in the spring (Figs. 4.7c-d), and northward shift during the boreal summer (Figs. 4.8c-d).

Large-scale anomalies also contribute to moisture convergence along the coastal regions during AMJ (Figs. 4.7e-f), and over the Sahel (Figs. 4.8e-f), with a magnitude almost equal to that of the mean flow. This suggests that precipitation over WA is primarily due to large-scale atmospheric features especially during the JAS season. The variability of large-scale atmospheric circulation features, such as those describe in chapter 1 (i.e., AEJ, TEJ, ITF, …), and the low-level moisture advection are considered to be the major factors influencing rainfall variability over WA (e. g., Nicholson and Grist 2003).

Synoptic-scale anomalies also contribute to moisture flux convergence and consequently, to precipitation, but the magnitude is smaller than that of the mean and the large-scale flows (Figs. 4.7g-h, Figs. 4.8g-h). The largest contributions of the small-scale anomalies are located over regions of frequent or intense mesoscale weather

phenomena, such as the Fouta Djalon highlands along the coast of Guinea Conakry and Sierra Leone, inland over the Mount Cameroon, and the Adamawa highlands, and on shores of the Gulf of Guinea where land-sea breeze storms have mesoscale organization.

To further characterize the strength of the relationship between moisture transport and precipitation over WA, a moisture transport index is defined as the area average of the divergence field across the Sudan-Sahel region bounded between 17.5^{o}W-10^{o}E and 10^{o}-20^{o}N. This region is chosen because of the strong interannual rainfall variability that characterizes its summer season, and the long period of drought that has experienced the region. The rainfall index used for correlation purposes is also defined as the average of the observed rainfall from stations within the domain. Figure 4.9 documents the interannual variation in the areal-averaged Sudan-Sahel precipitation and moisture flux convergence during 1960-2009. Interannual variations of JAS moisture flux convergence time series are significantly correlated with Sudan-Sahel JAS precipitation, with correlation coefficient of 0.60 (Table 4.1), exceeding the 99% confidence level according to a two-tailed Student's *t*-test (Wilks 2006, pp.131-135). The relationship between moisture transport and precipitation is positive, indicating that rainfall increases (decreases) with enhanced (diminished) moisture convergence the Sudan-Sahel region. The interannal variability of JAS moisture convergence (Fig. 4.9) also captures well the variability of precipitation in the sense that during the anomalously wet Sahel periods of the 1960s, anomalously positive atmospheric

moisture transported into the region was observed. Likewise, during the drought periods of the 1970s and 1980s, negative indices of moisture transport into the region have been observed. During the recent periods, often termed the "recovery period" by some reports (Nicholson 2005; Lebel and Ali 2009; Pu and Cook 2012), the Sudan-Sahel region was characterized by enhanced anomalous low-level moisture transport. However, the magnitude of this enhance moisture transport during the recovery is less than the magnitude of the wet 1960s period. This implies that the recovery is generally weak and limited in time and space, as suggested by Nicholson (2005) and Lebel and Ali (2009).

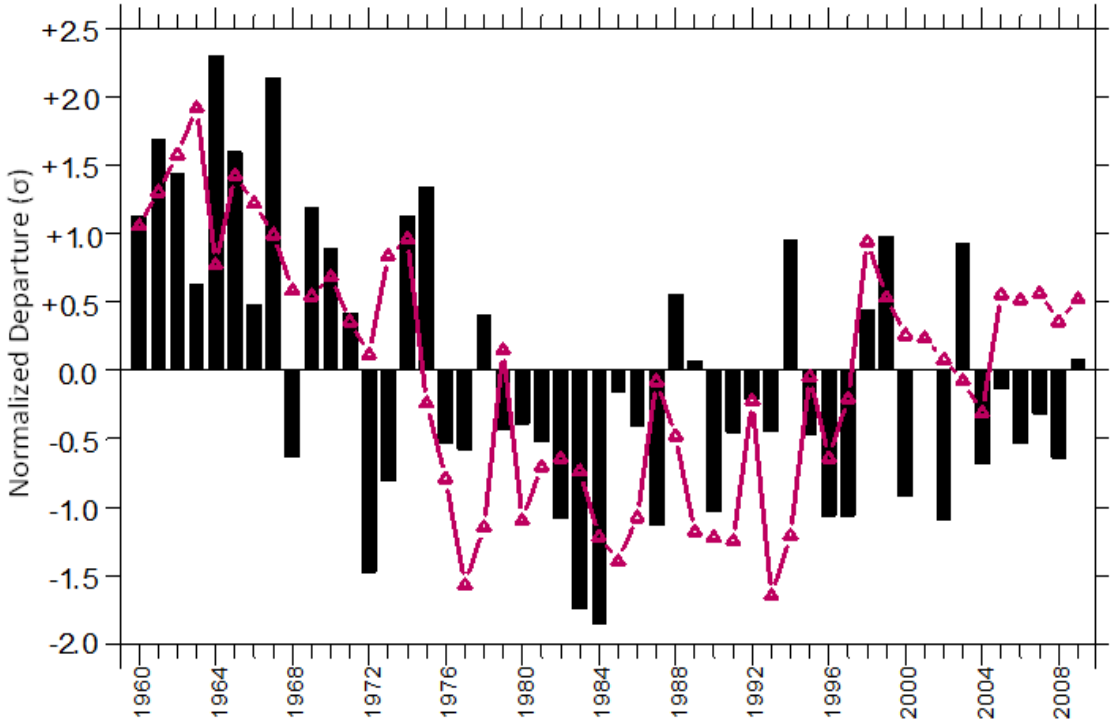

Figure 4.9: Time series (1960-2009) of normalized departure (σ) of JAS precipitation (bars) and moisture convergence (solid line) over Soudan-Sahel zone (17.5°W-10°E, 10°-20°N)

Moisture transport and Sudan-Sahel precipitation indices are also highly correlated in other months of the monsoon season. Table 4.1 portrays the correlation coefficients between precipitation and the different terms contributing to the total moisture convergence. Table 4.1 uses two to three months averages for each season to assess the association between the vertically integrated moisture convergence and precipitation. High and statistically significant correlations exceeding the 99% confidence level are found between the mean flow and the large-scale climate anomalies of moisture convergence, and rainfall over the Sudan-Sahel. The correlations are all positive, in agreement with previous spatial relationships found between the terms of the atmospheric moisture convergence and WAM rainfall variability. However, the strength of the association, although relatively high in the early rainy season months (June-July, JJ), becomes stronger as the season progresses. Note also that precipitation in most cases lags the moisture transport. For example, the averaged June-July mean and low frequency moisture convergence is highly correlated with precipitation during July-August (JA), June-July-August (JJA), and July-August-September (JAS), suggesting potential Sudan-Sahel rainfall predictability using the knowledge of the moisture flux and wind content. No significant correlations were found between precipitation and the high frequency component of the moisture transport which confirms that precipitation over Sudan-Sahel is dominated by large-scale anomalies.

Table 4.1 Correlation coefficients between rainfall and moisture convergence by the mean flow, the large-scale and the small scale anomalies over the Sudan-Sahel zone. Linear correlation coefficients, all of which are significant at the 1% (5%) level are in bold (underline) according to a two-tailed Student's *t*-test (Wilks 2006, 131–135). Time series consist of average of two and three month values for each year between 1960 and 2009. JJ represents the average of rainfall and moisture flux for June-July, JA is July-August, JJA is June-July-August, and JAS July-August-September.

Sudan-Sahel average rainfall index	Moisture convergence (mean flow)	Moisture convergence (climate anomaly)	Moisture convergence (synoptic anomaly)
		JJ	
JJ	0.32	**0.57**	0.03
JA	**0.45**	**0.79**	0.03
JJA	**0.49**	**0.79**	-0.01
JAS	**0.52**	**0.84**	0.02
		JJA	
JJA	**0.60**	**0.84**	0.19
JAS	**0.63**	**0.89**	0.23
		JAS	
JAS	**0.60**	**0.88**	0.11

In summary, this section focused on the interannual variability of the atmospheric moisture transport cycle and rainfall during two extreme years. Two dominant modes of seasonal rainfall are observed over West Africa during the WAM season: the Gulf of Guinea mode and the Sahelian mode. Large scale anomalies of moisture transport and convergence are the major contributors to these modes, except over higher terrain where the contribution of the small-scale anomalies is significant,

but still smaller than the large-scale anomalies. Detailed analysis of moisture transport over the Sudan-Sahel region suggests that the interannual variation in Sudan-Sahel summer precipitation is modulated by moisture transport variations from the Atlantic Ocean. This also suggests that atmospheric moisture transport could be part of the large-scale circulation changes in response to SST variations in the Atlantic Ocean, which provide forcing of Sahelian interannual-to-decadal rainfall variability (e.g., Lamb 1978a, b; Hastenrath 1990; Ward 1998; Giannini et al. 2003). However, while this might be true, it is not directly implied by the relationship between moisture transport/convergence over the region and the SST variations.

Correlation coefficients obtained based on the above methods could be biased estimators of the population coefficients. Hence, a nonparametric approach, it is often useful when the validity of assumptions underlying the traditional theoretical approaches is questionable. One may argue that the variance explained by the transport of moisture-rainfall relation is applicable only to the given sample used and may not be sufficient for some meteorological application decisions (e.g., prediction). In order to measure the uncertainty with the most meaningful absolute magnitude, it is useful to establish a confidence intervals range within which the unknown true correlation coefficient is likely to fall. Standard parametric confidence intervals can provide a measure of significance for correlation coefficients but they require Gaussian distribution assumptions which are difficult to achieve given the limited data available to studies like this to estimate the correlation coefficients. Alternative to the standard

parametric confidence intervals is the nonparametric method of using bootstrap estimates of the variability of the coefficient.

The close relationship between the confidence interval and hypothesis tests implied that the bootstrap confidence intervals can be used as the basis for nonparametric hypothesis tests. Thus, the bootstrap confidence interval of the correlation coefficients (Table 4.1) is designed in the way that it is consistent with *t*-test hypothesis. So, the 90% confidence interval for the correlation coefficients as estimated through their bootstrap distributions must encompass the acceptance region for the corresponding two-sided *t*-test. The null hypothesis that the correlation coefficient is equal to zero, previously rejected by the *t*-test (Table 4.1), will be rejected at the 5% level when the observed correlation coefficient lies outside of the bootstrap confidence interval. Otherwise, the statistical significance of the correlations coefficients previously obtained by the *t*-test will be strengthened by the bootstrap confidence interval which, investigate much more focused the null hypotheses.

The confidence levels were assessed by calculating the correlation coefficients with 1000 bootstrap with replications. Table 4.2 and 4.3 give the 90% confidence limits for the correlation coefficients, as given by the bootstrap percentiles, the bootstrap-*t*, and the bias-corrected and accelerated (BCa) techniques. It is seen that these three procedures yield results which are similar. Also, it is interesting to note that these methods provided substantially narrower limits except for when June-July (JJ) moisture

Table 4.2 Correlation coefficient and approximate bootstrap confidence intervals based on 1000 bootstrap replications for the association between the Sudan-Sahel rainfall and the moisture convergence by the mean flow.

	Mean flow	***Percentiles***	***Bootstrap-t***	***BCa***
Rainfall	**r**	**5^{th} , 95^{th}**	**5^{th} , 95^{th}**	**5^{th} , 95^{th}**
		JJ		
JJ	0.32	0.01, 0.59	0.04, 0.57	0.02, 0.60
JA	0.45	0.19, 0.64	0.19, 0.63	0.20, 0.65
JJA	0.49	0.20, 0.68	0.20, 0.67	0.21, 0.68
JAS	0.52	0.28, 0.70	0.26, 0.68	0.28, 0.71
		JJA		
JJA	0.60	0.38, 0.75	0.38, 0.75	0.39, 0.77
JAS	0.63	0.44, 0.77	0.46, 0.76	0.45, 0.77
		JAS		
JAS	0.60	0.39, 0.75	0.26, 0.68	0.40, 0.76

Table 4.3 Same as Table 4.2 but for moisture convergence by the climate anomaly.

	Climate anomaly	***Percentiles***	***Bootstrap-t***	***BCa***
Rainfall	**r**	**5^{th} , 95^{th}**	**5^{th} , 95^{th}**	**5^{th} , 95^{th}**
		JJ		
JJ	0.57	0.30, 0.75	0.31, 0.75	0.33, 0.78
JA	0.79	0.61, 0.88	0.64, 0.88	0.64, 0.88
JJA	0.79	0.61, 0.88	0.64, 0.88	0.64, 0.89
JAS	0.84	0.71, 0.91	0.73, 0.91	0.72, 0.91
		JJA		
JJA	0.84	0.69, 0.91	0.71, 0.91	0.72, 0.92
JAS	0.89	0.79, 0.94	0.81, 0.93	0.80, 0.94
		JAS		
JAS	0.88	0.78, 0.93	0.80, 0.93	0.79, 0.93

flux by the mean flow is used where the widths of the intervals are relatively wider (>0.40) for all the methods. Estimates of the correlation coefficients near the lower and upper ends of the confidence interval indicate that the relationship between the moisture convergence by the mean flow and the climate anomaly, and Sudan-Sahel rainfall is

strong over most of the case studies. Table 4.2 also suggests that variance estimates near the lower end of the limits still is distinctly weaker during the beginning of the rainy season (JJ; < 10%) but even then it still is moderately strong for the climate anomaly (JJ; 10% to 53%). Furthermore, except for the mean flow during JJ, these confidence limits do not include 0 which suggest the rejection of the null hypothesis and therefore, confirms that the correlation coefficients in Table 4.1 are indeed statistically significant at the 10% level as previously suggest by the standard *t*-test. These results further strengthen the convergence of moisture control on Sudan-Sahel rainfall.

4.4 Structure and Evolution of the Intraseasonal Variability Associated with Moisture Transport over West Africa

4.4.1 Overview of WAM Intraseasonal Variability

In the previous analysis, it was found that climate anomaly tends dominate the moisture transport over WA. It is therefore important to further investigate this variability and its contribution to monsoon rainfall. This because much of the WAM investigations in recent decades have focused on its seasonal variability, rather than its intraseasonal variability (e.g., Grodsky and Carton 2001; Matthews 2004), though for agricultural activities, weather over shorter periods has to be considered. An example of intraseasonal variation is shown in Fig. 4.10, where evidence of large-scale westward propagation of intense precipitation can be seen for each diagonal swath. More than six westward propagating convective events occur during the last 20 days of August 2005. The presence and evolution of these large-scale westward propagating systems are found to be associated with AEWs (e.g., Druyan et al. 2006) and thus linked to wet and dry periods over the region. In this Section, the underlying statistical relationship between the atmospheric moisture transport and the West African rainfall, with emphasis on the 30-90 day timescale variability was investigated.

The strong intraseasonal variations in precipitation over WA are obvious from inspection of the daily rainfall, such as those presented in Fig. 4.10. They have been known for a long period, and the dynamics behind such variability has been the subject of many studies (e.g., Park and Schubert 1993; Shapiro and Goldenberg 1993;

Matthews 2004; Foltz and McPhaden 2004; Gu and Adler 2004). The intraseasonal variability on the 10-25 day timescales has been intensively documented (e.g., Sultan and Janicot 2000; Janicot and Sultan 2001; Sultan et al. 2003; Mounier et al. 2008). However, more needs to be done on the still longer timescales, such as those related to the Madden-Julian oscillation (MJO, Madden and Julian 2005). For example, the impact of the global modes of intraseasonal variability on the WAM is far less understood.

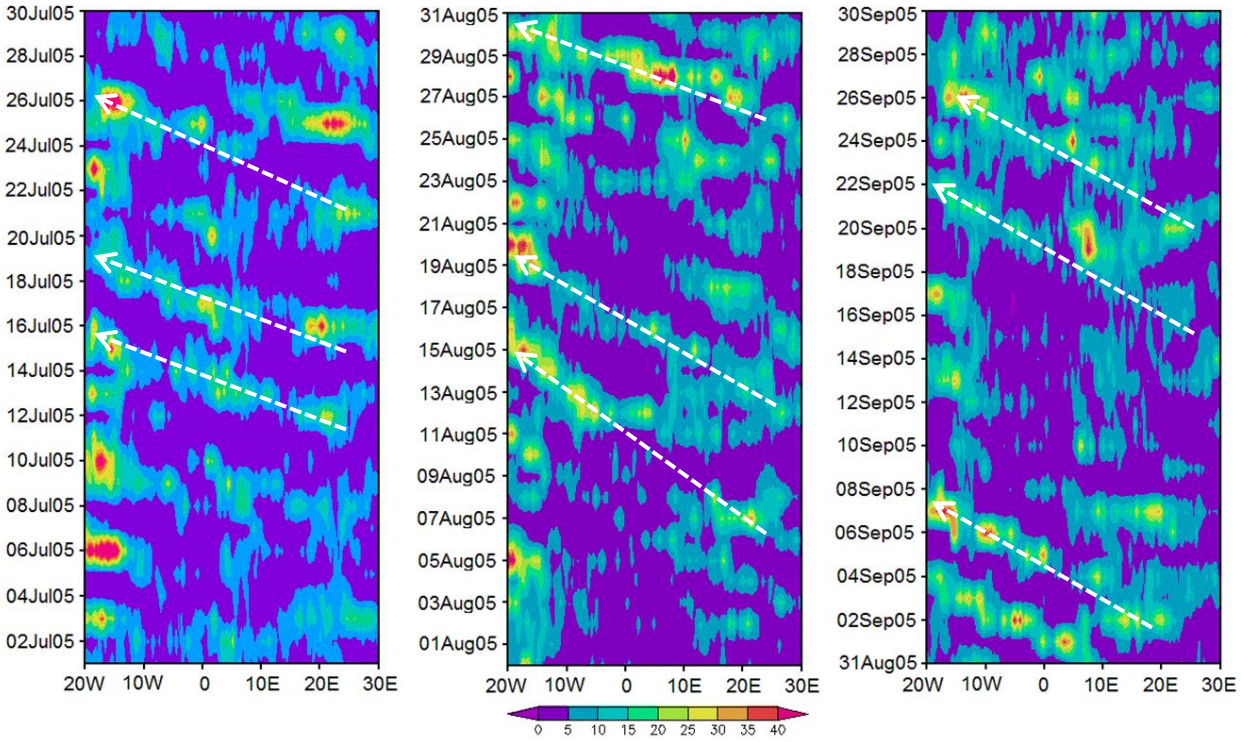

Figure 4.10: Time-space Hovmöller diagrams of TRMM precipitation (mm) averaged over 5°-15°N between July 1 and September 30, 2005. Broken arrows indicate the direction of the propagation.

While studies like those of Knutson and Weickmann (1987), Annamalai and Slingo (2001), and Wheeler and Weickmann (2001) found that the influence of the MJO on Sahelian precipitation is weak, it was found to be almost non-existent in other studies (e.g., Murakami et al. 1986, Maloney and Hartmann 2000a). However, the work by Matthews (2004), Janicot et al. (2009), and Janicot et al. (2011) suggest that strong MJO events can remotely influence the WAM system and modulate precipitation, winds, and AEW activity. Therefore, the investigation of the influence of the MJO on the WAM is important because skillful sub-seasonal forecasts could be made for the region if such a relation exists. So, the focus here will be more on the nature of the coupling between convection, large-scale atmospheric variability, and enhanced moisture transport into Sudan-Sahel zone. The understanding of moisture transport variations when convection is enhanced (active monsoon event) or when there is less precipitation (pause monsoon event) is important for short time prediction over the region.

4.4.2 Large-Scale Monsoon Index for West Africa

Before describing the 30-90 day mode of variability in the WAM region, a West African monsoon index that reflects the large-scale hydrological cycle is first developed. This index is developed because it is well known that monsoon phenomena are a combination of various parameters difficult to dissociate, and interacting at many different time and space scales (e.g., Redelsperger et al. 2002, Nicholson and Grist 2003, Redelsperger et al. 2006). Monsoon rainfall anomalies such as those observed

over WA are organized into large-scale patterns (e.g., Nicholson 1981, 1986; Janowiak 1988; Janicot 1992a; Nicholson and Palao 1993) which, suggests that the WAM rainfall variability is more a result of larger climate fluctuations occurring in summer over the entire WAM region rather than a single regional feature. Therefore, to objectively define the extent of the WAM and describe its variability over any timescale, the first task is to identify a rational monsoon index. A concise and meaningful index that characterizes the monsoon variability of a particular region can greatly facilitate empirical studies of the relationship between monsoon variability and lower boundary forcing (e.g., Wang and Fan 1999), and can aid in objectively assessing the capability of numerical models to reproduce monsoon variability over the region.

Several indices have been developed to characterize monsoon variation in recent decades. However, not only are the parameters involved in the development of these indices controversial (e.g., Webster and Yang 1992; Lau et al. 2000b), but most indices are for the Asian monsoon system. Over WA, seasonally-averaged precipitation over regional scales have been widely used as a measure of the WAM. While rainfall is a good indicator of the monsoon strength over localized areas, it is not clear how well it represents the larger-scale monsoon features. Consequently, a WAM Index (WAMI) which reflects the variability of the broad scale, needs to be developed for further monsoon-related research. In this study, a combination of fields is used to evaluate the applicability of a new WAMI that has a physical basis. The developed indices will be later used in identifying the onset and withdrawal dates of the boreal summer rainy season in WA.

4.4.2.1 Computation of West African Monsoon Index (WAMI)

It is often useful to look for combined modes of variations of many fields, and the combined EOF is the one of the technique that allows a simultaneous consideration of possible modes of variation of different variables (e.g., Kutzbach 1967; Navarra and Simoncini 2010; Carvalho et al. 2011). The computation of the WAMI utilizes a long term (1979-2008) pentad (5-day average) non-overlapping means of gridded field of precipitation (*p*) specific humidity (*q*), air temperature (*ta*), zonal (*u*), and meridional (*v*) wind components, at 2.5^{o} X 2.5^{o} spatial resolution. The pentad (P) means of the reanalysis data have been calculated in the same way as the precipitation pentad means where each year is divided into 73 pentads even if there are 366 days. So, the 12^{th} pentad contains an additional day to include February 29 in case of a leap year. The analysis covers the core of the rainy season period, June (P32)-September (P55), so that each grid cell time series for each of the fields total 720 pentads for this study period. The spatial domain is that of the WAM region, 10^{o}S-30^{o}N, and 20^{o}W-20^{o}E. WAMI is defined as the first or the second time coefficient of the combined EOF analysis of {*p, q, ta, u, and v*}. Prior to the combined-EOF computation, the time series of the fields were normalized to overcome the systematic deviations in the patterns that could be due to different units and quantities.

4.4.2.2 Illustration of Patterns

The combined-EOF analysis over WA yields 1191 eigenvectors and corresponding eigenvalues. The first 20 eigenvalues account for about 59% of the total

variance. The variance explained by the first three eigenvalues is summarized in Table 4.4. The first unrotated combined-EOF mode (combined-EOF-1) contains many atmospheric features previously found to be associated with the WAM. This Combined-EOF-1 explains about 19.63% of the total variance and is statistically different than the other modes according to the North et al. (1982) criteria. Combined-EOF-1 modes of precipitation, specific humidity, zonal, and meridional winds are shown in Fig. 4.11. The maximum positive loading for the anomalous precipitation field of 0.4 over the large east-west elongated area of the central Sudan-Sahel region (Fig. 4.11a) indicates that this mode explains about 16% of the intraseasonal precipitation variance in the region, while over the Guinean coast, a large area of negative correlation pattern is observed. Similarly, the maximum positive loading for *q* (Fig. 4.11b), zonal (Fig. 4.11c), and meridional (Fig. 4.11d) wind components are found along the central Sudan-Sahel (20^{o}W-15^{o}E), indicating that the intraseasonal variance of these fields are also explained by the combined-EOF-1 there. The patterns in Figure 4.11 indicated that for positive (negative) amplitudes of the combined-EOF-1 mode, enhanced (suppression) of *p*, enhanced (suppression) of *q*, and low-level westerly (easterly) and southerly (northerly) dominate the Sahelian (Guinean coast) regions.

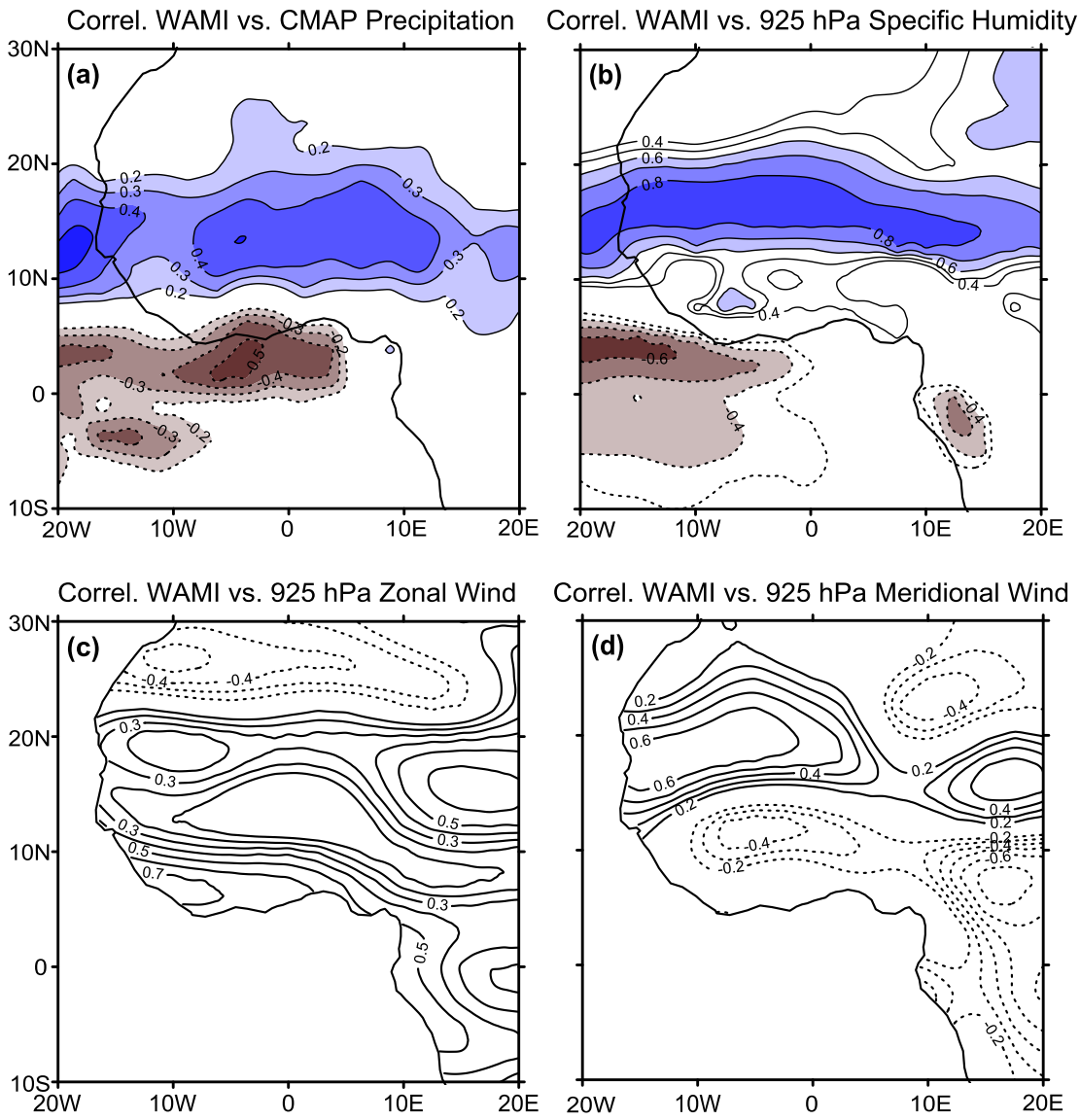

Figure 4.11: First combined-EOF patterns representing the correlation between WAMI (time series of the first Combined-EOF) and anomalies of (a) CMAP precipitation, (b) specific humidity, (c) zonal wind component, and (d) meridional wind component. Solid/dash contours represent positive/negative correlations.

Table 4.4 Percent variance explained by the first three combined-EOFs for June-July-August-September season.

Season	Combined-EOF 1	Combined-EOF 2	Combined-EOF 3
JJAS	19.6	12.3	7.1

The synoptic consistency of these departure patterns of climate variables in the Combined-EOF-1 representations can be assessed in a qualitative manner since the general relationships between the variables are well known. For example, the east-west oriented zone of strong positive correlation between the first combined principal component time series and precipitation, and between CPC1 and the specific humidity can be associated with the position of the ITCZ during this period. It is well known that during northern hemisphere high-sun season, the ITCZ migrates north from its southern position near the equator to about 20^{o}N. The contrast in correlation pattern between the Sahelian and the Guinean coast regions, suggests the enhancement of convective rainfall activities over the Sahelian zone and their suppression over the Guinean coast. The westerly and southerly wind anomalies over the Sahelian region, indicated by positive correlation in Figures 4.11c and d, are observed along with enhanced precipitation over that region, suggesting that moisture transported from the western and the southern Atlantic Ocean are important in supporting convection over the Sahelian zone in agreement with previous findings in this study.

From the above analysis, it is evident that combined-EOF-1 represents the main features of the Sahelian portion of the WAM variability because not only does it contain

many atmospheric features previously known, but these features are synoptically consistent. Also, the geographical extent as well as the time resolution of the positive phases of combined-EOF-1 is an indicator of the Sudan-Sahel phase of WAM. Therefore, the time coefficients for this first combined principal component can be used as an index to characterize the WAM variability over the Sudan-Sahel zone. Henceforth, the combined-EOF-1 time coefficients will be identified as the "West African Sudan-Sahel Monsoon Index (WASMI)" and will be used for further WAM variability investigations over the Sahelian zone. The second combined-EOF, which explains 12.34% of the total variance (not shown) is independent of the first according to the North et al. (1982) criteria. It is characterized mostly by the onset phase (in September) of the second monsoon season over the Guinean coast.

4.4.2.3 Interannual Variability of WASMI and rainfall over the Sudan Sahel Zone

Because the distribution of rainfall at the beginning of the monsoon season over WA is known to be spatially complex and variable, the decision to generate WASMI for the entire Sahelian region may appear questionable. Furthermore, as WASMI is based on few components of the monsoon cycle, its ability to characterize the monsoon rainfall variability is unclear. Does WASMI help describe the overall hydrological cycle in WA, or is the index merely a reflection of the low-level circulation?

Fig. 4.12a shows the time series of the WASMI for ten (1981-1990) summer monsoon seasons. The time series of pentad averages is characterized by seasonal-to-

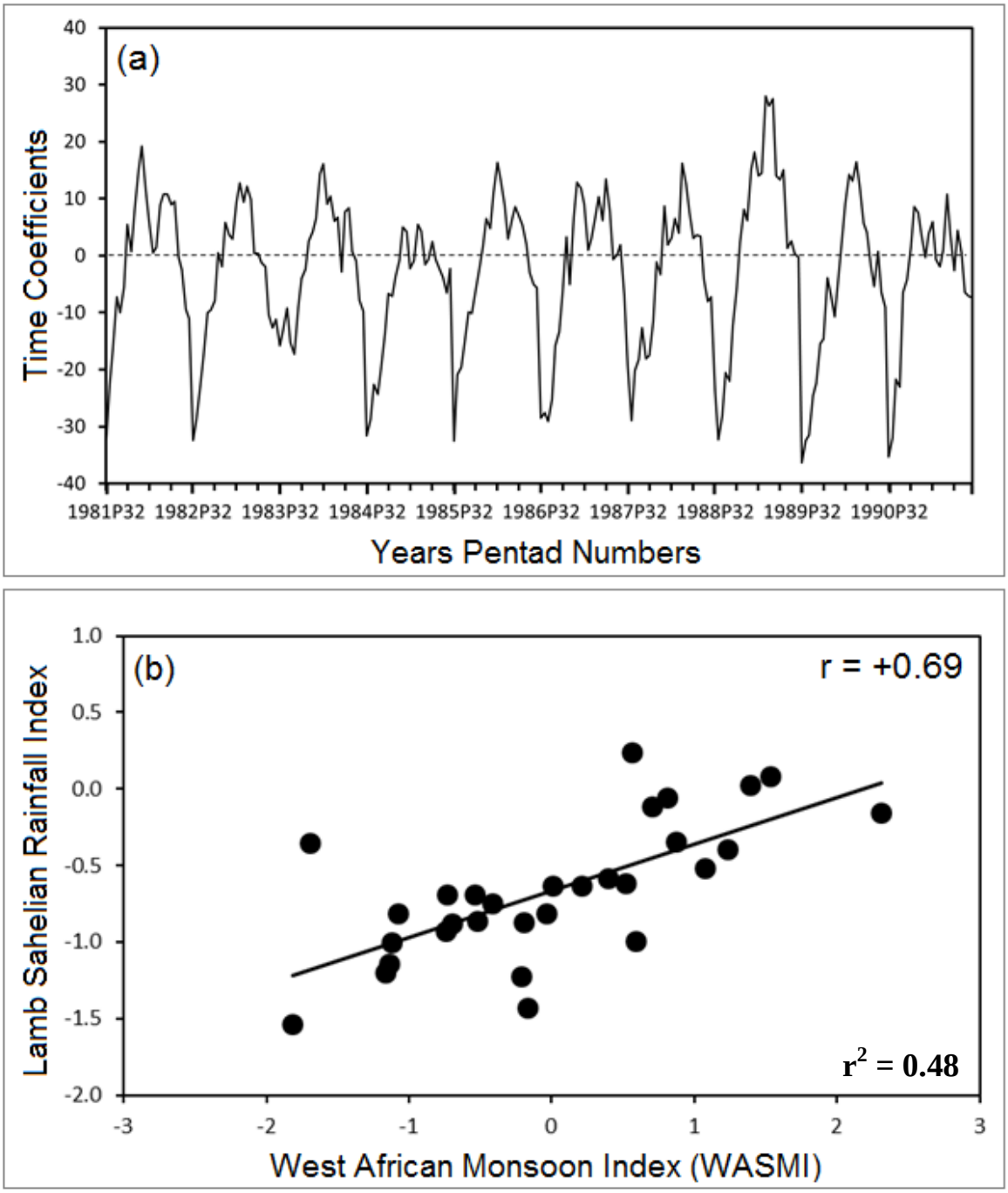

Figure 4.12: (a) Illustration of WASMI time series for 1981-1990. (b) Scatterplot and linear fit of June-September average normalized departure (σ) of WASMI versus Lamb Sahelian rainfall index for 1979-2008.

interannual variability. The annual cycles of WASMI show superimposed high frequency fluctuations, suggesting that WAM exhibits pronounced intraseasonal variability at timescales ranging from a few days to more than a month. It annual cycle also shows interannual variability, with persistent large negative anomalies throughout the drought years of 1982-1984 and 1987, and positive anomalies during the wet 1988 season (Fig. 4.12a). Positive monsoon anomalies generally begin in June around pentads 38 and 39 and increase gradually to early August (pentads 44-45) corresponding to the peak rainy season over the Sudan-Sahel region. The index starts to decrease rapidly from August to September and becomes negative again, marking the end of the (southwest) monsoon season. This WASMI seasonal cycle is in agreement to that of the ITF describe in Lélé and Lamb (2010).

To compare the WASMI time series with the widely-used Lamb Sahelian rainfall index (Fig. 1.1), JJAS seasonal average of WASMI was computed from the pentad mean values, and similar indices from monthly values of Lamb Sahelian rainfall index stations for 1979-2008. Fig. 4.12b shows the scatter diagram and the linear correlation coefficient, and Table 4.5 indicates the corresponding bootstrap confidence interval for the correlation coefficient according to the BCa bootstrap method. Since this interval does not include 0, the null hypothesize would be rejected at the 5% level (two-sided) indicating that the correlation coefficient is statistically significant at the 95% confidence interval. The relationship is positive, indicating that rainfall increases with increasing WASMI over the region.

Table 4.5 Correlation coefficient between West African Sudan-Sahel monsoon index (WASMI) and existing rainfall indices over central Sahel (10^{o}-20^{o}N, 18^{o}W-10^{o}E) and approximate bootstrap confidence intervals. The bootstrap method used is the bias-corrected (BCa).

	Pentad Scale Mean		Monthly Scale Mean	
	GPCP	CMAP	LAMB	GPCP
WASMI	0.95	0.87	0.69	0.40
CI_{lo}	0.89	0.89	0.36	0
CI_{up}	0.97	0.98	0.85	0.63
Length	0.08	0.09	0.49	0.63

Performances of WASMI vis-a-vis other sources of rainfall index over Sudan-Sahel were also tested. Table 4.5 summarizes the correlation between WASMI and other rainfall estimates over Sudan-Sahel for two different time averages, and their correspondence approximate bootstrap confidence intervals. These correlation coefficients are high when pentad time-scale is used. Also, the approximate bootstrap confidence intervals for these correlation coefficients at pentad time-scale does not include 0, indicating that they are statistically significant at the 95% confidence. This also suggests that the better WASMI can be simulated, the better the Sudan-Sahel monsoon rainfall variability can be predicted at pentad time-scale. However, it must be recognized that the fields used to construct WASMI are large scale fields, and therefore the index is only valid for the regional-scale rather than the local-scale. WASMI basically reflects the large-scale hydrological cycle and not the rainfall at a single point. It is applicable only to the Sudan-Sahel region due to the result of the EOF decomposition and not to other monsoon regions.

The WASMI-rainfall relationship however, weakens with increasing time-scale. For example, the correlation between WASMI and rainfall at the monthly time-scale (Table 4.5) is statistically significant at the 95% confidence interval using 1000 BCa bootstrap method only when the Lamb observed Sahelian index is used. On the other hand, the confidence interval for the correlation coefficient between WAMI and GPCP at this time-scale does include 0, suggesting that the null hypothesize could not be rejected. So, it can only, be argued that the correlation between WASMI and existing rainfall indices advocates that WASMI can be reasonably used to study the large-scale features of monsoon and its rainfall predictability over the Sudan-Sahel zone at time-scale less than a week.

4.4.2.4 WASMI and Worldwide Sea Surface Temperatures

Given that a contemporaneous relationship exists between rainfall and SSTs, it is of particular interest to explore if the same relationship exists between the WASMI index and SSTs. If so, to what extent are SST anomalies present in the months before WASMI onset? Answering these questions would motivate the use of SST as predictors in seasonal forecasting efforts for the Sahelian region.

Correlations between the June-September WASMI index and SSTs for different time-lags are displayed in Figures 4.13. The highest correlations are seen over the Atlantic and north Pacific Oceans. Negative correlations are depicted in the south equatorial Atlantic. These negative correlations increase and become widespread as the

WASMI onset in June is approached. Over the North Atlantic Ocean, however, positive correlations are present between the monsoon index and SST. This Atlantic basin dipole correlation pattern with the Sudan-Sahel monsoon index is consistent with some of the earliest work on the relationship between Sahelian rainfall and SST in the Atlantic (Lamb 1978a, b; Folland et al. 1986). Negative (positive) correlation means low (high) SST anomalies in a given ocean basin are a prelude to a strong (weak) WAM season. Therefore, the negative correlation with the tropical South Atlantic suggests that low SST temperatures in the Gulf of Guinea favor the enhancement of the southwesterly flow from the Atlantic Ocean into WA. This mechanism increases the flux convergence and rainfall in the Sudan-Sahel zone. A warmer South Atlantic weakens the ocean-land temperature gradient, and hence weakens the monsoon flow and the surface convergence over the Sudan-Sahel (e.g., Losada et al. 2010a). Hastenrath and Polzin (2010) also show that warmer (cooler) surface waters over the tropical North Atlantic are accompanied by lower (higher) surface pressure enhance (decrease) the cross-equatorial winds from the Southern Hemisphere and enhanced precipitation in the Sahel, in agreement with the correlation pattern found here.

The correlation of the WASMI with SSTs of the Central Pacific are weakly negative three months prior to the onset of WASMI, and suggests that the Pacific teleconnection to Sudan-Sahel monsoon variability is not as strong as the Atlantic teleconnection. However, the impact of ENSO on Sahel precipitation has been mentioned (Janicot et al. 1996; Ward 1998), and explained dynamically by Mohino et al. (2011) who suggest that a warming (cooling) in the Pacific is associated with

enhanced (decreased) large-scale subsidence over WA, resulting in decreased (increased) precipitation in the Sahel. Previous observational and modeling studies (e.g., Rowell 2003; Raicich et al. 2003; Fontain et al. 2010; Gaetani et al. 2010) also found a positive teleconnection between the Sudan-Sahel rainfall and SST anomalies in the Mediterranean. While the physical mechanism of this relationship needs to be clarified through modeling experiments, there is some agreement that the warming enhanced evaporation that provides additional moisture in the lower troposphere, which results in enhanced northerly moisture transport toward the Sahel.

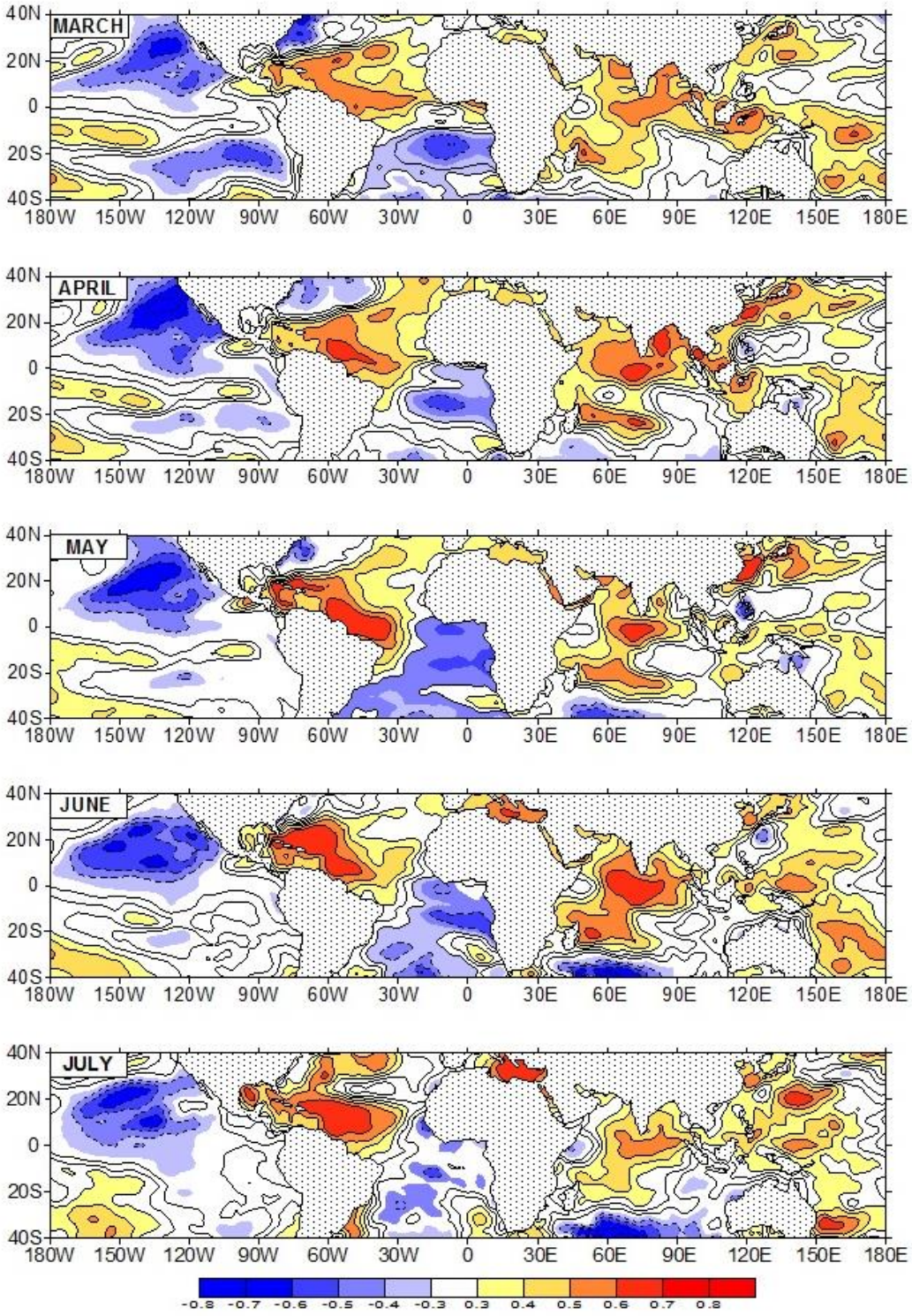

Figure 4.13: Lag-correlation patterns between average June-September WASMI index and monthly SSTs for the period 1979–2008.

4.5 Analysis of the 30-90 Day Mode of Variability

The wavelet decomposition and the Fourier transform of the divergence of moisture transport shown in section 4.2.2 indicates a significant power peak around the 30-60-day timescale - similar to that of the MJO. Hence, the intraseasonal variability of the West African moisture transport is examined, with the emphasis on the 30-90 day timescale. Temporal filtering is therefore employed to assess the MJO signal in time series of the different large scale circulation fields associated with the WAM variability and the vertically integrated moisture transport field in order to separate these timescales for cross-correlation and regression purposes.

The circulation variables such as the NCEP-NCAR reanalysis streamfunction field and the SLP, the NOAA-reconstructed OLR field, and the vertically integrated moisture transport field were bandpass filtered for 30 years of each June-October segment at each grid point, using a linear nonrecursive digital filter with half-power points at 30 and 90 days. The bandpass filtered data is used to assess the strength of the 30-90 day oscillations, and to compare the large-scale features associated with the intraseasonal oscillation (ISO) of the boreal rainfall season over WA.

4.5.1 WASMI Time Series of 30-90 Day Variance

A better representation of the spatial structure of the ISOs and their relationship to large-scale features can be achieved by constructing an index of monsoon ISOs (Goswami 2005). Such an index was constructed in this study based on the 30-90-day

bandpass filtered WASMI time series. The filtered time series is normalized by its own standard deviation and the resulting normalized departure (σ) time series is referred to as the West African Sudan-Sahel ISO index.

Figure 4.14 portrays the pentad average ISO index for the West African Sudan-Sahel zone during the June-September (1979-2008) period. Also shown in the Figure are examples of periods with indices exceeding +1 standard deviation (open blue circles), and those which indices that are below the -1 standard deviation threshold (red diamonds). Periods of ISO with indices > +1σ (< -1σ) represent the wet spell (dry spell) monsoon phases and often are referred to as active (break) monsoon periods.

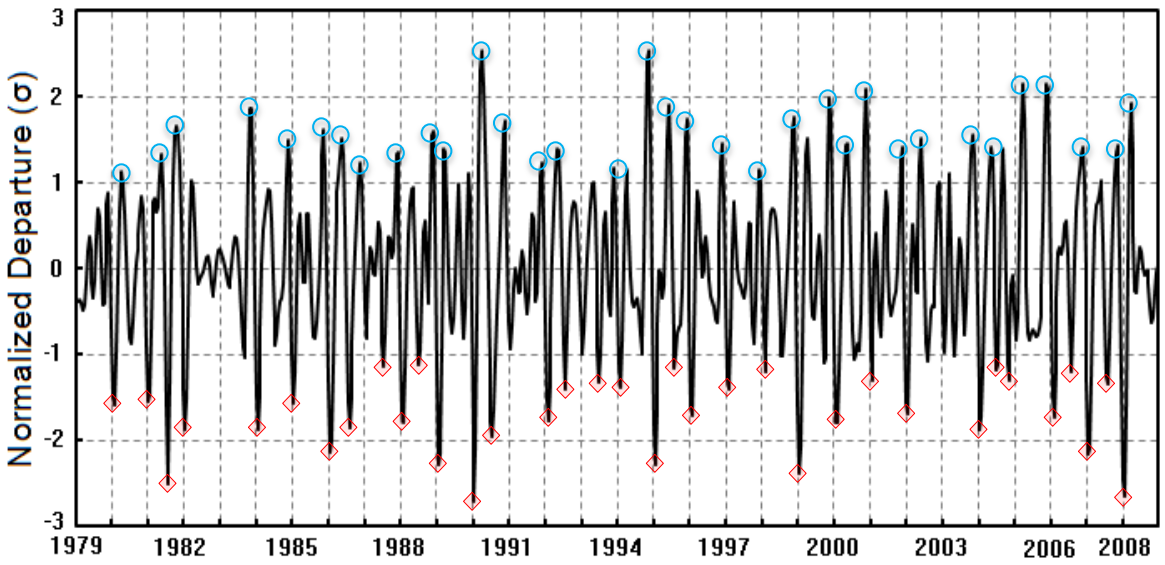

Figure 4.14: Time series (pentad values) of normalized departure (σ) of the June-September (1979-2008) West African Sudan-Sahel monsoon intraseasonal oscillation index (ISO), see text. Open blue circles indicate the peaks in the monsoon active phase or wet spells, and red diamonds indicate the break periods or dry spells.

Intraseasonal wet (dry) spell anomalies were defined when the ISO indices were above (below) +1σ (-1σ) of the ISO time series. In total, of the 720 pentad values of the Sudan-Sahel monsoon ISO index for June-September (1979-2008), 86 wet and 96 dry spells were identified and examined in this study. This represents a sufficiently large sample to generalize the space-time structure and convection associated with ISOs over the region.

4.5.2 Space-time Structure of the Atmospheric Circulation and Convection Associated with WAM Intraseasonal Oscillations

4.5.2.1 Composite Analysis

Understanding the space-time structure of large-scale atmospheric circulations and convection associated with the intraseasonal wet and dry spells is our main concern in this section. The description of the large-scale circulation is based on the 850-hPa streamfunction field. Streamfunction (ψ) has a distinct advantage to represent major low features somewhat more clearly since its field is a reflection of the quasi-nondivergent nature of large-scale atmospheric flow. Hence, previous studies (e.g., Rosen et al. 1979b) of the relationship between the global scale atmospheric circulation and the water vapor transport suggests that the later can be illustrated by means of the ψ. Since the large-scale atmospheric circulation is essentially nondivergent (except in the PBL near the ITCZ) (e.g., Chen and Wiin-Nielsen 1976; Chen 1985), it is not surprising that the large scale atmospheric water transport can be largely described by the nondivergence component (Rosen et al. 1979b).

Figure 4.15 portrays the composites of the average atmospheric moisture transport field and associated large scale convective zones for wet (Figs. 4.15a, c) and dry (Figs. 4.15b, d) monsoon spells. Both composites are shown for the zero lag only. The intraseasonal wet (dry) spell events are characterized by significant enhancement (suppression) of convection across the West Africa Sudan-Sahel region. Wet spell (dry spell) events in the Sahelian region (north of 10^{o}N) are accompanied with dry spell (wet spell) events in the Gulf of Guinea (South of 10^{o}N). During active monsoon events (Figs. 4.15a, c), a low-level cyclonic cell developed over the northwestern coast of WA, centered at approximately 25^{o}W and 18^{o}N. The associated monsoon trough extends inland over the west coast of Africa. A strong east-west circulation is present with westerly/southwesterly moisture flux into the Sahelian region. The low-level westerly flux approaches the Guinea highlands and stagnates over the west coast and central Sahelian regions where intense convection develops. The main area of convection lies near the Guinea highlands and over the Air Mountains, as indicated by both the OLR field (Fig. 4.15a) and the divergence of the moisture transport fields (Fig.4.15c). Regions of moisture sink (deep convection) during the intraseasonal wet spells are located west of the negative ψ (dashed contours) cell while regions of moisture source (suppressed convection) are located east of the positive ψ (solid contours) cell. This large-scale circulation feature during the active monsoon phase is consistent with the characteristic of the zonal-mean flow in low latitudes. That is, in the tropics, positive ψ anomalies are coupled with a clockwise east-west circulation and negative ψ anomalies with counterclockwise east-west circulation.

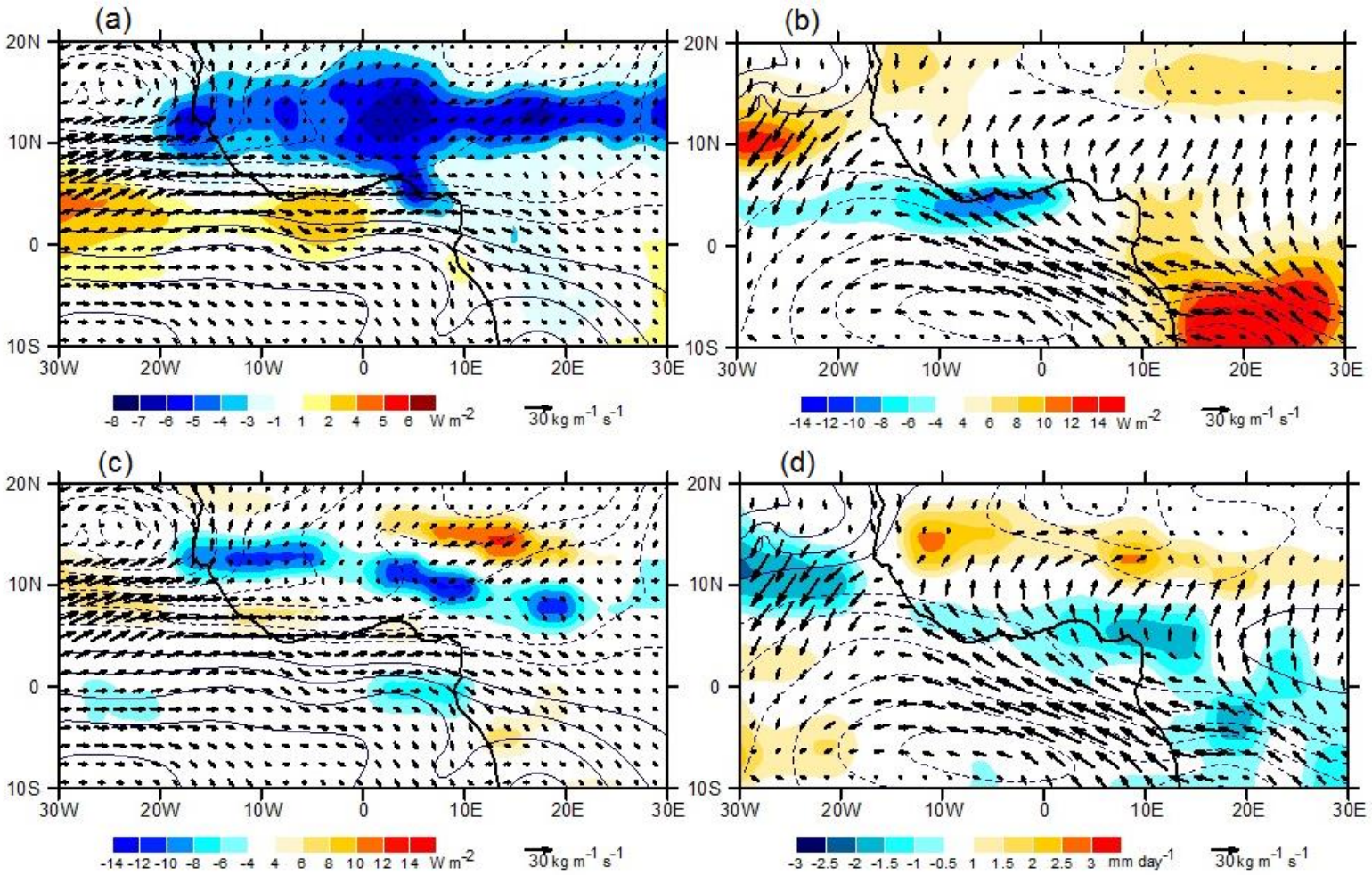

Figure 4.15: Composites of (a) pentad average OLR (shading, W m^{-2}), 850-hPa streamfuction (ψ, contour, 1 X 10^5 m^2 s^{-1}), and vertically integrated (from surface to 850-hPa) moisture flux (vectors, kg m^{-1} s^{-1}) with respect to the WASMI ISO index (Figure 4.13) for wet June-September (1979-2008) monsoon events. (b) Same as in (a) but for dry JJAS monsoon events. (c) and (d) Same as (a) and (b) respectively but with moisture transport divergence (shading, mm day^{-1}). Dashed/solid contours are negative/positive ψ.

During intraseasonal dry spell events (Figs. 4.15b, d), the low-level cyclonic circulation (negative ψ) associated with the monsoon trough initially centered over the northwestern coast of WA is replaced by a low-level anticyclonic circulation (positive ψ) and associated ridge. This induced northeasterly flow which suppress the westerly moisture flow from the eastern Atlantic Ocean into the Sahelian zone. Over South Atlantic however, a weak anticyclonic circulation is present, but its associated moisture transport supply the Guinea coast region only. As result of all of the above, weak convective activities appear in the Guinea coast while the Sudan-Sahel remains dry.

The description above suggests that large-scale intraseasonal changes in the tropical circulation have accompanied the dislocation of convection from the Sahelin zone, in agreement with Ward (1998) who also found that a wetter Sahel is accompanied by a lower sea level pressure (SLP) trough in the tropical north Atlantic, northern Indian Ocean, and equatorial western Pacific Ocean. These changes in the circulation induce a significant decrease in moisture transport and convergence over the Sahel. For instance, the transport of moisture from South Atlantic barely sustains its northward latitudinal progression. Its magnitude during the dry spell events is weaker in the Sahelian region compared to during the wet spell events, but remains stronger over the Guinea region. In addition, suppression of the westerly moisture flow is observed due to the intensification of the high pressure system in the North Atlantic Ocean. This intensification of the Azores high pressure circulation favors the enhancement of the hot and dry northeasterly Harmattan flow, emanating from the Sahara resulting in a dry

spell condition in the Sahel region while a relatively wet spell condition is observed over the Gulf of Guinea.

4.5.2.2 Cross-Correlation and Lag Regression Analysis

To further illustrate the time evolution of convection and associated large-scale circulation during a typical intraseasonal event, cross-correlation and lag-linear regression technique using the WASMI ISO index as predictand was applied. Lag regression analysis of the 30-90 days bandpass filtered variables at a number of vertical levels, and 30-90 days filtered WASMI permits depiction of the life cycle of convection over WA and its relationship to the ISOs. Although both the wet and the dry spell composites are generated separately, comparable fields can be obtained by using only the wet or dry spell events, and then generating the others as a function of time lag. Here, the study make used of the wet spell events which consist of the ensemble of strong ($> +1\sigma$) deviations of the 30-90 days bandpass filtered WASMI time series to investigate the life cycle of summertime intraseasonal convection and its associated large-scale circulation over West Africa.

Figures 4.16 and 4.17 display maps of the lagged cross-correlation and linear regression coefficients of 30-90-day filtered OLR, 925 hPa ψ, and vertically integrated moisture flux and its divergence upon the identically filtered WASMI ISO index. Recall that OLR data (Liebmann and Smith 1996) is used as proxy for tropical deep convection, where low OLR values correspond to cold cloud tops associated with

convective activity and high precipitation in the tropics. Therefore, the life cycle of convection relative to the West African summer intraseasonal variation is indicated by the shaded contours in both Figs. 4.16 and 4.17 where only grid point values that are statistically significant from zero at the 95% confidence level of the Student's *t*-test (Wilks 2006, 131-135) are displayed. The spatial pattern of convection over West Africa during wet events (Lag 0) and dry events (i.e. Lag +4) corresponds well with the wet (dry) patterns describe in other studies (e.g., Matthews 2004; Maloney and Shaman 2008; Janicot et al. 2011).

The relationship between WASMI and OLR fields (Fig. 4.16 and Figs 4.17) shows that when the Sahelian index lags the moisture transport by 4 pentads (20 days), a negative OLR anomaly (enhanced convection) is only apparent over the South Atlantic Ocean, centered at about 4^{o}W-3^{o}N, and only affects the coastal regions of the continent while the rest of WAM domain is characterized by nil to positive OLR anomalies. At Lag -3, the convective cell initially over the Ocean has moved northeastwards and occupies the Gulf of Guinea regions. Negative OLR anomalies also appear over the region of the Air Mountains and over the Ethiopian highlands, indicating the presence of weak convective activity. These new regions of convection, grow in time, propagate westwards, and straddle the central Sahel at Lag -2 and Lag -1. Beginning at Lag 0, an east-west elongated convective band that extends northerly to about 17^{o}N, developed across the Sahel and the West Atlantic Ocean. At this time a dipole structure is observed over the region with enhanced convection (large area of negative OLR anomalies) over central Sudan-Sahel and their suppression (positive OLR

anomalies) over the Gulf of Guinea region. Regions of convective activity over the central Sahel seems to continue propagating westwards and eventually dissipate over the western coast of Africa three pentads later.

The spatial evolution of cloudiness described by the OLR anomaly in Figs. 4.16 and Figs. 4.17 is also well illustrated by the lag regression of the divergence of moisture transport upon WASMI ISO index (Fig. 4.18 and Figs. 4.19). The life cycle of precipitation calculated from the divergence of moisture flux within WAM region (Fig 4.19) is very similar to that obtained from station data (Fig. 3.2) and indicates that the 30 to 90-day monsoon intraseasonal variability with wet and dry events is not confined to the WAM region, but has a much larger spatial scale - extending from the western Atlantic Ocean to the eastern and central Africa. One important characteristic of the WAM interannual variability describes by observational analysis and other diagnostic studies is the dipole-like structure over the Gulf of Guinea and the central Sahelian region. This analysis confirms the North-South dipole in precipitation at the intraseasonal timescale characterized by wet (dry) spell conditions being associated with enhanced (decreased) precipitation over central Sudan-Sahel and decreased (enhanced) precipitation over the Gulf of Guinea region.

4.5.3 Moisture Build-Up Mechanism

The water vapor transport anomalies associated with typical intraseasonal anomalous rainfall patterns can also be estimated by regressing the vertically integrated

moisture transport anomalies with the WASMI ISO index. The structure of 30 to 90-day time sequences of moisture transport associated with anomalously wet (dry) spells is illustrated by the flux transport vectors in Figs. 4.16-19 superimposed on the 925-hPa ψ contours. While only those moisture vectors where the local correlation coefficient is statistically significant at the 95% confidence interval are shown for either the zonal or meridional components, the ψ however, is displayed regardless of the statistical significance.

The ψ structure during suppressed convective activity (Lag -4 in Fig. 4.18), shows an anticyclonic cell over the southern Gulf of Guinea, centered near 3˚W, 4˚S. Due to the structure of this cell only a small moisture flux reaches the northern coast of the Gulf of Guinea. Fifteen days prior to the wet spell (Lag -3), the anticyclonic cells located over the Ocean intensify, and another cell develops over land, and centered just above of the oceanic cell. The southeasterly transport of water vapor by the marine cell becomes stronger, and often reaches the coast of Africa where it changes direction to become southwesterly flow, due to the influence of the continental anticyclone and the coriolis effect. As a result, moisture flux from South Atlantic begins to penetrate into the continent. In addition, there is a well-developed wave train over the continent in the regions north of 10^{o}N extending from the northwestern Atlantic Ocean through the Eastern part of Africa, contributing to the enhancement of West African moisture build-up.

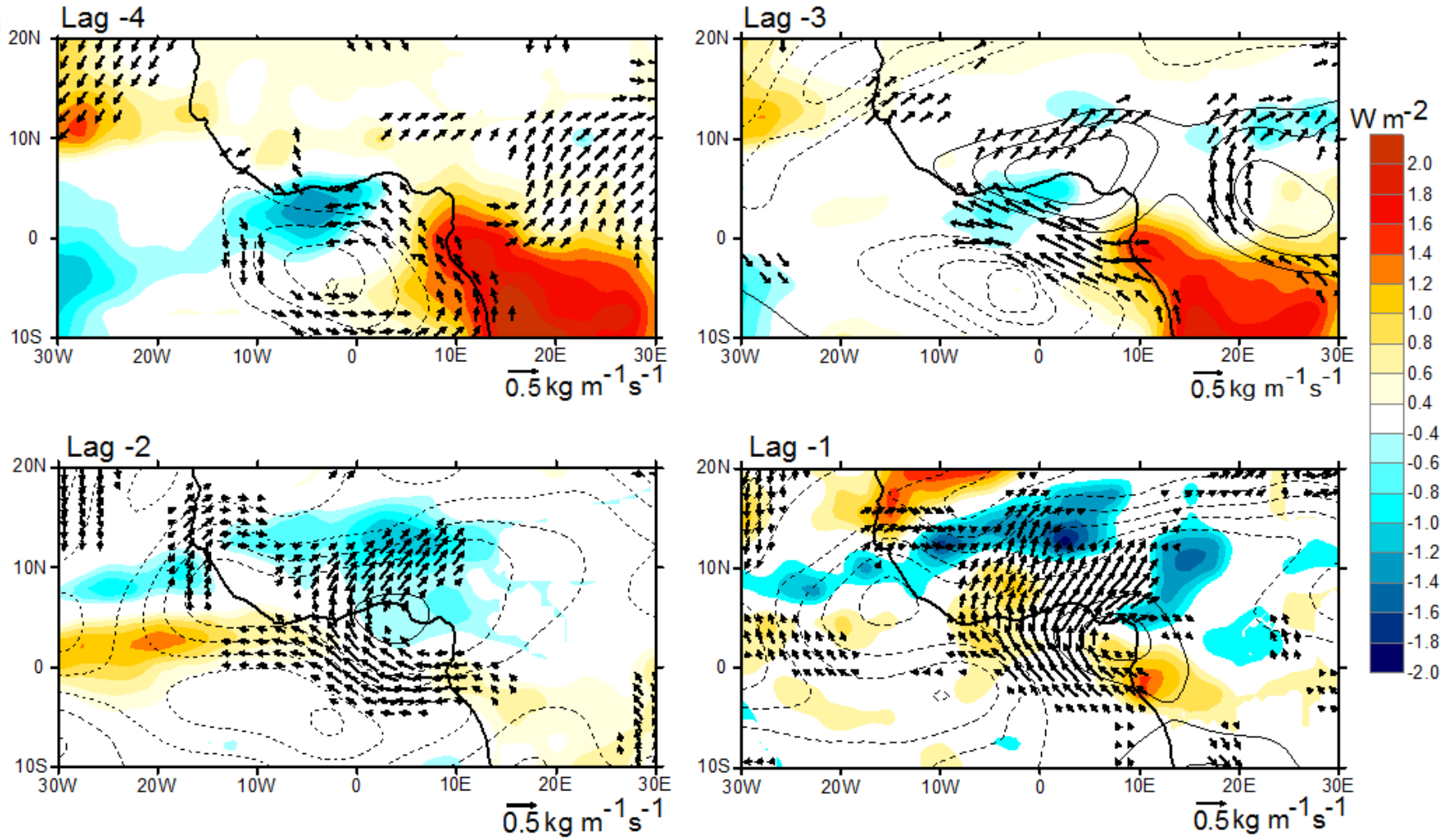

Figure 4.16: Horizontal structure of dominant intraseasonal variability. Lag regressions of OLR (shading, W m^{-2}), 925-hPa streamfuction (ψ, contour, 0.4 X 10^5 m^2 s^{-1}), and vertically integrated (surface to 850-hPa) moisture flux (vectors, kg m^{-1} s^{-1}) anomalies upon WASMI ISO index associated with +1σ deviation. Lagged regressions are for JJAS pentad averages between -4 and +3 pentads. Only locally significant grid point values at the 95% level OLR and moisture flux are displayed.

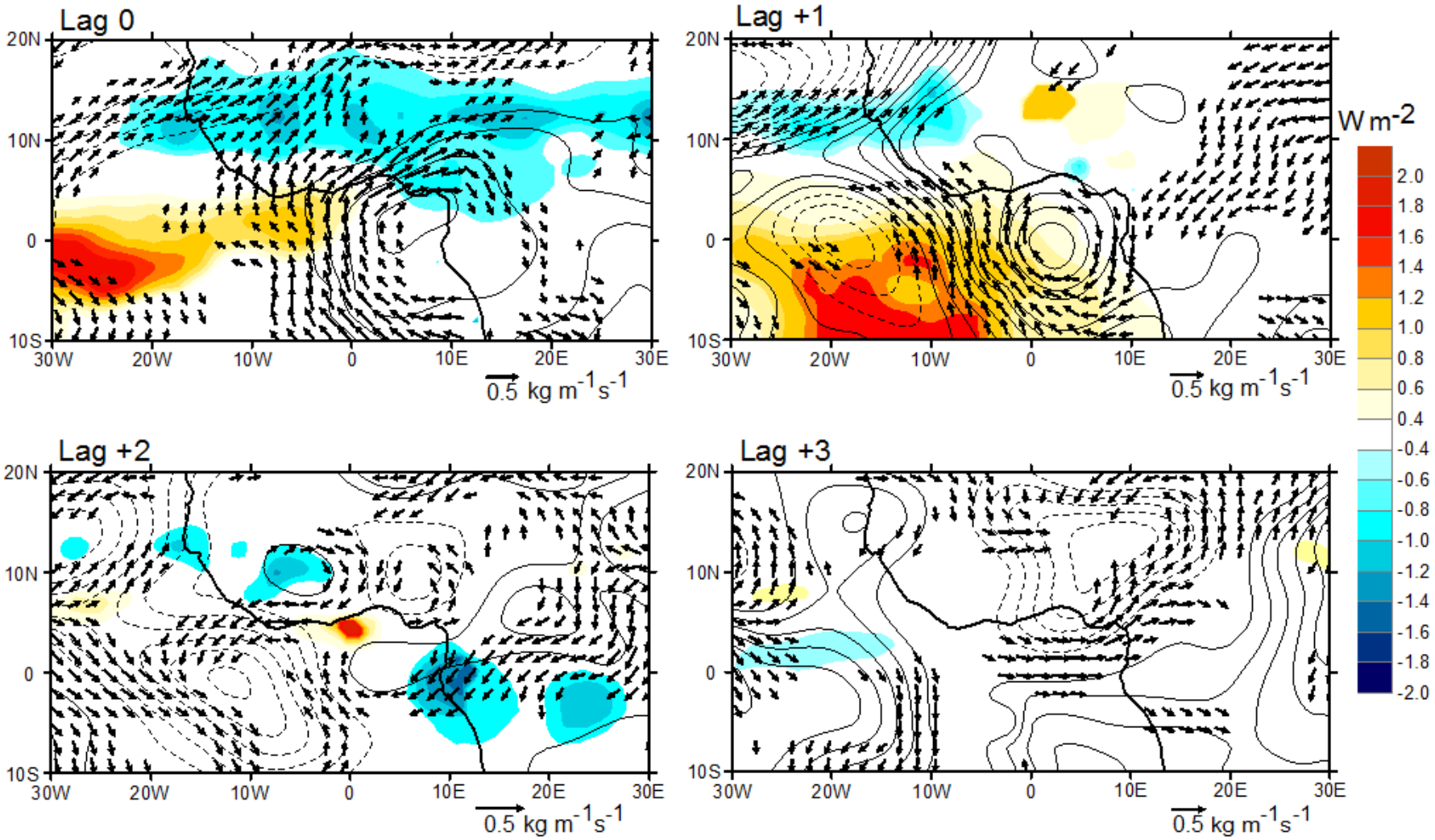

Figure 4.17: Continued of Figs. 4.16 for Lag 0, Lag +1, Lag +2, and Lag +3.

The anticyclonic cell on Lag -4 moves northward and intensifies by Lag -1. This increases the southwesterly flux over the Guinean coast and the flux reaches its greatest northward intensity by Lag +1, when the anticyclonic cell has moved westward to be centered at about 0^{o} latitude and 20^{o}W and is no longer intense. The southwesterly flux was enhanced by a well-developed cyclonic cell centered over the Gulf of Atlantic Ocean that extends inland, and its associated cyclonic moisture transport penetrates deeper inland and provides sufficient moisture for the Sahelian region. A low-level jet of westerly moisture transport develops as a wave train over the west coast of Africa and becomes stronger by the time of the active monsoon phase. By Lag 0, both the southwesterly and the westerly fluxes have intensified and have reached the Sahelian region where convection is favored. By Lag +3 the features evident early in the cycle are no longer present over the Sahelian zone. Instead, the Sahelian region is characterized by a well-developed cyclonic cell centered at about 10^{o}E-10^{o}N, and by the suppression of moisture inflow over WA. Prior to the suppression of the westerly and southwesterly transport of moisture, two adjacent cells are visible along the Equator by Lag +1. One is an anticyclonic cell centered along 20^{o}W and 0^{o} latitude, which favors a southeasterly moisture transport over the southwestern coast of the continent. The second, a cyclonic cell is centered at about 2^{o}E and 0^{o} latitude. Consequently, the envelope of enhanced convection begins to shrink over the central Sahel, due to the dry northeasterly flows that began to penetrate into the region.

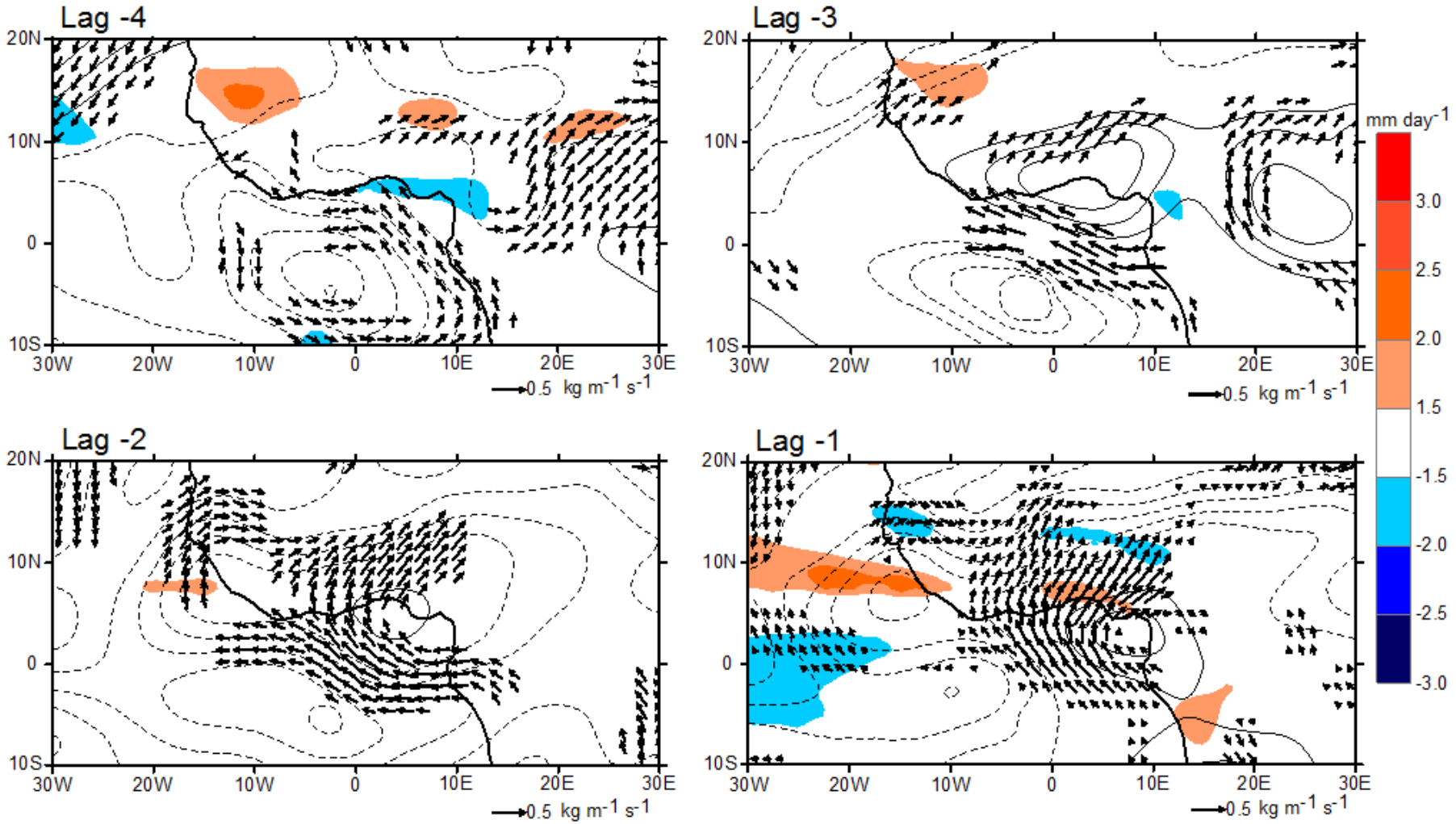

Figure 4.18: Same as Fig. 4.16 except for moisture convergence (shaded).

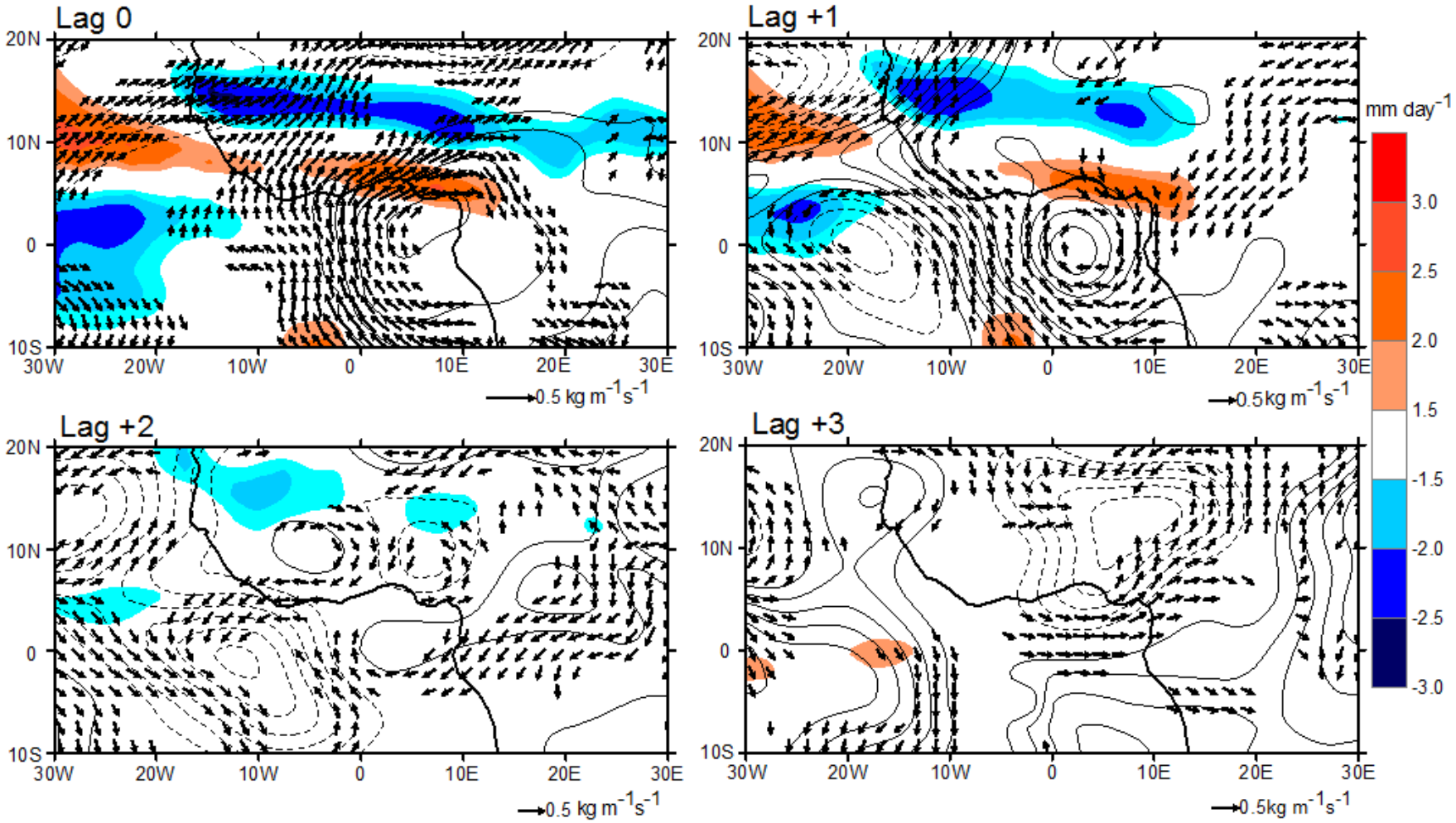

Figure 4.19: Same as Fig. 4.17 except for moisture convergence (shaded).

Interestingly, the statistically significant westerly/southwesterly moisture flux anomalies associated with the two branches of water vapor transport are accompanied by wet spell events, as convection reaches a peak over the Sahel, along with the downstream cyclone-anticyclone coupled, indicative of the amplification of waves across the region. The convective activity over the Atlantic is also enhanced. Note that the anomalously convective signal develop over regions east of 10^{o}E, starting at Lag -2, have moved westward in agreement with the westward propagation characteristic of West African convective activities (Fig. 4.11). Also, a northwestwardly oriented convective envelope is apparent and extends from the south Atlantic to about 20^{o}N. This feature is illustrated in Fig. 4.20 which portrays the Hovmöllor time-latitude representation of convection along 10^{o}W, 0^{o}, and 10^{o}E. Intraseasonal convection along these longitudes has some active and pause events as the convection envelope seasonal cycle moves northwestward.

Analysis of the intraseasonal variability of convection and moisture transport provides insight into the mechanisms controlling the space-timescales variability of convection over WAM region. The coherence evolution of the divergence of moisture transport and OLR is associated with the 30-90 days mode of intraseasonal oscillation. This characteristic of the intraseasonal evolution of WAM provides an insight for potential predictability of its variables beyond the skill of current numerical weather models. The mechanism of westward propagating convective activities was suggested by Lavender et al. (2009). In a GCM simulation with and without soil

moisture coupling at intraseasonal scales, the authors suggested that westward propagating convective activity probably is controlled by an internal atmospheric mode, although they did not specify which mode. This prompted the study by Janicot et al. (2011) which suggested that this atmospheric mode might be due to a convectively coupled equatorial Rossby wave signal which also propagates westwards.

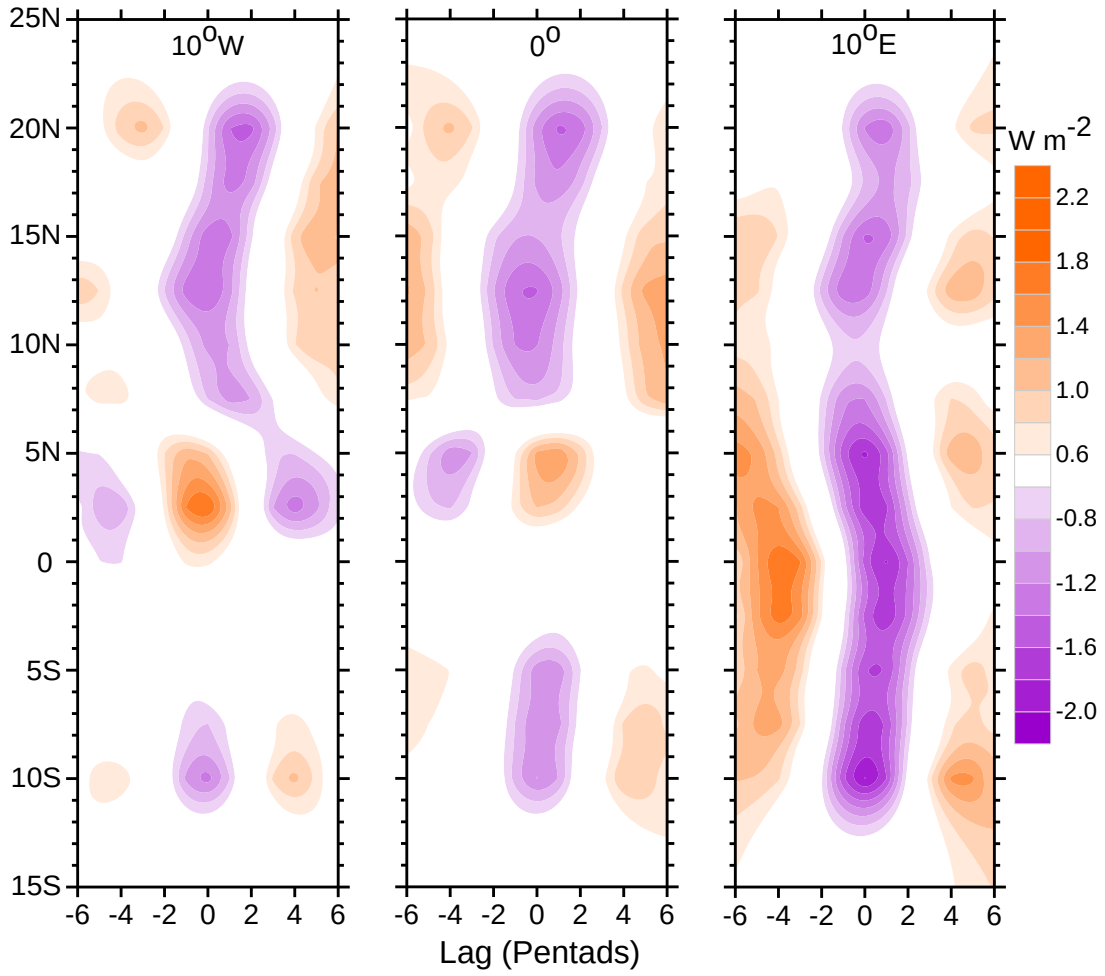

Figure 4.20: Lag-latitude cross-sections along 10°W, 0°, and 10°E of regressed OLR. Purple indicates convergence, and orange indicates divergence.

4.5.4 Circulation Associated with the 30-90 day Moisture Transport

The structure of the cross-correlation between WASMI and the upper and low-level circulation of the 30 to 90-day mode over WA and adjacent ocean is illustrated in Figs. 4.21-23. Again, only wind vectors in these figures that are statistically significant at the 95% confidence level are shown.

Fifteen days prior to convection, the upper level circulation is characterized by a strong easterly jet, namely the TEJ. This suggests that the 30-90-day of intraseasonal wet spell is associated with a strong TEJ, in agreement with previous studies of the interannual timescale relationship of the TEJ and WAM rainfall during contrasting years (e.g., Chen and van Loon 1987; Grist and Nicholson 2001). These studies have shown the decrease of the TEJ during dry monsoon years. As the convection period approaches (Lag -1), the TEJ is stronger, but the jet axis has also shifted northward, consistent with its characteristics during wet periods (e.g., Nicholson et al. 2007). On the day of maximum cloudiness (Lag 0), the jet core is tilted southwest-northeast, associated with the intensification of a cyclonic gyre that flanks the equator southwest of the enhanced continental convection zone. These upper-level gyres were found in other studies and have been associated with the Rossby wave response to the equatorial heating (e.g., Webster 1972; Gill 1980; Sardeshmukh and Hoskins 1988). After convection (Lag +1), the TEJ weakens.

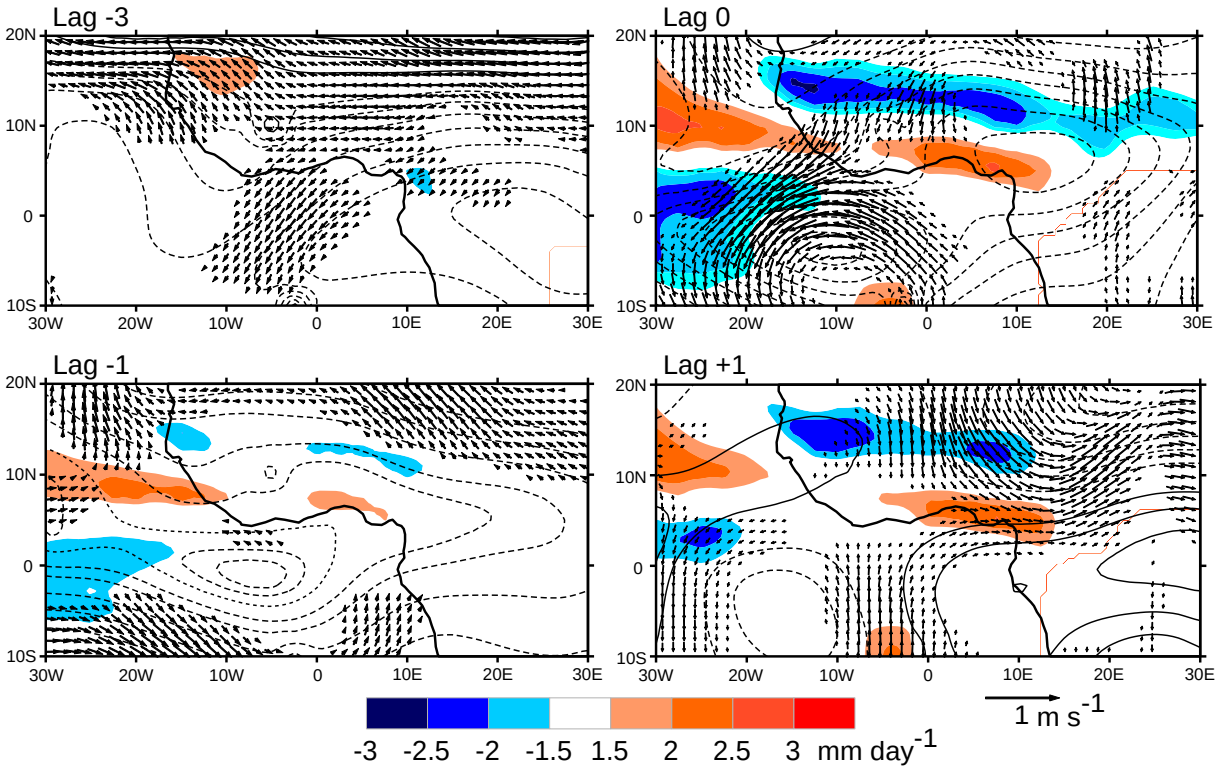

Figure 4.21: Spatial structure and amplitude of the 30-90 days June-September mode of variability. Regressed 30-90 days filtered of moisture flux convergence (shaded) 200-hPa winds (vectors), and 200-hPa streamfunction anomalies upon the WASMI ISO time series. Lagged regressions between -3 and +1 pentads are shown. Only regressed moisture flux convergence and wind anomalies significant at 95% confidence level are plotted. Streamfunction contour is 0.4 x 10^5 m^2 s^{-1} with zero contours omitted.

The low-level winds associated with the 30-90 day mode are shown in Figs 4.22 and Figs. 4.23 for the 850-hPa, and 925-hPa, respectively. Their structure is generally similar to that of the mode of the vertically integrated low-level moisture transport, and also to that of the seasonal mean, strengthening (weakening) prior (after) the occurrence of convective activities. At the 850-hPa level, significant southeasterly wind anomalies, that changed later to southwesterly over the continent, occurred in two locations. One is

centered at 0^{o} longitude, and the other at 30^{o}E, suggesting the regional character of WAM. Interestingly, the strong trade winds at 850-hPa are not accompanied with significant convection of the Gulf of Guinea, a phenomenon also found by Maloney and Shaman (2008). The passage of the Kelvin wave is be noted at 925-hPa as the anomalous easterlies to the west of the convergence zone appear at Lag -1 cycle. The passage of the wave is followed by westerly wind anomalies which lead to an enhancement of the zonal moisture flux component inland and off the west coast, at the location of the westerly low-level jet.

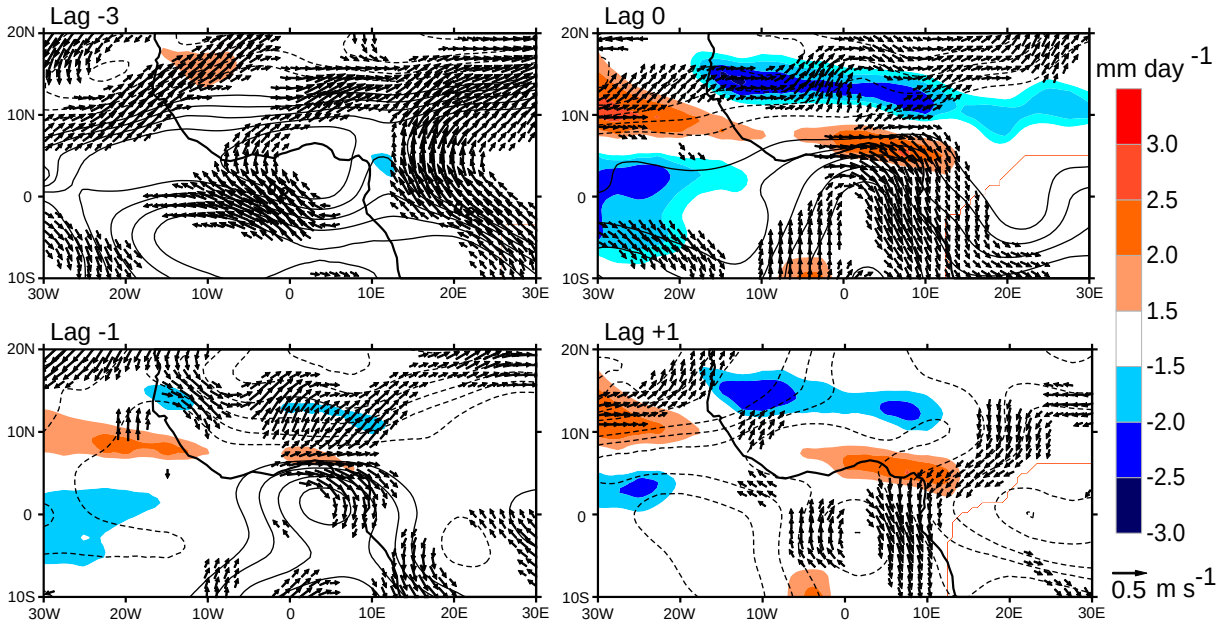

Figure 4.22: Same as 4.20 except for 850 hPa.

The 30-90 day mode of intraseasonal variability of the WAM is investigated in this section with emphasis on the variability of water vapor transport. A large-scale and temporal structure, as well as the regional propagation characteristic of the WAM, is presented. ISO activity may modulate the total summer monsoon rainfall over Africa, and therefore need to be taken into consideration for prediction purposes. It is found that summer moisture build-up over WA starts over the Guinean coast 20 days prior to the occurrence of convective activities over the Sahelian region, and progressively continues to build-up as time evolves. A North-South dipole in precipitation exists at the intraseasonal timescale with wet (dry) spell conditions being associated with enhanced (decreased) precipitation over central Sahel and decreased (enhanced) precipitation over the Gulf of Guinea region.

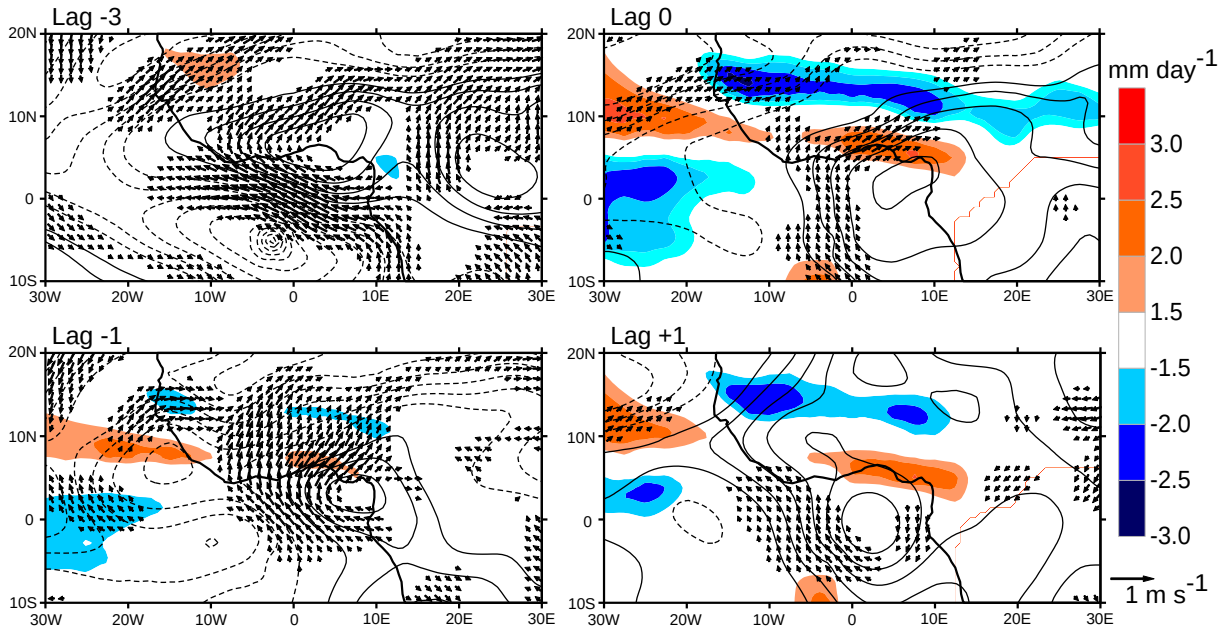

Figure 4.23: Same as 4.20 except for 925 hPa.

Matthews (2004) suggested that the equatorial Kelvin waves and Rossby waves could link the MJO in the Indian sector with the longer intraseasonal timescale mode (e.g., 30-90 days) of the African monsoon. The mechanism proposed by Matthews (2004) is that, in response to the changes in the equatorial warm pool convection, a Kelvin wave response propagates eastward and an equatorial Rossby wave response propagates westward. After completing a circuit of the Earth, they meet 20 days later over Africa, where the negative mid-tropospheric anomalies in the Kelvin and Rossby waves favor deep convection. However, due to the dominant westward propagation of the 30 to 90-day mode of convection, it can be argued that convectively coupled Rossby wave signals dominate the mode of intraseasonal variability over WA, also suggested by Janicot et al. 2009, 2011, and by Lavender and Matthews 2009.

The mechanism of the poleward propagation of the 30-90 day mode of moisture transport and associated convergence areas can explain the appearance and the characteristics of the stationary waves across the region during the wet episode of the monsoon season, and their relationship to the east-west circulation. It is well known (e.g., Lau 1979) that in the midlatitudes, the upward motion is observed ahead of the trough and downward ahead of the ridge. This circulation pattern reversed in the tropics when dealing the streamfuction, so that in the lower level, the upward motion occur east of the positive ψ cell, while the downward motion branches manifest west of the negative ψ cell. This mechanism summarized in Fig 4.24, and known as the Sverdrup regime, enhanced the northward shift of the rain producing system during the seasonal cycle of WAM.

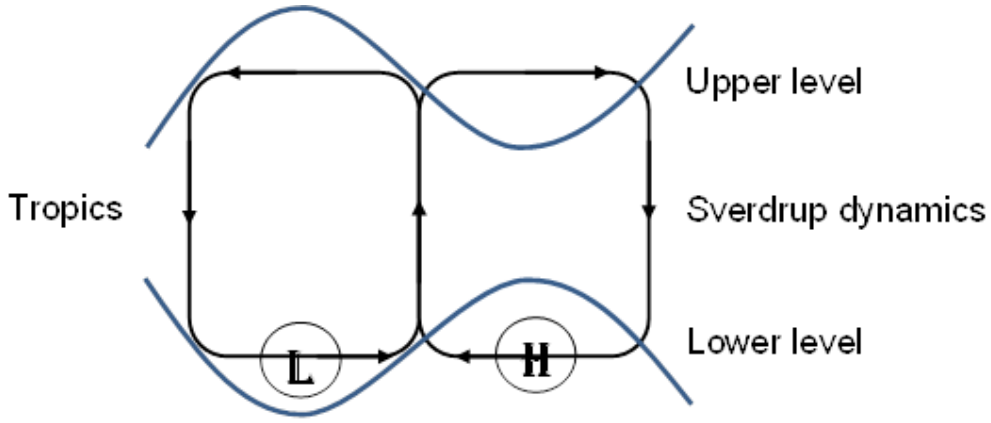

Figure 4.24: A schematic diagram of the relationships between stationary waves (thick-solid sinusoidal blue lines) and the east–west circulation (thin-solid lines with shafts) in the Tropics. Adapted from Chen (2005).

Chapter 5

5. Predictability of West African Monsoon Onset and Withdrawal Dates and Numerical Simulations of its Features using the Weather Research and Forecasting (WRF) Model

5.1 Background

Since more than 60% of the world population resides in monsoon regions, the ability to forecast monsoon features has great socio-economic importance (e.g., Ramage 1971; Webster et al. 1998; Lau et al. 2000a, 2000b; Webster and Yang 1992). These monsoon regions include the WA Sudan-Sahel zone which comprises countries with the most rapidly growing populations on the planet, and where most people are subsistence farmers. Hence, the coming and goings of the monsoon are vital to the livelihood of people to grow food and feed themselves. Unfortunately, predicting the WAM remains a challenge for both weather and climate models. From the IPCC AR4 (2007) report, it is apparent that current climate models have difficulty in simulating key elements of African climate, including the WAM. Such limitations are due not only to the poor observational coverage over the region, but also to the coarse spatial resolution of current GCMs. In this regard, Regional Climate Models (RCMs) forced by GCM output, have become valuable tools for studying the multiple interactions between

components of a regional climate system. This method offers the possibility of increasing the horizontal resolution of climate models while keeping the computational cost reasonable.

Over the last decade, research in regional climate modeling in many parts of the world has demonstrated the usefulness of downscaling tools for providing climate information at scales appropriate for societal use. However, until recently, few of these studies have been conducted over WA. After the AMMA (Redelsperger et al. 2006) field experiment substantial modeling efforts have been conducted. These have included the AMMA land-surface Model Intercomparison Project (ALMIP; Boone et al. 2009), the AMMA "Couplage de l'Atmosphere Tropical et du Cycle Hydrologique" (AMMA-CATCH) project (Lebel et al. 2009), the AMMA Model Intercomparison Project (AMMA-MIP; Hourdin et al. 2010), the West African Monsoon Modeling and Evaluation (WAMME) project (Xue et al. 2010; Druyan et al. 2010), and the Ensembles-based Predictions of Climate Change and their Impacts (ENSEMBLES) African project (Paeth et al. 2011).

Some of the previous climate simulations for WA have used versions of the International Center for Theoretical Physics (ICTP) Regional Climate Model (RegCM). This study uses the WRF model to investigate its ability to realistically simulate WAM features and to study the processes responsible for WAM precipitation. First, an empirical investigation of the large-scale WAM onset and cessation is described using the WASMI time series developed in the previous chapter.

5.2 WAM Onset and Withdrawal

Forecasting the WAM onset and withdrawal dates has great economic significance for the Sudan-Sahel region because of the shortness of the rainy season. However, objectively defining the timing of the onset and withdrawal is a difficult task. Previously, it has been shown that the onset of the Sudan-Sahel summer monsoon season is characterized by a large-scale northward shift of the ITF/ITCZ and associated rain band (e.g., Sultan and Janicot 2000, 2003; Sultan et al. 2003; Fontaine and Louvet 2006; Lélé and Lamb 2010), and the withdrawal is characterized by a fast southward shift of the ITF/ITCZ. However, reliable forecasts of the onset and cessation dates currently are lacking, and are unable to assist farmers and decision-makers who need the information ahead of time.

5.2.1 Definition of Onset and Withdrawal dates

Our definition of onset and cessation is based on the Fasullo and Webster (2003) criteria. These dates must be i) associated with the establishment of the large-scale processes that drive the monsoon circulation ii) relatively insensitive to individual synoptic disturbances, and bogus monsoon onsets and active-break transitions that occur within the monsoon season iii) based on fields that have been well observed over an extended period, so that the method can be employed over an extended climatology, and iv) based on fields that experience large and rapid variability during monsoon onset and withdrawal. Accordingly, a 3-day running mean is applied to the WASMI time

series to mask the influence of small-scale synoptic variability. Since the onset (withdrawal) is a transition from dry (wet) to a sustained wet (dry) condition, the onset occurs when WASMI becomes positive (i.e., enough moisture in the region to initiate rainfall), and the withdrawal is when the index falls below zero. as shown in Fig. 5.1. And because the wet period must be sustained, the length of the season is simply the difference between the cessation and onset dates.

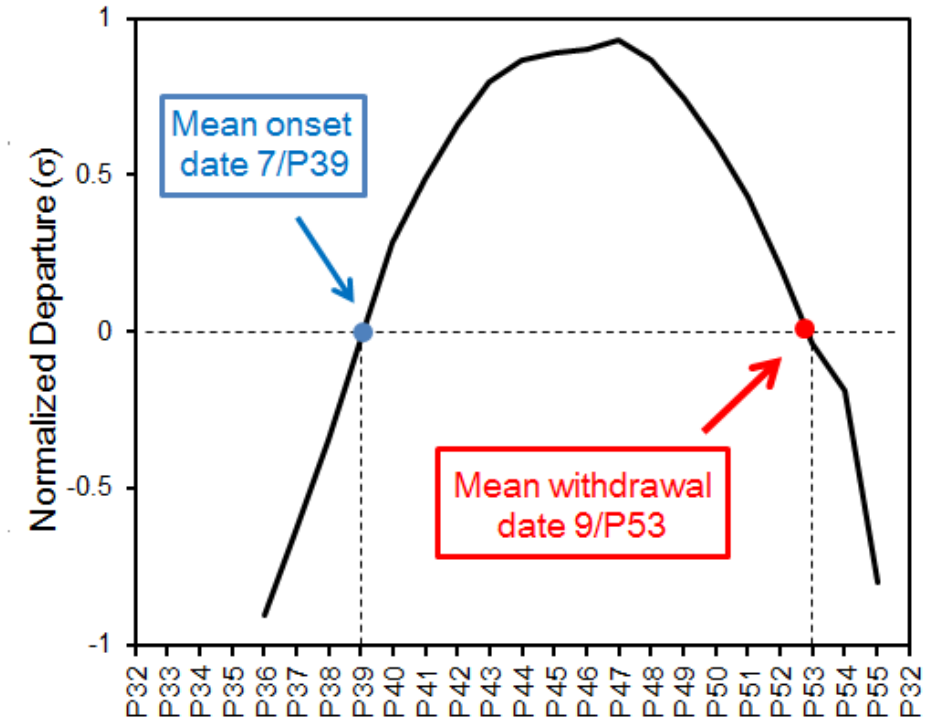

Figure 5.1: Method of finding the onset and withdrawal dates for Sudan-Sahel monsoon season and the climatological mean onset date (blue dot) and withdrawal (red dot) based on WASMI time series. Abscissa is labeled in pentads starting with pentad 32 in June.

5.2.2 Interannual Variability of the Onset and Withdrawal Dates

5.2.2.1 Seasonal Cycle

Based on the above definitions, the WASMI long-term mean (Fig. 5.1) indicates a clear transition period from dry (negative amplitudes) to wet (positive amplitudes). The wet period is sustained after the onset and before the withdrawal occurs. On average, the onset occurs on the 39th pentad (10-14 July) with a standard deviation of ±1.4 pentad, and the mean withdrawal on the 53rd pentad (18-22 September) with ±2 pentad standard deviation. This suggests a climatological length of the Sahelian rainy season of about 14 pentads - a clear indication of the shortness of the Sahelian monsoon season. Compared to other rainfall based methods, this mean onset date is in agreement with Ndiaye (2010) who identified the large scale and true onset in northern Senegal. His criteria for large scale onset was when a 3-day period of rain greater than 20 mm occurred in at least three stations within a homogeneous zone while, for the true onset, the condition of no dry spell of 7 consecutive days or more at any time during the following 10 days being recorded is added. For Ndiaye (2010), the large scale mean onset date for 1981-2008 is 11 July ±17 days, and the true onset 25 July ±14 days. However, Sultan and Janicot (2003) found the mean WAM onset to be earlier than the WASMI based mean onset (24 June ±8 days). The WASMI based the uncertainty in onset date is far less than the rainfall based onset uncertainty advocated by Ndiaye (2010), but it is almost equal to the uncertainty on the WAM onset in Sultan and Janicot (2003).

5.2.2.2 Interannual variability

Figures 5.2a-b show, respectively, the interannual variations in the onset and withdrawal dates. The earliest onset date in the study period occurs in 2005 (P36; 25-29 June), while the latest onset occurs in 1989 (P43; 30 July-3 August). The earliest cessation date occurs during the 1983 drought year (P50; 3-7 September), and the latest cessation during the 1988 wet year (P55; 28 September-2 October).

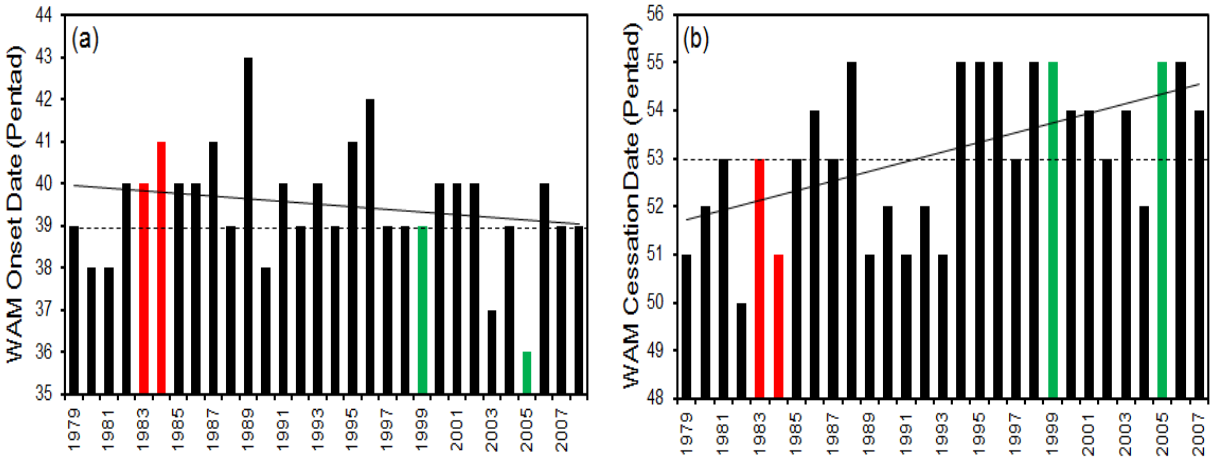

Figure 5.2: Interannual variations of Sudan-Sahel monsoon (a) onset and (b) withdrawal dates for the 1979-2008 period. Horizontal dashed lines indicate the climatological onset and withdrawal means. Solid oblique lines indicate the linear trend. The red/green bars indicate the years taken for illustration in the text.

Figure 5.2 suggests that wet years (e.g., 1988, 1994, 1998, 1999, 2003, and 2005) usually have an early onset date and a late cessation date, whereas dry years (e.g., 1982, 1983, 1984, 1985, 1986, 1987) usually have a late monsoon onset date and an early cessation date. Therefore, wet years are characterized by much longer rainy

seasons than drought years. For example, the lengths of 1999 and 2005 wet years are 16 and 19 pentads respectively, while those of 1983, 1984 drought years are 13 and 10 pentads.

5.2.2.3 Sensitivity to Synoptic Disturbance

The monsoon season frequently is characterized by false, or bogus, monsoon onsets associated with propagating tropical intraseasonal disturbances (e.g., Flatau et al. 2001; Ndiaye 2010). The false onset is usually characterized by enhanced convection and large-scale precipitation. These precipitation events encourage farmers to plant their crops, but it often is followed by a large-scale dry spell which eventually destroys the crops. Hence, the reliability of the WASMI-based onset estimates depends on its insensitivity to these bogus monsoon onsets. Figure 5.3 shows the seasonal cycle of WASMI for two years with strong bogus monsoon. Interestingly, the monsoon only becomes fully established after WASMI indicate an onset for each year. That is, there is no fluctuation around the onset date that could influence a false alarm onset prediction for these years. The fact that no other transition period from positive to negative appear in WASMI until the withdrawal date suggests that the method is not sensitive to active or break monsoon periods that could jeopardize the determination of the onset and the withdrawal date.

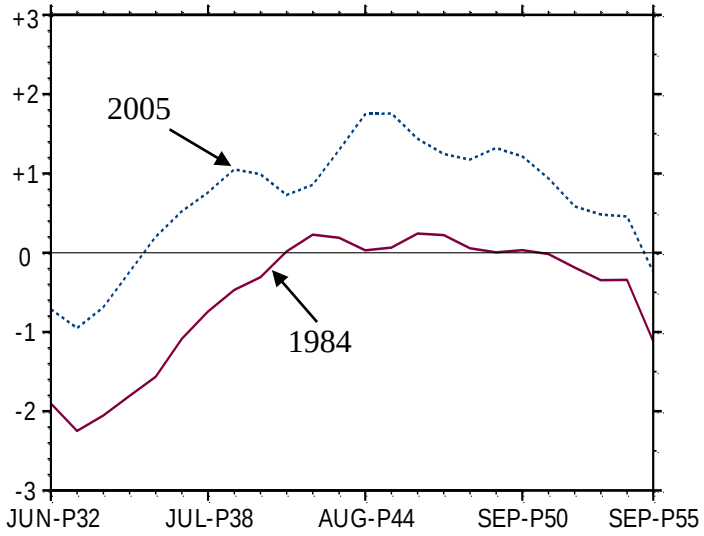

Figure 5.3: Variations of WASMI during an anomalously dry year (1984; solid line) and wet year (2005; dotted line).

5.2.2.4 Relationship Between Monsoon Onset and Rainfall Total

The importance of monsoon onset over the Sudan-Sahel region requires us to assess carefully the above newly developed technique in computing the WAM onset. The objective here is to determine the relation between the onset date and the seasonal rainfall that follows. Hence, the WASMI was used to estimate the time series of the duration of WAM for the study period. The climatological duration of WAM is 14 pentads with a standard deviation of 2 pentads. WAM duration is negatively correlated to its onset date as shown in Fig. 5.4, with a -0.70 correlation coefficient that is statistically significant at the 95% confidence interval using the BCa bootstrap replication. Furthermore, WAM duration is also negatively correlated with the onset

date (r = -0.78; Fig. 5.5a), but positively correlated with the rainfall total (r = +0.61; Fig. 5.5b), and both correlation coefficients are statistically significant at the 95% confidence interval. These associations suggest that an early (late) onset is associated with a longer (shorter) monsoonal season, with wetter (dryer) condition. This is very useful for seasonal rainfall prediction over the Sudan-Sahel zone, although the correlation between the duration and rainfall total is relatively weak. For example, in 2003 and 2005, the Sudan-Sahel has been wet compared with the long term average (Fig. 1.1), and WASMI gives an anomalously long monsoon season (+2.4σ, and +3.7σ) respectively, and a substantial cumulative rainfall (+0.08σ, and - 0.16σ) as shown by green dots in Figs. 5.5a, b. this

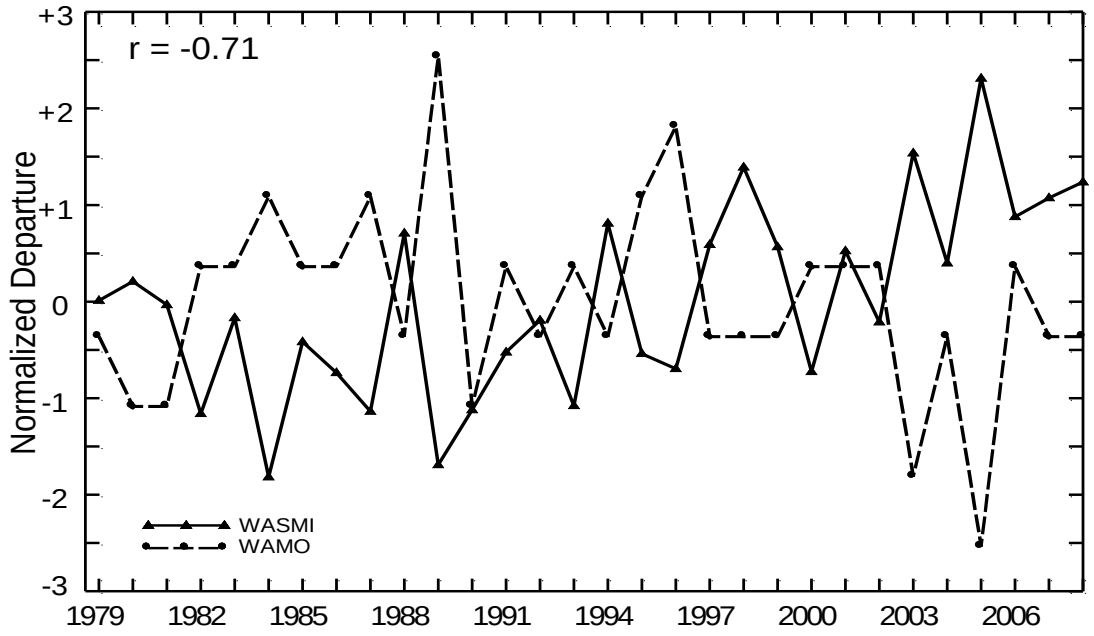

Figure 5.4: Relationship between the normalized departure (σ) of the WASMI time series (solid line) and the WAM onset dates (dash line). The Correlation coefficient between the two time series (*r*) is statistically significant at the 95% confidence interval according to the BCa bootstrap replication.

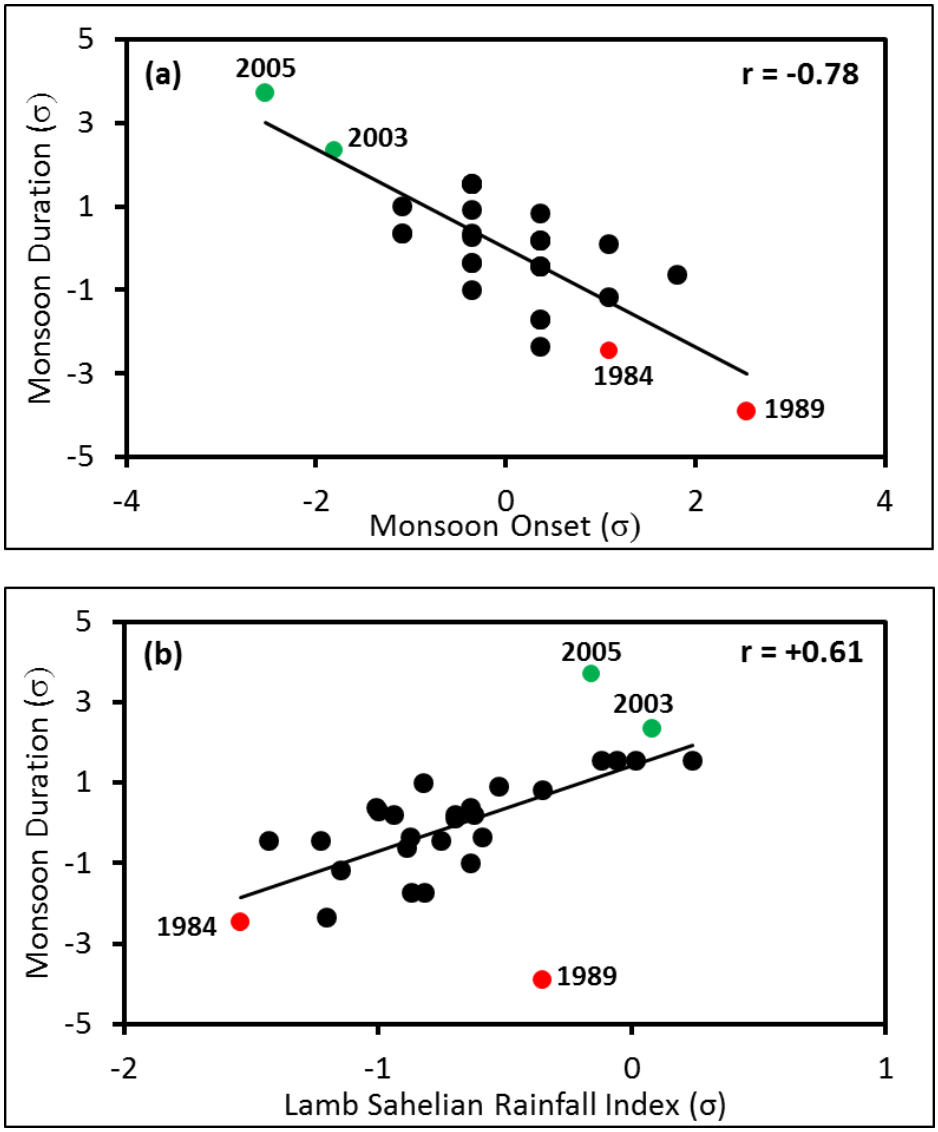

Figure 5.5: Scatter diagrams and linear correlation coefficients between WAM duration and (a) WAM onset and (b) Lamb Sahelian rainfall index for 1979-2008. Green (red) dote indicates wet (dry) monsoonal seasons use for illustration in the text. Correlation coefficients are all significant at the 95% confidence interval according to the BCa bootstrap replication.

early onset-rainfall amount relation is in agreement with the study of Fontaine and Louvet (2006) and Dalu et al. (2009) who also reported that the 2003 summer monsoon season was characterized by an early onset, a longer than average duration, and more cumulative rainfall. On the other hand, 1984 and 1989 (red dots) were extremely dry. These years also recorded both a late onset and a short monsoon season (Fig. 5.5a, b).

Monsoon duration is positively correlated with the withdrawal dates, with a coefficient of +0.77, statistically significant at the 95% confidence interval according to the BCa method. However, the correlation is weaker between the cumulative rainfall and the cessation (+0.56), using the Lamb index. Early (late) withdrawal preludes to deficient (abundant) monsoon season, in agreement with previous analysis, that is an early (late) monsoon onset are usually associated with a long (short) monsoonal season, because the season ends late (earlier). This is very important for farmers over WA who can rely on the onset and length of the rainy season to select crop species best suited to the season to the coming season (e.g., drought resistant varieties and high-value products for a short monsoon season will certainly raise farmers' incomes substantially and eliminate the subsequent famine).

5.2.3 Monsoon Onset and Worldwide Sea Surface Temperature

Because the WAM onset and withdrawal are large-scale phenomena, their index must reflect the changes in both rainfall and large-scale circulation. Variability of WAM onset from one summer to the next is also substantial, and the causes of these

variations is important to understand. Thus, the relationship between the onset dates and global Sea Surface Temperature (SST) patterns was explored on monthly basis.

Figure 5.6 shows the correlation patterns between the WAM onset anomalies and the global SST anomalies. Positive and negative correlations are found in the equatorial tropical South Atlantic (~ 0-20^{o}S, 30^{o}W-10^{o}E) and North Atlantic (~ 5-20^{o}N, 60^{o}-30^{o}W), respectively. These high correlations persist from March to June. In June, the correlation coefficients in the equatorial South Atlantic are higher while there are become weak in the north Atlantic. Moderate negative correlations are found over much of the western and northern Indian Ocean and the Mediterranean Sea. In the Pacific however, the correlations are weak and not statistically significant at the 5% level. The correlation distribution in the tropical Atlantic Ocean indicates that late (early) onsets are characterized by warm (cold) SST in the South Atlantic, and cold (warm) SST in the North.

This WAM – Atlantic Ocean teleconnection is in agreement with earlier analysis regarding the relationship between the monsoon index and global SSTs, and confirms that warmer (cooler) tropical South Atlantic SSTs prelude a late (early) onset, with a dry (wet) monsoon season. It is also in agreement with earlier studies (i.e., Lamb 1978; Hastenrath 1984; Lough 1986; Janowiak 1988) and with more recent studies (i.e., Janicot et al. 1998; Ward 1998; Fontaine et al. 1999). The distinctive SST anomaly patterns in the late and early onset years suggest that the large-scale SST anomaly pattern in the tropical Atlantic (dipole) is a fundamental driver of the anomalous WAM onset.

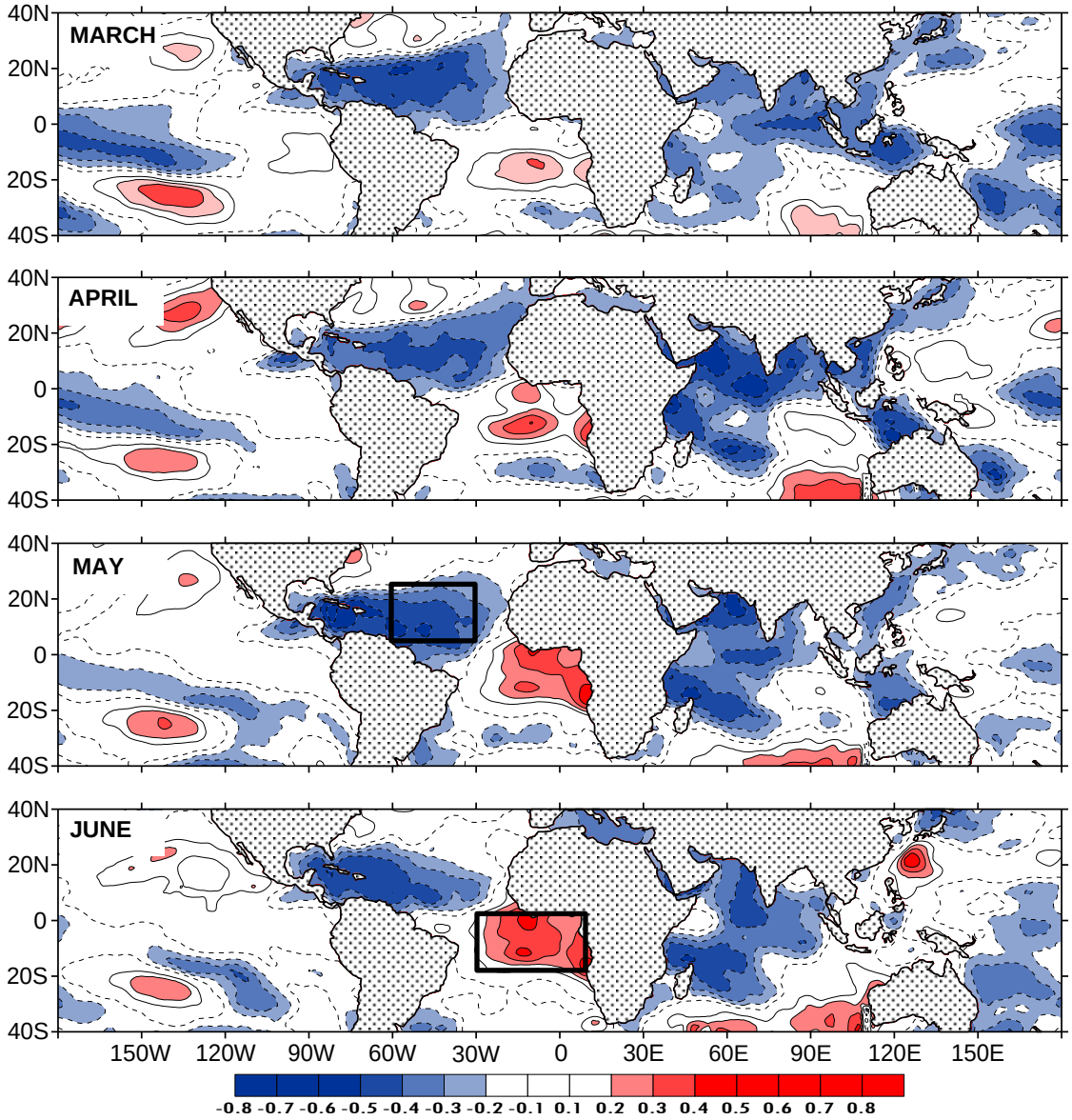

Figure 5.6: Correlation map of the West African Sudan-Sahel monsoon onset anomaly with worldwide sea surface temperature in March, April, May, and June during 1979-2008. Only correlation coefficients significant at the 5% level according to a two-tailed Student's *t*-test (Wilks 2006, 131–135) are shaded. The boxes indicate the area for which time series of SSTs have been used; in the North Atlantic Ocean (ATL_N), and South Atlantic Ocean (ATL_S).

The weak correlation between WAM onset and the central Pacific SST suggests a lesser role of the Pacific Ocean SSTs on Sahelian rainfall variability. This role remains unclear because some studies (Rowell et al. 1992; Janicot et al. 1996; Ward 1998; Rowell 2001; Joly et al. 2007; Losada et al. 2012) have shown these SSTs to play a key role while others (Nicholson and Entekhabi 1986; Ropelewski and Halpert 1987; Janowiak 1988; Nicholson and Kim 1997) have suggested a passive relation between Pacific Ocean SSTs and WAM variability. The intrinsic impact of ENSO is also difficult to estimate, especially from observations alone.

The WAM onset-SST anomaly relationship can be further assessed by a correlation analysis between the onset and the Climate Prediction Center (CPC) area-averaged SST time series in the equatorial South Atlantic (0-20^{o}S, 30^{o}W-10^{o}E) and the tropical North Atlantic (5-20^{o}N, 60^{o}-30^{o}W). These regions were selected because of their proximity to the WAM domain and the result of the large-scale correlation patterns (Fig. 5.5). Figure 5.6a shows the concurrent correlation between the springtime month's average SST anomalies in the two grid boxes and early summertime monsoon onset indices. Positive correlations were found between the onset index and the South Atlantic SST anomalies (Fig. 5.6a, solid line) with peak correlations in May-June. Conversely, negative correlations were depicted with the North Atlantic SST anomalies, with the peak correlation coefficients occurring also in May-June. These positive (negative) correlations in the equatorial South (North) Atlantic are in agreement with the correlation patterns previously described when the worldwide SST anomalies were

used, and an indication that SST of these months could be used as predictor for WAM onset.

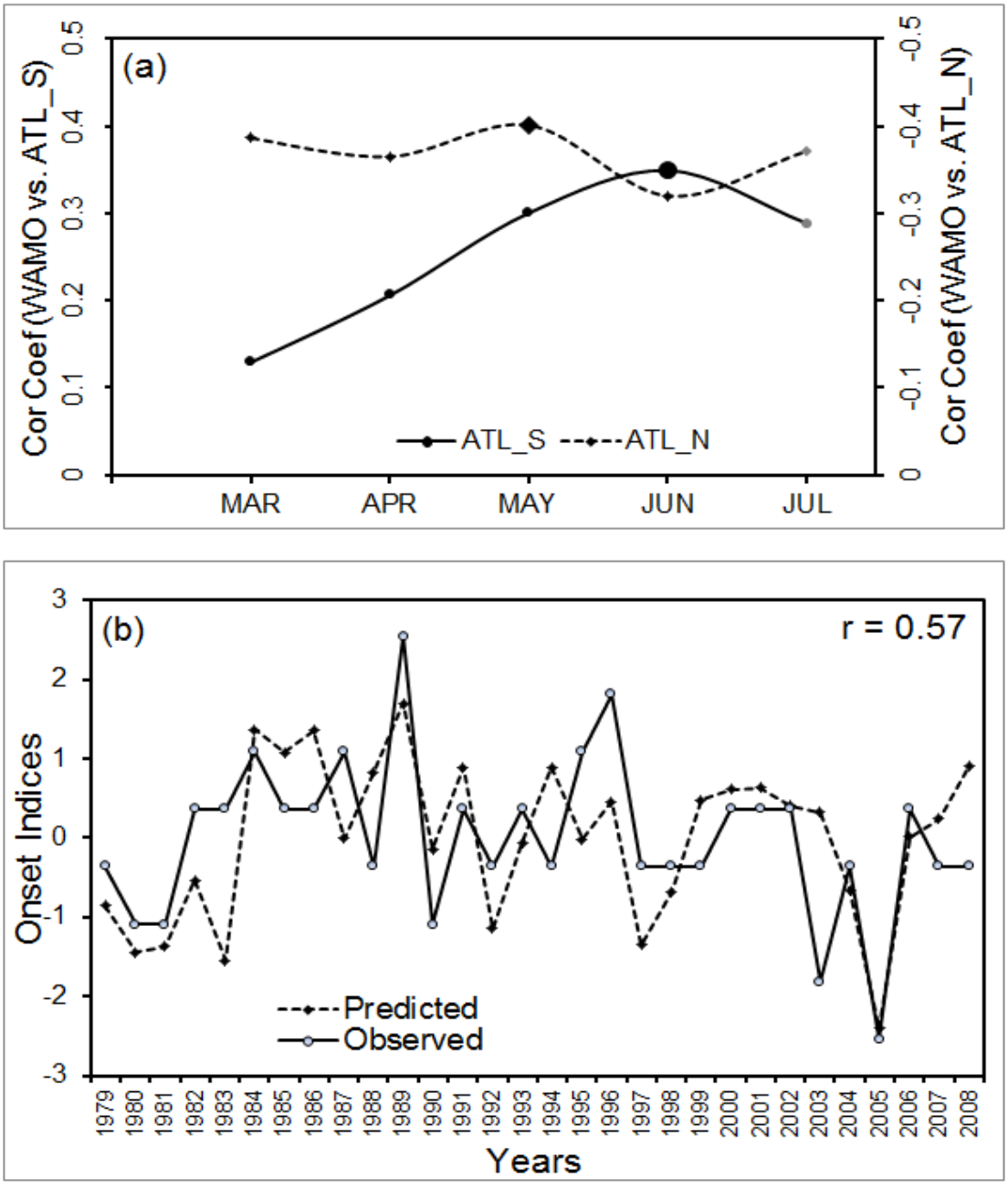

Figure 5.7: (a) Correlation between WAMO indices and area averaged SST anomalies in the tropical South Atlantic (ATL_S, 0-20°S, and 30°W-10°E) and the tropical North Atlantic (ATL_N, 5-20°N, 60°-30°W). (b) Cross-validation time series of predicted versus observed monsoon onset indices.

To further strengthen the argument regarding the onset prediction using the equatorial SST anomalies, a linear regression was applied to the SST-onset index time series. The best linear regression fit was obtained when the May SST index of the tropical North Atlantic was used simultaneously with the June SST index of the tropical South Atlantic. This multiple linear regression model provides an adequate description of the relationship between the mean onset and the SST anomalies as shown in Figure 5.6a, although the model is sensitive to other large-scale circulation features. The multiple linear regressions for prediction of WAM onset (in pentads), using SST anomalies (in ^{o}C) is given by the expression

$$WAMOI = 0.041 - 0.944\ ATL\_N + 0.812\ ATL\_S \tag{5.2}$$

The performance of Eq 5.2 has been evaluated using a cross-validation method (Wilks 2006, pp. 215-217). This method was chosen for the model evaluation because of its superior evaluation performance over the residuals method which does not address the over-fitting problem (e.g., Schneider and Moore 1997). Here, the leave-one-out cross-validation method was employed. This method consists of training the model using all the data except for one point and a prediction is made for that point. Comparison of the predicted onset against the observed values is shown in Figure 5.6b. Except for the few discrepancies for the years shown in boxes, the model has been able to correctly predict the observed onset. In addition, the cross validation result shows that the model is stable throughout the training period. The skill of the model (correlation between the predicted and the observed of +0.57) gives confidence that the

model can be used in the operational onset forecasting. The lead time of such a forecast is short (about a month) if observed SST must be employed, but can be increased by using the forecast SST rather than the observed.

5.3 Simulation of WAM Features using the WRF Model

5.3.1 Overview of the WRF Model

Chapter 3 and 4 established the importance of moisture transport, and its convergence over WA, for the onset of the WAM season, and that the description in the previous chapters is consistent with other studies. In this section the third-generation Weather Research and Forecasting (WRF) model (Skamarock et al. 2008) was used to study the model performance in simulating the key elements of the West African climate, including the WAM. The WRF model is useful not only for idealized research simulations but also for operational forecasting (Klemp 2006). A research version of the WRF model is maintained by the NCAR Mesoscale and Microscale Meteorological Division and available at http://www.mmm.ucar.edu/wrf/users/. One of the objectives of the model developers is the transfer of advances in research to operational and, because it is freely distributed, makes the WRF model attractive to large number of users. So far, the model has been tested and evaluated thoroughly mainly in the Unites States (e.g., Klemp 2006; Coniglio et al. 2010) and countries in the world, but its use in WAM forecasting is very limited to case studies. Although the WRF model allows forecasts to be made on a global scale, in this study it is used as a limited-area model. In doing so, one can reduced the computational expense but recognizes that the WRF needs to obtain its initial and lateral boundary conditions from other models that cover an area wider than the WRF domain - usually a global analysis. This involves interpolating other model's data to WRF grids, which could results in systematic errors.

5.3.2 Model Setup and Analysis Method

The model configuration consisted of a one-way interacting nested domains (36, 12, and 4 km), defined on a Mercator projection, for all the case studies (Fig. 5.8). The coarse domain (220 x 170 horizontal grid points) extends from 20^{o}S to 35^{o}N and from 35^{o}W to 35^{o}E. The second nested domain covers most of the WAM inland domain and has a horizontal grid array of 400 x 187 points. The innermost nested array covers the AMMA-CATCH mesoscale site (262 x 190 grids points). The domain boundaries are located mostly over flat land points or ocean points to avoid vertical interpolation problems due to the differences in topography between the forcing data and WRF (Fig.5.8). The domain boundaries are far from WAM area to minimize the large scale forcing of the WRF model behavior. However, the eastern boundary does not include the Indian Ocean basin; consequently, interaction between this Ocean and WAM are not simulated by the model but imposed by the lateral boundary conditions. This forces the model to determine the regional features without bias due to large-scale processes.

The WRF coarse domain initial and lateral boundary conditions are taken from the 1° x 1° resolution and 24 levels (surface to 10 hPa) final global analysis (FNL) of the National Centers for Environmental Prediction (NCEP) and the lateral boundary conditions are updated every 6 h. The details of the NCEP FNL are available at http://dss.ucar.edu/datasets/ ds083.2. For the lower boundary conditions over water, the Real Time Global SST analysis (RTG_SST, 0.5° X 0.5°, daily), provided by the

NCEP/Marine Modeling and Analysis Branch (NCEP/MMAB), is used. The primary physics options selected in this simulation are also shown in Table 1.

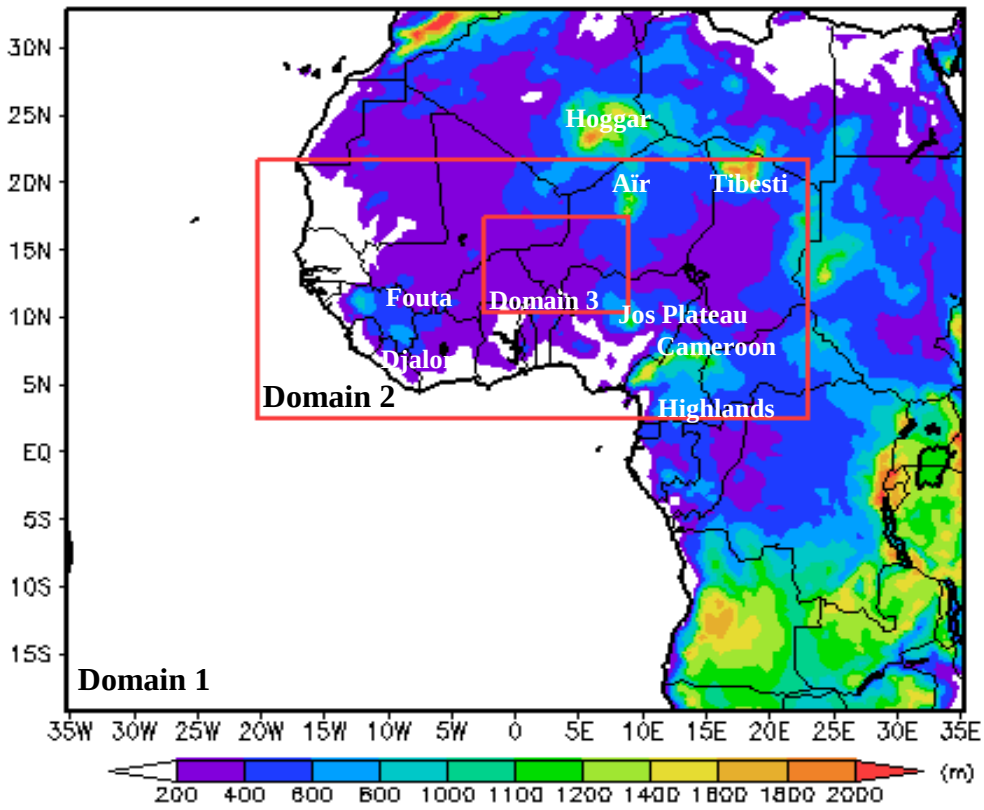

Figure 5.8: Topography of West Africa and WRF model domains with two nests (domains 1, 2, 3). Shadings represent terrain height (m).

Simulations were performed with surface layer processes handled by the Monin-Obukhov scheme, and the unified Noah land-surface model (LSM) to provide sensible and latent heat fluxes to the planetary boundary layer (PBL). The Noah LSM (Chen and Dudhia 2001) is a detailed 4-layer soil temperature and moisture model, which includes

canopy moisture, snow cover prediction, evapotranspiration, soil drainage, runoff, vegetation categories, monthly vegetation faction, and soil texture. Planetary Boundary layer fluxes and vertical diffusion are calculated by the Yonsei University (YSU PBL) scheme (Hong et al. 2006), and the longwave radiation is represented by the Rapid Radiative Transfer (RRTM; Mlawer et. al. 1997) model, while the shortwave radiation adopts Goddard short wave radiative transfer (Chou and Suarez 1994).

5.3.3 Sensitivity Experiments

The quality of climate model simulations depends critically on the performance of the models' parameterizations of physical processes (Druyan et al. 2009). Regional climate models are very sensitive to the choice of parameterizations, and thus it is important to investigate and quantify this sensitivity. Moist convective processes, on the other hand, occur on scales smaller than the typical resolution of limited-area models and they also depend on a variety of physical forcing (e.g., Giorgi, 1991). This fact makes the representation of moist convection in numerical model very difficult, and if not handled properly; the simulated precipitation could strongly depend on the model physics employed. Moist convection accounts for the major source of precipitation over WA. Therefore, it is important to assess the sensitivity of the WRF model to different combinations of convective schemes and microphysics to find the configuration best suited for accurately simulating WAM features. To date there has been no comprehensive assessment of the performance of convective parameterization schemes (CPSs) in simulating convection over the WAM region using the WRF model. Thus, an

important goal was to provide quantitative assessment and evaluation of some CPSs available in the WRF from various model configurations, and to validate the relative performance of these CPSs in simulating the WAM by comparison with observed data.

Table 5.1 summarizes a matrix of 9 WRF members with different physics combinations used for the sensitivity test. The model is run for the month of August 2006 for these case studies and re-run for the entire year after the combination of physics has been selected. August is selected for the case studies because it is the peak rainfall month for WA summer season. The three different CPSs selected for this study are the modify version of Kain-Fritsch (KF), based on Kain and Fritsch (1990; 1993), the Betts-Miller-Janjic (BMJ; Betts 1986; Betts and Miller 1986; Janjic 1994; 2000), and the Grell-Devenyi (GR) ensemble Grell and Devenyi (2002). These cumulus physics schemes vary in their representation of the physical processes, ranging from the relatively simple profile adjustment to the entraining-detraining mass flux (Gochis et al. 2002). For each of these three choices, three microphysical schemes were used, the Kessler simple warm cloud scheme (Kessler, 1969), the Lin et al. (1983) six classes of hydrometeors, and the WRF Single-Moment 6-Class (WSM6; Hong et al. 2004; Hong and Lim, 2006) scheme.

Table 5.1 Physical parameterization schemes used in the WRF model for sensitivity test to microphysics and cumulus parameterization studies.

Name of Experiment	Microphysics Scheme	Cumulus Scheme	Fixed Physical Schemes
KKF	Kessler	Kain-Fritsch	Surface layer: Monin-Obukhov
KGR		Grell Devenyi	Land-surface: Noah land-surface model
KBM		Betts-Miller-Janjic	
LKF	Lin et al.	Kain-Fritsch	Planetary Boundary Layer: Yonsei University (YSU)
LGR		Grell Devenyi	
LBM		Betts-Miller-Janjic	Longwave radiation: Rapid Radiative Transfer Model (RRTM)
WKF	WSM6	Kain-Fritsch	
WGR		Grell Devenyi	Shortwave radiation: Goddard shortwave
WBM		Betts-Miller-Janjic	

5.3.4 Model Evaluation Tools

The evaluation of the WRF downscaling experiments is performed by a variety of statistical techniques over the region of study, by comparing the gridded model values with different observed data. To facilitate the comparison, the observational data are bilinearly interpolated into the WRF grid. Relationships between the paired simulated and observed of these fields are then assessed by the mean error (*ME*) or bias, and regional root-mean-squared error (*RMSE*) over the physiographically similar regions. The ME helps to us to know the inherent biased nature of the particular model;

that is, if it underestimates or overestimates a certain quantity and by how much, and the RMSE gives an overview of the accuracy of simulations. If P is the predicted variable, O the observed variable, and N the total number of verification grid point (e.g., Lo et al., 2008), then, the ME and the RMSE formula can be defined as:

$$ME = \frac{1}{N}\sum_{i=1}^{N}(P_i - O_i), \tag{5.1}$$

$$RMSE = \sqrt{\frac{1}{N}\sum_{i=1}^{N}(P_i - O_i)^2}. \tag{5.2}$$

The corresponding wind vector RMSE (*WRMSE)* can also been obtained from equation 5.2 and is defined as:

$$WRMSE = \frac{1}{N}\left[\sqrt{(uP_i - uO_i)^2 + (vP_i - vO_i)^2}\right], \tag{5.3}$$

where *u* and *v* subscripts indicate the zonal (u), and meridional (v) wind components. For precipitation verification, the accuracy of simulated precipitation is determined by quantities such as the bias score (*BS),* which measures the tendency of a model to over or under estimate the fractional area coverage of precipitation for a certain threshold. It is defined as:

$$BS = \frac{P}{O}. \tag{5.4}$$

The threat score (*TS*) is also used to measure the skill in predicting the area of precipitation amounts over any threshold. The *TS* is the same as the critical success index (CSI) and it is defined by:

$$TS = \frac{H}{(P+O-H)}, \tag{5.5}$$

where H is the number of grid points correctly forecast to receive a threshold amount of precipitation, P is the number of grid points in which the threshold amount of precipitation was simulated, and O the number of grid points that the threshold amount was observed. The threshold amounts used is 8 mm. The correlation coefficient (*CC*), which indicated the strength and direction of the linear relationship between the simulated and observed values is also used, and is given by:

$$cc = \frac{\frac{1}{N-1}\left\{\sum_{i=1}^{N}[(P_i - \bar{P})\,(O_i - \bar{O})]\right\}}{\left[\frac{1}{N-1}\left[\sum_{1=1}^{N}(P_i - \bar{P})^2\right]\right]^{\frac{1}{2}}\left[\frac{1}{N-1}\left[\sum_{i=1}^{N}(O_i - \bar{O})^2\right]\right]^{\frac{1}{2}}}, \tag{5.6}$$

where the bar denotes the mean of that variable.

The evaluation is performed over different subregions of the WAM domain (20^{o}W-30^{o}E and 10^{o}S-20^{o}N). A western subregion encloses the region from 20^{o}W-5^{o}W and 6^{o}-15^{o}N. A central region is between 5^{o}W-5E and 6^{o}-15^{o}N, whereas an eastern domain encloses the region from 5^{o}E-15^{o}E and 3^{o}N-15^{o}N. These subdomains were selected according to the August mean rainfall pattern of WA.

5.3.5 Spatial Pattern of the Modeled West African Rainfall

Figure 5.9 shows the spatial distribution of modeled precipitation rate for the nine simulations along with AMMA rain gauges observation, the TRMM 3B42 satellite-derived estimate of precipitation, and the GPCP data. TRMM 3B42 estimated rainfall has been verified against rain gauges rainfall over WA, and has been shown to yield satisfactory results, although it shows some degree of overestimation in areas to the north of the rainbelt (Nicholson et al. (2003b). In August 2006, observed monthly mean precipitation distribution is characterized by an east-west band of precipitation (ITCZ) and two centers of maximum precipitation located over the orographic areas: one over the Guinea Highlands to the west coast, and another over the Cameroon Mountains (10^{o}E, and 4.5^{o}-10^{o}N). Low rainfall characterized the region in between these two maxima. Both the GPCP and TRMM used here as observed data also show these rainfall characteristics with an overestimation of the precipitation maxima. However, while both the GPCP and TRMM rationally give the same northward extent of precipitation as the rain gauge observations, the GPCP exhibits higher precipitation values than the TRMM.

The simulation with the WRF Single-Moment 6-Class scheme and Kain-Fritsch (WKF; Fig. 5.9) shows a stronger ITZC than observations and rainfall maxima, only over the west coast of WA, and fails to locate the heavy observed rainfall over the Cameroon Mountains. This rainfall maxima is displaced further north over the Lake Chad regions. However, the band of heavy rainfall, located between 10^{o}-15^{o}N is in agreement with observation. The combined WKF thus, overestimates rainfall in most

regions especially over the Fouta Djalon Mountains, and the central Sahelian regions, and underestimates over the Jos Plateau areas (Fig. 5.9b, d). On the other hand, the model captures very well the extent of the little dry season area of the Gulf of Guinea and the location of the West coast rainfall maxima.

The WRF Single-Moment 6-Class scheme and Grell-Devenyi (WGR; Fig. 5.9) experiment, produces a spatial distribution of rainfall that resembles the observation, but underestimates rainfall over the entire region. Both precipitation maxima previously describe are well captured. The magnitude and extent of the maximum over the west coast regions are comparable to the observation. However, WRG significantly underestimates the rainfall over the Cameroon Mountains regions. The little dry season over the Gulf of Guinea is also well simulated. Compare to the WKF, the WGR significantly underestimates the August 2006 rainfall over WA Sudan-Sahel regions.

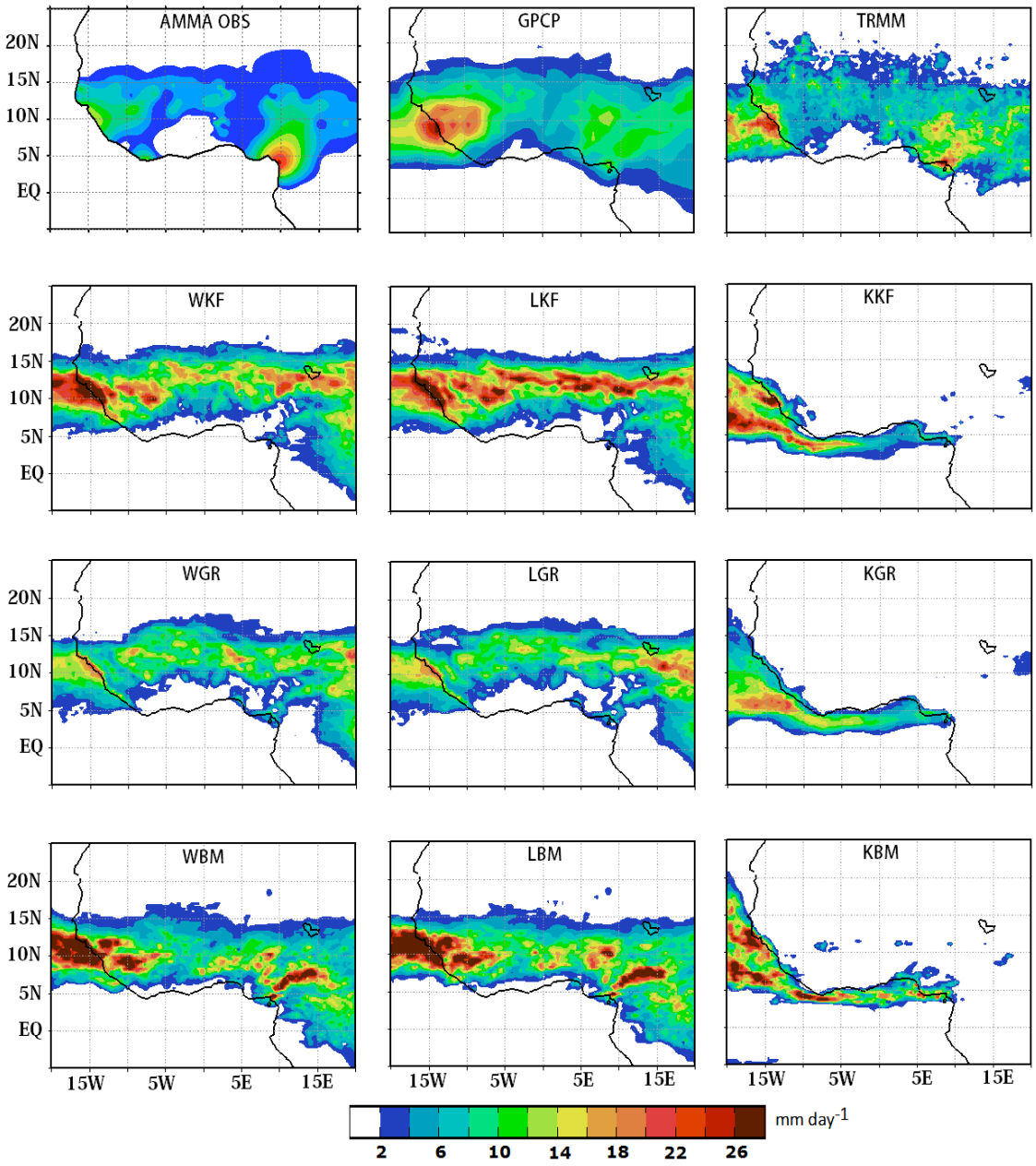

Figure 5.9: August 2006 observed rainfall rate (mm day-1) over WA Sudan-Sahel zone from the 2006 AMMA field campaign rain gauges (AMMA OBS), the global precipitation climatology project (GPCP), and the tropical rainfall measuring mission (TRMM), and simulated using different physics. The first letter of each experiment name indicates the microphysics used (W for WRF single-moment 6-class, L for Lin et al, and K for Kessler), and the other letters indicate the cumulus physics (KF for Kain-Fritsch, GR for Grell-Devenyi, and BM for Betts-Miller-Janjic).

Simulations with the WRF Single-Moment 6-Class scheme and Betts-Miller-Janjic (WBM; Fig. 5.9) shows the two rainfall maxima at their appropriate locations. However, the ITCZ is displaced southward compared to observations and to the WKF, and WGR simulations. As a result, the northern portion of the Sahelian region is dry whereas the model produces rainfall in the regions immediately north of the Gulf of Guinea. The WBM experiment produces the low rainfall observed in between the two rainfall maxima, but overestimates the mountainous area rainfall (over 26 mm day^{-1}).

Simulation using Lin et al. (1983) microphysics, together with the Kain-Fritsch CPS, (LKF; Fig. 5.9) produces a very strong ITCZ with excessive precipitation exceeding 26 mm day^{-1} over central Sahelian regions between 10^{o}-15^{o}N. The rainfall maximum over the west coast of the region is well simulated but the model fails to simulate the maximum over the Cameroon Mountains. It also fails to shows the low rainfall between the western and the eastern rainfall maxima of the region. The northern extent of the rain band is slightly southward compare to observations and the extent of region in the Guinea coast that experience the little dry season is poorly captured, suggesting that the rain belt is misplaced to the south.

Lin microphysics combined with the Grell-Devenyi (LGR; Fig. 5.9) experiment gives rainfall amounts close to rain gauge observation. The ITCZ is well captured, and the northern limit of the rain band as well. The maximum over the western coast is quite well simulated, but that over the Cameroon Mountains is underestimated. When the Lin et al. scheme is used with the Betts-Miller-Janjic CPS (LBM; Fig. 5.9), the precipitation

band is displaced southward and the northern limit is approximately 15^{o}N, which means that no precipitation is produced over the northern Sahelian countries. Nevertheless, the two rainfall maxima were well captured.

Experiments using the Kessler microphysics, and the three cumulus parameterization schemes used, only produced rainfall in the ocean along the coast of WA and completely fail to generate rainfall inland. This failure of the Kessler microphysics may results from its difference formulation compared to the other. Microphysics schemes are used to parameterize the various forms of water substance at grid cell in the models. These forms include water vapor, cloud water, cloud ice, rain, snow, and hail. Kessler microphysics only includes water vapor, cloud water, and rain while, the Lin et al. and WSM6 schemes has all six variables. In addition, there is no ice-phase nor mixed-phase processes in the Kessler scheme unlike the other two. Hence, this scheme is not appropriate in simulating tropical weather variability.

The inadequacy of some experiments to correctly simulate rainfall over the Sudan-Sahel could be due to errors introduced at the lateral boundaries. We mentioned in section 5.3.1 that the use of global model output for lateral boundaries condition could result in a systematic error (e.g., mismatch in the large scale and model resolutions) which can contaminate the simulated results. In particular, spurious precipitation may form at the lateral boundaries, since the internal model dynamics would not freely evolve there, and cloud water is not provided by lateral boundary conditions for the model to develop accurate cloud distribution (e.g., Giorgi and Mearns

1999). Errors could also be related to the schemes' inability in representing convection. For example, we do not know if the parameterization of the effects of cumulus convection could depend on the dynamic and thermodynamic structure and evolution of the resolvable scale (such as moisture convergence or rate of destabilization and the vertical temperature and moisture structure), and if the effect of nonprecipitating clouds is been considered in the surface energy budget by relating the amount of these clouds to the mean layer relative humidity (e.g., Anthes 1983). Since most of the West African summer monsoon precipitation is associated with convection, it suggests the Kain-Fritsch convective parameterization produces too such cumulus convection, thereby resulting in an overestimation of precipitation (WKF, LKF; Fig. 5.9).

5.3.6 Precipitation Verification

Figures 5.10 and 5.11 show the downscaling skill of the microphysics and cumulus physics experiments on simulating August 2006 accumulated precipitation and the tabulated statistical skill scores and correlation coefficients against observation are in tables 5.2 and 5.3 respectively. The WKF, WGR and WBM experiments generally show an improved model-simulated areal coverage of precipitation over the WAM domain, the western and eastern regions than over the central region (Figs. 5.10a, b). However, using the WGR does not improve significantly upon the simulation of the mean precipitation magnitude in the western region of WA (Fig. 5.10b); the WGR configurations generally underpredict the mean precipitation magnitude, while the WKF

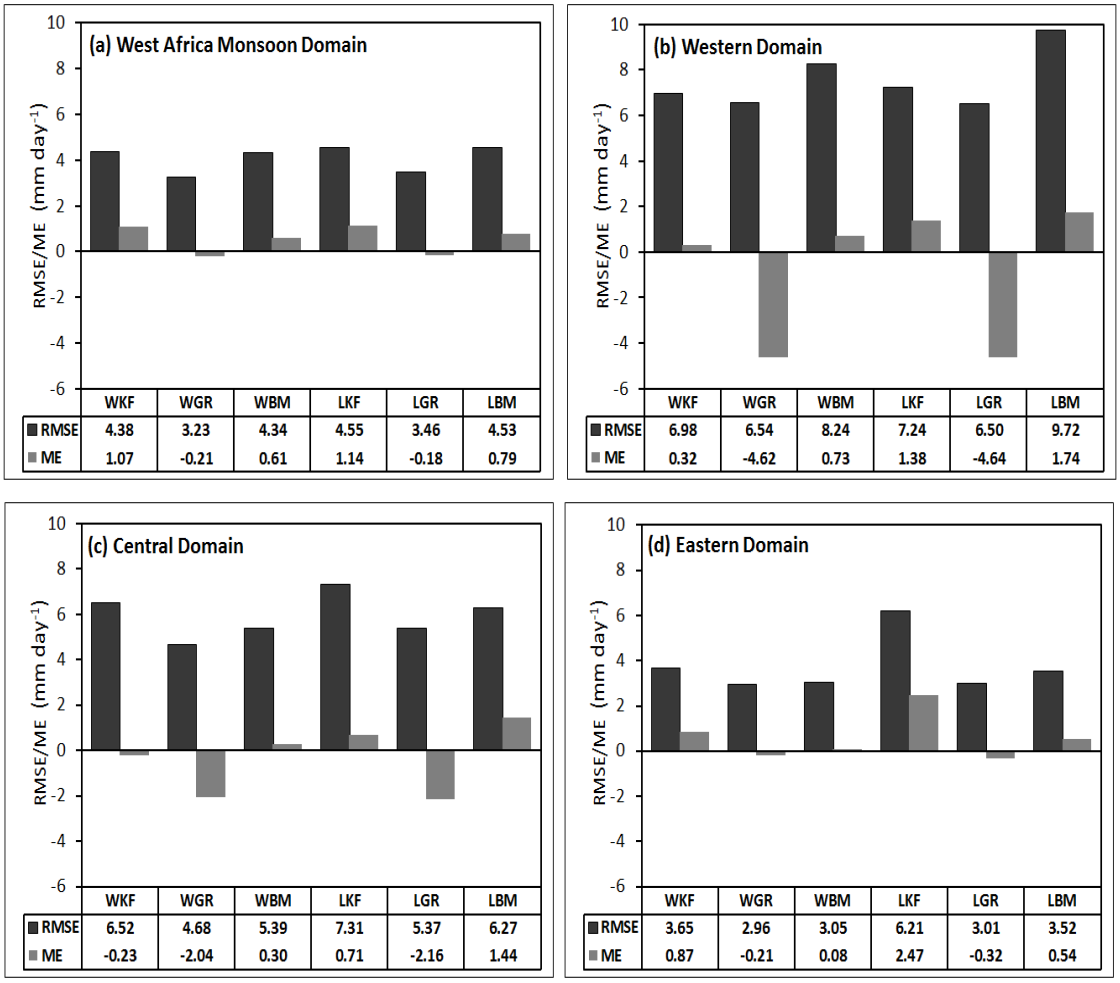

Figure 5.10: Root mean square errors (RMSE; black bars) and mean errors (ME; gray bars) for simulated precipitation in comparison with the GPCP precipitation over (a) the WAM domain, (b) the western domain, (c) the central domain, and (d) the eastern domain. Unit is mm day^{-1}.

and WBM experiments generally overpredict the mean precipitation magnitude for the western region. Similarly, the LKF, LGR, and LBM model-simulated areal coverage of precipitation does well over the WAM domain, the western and eastern regions than the

central domain (Figs. 5.11c, d). WKF, WBM, LKF, and LBM experiments seem to perform better in term of areal coverage of precipitation in the western domain than in the other domains, thereby showing a lower bias in the precipitation simulations both in the fractional areal coverage (Fig. 5.11a, b) and the mean magnitude (Fig. 5.10b), and also a higher TS (Fig. 5.11c, d). The deterioration in precipitation simulation in the central domain might results from its topography which is lower than that of the west, and to the distance between the region and the ocean. This might also result from the large differences in topography between the coarse-resolution FNL and the WRF downscaling domain.

Table 5.2 Threat (bias) scores for 10 mm day^{-1} threshold for the West African monsoon domain (WAM) and the western and eastern regions, and for 5 mm day^{-1} threshold for the central region.

	Precipitation			
	WAM domain	West domain	East domain	Central domain
WKF	0.27 (2.17)	0.60 (0.89**)**	0.08 (1.29)	0.77 (0.82)
WGR	0.23 (1.31)	0.35 (0.43)	0.07 (0.76)	0.68 (0.69)
WBM	0.41 (1.38)	0.58 (0.76)	0.48 (1.44)	0.55 (0.77)
LKF	0.27 (2.17)	0.59 (1.02)	0.14 (1.25)	0.77 (0.84)
LGR	0.21 (1.43)	0.35 (0.46)	0.04 (0.76)	0.66 (0.69)
LBM	0.40 (1.55)	0.61 (0.84)	0.48 (1.72)	0.59 (0.81)

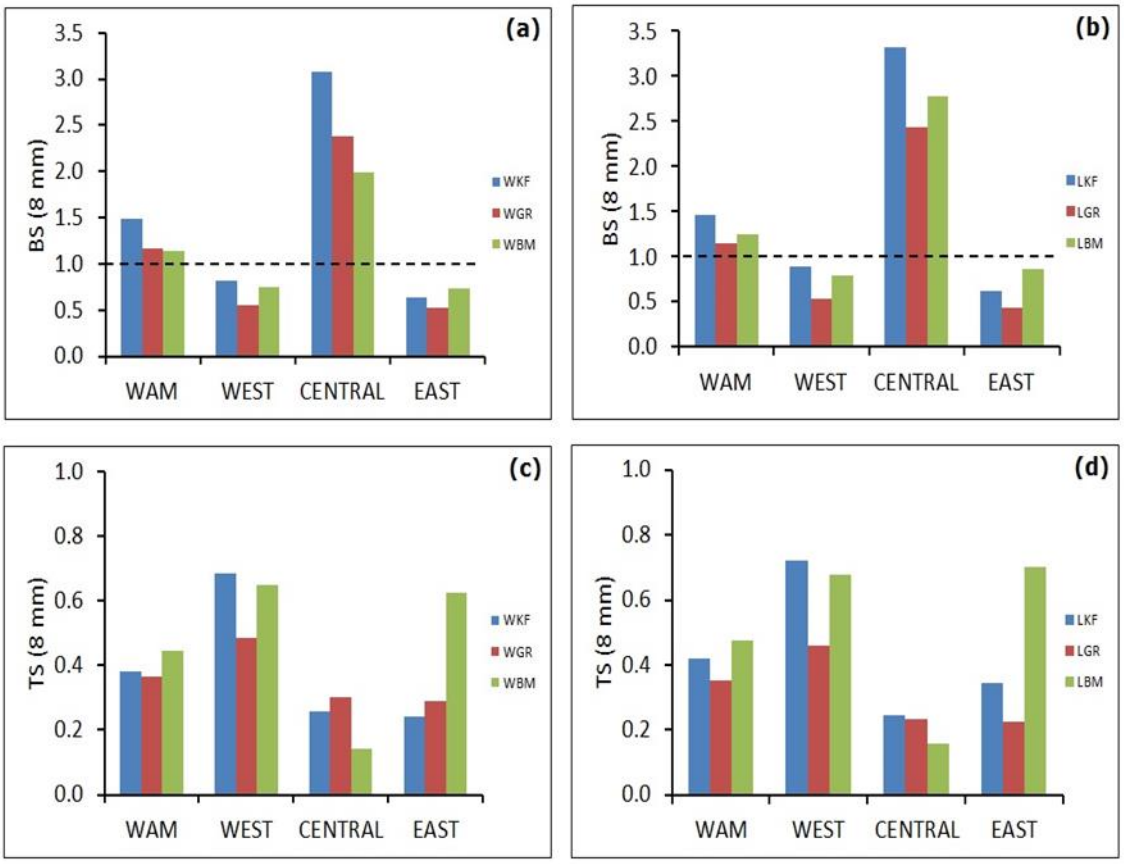

Figure 5.11: Precipitation skill scores for WRF experiments during August 2006 in the WAM, western, central and eastern domains. (a) and (c) Bias scores at the threshold 10 mm, (b) and (d) threat scores at the threshold 10 mm. The horizontal broken line indicates the perfect prediction ($P = O$).

Table 5.3 Correlations between time series of simulated August 2006 accumulated precipitation and the observed rainfall over WA domains

	Precipitation			
	WAM domain	West domain	East domain	Central domain
WKF	0.75	0.46	0.04	0.66
WGR	0.74	0.48	0.29	0.71
WBM	0.75	0.52	0.59	0.30
LKF	0.74	0.41	0.21	0.61
LGR	0.72	0.50	0.20	0.66
LBM	0.76	0.48	0.61	0.33

For a large domain equivalent to the size of WAM domain, the WRF model performance in reproducing areal precipitation pattern is quite poor (TS < 0.5) for all parameterization schemes. However, the WBM and LBM perform better, with threat scores of 0.45 and 0.48 respectively. The performance improves slightly with a reduced simulation domain. Except for the LGR, the other model configurations does well in reproducing the areal patterns of precipitation with threat scores approaching 0.7 over the western and eastern region, but does a poor job in the central Sahelian region with the threat score varying between 0.14 to 30 for all the combination of microphysics and convective schemes, including the LGR experiment. However, the scores decrease as the threshold increases and increase as the threshold decreases. Table 5.2 shows the threat score and the bias score for 10 mm day^{-1} for the western, eastern, and the WAM domain as whole, and for 5 mm $day^{-1}$for the central region. These scores are relatively large for the central region, due to the low rainfall threshold.

Verification of the model-simulated areal precipitation pattern suggests that there is no single model configuration adequate in simulating precipitation over WAM domain. The WRF Single-Moment 6-Class scheme and Betts-Miller-Janjic perform better over the entire domain for 10 mm day^{-1} threshold, and the overall correlation coefficient is relatively high (0.75). More precipitation is simulated by the Lin et al. (1983) than by the WSM6 and this result in the deterioration of the bias score for precipitation. Another distinct impact is that compared to the results from the Lin et al. (1983) microphysics experiments, the WSM6 scheme shifts the major precipitation band southward toward the observed, leading to improved correlation coefficients in the

case of the WBM over the western and eastern domains where maximum precipitation occurred. Over the western portion of WA, the Kain-Fritsch cumulus physics combined with ether the WRF Single-Moment 6-Class or the Lin et al. scheme performs better than the rest when considered the threat and the bias scores for the 10 mm day^{-1} threshold. However, their area-average correlation coefficients with the observed precipitation are low (r = 0.46, 0.41) respectively. Over the eastern zone, again the WRF Single-Moment 6-Class and Betts-Miller-Janjic is superior with a correlation coefficient of 0.59 for areal-average precipitation, whereas over the central region and for low rainfall rate, the Kain-Fritsch cumulus physics associated to WRF Single-Moment 6-Class or the Lin et al. microphysics schemes perform better.

5.3.7 Verification of Circulation Fields

5.3.7.1 Validation of the African Easterly Waves

African Easterly Waves (AEW) are a key component of the WAM system because of their role in the rainfall modulation (e.g., Burpee 1974; Payne and McGarry 1977; Mekonnen et al. 2006). Druyan et al. 2006 noted that AEW that traverse WA cause periodic wind fluctuations, most prominently in the meridional component of the circulation, with strongest amplitudes in the mid-troposphere, usually at about 700 hPa.

Figure 5.12 and Figure 5.13 show the Hovmöller time-longitude diagram of the 700 hPa meridional wind component, averaged between 5^{o}-15^{o}N for the ECMWF-

AMMA reanalysis data and the WRF simulated of all the experiments. The observation of the 700 hPa meridional wind component shows a pattern of westward propagating system of negative and positive centers (Figs. 5.12a, 5.13a). These negative (positive) centers of westward propagating systems represent an alternation of southerly (northerly) circulation associated with convective activities over the region. August 2006 is characterized by less westward propagating systems during the first halve of the month than during the second. Druyan et al. (2006) also describe these alternating positive and negative bands and estimated their speed of about 5^{o}-10^{o} per day (5.8-11.6 m s^{-1}). Next, the ability of the model to simulate these features of the 700 hPa circulation describe in Fig. 5.12a was examined.

Figure 5.12b-d compare the 700 hPa daily variations of the latitudinal mean meridional circulation during August 2006 period of the simulated to the observed (Fig. 5.12a). The letters A and B used with dashed axes in the figures denote major weather systems that give significant precipitation over the region. Significant daily variations of westward propagating systems similar to the observation are evident across the longitudes 30^{o}E to 20^{o}W in all the simulated cases with the WRF Single Moment 6-class microphysics. Of interest is that the timing for each simulate band of westward propagating system is closely synchronized with the observation and with each other, although their magnitude and extent slightly varies from each other.

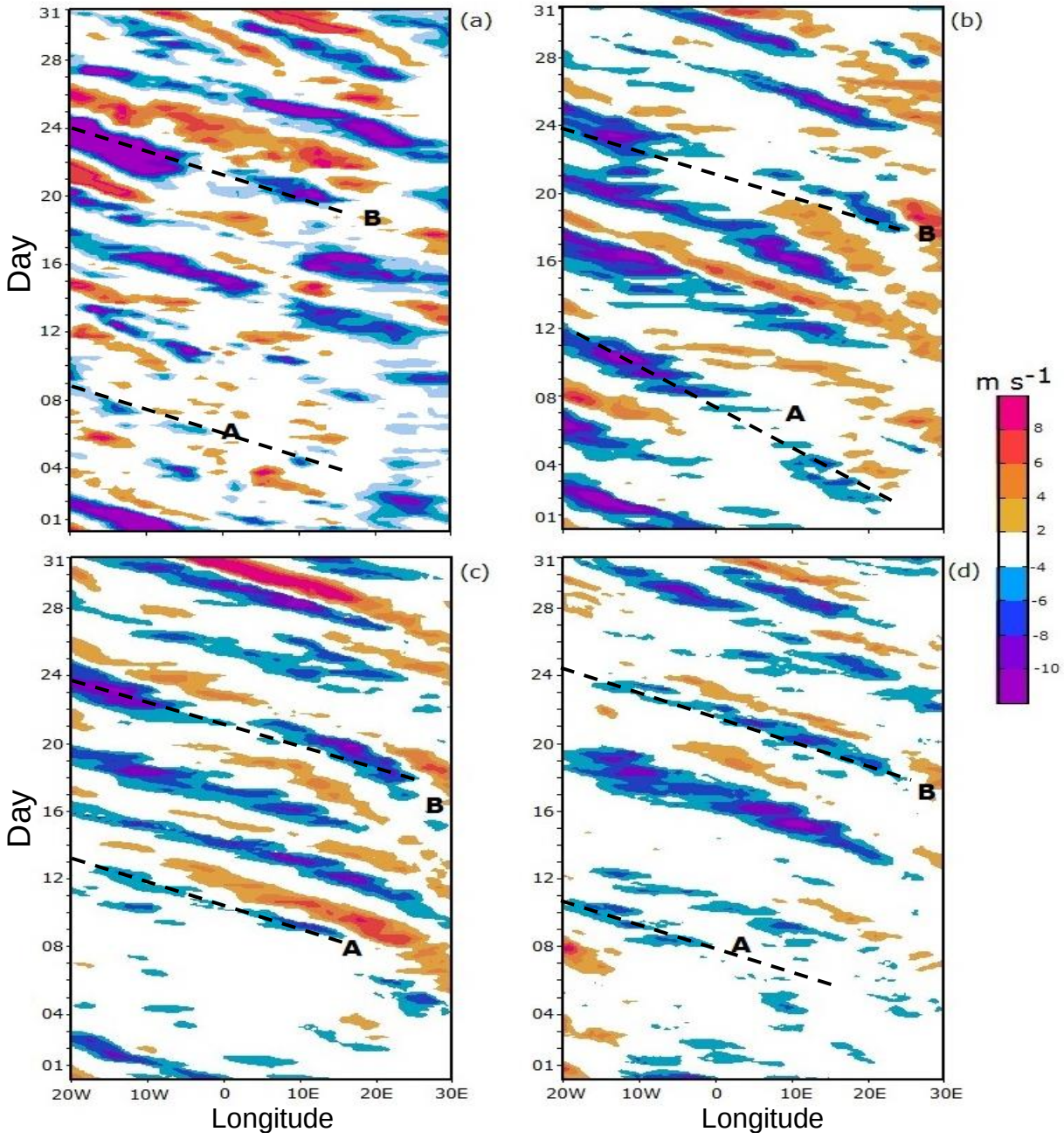

Figure 5.12: Comparison of the time-longitude (from 20°W to 30°E) cross-section, or Hovmöller diagram, of 6-hourly meridional wind (shaded; m s^{-1}) at 700 hPa averaged over 5°-15°N for August 2006 period between (a) the observed (ECMWF-AMMA reanalysis) and the simulated with the WRF Single-Moment 6-Class microphysics associated with (b) the Kain-Fritsch, (c) the Grell-Devenyi, and (d) the Betts-Miller-Janjic cumulus parameterization schemes. Capital letters A – B used with dashed axes denote major weather systems that give significant precipitation over the region.

The model also captured very well the systems that produce the storms A (11-12 August) and B (24 August) around the Niamey area, according to the MIT radar images (not shown). The WBM experiment (Fig. 5.12d) clearly shows fewer systems than the observations and the corresponding simulations as well, and certainly has fewer extreme positive values. Simulations using the WKF (Fig. 5.12b) shows weak systems with negative values in the interior of the continent. These systems then increased in intensity as they moved westward and become strongest over the west coast of WA. It is probably the reason why this combination of physics gives excessive precipitation over the west coast compared with the observed precipitation. The WGR experiment (Fig. 5.12c) clearly shows weaker systems than the observations, suggesting that the amplitude of the AEW is not well simulated when the Grell-Devenyi scheme is used with the WRF single moment 6-class scheme. This also is reflected in the simulated precipitation pattern, with an underestimation of rainfall over the entire WAM domain.

Comparisons with the Lin et al. (1983) simulations in combination of the cumulus physics used (Fig. 5.13) suggest that WRF is able to simulate the westward propagation of an AEW across WA during the August 2006. The two storm systems chose for reference are also been simulated in each of the experiments. However, the amplitude of the alternating positive (negative) values of the circulation is also stronger in the LKF simulation (Fig. 5.13b) during the last 15 days of the month than during the first, and also stronger than observation. Comparatively, this experiment overwhelmingly overestimated the August precipitation pattern over WA. Simulations with LGR (Fig. 5.13c) resemble that of the WRF Single-Moment 6-Class microphysics

associated with the Grell-Devenyi (Fig. 5.12c), as so does the WBM experiment (Fig. 5.13d).

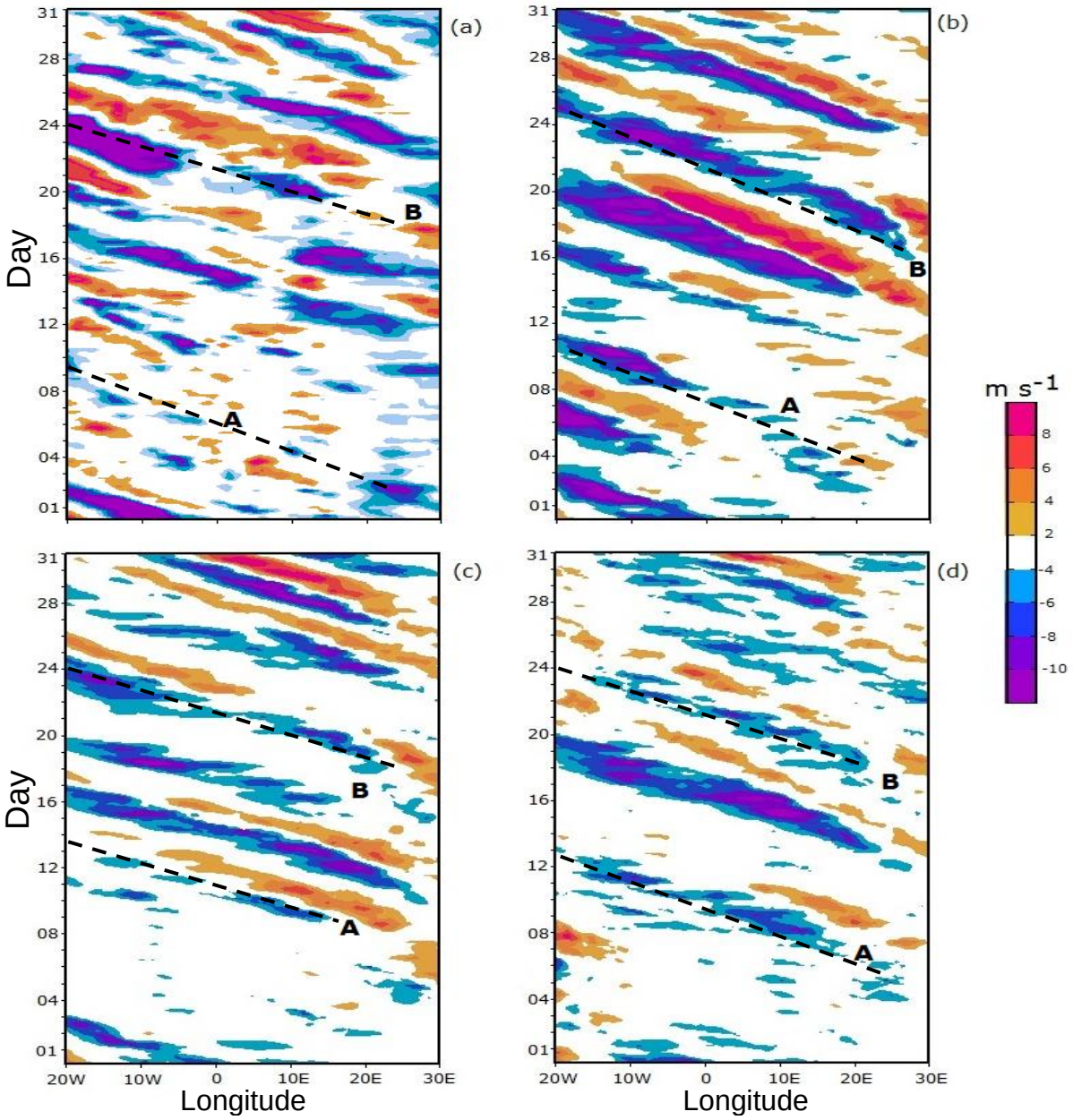

Figure 5.13: Same as Fig.5.12 but for Lin et al. microphysics experiments and (b) the Kain-Fritsch, (c) the Grell-Devenyi, and (d) the Betts-Miller-Janjic cumulus parameterization schemes.

In summary, WRF is capable of simulating many regional climate features over WA, such as the area averaged precipitation and the propagation of AEW at 700 hPa at the daily to monthly timescales. Results indicate that all the microphysics and cumulus schemes perform adequately in WRF simulations of the AEW disturbances, including those that are associated with precipitation such as the system of 11-12, and 24 August 2006. However, model dependence is reflected in the occasional discrepancies in the locations of the extreme positive negative values of the meridional wind.

5.3.7.2 Validation of the African Easterly Jet Core Speed and Location and the Monsoon Depth

The AEJ is another prominent feature of the WAM system because of its strong influence on the occurrence, intensity, and frequency of the West African weather systems. The jet is formed due to vertical wind shear created by the atmosphere to maintain thermal wind balance because of the gradient in temperature and moisture between the Gulf of Guinea and the Sahara during the boreal summer season (e.g., Cook 1999), and has its maximum in the mid-troposphere near 600 mb. Because it is poorly represented in numerical models and low-resolution global analysis datasets, an investigation of how well WRF simulates the August 2006 observed AEJ structure is necessary. Comparisons of the daily average cross-sections along 0^{o} of WRF simulated zonal wind component and ECMWF-AMMA reanalysis are presented in Figure 5.14. During August 2006, the AEJ is confined between 10^{o} and 20^{o}N, with a core centered at 15^{o}N and maximum velocity of about 12 m s^{-1} (Fig. 5.14a).

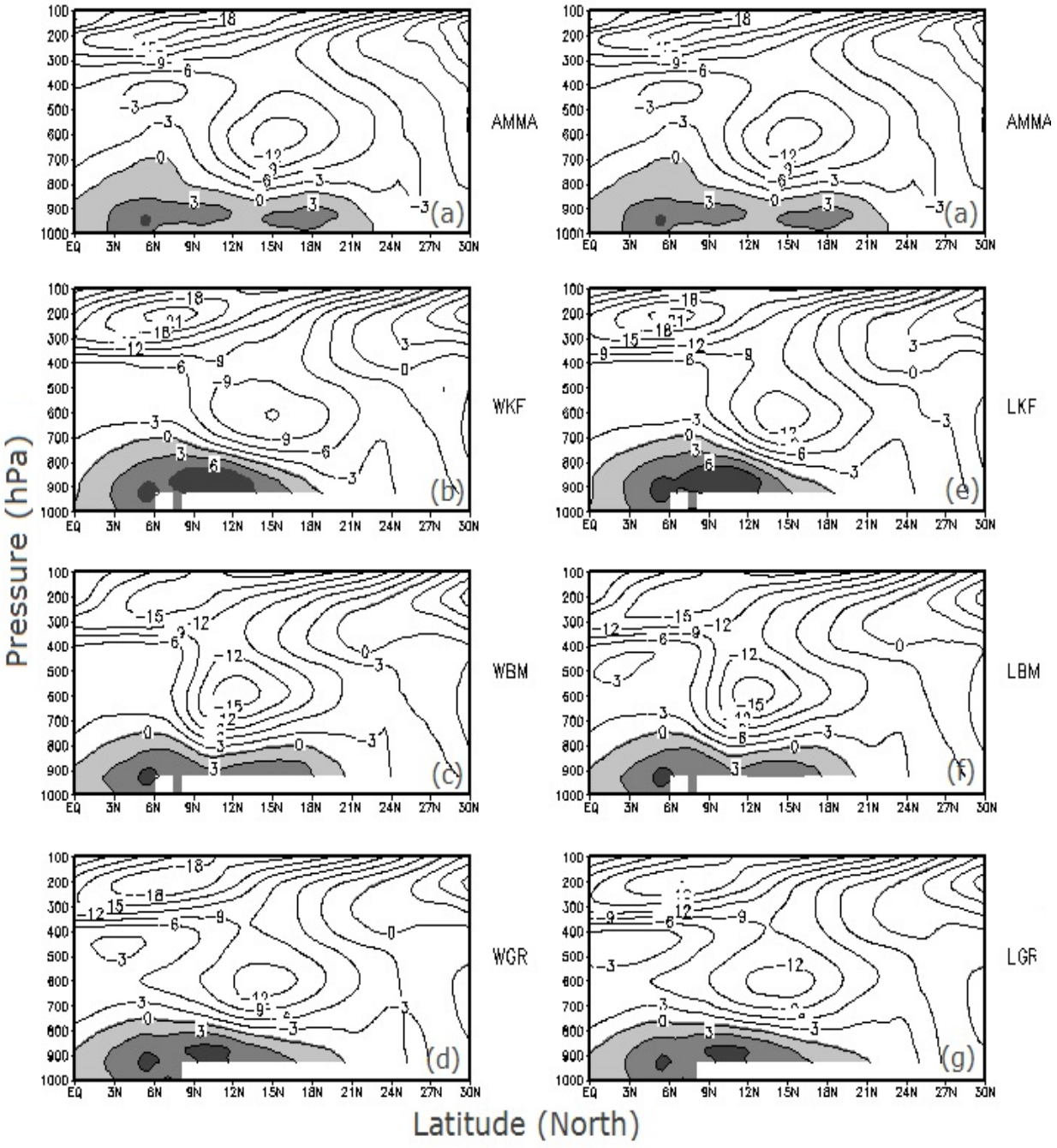

Figure 5.14: Comparison of the daily average cross-sections along 0^{o} of the zonal wind (m s^{-1}) over August 1-31, 2006 period between (a) the ECMWF-AMMA reanalysis; (b), (c), and (d) the simulated with WRF Single-Moment 6-Class microphysics and the Kain-Fritsch (WKF), the Betts-Miller-Janjic (WBM), and the Grell-Devenyi cumulus schemes respectively. (e), (f), and (g) are the same as (b), (c), and (d) but for the Lin et al. microphysics. Shading areas indicate the depth of the monsoon.

The low-level monsoon westerlies cross the coast of WA and penetrates inland up to 22^{o}N. The monsoon depth varies from the coast, where it is deeper (up to 800 hPa), to the Sahelian region where it is limited to 850 hPa.

Simulation of the jet using the Kain-Fritsch cumulus physics and WRF Single Moment 6-class (Fig. 5.14b) and the Lin et al. (1983) (Fig. 5.14e) microphysics placed the jet core at the same location as the observed. However, the core speed is weaker in the WKF experiment, whereas is about the same to the observation in the LKF experiment. The simulated southwesterly are stronger in both cases than the observation, but the northward extent of the monsoon is southward (~18^{o}N) compare to observation (22^{o}N). Experiments with Betts-Miller-Janjic cumulus physics and WRF Single-Moment 6-Class (Fig. 5.14c), and Lin et al. (Fig. 5.14f) microphysics placed the jet at 600 hPa just as the observation, but shifted its core southward at about 12^{o}N, and produced a strong core speed (~15 m s^{-1}). The simulated monsoon layer is shallower compare to observation. Finally, the Grell-Devenyi cumulus schemes combined with WRF Single-Moment 6-class (Fig. 5.14d) and with Lin et al. (Fig. 5.14g) microphysics located the jet at 15^{o}N, but its core speed is weaker especially for the WGR experiment. The WRF experiment suggests that in general, a strong and slightly southward displaced of the AEJ core is associated with weak near-surface westerlies, and shallow monsoon depth (e.g., Fig 5.14c).

5.3.7.3 *Validation of Upper-Level Circulations*

Vertical profiles of simulated potential temperature, wind speed, and relative humidity at standard pressure levels from the 12 km grid run are compared with radiosonde observations from three operational weather stations (Dakar, Bamako, and Niamey) in WA. Previous analyses of the simulations show that the Lin et al. (1983) microphysics does reasonably well over WA and hence an analysis of results using this scheme is presented here in the form of the differences between the simulated and the observed variables (Fig. 5.15). Simulations with the LKF and LGR overestimate potential temperature (Fig. 5.15a) in the layer 1000-500 hPa compared to the observation, but are close to it in the layer above over Bamako and Niamey. However, this overestimation of the potential temperature is less over Dakar than over Bamako and Niamey. The LBM simulation and observation almost exhibited identical potential temperature profile over Dakar. Analysis indicates in all cases that wind speeds (Fig. 5.15b) are slightly under-predicted especially at the location of the AEJ (700 hPa) but all the schemes have correctly located the jet core when compared with observations. In general, simulated wind speeds are close to observations in the lower levels. This simulated result regarding the low-level wind speeds is very important for monsoon predictability and should be further investigated.

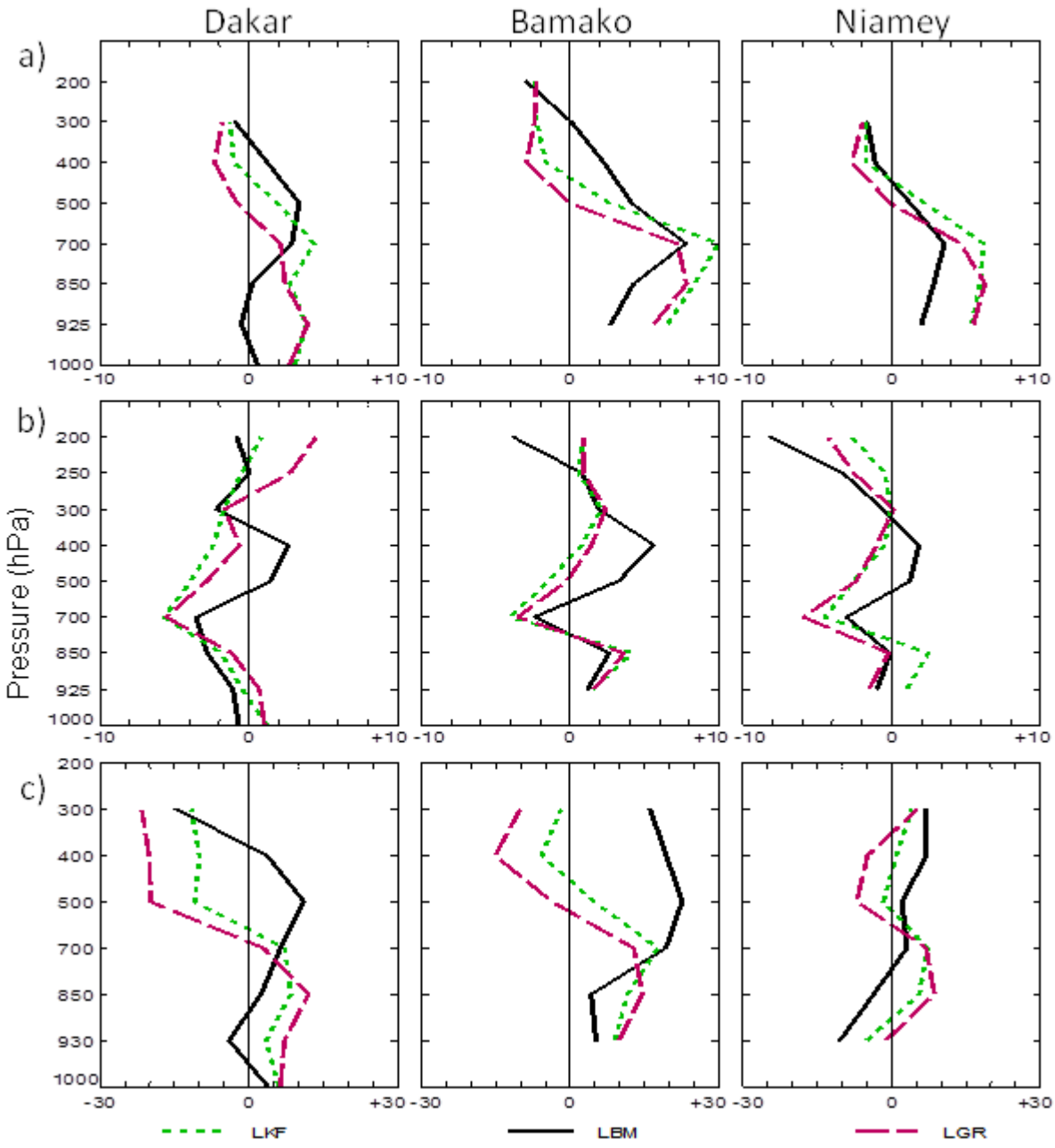

Figure 5.15: Differences between modeled and observed at standard pressure levels for a) potential temperature (^{o}K), b) wind speed (m s^{-1}), and c) relative humidity (%). Dotted line indicates the simulation using the LKF schemes, solid line is for LBM schemes, and dashed line is for the LGR schemes.

The relative humidity (Fig. 5.15c) from 1000 hPa to the level of the AEJ over Dakar and Niamey are well simulated by all the schemes, but are over-predicted over Bamako. LKF and LGR under-predicted the relative humidity in the upper levels over Dakar and Bamako but, over Niamey, the simulations are close to observations. Simulations with LBM show results that are reasonably similar to observations except for the relative humidity over Bamako where an over-estimation is observed across all levels.

Chapter 6

6. Summary and Conclusions

The West Africa Sudan-Sahel zone experienced relatively abundant rainfall during the 1950s but, by the end of the 1960s, the region was experiencing dry conditions including severe and lengthy droughts over the Sahelian zone such as those of 1973-1974, 1983-1984, and 1987 (Fig. 1.1). This drying trend, coupled with marked interannual variations, had devastating socio-economic consequences on the region. Hence, understanding and predicting the nature and causes of the wet and dry spell events have been of great interest because of their impact on the total seasonal monsoon rainfall. Prolonged dry/wet spells during a season can lead to a deficient/abundant monsoon season, and the timing of wet and dry spells also has a considerable socio-economic impact over the region and is particularly important to farmers and water managers.

Any effort to understand WAM climate fluctuations requires an accurate estimation of the hydrological cycle over the region and its linkages to regional-scale features. This because water cycle is an integral part of the global energy cycle and therefore plays a fundamental role in determining large-scale circulation and precipitation patterns. However, its accurate representation is one of the most

challenging problems facing the atmospheric modeling community because of the complex web of feedbacks linking hydrological processes; and because they operate over a range of time and space scales.

In this study, the origins and transport of moisture into WA during the summer monsoon season and its impact on rainfall variability are examined through observations analyses, and numerical simulations. The full range of interannual and intraseasonal variability of the fluxes of moisture entering the WAM region has been examined. The primary objective was to improve our understanding of the underlying dimensions of atmospheric moisture variability on which WAM rainfall depends. This aspect of the WAM climate system has been under-investigated in the past. There has been a need to describe the relationship between intraseasonal variability, the annual cycle, and interannual variability of moisture convergence and the significance it has for rainfall predictability including the onset and withdrawal date of the WAM. An improved treatment of the intraseasonal variability, including wet and dry spells is important for high resolution dynamical and climate models to better simulate the annual and interannual time-scales of rainfall variability. The ability of the WRF regional climate model to simulate seasonal variability of aspects of the WAM was also considered.

The first part of this study dealt with the mechanisms of the low level moisture transport and moisture convergence into WA. The observed tropical Atlantic moisture transport/convergence-WAM interannual relationship has been investigated by

analyzing the vertically integrated fluxes and flux divergences of water vapor computed for the 49 summers of 1960-2008. We used the NCEP/NCAR reanalysis data to examine both spatial structure and primary time-scales of the fluxes using a compositing technique that is keened on the low-level moisture fluxes into WA. The seasonal evolution of the moisture fluxes, their convergence, the movement of the ITF, and associated rainfall is strongly affected by the intensity and latitude position of the equatorial Atlantic cold tongue, the Atlantic semi-permanent high pressure systems, the West African westerly jet, and the Saharan heat low. The transport of moisture occurs mainly in phases and starts from the pre-monsoon season in the South Atlantic Ocean to the fully developed monsoon phase inland. The pre-monsoon onset in March-April is characterized by the cross-equatorial southwesterly moisture flow over the Gulf of Guinea coast. This relatively weak southwesterly flow off the Guinea coast transports a substantial amount of moisture into the Gulf of Guinea, and is associated with the northward shift of the ITF from its winter position near the Guinea coast to around 10^{o}N in April.

The May to June season is characterized by an enhanced southwesterly monsoon flows and the sudden northward latitude shift of the ITF as the result of the development of two branches of moisture fluxes transport from the Atlantic Ocean. The first branch is a strong cross-equatorial southwesterly moisture transport belt or "moisture river" from the South Atlantic Ocean, and the second is the northwestern branch of moisture flux originates from the northeast Atlantic and merges with the westerly flow to form the West African westerly jet (WAWJ). These two branches of

moisture transport are responsible for a strong moisture build-up along the Guinean coast during June. During the peak monsoon season, the southwesterly transport from the South Atlantic Ocean progressively weakens, while the transport by the WAWJ becomes stronger and supplies the Sahelian region. These stages of moisture transport are associated with centers of moisture flux convergence which progressively migrate northward between June and August. The study found two latitudinal moisture convergence zones located respectively over the Guinean coast and the Sahelian zone. The convergence is stronger during the April-June period, suggesting that the moistening of the atmospheric column in WA occurred during the pre-monsoon season rather than during the peak summer monsoon season in July-September, although the enhanced moisture flux into the region is clearly associated with a low-level southwesterly circulation flow, and a large region of enhanced precipitation across the coastal areas in the spring season and further inland in the summer season. Convergence of water vapor generally prevails north of the Equator and the center of the maximum flux convergence is located south of the ITF latitude. This is consistent with the observation that show rainfall over WA generally occurs more than 400 km south of the ITF (Hastenrath 1991; Lélé and Lamb 2010). In the period from March to May the peak of moisture convergence is over 8 mm day^{-1} over the Gulf of Guinea region (5^{o}-10^{o}N), but only 0-2 mm day^{-1} over the Sahelian zone. By August, the moisture flux convergence increases to about 4 to 8 mm day^{-1} in the Sahel where the peak of WAM rainfall is observed.

On the interannual time-scale, observational analysis revealed a significant year-to-year variability in moisture transport. Drought years are generally associated with large decreases in moisture content in the surface-850 hPa layer due to the weakening of the southwesterly monsoon flow, a much farther southward extent of moisture across WA, and a southward ITF latitude position compared to its long-term average latitude position. Moreover, during the extremely wet years, the transport of moisture flux extend further north due to the strengthening of the westerly and southwesterly inflow, and the ITF reaches its northernmost latitude position. It is also found that during an extremely wet monsoon season, the zonal moisture transport crossing the western boundary of West African domain is larger than the meridional moisture transport crossing it southern boundary. However, the zonal and meridional outflow is always of magnitude smaller than the inflow of the zonal and meridional moisture flux components regardless of the season. Correlation between components of moisture transport and rainfall confirm the strong association between the zonal moisture transport and Sahelian precipitation. While significant positive correlation coefficients exist between the zonal component of moisture transport and rainfall starting from zero lag, they appear only at Lag 3 between the meridional component and Sahelian rainfall. The study found statistically significant positive correlations (beyond the 5 % level) between the zonal moisture flux and Sudan-Sahel rainfall total. This relationship is most pronounced when the zonal flux lead by 1 to 4 pentads ($r = +0.44$ *to* $+0.50$). However, the correlations are weak, but are statistically significant at the 5 % level and at lag 3 to lag 4 when the meridional moisture flux is employed ($r = +0.3$). Comparison of June-September simultaneous correlation (Lag 0) with other lag relationships reveals that the

precipitation occurrences over the Sahelian region lag the moisture inflow into the region, which is in agreement to the fact that most of the moistening of the atmospheric column over WA occurs during the pre-monsoon season.

The contributions of both the synoptic- and climate- time scales anomalies of moisture transport over the WAM region has not been shown previously. An application of wavelet and spectral analysis on the vertically integrated moisture flux shows a rich spectrum of variability, with associated well-defined synoptic- and larger-scale circulation features that evolve over a range of period. In particular, the flux variability is mostly dominated by spectral peaks centered near periods of 15 days and 50 days. These time-scales are consistent with those found in other studies (e.g., Janicot and Sultan 2001; Grodsky and Carton 2001; Sultan et al. 2003; Lavaysse et al. 2006; Maloney and Shaman 2008). This study has confirmed and further elucidated the link between enhanced transport over the south and west coasts of Africa and the AEW (3-8 day) time-scales, and at the MJO time-scale (30-90 day). The moisture transport was further partitioned into synoptic (high frequency) and large- (low frequency) scale transport anomalies, to assess their relative contribution to the summer monsoon circulation and resulting rainfall. The results suggest that during the WAM season, the climate and synoptic anomalies play a significant role in the atmospheric transport of moisture from the Atlantic Ocean to land. However, the large-scale atmospheric moisture transport dominates the mean moisture flux transport and moisture flux convergence. Large-scale anomalies of moisture transport and convergence are the major contributors to precipitation over the Gulf of Guinea and the Sahel except over

the topographic regions, where the contribution of synoptic-scale anomalies is substantial. This suggests that atmospheric moisture transport mechanism is part of the large-scale circulation changes in response to SST variations in the Atlantic Ocean, which provide forcing of Sahelian interannual-to-decadal rainfall variability (e.g., Lamb 1978a, b; Hastenrath 1990; Ward 1998; Giannini et al. 2003).

Comparison of the seasonal cycles of moisture convergence of the two AMMA years (2005-2006) suggests that large-scale anomalies of moisture convergence contribute more than that of the synoptic anomalies to the total moisture convergence along the coastal regions during the spring season (April-June), and over the Sahel during the summer season (July-September). The magnitude of moisture convergence by the climate anomalies is almost equal to that of the mean flow suggesting that precipitation over WA is primarily due to large-scale atmospheric features especially during the July-August season. On the other hand, the largest contribution of the synoptic-scale anomalies of moisture convergence are located over regions of frequent or intense mesoscale weather phenomenon, such as the orographic areas and on the shores of the Gulf of Guinea where land-sea breeze storms have mesoscale organization. A positive and statistically significant relationship was found between moisture convergence and Sahelian rainfall (*JAS, r = +0.60*). This supports the hypothesis that rainfall increases (decreases) with the enhanced (diminished) anomalously moisture convergence over the Sudan-Sahel region. On the interannual scale of variability, it was found that extremely wet Sudan-Sahel rainfall years are characterized by positive anomalously atmospheric transport of moisture, while dry

years are characterized by anomalously negative moisture transport into the region. This study also found an enhanced anomalous low-level moisture transport during the Sahelian "recovery" rainfall period; although the magnitude of this enhanced moisture transport is less than the magnitude of the wet period of the 1960s.

The spatial and temporal structure of the WAM 30-90 day intraseasonal moisture variability also is described in this study. The study first developed a large-scale monsoon index for WA Sudan-Sahel zone and reflects the hydrological cycle of the entire region, but not rainfall at a single point. The first combined-EOF mode of monsoon circulation variables characterized such index named the West African Sudan-Sahel Monsoon Index (WASMI). The index is positively correlated to the observed rainfall with correlation coefficients of about +0.95 exceeding the 95% confidence interval, suggesting that years associated with strong monsoon index are accompany with abundant monsoon rainfall. Furthermore, WASMI is negatively correlated with SST in the tropical South Atlantic and positively correlated with SST in the tropical North Atlantic. This confirmed the dipole structure describe in previous studies, that is, a warming (cooling) in the equatorial South Atlantic SST is synchronized with dry (wet) Sahelian rainfall, while the warming (cooling) in the North Atlantic is generally synonym of wet (dry) Sahelian rainfall season. The correlation with the tropical Pacific SST however, is weak and not statistically significant according to the Student *t*-test, in agreement of the weak ENSO signal upon the West African rainfall variability.

The space-time structure of large-scale atmospheric circulations and convection associated with the intraseasonal WET and DRY spell events was investigated through composite analysis. It was found that the intraseasonal wet (dry) spell events were characterized by a significant enhancement (suppression) of convection across WA Sudan-Sahel region. Wet spell (dry spell) events in the Sahelian region (north of 10^{o}N) were accompanied with dry spell (wet spell) events in the Gulf of Guinea (South of 10^{o}N). During active monsoon events, a low-level cyclonic circulation developed over the northwestern coast of WA and favors a strong east-west circulation which transports westerly and southwesterly moisture fluxes into the Sahelian region in a stationary wavelike. We also found that regions of moisture sink (deep convection) during the intraseasonal wet years are located west of the negative ψ cell while regions of moisture source (suppressed convection) are located east of the positive ψ cell, which could explain the mechanism of the northward propagation of convection during the monsoon season. It is known that in the tropics positive ψ anomalies are coupled with a clockwise east-west circulation, and negative ψ anomalies with a counterclockwise east-west circulation, consistent with the characteristic of the zonal-mean flow in low latitudes. Moreover, during the intraseasonal dry spell events a low-level anticyclonic circulation (positive ψ) and associated ridge occupies the northwestern coast of WA. The northwesterly transport of moisture into the Sahelian region is suppressed and becomes northeasterly.

The life cycle of convection relative to WAM intraseasonal variation is highlighted and provides insight for the mechanisms controlling the space-time scales variability of convection over WAM region. The coherence evolution of the divergence of moisture transport and OLR is associated with the 30-90 days mode of intraseasonal oscillation. This characteristic of the intraseasonal evolution of WAM is an insight for potential predictability of its variables beyond the skill of current numerical weather models.

This study also investigated the predictability of the WAM onset and withdrawal through statistical analysis. A large-scale index of monsoon onset and withdrawal based on key features of the monsoon circulation has been developed that provides new insight into the seasonal transitions of the WAM and their relationships to both monsoon rainfall total and tropical Atlantic temperature anomalies. The index is intended to act as an indicator of interannual variability in the large-scale WAM system, rather than as a localized onset and withdrawal criterion, and is developed to further understand the monsoon relationship to regional scale circulation patterns. The results are consistent with previous rainfall based methods. Although the onset and withdrawal index characterizes the large-scale, they are less sensitive to synoptic variability while being indicative of the rapid variations that occur during the monsoon transitions.

Correlation analysis revealed an important association between rainfall totals and the monsoon duration, onset, and withdrawal. The monsoon onset is negatively correlated to WAM rainfall total ($r = -0.70$), and to the monsoon duration ($r = -0.78$), but the duration is positively correlated to the rainfall total ($r = +0.61$). These associations suggest that an early (late) onset is likely to be associated with a longer (shorter) monsoonal season, with wetter (dryer) condition. This finding is very useful for seasonal rainfall prediction over the Sudan-Sahel zone, although the correlation between the duration and rainfall total is relatively weak. In addition, positive (negative) correlations of worldwide SST anomalies with the onset dates are found in the tropical south (north) Atlantic Ocean, indicating that warmer (cooler) tropical South Atlantic preludes a late (early) onset, with a dry (wet) monsoon season.

Finally, assessment of the methodologies of regional climate downscaling has been performed using a regional model (WRF), with initial conditions and boundary conditions driven by coarse-resolution FNL reanalysis. The sensitivity of the WRF model to the combinations of different convective parameterizations with the microphysics schemes has been evaluated in 9 case studies. The aim was to find the WRF configuration most suitable for operational forecasts at the West African weather centers. Our evaluation has focused on the landmass of the WAM domain during August 2006. Compared to available observations, the WRF model reproduces many regional features such as the pattern and magnitude of the monthly accumulated precipitation, the time series of area-averaged precipitation, and the low- and upper-level winds, the AEJ, and the monsoon depth as well. The model also reasonably

simulates the timing and passage of important storms including the westward propagating storms crossing the West African domain.

Inter-comparisons between simulations of different model configurations revealed that there are substantial differences in circulation and thermodynamic structure of the simulated WAM with the different CPSs. In addition to entire domain error tendencies, stations error tendencies are also prevalent (not shown) and some of the simulation differences are statistically significant. Using the Grell-Devenyi convective parameterization results in more tropospheric instability than using the Kain-Fritsch cumulus physics. It is significantly more unstable than using the Betts-Miller-Janjic scheme. The experiments using the Kessler microphysics and either the Kain-Fritsch, the Grell-Devenyi, and the Betts-Miller-Janjic cumulus parameterization schemes produced unrealistic patterns of the Sudan-Sahelian rainfall. This failure of the Kessler microphysics to locate WAM rain-bands at the correct locations indicate that the scheme is not appropriate for the tropical weather systems due to its different formulations compared to the other microphysics used. Experiments with the Lin et al. and Kain-Fritsch schemes tended to overestimate the Sahelian rainfall. This suggests that changes in convective parameterization schemes result in marked differences in the regional moisture transports into and out of a particular sub-region and, so, convective parameterizations choices should depend on the purpose of the simulation.

The reasons for the poor performance of the parameterization schemes within the WRF model in simulating WAM rainfall variability essentially result from two main

sources. The first was related to issues present in the tropical weather system, and the second was related to the uncertainties in formulating cloud and associated processes. Many factors characterize tropical weather systems, such as weak synoptic forcing and a diminishing Coriolis parameter (e.g., Endlich and Mancuso 1964). The effects of the local circulations and diurnal variations are also important. In addition, the monsoon rainfall variability over WA results from a complex nonlinear dynamical system, with spatial variability on scales ranging from individual clouds to large-scale circulations in the atmosphere and ocean, and temporal variability ranging from minutes to weeks, and with the majority of rainfall occurring being produced by organized disturbances (Omotosho, 1985) that the WRF model did not capture well. The uncertainties in the physics also is related to that fact the current parameterization schemes are unable to correctly describe the nature of the convective-large scale interaction for several general reasons. For example,

(i) our current knowledge about the physical processes and feedback mechanisms limits the ability of current parameterization schemes to correctly mimic the impacts of moist convection upon their environment.

(ii) the trigger function, which is the criteria that determines when and where convection is activated within the model, is based upon what parameterization developers thought was important for convective development, and that differs substantially between the individual convective parameterizations used in this study.

(iii) the above led to a number of uncertainties in modeling clouds and their associated processes which also results from the lack of a unified cloud system model framework for implementing detailed formulations of processes needed for

parameterization (Arakawa 2004). As a result, the objective of the parameterization is to have moist convection in the right place, at the right time, with the correct evolution and intensity.

More disturbing for the African continent, is that the current parameterization schemes were developed based on the understanding of the mid-latitude weather system processes and not specifically for the tropics. This is particularly true in view of the relatively good performance of these schemes in the mid-latitude regions compared to their poor performance in the tropical regions. Hence, it is very important for African scientists, especially, and for those interested in tropical weather systems in general, to propose a sufficiently general framework of a tropical cloud system model, and implement detailed formulations processes for the purpose of tropical deep convection parameterization. The focus is to implement, test and further develop existing physical parameterization such as cloud microphysics, radiation, surface fluxes and turbulent mixing with a new multi-scale atmospheric modelling framework. This can only be achieved if the WAM physical processes is better understood by enhanced observational data such as those collected by the ARM mobile facility (AMF) deployment in Niamey (Niger) during the 2006 monsoon season. This kind of deployment should be encouraged and repeated in the future in order to collect sufficiently large data samples. For example, the data collected during 2006 by the AMF can be used to enhance insight into the roles of monsoon convective clouds and atmospheric mineral dust and biomass burning aerosols for the West African weather system, and can also provide a basis for improving the treatment of cloud and aerosol

interactions in numerical weather prediction models, regional climate models, and even global climate models.

Bibliography

Agustí-Panareda, A., A., Beljaars, M., Ahlgrimm, G., Balsamo, O., Bock, R., Forbes, A., Ghelli, F., Guichard, M., Köhler, R., Meynadier, and J-J., Morcrette, 2010: The ECMWF re-analysis for the AMMA observational campaign. *Q. J. R. Meteorol. Soc.* **136**: 1457–1472

Albignat, J. P., R. J. Reed, 1980: The Origin of African Wave Disturbances during Phase III of GATE. *Mon. Wea. Rev.*, **108**, 1827–1839.

Annamalai, H. and J. M. Slingo, 2001: Active/break cycles: Diagnosis of the intraseasonal variability of the Asian summer monsoon. *Climate Dyn*, **18**:85–102.

Anthes, R. A., 1983: Regional models of the atmosphere in middle latitudes, *Mon. Wea. Rev.*, **111**, 1306-1335.

Arakawa, A., 2004: The cumulus parameterization problem: Past, Present, and Future. *J. Climate,* **17**, 2493–2525.

Aspliden, C. I., and D. Adefolalu, 1976: The Mean Troposphere of West Africa. J. *of Appl. Meteor.,* **15**, 705-716.

Barrios, S., L. Bertinelli, and E. Strobl, 2010: Trends in Rainfall and Economic Growth in Africa: A Neglected Cause of the African Growth Tragedy. *Review of Economics and Statistics* **92** (2) 350-366.

Bell, M. A., P. J. Lamb, 2006: Integration of Weather System Variability to Multidecadal Regional Climate Change: The West African Sudan–Sahel Zone, 1951–98. *J. Climate,* **19**, 5343–5365.

Benson C., and E. J. Clay, 1998: The impact of drought on sub-Saharan African economies: A preliminary examination. World Bank Tech. Paper 401, World Bank Publications, 80 pp.

Berry, G., C. Thorncroft, and T. Hewson, 2007: African Easterly Waves during 2004-Analysis Using Objective Techniques. *Mon. Wea. Rev.*, **135**, 1251-1267.

Betts, A. K., 1986: A new convective adjustment scheme. Part I: Observational and theoretical basis. *Q. J. R. Meteor. Soc.*, **112**, 677-691.

Betts, A. K., and M. J. Miller, 1986: A new convective adjustment scheme. Part II: Single column tests using GATE wave, BOMEX, ATEX and arctic air-mass data sets. *Quart. J. Roy. Meteor. Soc.*, **112**, 693-709.

Biasutti, M., D. S. Battisti, E. S. Sarachik, 2003: The Annual Cycle over the Tropical Atlantic, South America, and Africa. *J. Climate*, **16**, 2491-2508

Biasutti, M., I. M. Held, A. H. Sobel, A. Giannini, 2008: SST Forcings and Sahel Rainfall Variability in Simulations of the Twentieth and Twenty-First Centuries. *J. Climate*, **21**, 3471–3486.

Bielli, S. and R. Roca, 2009: Scale decomposition of atmospheric water budget over West Africa during the monsoon 2006 from NCEP/GFS analyses. *Climate Dynamics*, **35**. 143–157.

Boone, A., and Coauthors, 2009: The AMMA Land Surface Model Intercomparison Project (ALMIP). *Bull. Amer. Meteor. Soc.*, **90**, 1865–1880.

Brubaker, K.L., A. Entekhabi, and P.S. Eagleson, 1993: Estimation of continental precipitation recycling. *J. Climate*, **6**, 1077-1089.

Burke, M.B., E. Miguel, S. Satyanath, J. A. Dykema, and D. B. Lobell, 2009: Warming Increases the Risk of Civil War in Africa. *Proceedings of the National Academy of Sciences*, 106 (49), 20670-20674. *doi:10.1073/pnas.0907998106*

Burki, S. J., 1986: The African Food Crisis: Looking Beyond the Emergency. *Journal of Social Development in Africa*, **1**, 5-22.

Burpee, R. W., 1972: The Origin and Structure of Easterly Waves in the Lower Troposphere of North Africa. *J. Atmos. Sci*., **29**, 77-90.

——, 1974: Characteristics of North African easterly waves during the summers of 1968 and 1969. *J. Atmos. Sc*., **31**, 1556-1570.

——, 1975: Some features of synoptic-scale waves based on compositing analysis of GATE data. . Mon. Wea. Rev., 103, 921-925.

Cadet, D. L., and O. Nnoli, 1987: Water vapour transport over Africa and the Atlantic Ocean during summer 1979, *Q. J. R. Meteorol. Soc.*, **113**, 581–602.

Camberlin, P., 1997: Rainfall Anomalies in the Source Region of the Nile and Their Connection with the Indian Summer Monsoon. *J. Climate*, **10**, 1380-1392.

Cappelaere, B., L. Descroix, T. Lebel, N. Boulain, D. Ramier, J.-P. Laurent, G. Favreau, S. Boubkraoui, M. Boucher, I. Bouzou Moussa, V. Chaffard, P. Hiernaux, H.B.A. Issoufou, E. Le Breton, I. Mamadou, Y. Nazoumou, M. Oi, C. Ottlé, G. Quantin, 2009: The AMMA-CATCH experiment in the cultivated Sahelian area of south-west Niger – Investigating water cycle response to a fluctuating climate and changing environment. *Journal of Hydrology*, **375**, Issues 1–2, 34-51.

Carvalho, L. M. V., A. E. Silva, C. Jones, B. Liebmann, P. L. S. Dias, H. R. Rocha, 2011: Moisture transport and intraseasonal variability in the South America monsoon system. *Clim Dyn*, **36**,1865–1880.

Chauvin, F., R. Roehrig, and J-P., Lafore, 2010: Intraseasonal Variability of the Saharan Heat Low and Its Link with Midlatitudes. *J. Climate*, **23**, 2544-2561.

Chen, T-C., and A. Wiin-Nielsen, 1976: On the kinetic energy of divergent and nondivergent flow in the atmosphere. *Tellus*, **28**, 486-498.

_____, 1985: Global water vapor flux and maintenance during FGGE. *Mon. Wea. Rev.*, **113**, 1801-1819.

_____, and H. van Loon, 1987: Interannual Variation of the Tropical Easterly Jet. Mon. *Wea. Rev*., **115**, 1739-1759.

Chen, F., and J. Dudhia, 2001: Coupling an advanced land-surface/ hydrology model with the Penn State/NCAR MM5 modeling system. Part I: Model description and implementation. *Mon. Wea. Rev*., **129**, 569–585.

Chou M.-D., and M. J. Suarez, 1994: An efficient thermal infrared radiation parameterization for use in general circulation models. *NASA Tech. Memo*. *104606*, **3**, 85pp.

CLIVAR, 2000: CLIVAR Africa Implimentation Plan. *ICPO Publication Series No.35*, 34pp.

Coniglio, M. C., K. L. Elmore, J. S. Kain, S. J. Weiss, M. Xue, and M. L. Weisman, 2010: Evaluation of WRF model output for severe-weather forecasting from the 2008 NOAA Hazardous Weather Testbed Spring Experiment. *Wea. Forecasting*, **25**, 408-427.

Cook, K. H., 1999: Generation of African Easterly Jet and Its Role in Determining West African Precipitation. *J. Climate,* **12**, 1165-1184.

Cook, K. H., and E. K. Vizy, 2006: Coupled Model Simulations of the West African Monsoon System: Twentieth- and Twenty-First-Century Simulations. *J. Climate*, **19**, 3681–3703.

Couttenier, M., and R. Soubeyran 2012: Drought and Civil War in Sub-Saharan Africa. *Working Papers*, LAMETA, University of Montpellier, revised Oct 2012. *Journal of Economic Literature (JEL)* codes: O10, O55, P0, Q0.

Cunnington, W. M. and P. R. Rowntree, 1986: Simulations of the Saharan atmosphere-dependence on moisture and albedo. *Quart. J. Roy. Meteor. Soc.* **112,** 971-999.

Dai, A., P. J. Lamb, K. E. Trenberth, M. Hulme, P. D. Jones, and P. Xie, 2004: The recent Sahel drought is real. *Int. J. Climatol,* **24**, 1323-13331.

Dalu, G. A., M. Gaetani, and M. Baldi, 2009: A hydrological onset and withdrawal index for the West African monsoon, *Theor, Appl. Climatol.,* **96**, 179-189, doi:10.1007/s00704-008-0022-8.

Diatta, S. and A. H. Fink, 2014: Statistical relationship between remote climate indices and West African monsoon variability. *Int. J. Climatol*, doi: 10.1002/joc.3912

Dickinson, M., and J. Molinari, 2000: Climatology of Sign Reversals of the Meridional Potential Vorticity Gradient over Africa and Australia. ***Mon. Wea. Rev.***, **128**, 3890–3900.

Diedhiou, A., S. Janicot, and A. Viltard, 1999: Easterly wave regimes and associated convection over West Africa and tropical Atlantic Ocean: Results from NCEP/NCAR and ECMWF reanalysis. *Climate Dyn.*, **11**, 795–822.

Druyan, L. M., and R. J. Koster, 1989: Sources of Sahel precipitation for simulated drought and .rainy seasons. *J. Clim.*, **2**, 1438-1446.

——, M. Fulakeza, P. Lonergan, 2002: Dynamic Downscaling of Seasonal Climate Predictions over Brazil. *J. Climate,* **15**, 3411–3426.

——, ——, and ——, 2006: Mesoscale analyses of West African summer climate: Focus on wave disturbances, *Clim. Dyn.*, **27**, 459– 481.

——, ——, ——, and E. Noble, 2009a: Regional Climate Model Simulation of the AMMA Special Observing Period #3 and the Pre-Helene Easterly Wave. ***Meteorol. Atmos. Phys.***, **105**, 191–210.

——, J. Feng, K. H. Cook, Y. Xue, M. Fulakeza, S. M. Hagos, A. Konaré, W. Moufouma-Okia, D. P. Rowell, E. K. Vizy, S. S. Ibrah, 2009b: The WAMME Regional Model Intercomparison Study. ***Clim. Dyn. DOI 10.1007/s00382-009-0676-7.***

——, M. Fulakeza, P. Lonergan, and R. Worrell, 2010: Regional model nesting within GFS daily forecasts over West Africa. *Atmos. Sci. J., **4**,* 1-11,

Duvel, J. P., 1989: Convection over tropical Africa and the Atlantic Ocean during northern summer. Part I: Interannual and diurnal variations. *Mon. Wea. Rev.*, **117**, 2782–2799.

——, 1990: Convection over tropical Africa and the Atlantic Ocean during northern summer. Part II: Modulation by easterly waves. *Mon. Wea. Rev.*, **118**, 1855–1868.

Efron B., R. J. Tibshirani, 1993: An Introduction to the Bootstrap. Chapman & Hall, London, pp 436.

Eldridge R. H., 1957: Asynoptic study of West African Disturbance Lines *Int. J. Climatol.* **9**, 5, 1030–1042.

Eltahir, E. A. B. and R. L. Bras, 1996. Precipitation Recycling, *Reviews of Geophysics*, 34(3): 367-379.

Endlich, R. M. and R. L. Mancuso, 1964: A direction method of stream-function computation. *Tellus*, **XVI**, I, 32-39.

Fasullo, J. and P. J. Webster, 2003: A hydrological definition of the Indian summer monsoon onset and withdrawal. *J. Climate*, **16**, 3200-3211.

Findley, S. E., 1994: Does drought increase migration? A study of migration from rural Mali during the 1983–1985 drought. *Int. Migr. Rev.*, **28**, 539–553.

Fink, A. H., and A. Reiner, 2003: Spatio-temporal variability of the relation between African Easterly Waves and West African Squall Lines in 1998 and 1999. *J. Geophys. Res.*, **108,** 4332, doi:10.1029/2002JD002816.

Flaounas, E., S. Bastin, and S. Janicot, 2011: Regional climate modelling of the 2006 West African monsoon: sensitivity to convection and planetary boundary layer parameterisation using WRF. *Clim. Dyn*., **36**:1083–1105.

Flaounas, E., S. Janicot, S. Bastin, and R. Roca, 2012: The West African monsoon onset in 2006: sensitivity to surface albedo, orography, SST and synoptic scale dry-air intrusions using WRF. *Clim. Dyn*., **38**: 685-708.

Flatau, Maria K., Piotr J. Flatau, Daniel Rudnick, 2001: The Dynamics of Double Monsoon Onsets. *J. Climate*, **14**, 4130–4146.

Folland, C. K., T. N. Palmer, and D. E. Parker, 1986: Sahel rainfall and worldwide sea surface temperatures 1901-85. *Nature*, **320**, 602-607.

Folland, C. K., J. Owen, M. N. Ward, and A. Colman, 1991: Prediction of seasonal rainfall in the Sahel region using empirical and dynamical methods. *J. Forecasting*, **10,** 21–56.

Foltz, G. R., and M. J. McPhaden, 2004: The 30-70 day oscillations in the tropical Atlantic. *Geophys. Res. Lett.*, **31**, L15205.

Fontaine, B., and S. Janicot, 1992: Wind-Field Coherence and Its Variations over West Africa**.** *J. Climate*, **5**, No. 5, 512–524.

——, S. Janicot, and P. Roucou, 1999: Coupled ocean–atmosphere surface variability and its climate impacts in the tropical Atlantic region. *Clim. Dyn.*, **15,** 451–473.

——, P. Roucou, and S. Trzaska, 2003: Atmospheric water cycle and moisture fluxes in the West African monsoon: mean annual cycles and relationship using NCEP/NCAR reanalysis. *Geophys. Res. Lett*., **30**, 1117, doi:10.1029/2002GL015834.

——, and S. Louvet, 2006: Sudan-Sahel rainfall onset: Definition of an objective index, types of years, and experimental hindcasts. *Geophy. Res. - Atmospheres*, **111**. D20103.

——, J. Garcia-Serrano, P. Roucou, B. Rodriguez-Fonseca, T. Losada, F. Chauvin, **S.** Gervois, S. Sijikumar, P. Ruti, and S. Janicot, 2010: Impacts of warm and cold situations in the Mediterranean basins on the West African monsoon: Observed

connection patterns (1979–2006) and climate simulations, *Clim. Dyn.*, **35**, 95–114, doi:10.1007/s00382-009-0599-3

Gaetani, M., B. Fontaine, P. Roucou, and M. Baldi, 2010: Influence of the Mediterranean Sea on the West African monsoon: Intraseasonal variability in numerical simulations. *J. Geophys. Res*, **115**, doi:10.1029/2010JD014436.

Giannini, A., R. Saravanan, and P. Chang, 2003: Oceanic forcing of Sahel rainfall on interannual to interdecadal time scales. *Science*, **302,** 1027–1030. doi:10.1126/science.1089357.

Gill, A. E., 1980: Some simple solutions for heat-induced tropical circulation. *Q.J.R. Meteorol. Soc.*, **106**, 447–462. doi: 10.1002/qj.49710644905

Giorgi, F., 1991: Sensitivity of simulated summertime precipitation over the western United States to different physics parameterization. *Mon. Wea. Rev.*, **119,** 2870–2888.

Giorgi, F., and L. O. Mearns, 1999: Introduction to special section: Regional climate modeling revisited. *J. Geophys. Res*., **104**, D6, doi:10.1029/98JD02072.

Glantz, M., 1977: The Value of a Long-Range Weather Forecast for the West African Sahel. *Bull. Amer. Meteor. Soc.*, **58**, 150–158.

Gochis, D. J., W. J. Shuttleworth, Z-L. Yang, 2002: Sensitivity of the Modeled North American Monsoon Regional Climate to Convective Parameterization. *Mon. Wea. Rev.*, **130**, 1282–1298.

Gong, C. and E. Eltahir, 1996: Sources of moisture for rainfall in West Africa. *Water Resources Research*, *32*, 3115-3121.

Goswami, B. N., 2005: South Asian Monsoon: in *Intraseasonal Variability of the Atmosphere-Ocean Climate System*, Eds. William K. M. Lau and Duane E.Waliser Chapter 2, Praxis, Springer Berlin Heidelberg, 19-61 pp.

Grams, C. M., S. C. Jones, J. H. Marsham, D. J. Parker, J. M. Haywood, and V. Heuveline, 2010: The Atlantic Inflow to the Saharan heat low: Observations and Modelling. *Q. J. R. Meteorol. Soc.* **136(s1)**: 125–140

Grell, G. A., and D. Devenyi, 2002: A generalized approach to parameterizing convection combining ensemble and data assimilation techniques. *Geophys. Res. Lett*., **29**(14), Article 1693.

Grimes, D et al, 1999: Optimal areal rainfall estimation using raingauges and satellite data, *J. of Hydrology*, **222**, 93-108

Grist, J. P. and S. E. Nicholson, 2001: A study of the dynamic factors influencing the interannual variability of rainfall in the West African Sahel. *J. Climate*, **14**:1337–1359.

Grodsky, S. A. and J. A. Carton, 2001: Coupled land/atmosphere interactions in the West African monsoon. *Geophys. Res. Lett*, **28**:1503–1506.

Grodsky, S.A., J.A. Carton, and S. Nigam, 2003: Near surface westerly wind jet in the Atlantic ITCZ. *Geophysical Research Letters* **30***:* doi: 10.1029/2003GL017867.

Gu, G., and R. F. Adler, 2004: Seasonal Evolution and Variability Associated with the West African Monsoon System. *J. Climate*, **17**, 3364–3377.

Hagos, Samson M., Kerry H. Cook, 2007: Dynamics of the West African Monsoon Jump. *J. Climate*, **20**, 5264–5284.

Hagos, S. and C. Zhang, 2009: Diabatic heating, divergent circulation and moisture transport in the African monsoon system. *Q. J. R. Meteorol. Soc.* **136**, 411-425.

Hamilton, R. A. and J. W. Archbold, M.A. 1954: Meteorology of Nigeria and adjacent territory. *Quart. J. Roy. Met. Soc.* **669**, 551.515: 551.582.

Hamilton, R. A. and J. W. Archbold, M.A. 1954: Meteorology of Nigeria and adjacent territory. *Quart. J. Roy. Met. Soc* **71**, 231-264.

Hammer, Ø., 2010: Time series analysis with Past, *available online at:* http://nhm2.uio.no/norlex/past/TimeseriesPast.pdf

Hare, K. F., 1977: Takoradi-Khartoum air route. *General Synoptic Climate University of Toronto, Canada.*

Hastenrath, S., 1984: Interannual variability and annual cycle: Mechanisms of circulation and climate in the tropical Atlantic sector. *Mon. Wea. Rev.,* **112,** 1097–1107.

——, 1990: The Relationship of Highly Reflective Clouds to Tropical Climate Anomalies. ***J. Climate***, **3**, 353–365.

——, 1991: Climate Dynamics of the Tropics. *Kluwer Academic Publishers, Dordrecht*, 488 pp.

——, 2000: Interannual and longer term variability of upper-air circulation over the tropical Atlantic and West Africa in boreal summer. *Int. J. Climatol*. **20**: 1415–1430.

——, and D. Polzin, 2010: Long-term variations of circulation in the tropical Atlantic sector and Sahel rainfall. *Int. J. Climatol.*, **31**: 649–655.

Hartmann, L.D. 1994 Global Physical Climatology, Academic Press, San Diego, 411pp.

Henson, R., 2008: The Rough Guide to Climate Change. Rough Guide Ltd.

Hong, S.-Y., J. Dudhia, and S.-H. Chen, 2004: A Revised Approach to Ice Microphysical Processes for the Bulk Parameterization of Clouds and Precipitation, *Mon. Wea. Rev*., **132**, 103–120.

——, Y. Noh, and J. Dudhia, 2006: A new vertical diffusion package with an explicit treatment of entrainment processes. *Mon. Wea. Rev.*, **134,** 2318–2341.

——, and J.-O. J. Lim, 2006: The WRF Single-Moment 6-Class Microphysics Scheme (WSM6), *J. Korean Meteor. Soc*., **42**, 129–151.

——, K-S. S. Lim, J-H. Kim, J-O. J. Lim, J. Dudhia, 2009: Sensitivity Study of Cloud-Resolving Convective Simulations with WRF Using Two Bulk Microphysical Parameterizations: Ice-Phase Microphysics versus Sedimentation Effects. *J. Appl. Meteor. Climatol.*, **48**, 61–76.

Hodges, KI, Thorncroft CD. 1997. Distribution and statistics of African mesoscale convective weather systems based on the ISCCP Meteosat imagery. *Mon. Wea. Rev.*, **125**, 2821-2837.

Hoerling, M., J. Hurrell, J. Eischeid, and A. Phillips, 2006: Detection and Attribution of Twentieth-Century Northern and Southern African Rainfall Change. *J. Climate*, **19**, 3989–4008.

Hourdin, F., I. Musat, F. Guichard, P. M. Ruti, F. Favot, M.-A. Filiberti, M. Pham, J.-Y. Grandpeix, J. Polcher, P. Marquet, A. Boone, J.-P. Lafore, J.-L. Redelsperger,

A. Dell'Aquilla, T. Losada Doval, A. K. Traore, and H. Gallée, 2010: AMMA-Model Intercomparison Project. *Bull. Amer. Meteor. Soc*, **91**, 95–104.

Houze, R. A., Jr., and A. K. Betts, 1981: Convection in GATE. *Rev. Geophys. Space Phys.*, **19,** 541–576.

Hulme, M., and N. Tosdevin, 1989: The Tropical Easterly Jet and Sudan Rainfall: A Review. *Theor. Appl. Climatol*., **39**, 179-187.

Hulme, M., R. Doherty, T. Ngara, M. New, D. Lister, 2001: African climate change: 1900 – 2100. *Climate Research*, **17**: 145-168.

Huffman, G. J., F. R. Adler, T. D. Bolvin, G. Gu, J. E. Nelkin, P. K. Bowman, Y. Hong, F. E. Stocker, and B. D. Wol¤, 2007: The TRMM Multi-satellite Precipitation Analysis (TMPA): Quasiglobal, multi-year, combined-sensor precipitation estimates at fine scales. *J. Hydrometeor*., **8**, 38–55.

IPCC, 2007: Climate Change 2007: The Physical Science Basis. Contribution of Working Group I to the Fourth Assessment Report of the Intergovernmental Panel on Climate Change [Solomon, S., D. Qin, M. Manning, Z. Chen, M. Marquis, K.B. Averyt, M.Tignor and H.L. Miller (eds.)]. Cambridge University Press, Cambridge, United Kingdom and New York, NY, USA.

Janjic, Z. I., 1994: The step-mountain eta coordinate model: further developments of the convection, viscous sublayer and turbulence closure schemes. *Mon. Wea. Rev.*, **122**, 927-945.

Janjic, Z. I., 2000: Comments on "Development and Evaluation of a Convection Scheme for Use in Climate Models", *J. Atmos. Sci*., **57**, 3686.

Janicot, S. 1992a: Spatiotemporal Variability of West African Rainfall. Part I: Regionalization and Typings. *J. Climate*, **5**, N^{o}. 5, 489–497.

——, 1992b: Spatiotemporal Variability of West African Rainfall. Part II: Associated Surface and Airmass Characteristics. *J. Climate,* **5**, N^{o}. 5, 499–511.

——, V. Moron, and B. Fontaine, 1996: Sahel droughts and ENSO dynamics. *Geophy. Res. Lett.*, **23**, 515-518.

——, A. Harzallah, B. Fontaine, and V. Moron, 1998: West African monsoon dynamics and eastern equatorial Atlantic and Pacific SST anomalies (1979–88). *J. Climate*, **11,** 1847–1882.

——, and B. Sultan, 2001: Intra-seasonal modulation of convection in the West African monsoon. *Geophys. Res. Lett*, **28**:523–526.

——, F. Mounier, N. M. J. Hall, S. Leroux, B. Sultan, G. N. Kiladis, 2009: Dynamics of the West African Monsoon. Part IV: Analysis of 25–90-Day Variability of Convection and the Role of the Indian Monsoon. *J. Climate*, **22**, 1541–1565.

——, and co-authors, 2008: Large-scale overview of the summer monsoon over West Africa during the AMMA field experiment in 2006. *Ann. Geophys.*, **26**, 2569–2595.

——, G. Caniaux, F. Chauvin, G. de Coëtlogon, B. Fontaine, N. Hall, G. Kiladis, J.-P. Lafore, C. Lavaysse, S. L. Lavender, S. Leroux, R. Marteau, F. Mounier, N. Philippon, R. Roehrig, B. Sultan, and C. M. Taylor, 2011: Intraseasonal variability of the West African monsoon. *Atmosph. Sci. Lett*., **12**: 58–66.

Janowiak, JE, 1988: An investigation of interannual rainfall variability in Africa. *J. Climate,* **1,** 240–255.

Jolliffe, I. T., 1986: Principal component analysis, 2nd ed. Springer Series in Statistics, ISBN 0-387-95442-2 New York, Inc 487pp.

Joly, M., A. Voldoire, H. Douville, P. Terray, and J-F., Royer, 2007: African monsoon teleconnections with tropical SSTs: validation and evolution in a set of IPCC4 simulations. *Climate Dyn*, **29**, 1-20.

Joly, M., A. Voldoire, 2010: Role of the Gulf of Guinea in the inter-annual variability of the West African monsoon: what do we learn from CMIP3 coupled simulations? *Int. J. Climatol.* **30**: 1843–1856.

Kain, J. S., and J. M. Fritsch, 1990: A one-dimensional entraining/ detraining plume model and its application in convective parameterization, *J. Atmos. Sci.*, **47**, 2784–2802.

Kain, J. S., and J. M. Fritsch, 1993: Convective parameterization for mesoscale models: The Kain-Fritcsh scheme, *The representation of cumulus convection in*

numerical models, K. A. Emanuel and D.J. Raymond, Eds., Amer. Meteor. Soc., 246 pp.

Kaiser, G., 1994: *A Friendly Guide to Wavelets.* Birkhäuser, 300 pp.

Kalnay, E., Kanamitsu M., Kistler R., Collins W., Deaven D., Gandin L., Iredell M., Saha S., White G., Woollen J., Zhu Y., Leetmaa A., Reynolds B., Chelliah M., Ebisuzaki W., Higgins W., Janowiak J., Mo K.C., Ropelewski C., Wang J., Roy J., and Joseph D., 1996: The NCEP/NCAR 40-Year Reanalysis Project. *Bull. Amer. Meteor. Soc.*, 77, 437–471.

Kessler, E., 1969: On the distribution and continuity of water substance in atmospheric circulation, *Meteor. Monogr.*, 32, Amer. Meteor. Soc., 84 pp.

Kidson, J. W., 1977: African rainfall and its relation to the upper air circulation. *Quart. J. Roy. Meteor. Soc.*, **103**, 441-456.

Klemp, J. B., 2006: Advances in the WRF model for convection-resolving forecasting, *Adv. Geosci*., **7**, 25-29. doi:10.5194/adgeo-7-25-2006.

Knutson, D. R. and K. M. Weickmann, 1987: 30–60 day atmospheric oscillations: Composite life cycles of convection and circulation anomalies. *Mon. Wea. Rev*, **115**:1407–1436.

Koohafkan, A. P., 1996: Desertification, drought and their consequences. *Sustainable Development, Food and Agriculture Organization (FAO)* of the United Nations. Available online at: http://www.fao.org/sd/EPdirect/EPan0005.htm

Koteswaram, P., 1958: The Easterly Jet Stream in the Tropics, *Tellus*, **10**, 43– 57.

Kutzbach, J. E., 1967: Empirical eigenvectors of sea-level pressure, surface temperature and precipitation complexes over North America. *J. Appl. Metor*., **6**, 791-802.

Lamb, P. J., 1978a: Case studies of tropical Atlantic surface circulation patterns during recent sub-Saharan weather anomalies: 1967 and 1968. *Mon. Wea. Rev.*, **106,** 482–491.

——, 1978b: Large-scale tropical Atlantic surface circulation patterns associated with subsaharan weather anomalies. Tellus, **30**, 240-251.

——, 1979: Some perspectives on climate and climate dynamics. Progress in Physical Geography, **3**, 215-235.

——, 1980: Sahelian Drought. *New Zealand J. of Geography* N^{o} **68**, 12-16.

——, 1982: Persistence of subsaharan drought. Nature, **299**, 46-47.

——, 1983a: Subsaharan rainfall update for 1982: Continued drought. *J. of Climatol.*, **3**, 419-422.

——, 1983b: West African water vapor variations between recent contrasting sub-Saharan rainy seasons. *Tellus,* **35A**, 198-212.

——, R.A. Peppler and S. Hastenrath, 1986: Interannual variability in the tropical Atlantic. *Nature*, **322**, 238-240.

——, and R.A. Peppler, 1992: Further case studies of tropical Atlantic surface atmospheric and oceanic patterns associated with sub-Saharan drought. *J. Climate*, **5**, 476- 488.

Lau, N.-C., 1979: The observed structure of tropospheric stationary waves and the local balances of vorticity and heat. *J. Atmos. Sci.,* **36,** 996–1016.

Lau, K.-M., K.-M. Kim, and S. Yang, 2000b: Dynamical and boundary forcing characteristics of regional components of Asian summer monsoon, *J. Climate,* **13**, 2461–2482.

Laurent, K., M. Grippa, A. Baille, L. Eymard, R. Lacaze, E. Mougin, C. Ottlé, T. Pellarin, J. Polcher, P. de Rosnay, J.-L. Roujean, I. Sandholt, C. M. Taylor, I. Zin, and M. Zribi, 2011: Remote sensing of the land surface during the African Monsoon Multidisciplinary Analysis (AMMA). *Atmos. Sci. Let.* **12**: 129–134.

Lavaysse, C., A. Diedhiou, H. Laurent, T. Lebel, 2006 : African easterly waves and convective activity in wet and dry sequences of the west African monsoon. *Clim. Dyn.* **27**: 319–332.

——, C. Flamant, S. Janicot, D. J. Parker, J-P. Lafore, B. Sultan, and J. Pelon, 2009: Seasonal evolution of the West African heat low: A climatological perspective. *Climate Dyn.*, **33,** 313–330.

——, ——, ——, and P. Knippertz, 2010: Links between African easterly waves, midlatitude circulation and intraseasonal pulsations of the West African heat low. *Q. J. R. Meteorol. Soc.*, **136**, 141-158.

Lavender, S. L., and A. J. Matthews, 2009: Response of the West African monsoon to the Madden-Julian oscillation. *J. Climate*, **22**. 4097–4116.

Lavender, S. L., C. M. Taylor, & A. J. Matthews, 2009: Coupled land-atmosphere intraseasonal variability of the West African monsoon in a GCM. *J. Climate*, **23**, 5557–5571.

Le Barbé, L., T. Lebel, and D. Tapsoba, 2002: Rainfall variability in West Africa during the years 1950–90. *J. Climate*, **15**:187–202.

Lebel, T., D. J. Parker, C. Flamant, B. Bourlès, B. Marticorena, E. Mougin, C. Peugeot, A. Diedhiou, J. M. Haywood, J. B. Ngamini, J. Polcher, J.-L. Redelsperger, and C. D. Thorncroft, 2010: The AMMA Field Campaigns: Multiscale and Multidisciplinary Observations in the West African Region. *Q. J. R. Meteorol. Soc*,. **136**, 8–33.

——, B. Cappelaere, S. Galle, N. Hanan, L. Kergoat, S. Levis, B. Vieux, L. Descroix, M. Gosset, E. Mougin, C. Peugeot, L. Seguis, 2009: AMMA-CATCH studies in the Sahelian region of West-Africa: An overview. *J. of Hydrology*, **375**, Issues 1–2, 3-13.

——, and A. Ali, 2009: Recent trends in the Central and Western Sahel rainfall regime (1990–2007) *Journal of Hydrology*. **375**, 52–64

Lélé, I. M., and P. J. Lamb, 2010: Variability of the Intertropical Front (ITF) and Rainfall over the West African Sudan–Sahel Zone. *J. Climate*, **23**, 3984-4004

Leung, L. R., Y. Qian, 2003: The Sensitivity of Precipitation and Snowpack Simulations to Model Resolution via Nesting in Regions of Complex Terrain. *J. Hydrometeor*, **4**, 1025–1043.

——, Y. Qian, X. Bian, 2003: Hydroclimate of the Western United States Based on Observations and Regional Climate Simulation of 1981–2000. Part I: Seasonal Statistics. *J. Climate*, **16**, 1892–1911.

——, Y. Qian, X. Bian, A. Hunt, 2003: Hydroclimate of the Western United States Based on Observations and Regional Climate Simulation of 1981–2000. Part II: Mesoscale ENSO Anomalies. *J. Climate*, **16**, 1912–1928.

——, L. O. Mearns, F. Giorgi, and R.L. Wilby, 2003: Workshop on regional climate research: Needs and opportunities. *Bull. Amer. Met. Soc.*, **84**, 89-95.

Liebmann, B., and C. A. Smith, 1996: Description of a complete (interpolated) outgoing longwave radiation dataset. *Bull. Amer. Meteor. Soc.,* **77**, 1275–1277.

Li, J. and Q. Zeng, 2002: A unified monsoon index. *Geophys. Res. Letts*, **29**, NO. 8, 1274, 10.1029/2001GL013874

Lin, X., and R. H. Johnson, 1996: Kinematic and thermodynamic characteristics of the flow over the western Pacific warm pool during TOGA COARE. *J. Atmos. Sci.*, **53**, 695-715.

Lin, Y.-L., R. D. Farley, and H. D. Orville, 1983: Bulk parameterization of the snow field in a cloud model. *J. Climate Appl. Meteor.*, **22**, 1065–1092.

Lo, J. C-F, Z-L. Yang, and R. A. Pielke Sr., 2008: Assessment of three dynamical climate downscaling methods using the Weather Research and Forecasting (WRF) model. *J. of Geophysical Res.*, **113**, D09112, doi:10.1029/2007JD009216.

Long, M., D. Entekhabi, and S.E. Nicholson, 2000: Interannual variability in rainfall, water vapor flux, and vertical motion over West Africa. *J. Climate,* **13,** 3827-3841.

Lorenz, D. J., and D. L. Hartmann, 2006: The Effect of the MJO on the North American Monsoon. *J. Climate*, **19**, 333–343.

Losada, T., B. Rodriguez-Fonseca, S. Janicot, S. Gervois, F. Chauvin, and P. Ruti, 2010a: A multimodel approach to the Atlantic equatorial mode: Impact on the West African monsoon, *Clim. Dyn*., **35**, 29–43.

Losada, T., B. Rodriguez-Fonseca, E. Mohino, J. Bader, S. Janicot, CR. Mechoso, 2012: Tropical SST and Sahel rainfall: a nonstationary relationship. *Geo. Res Lett*, **39**, 1-7.

Loschnigg, J., and P. J. Webster, 2000: A Coupled Ocean–Atmosphere System of SST Modulation for the Indian Ocean. *J. Climate*, **13**, 3342–3360.

Lough, J. M., 1986: Tropical Atlantic sea surface temperatures and rainfall variations in sub-Saharan Africa. *Mon. Wea. Rev.,* **114,** 561–570.

Louvet, S., B. Fontaine, and P. Roucou, 2003: Active phases and pauses during the installation of the West Africa monsoon through 5-day CMAP rainfall data (1979-2001). *Geophys. Res. Lett*., **30** (24), 2271, doi:10.1029/2003GL018058.

Madden, R. A., and P. R. Julian, 2005: Historical perspective. Intraseasonal Variability in the Atmospheric–Ocean Climate System, *K. M. Lau & D. E. Waliser, Eds.*, Springer, 1–18.

Maloney, E. D., and D. L. Hartmann, 2000: Modulation of eastern north Pacific hurricanes by the Madden-Julian oscillation. *J. Climate* , **13** , 1451-1460.

Maloney E. D. and J. Shaman, 2008: Intraseasonal variability of the West African monsoon and Atlantic ITCZ. *J. Climate*, **21**, 2898-2918

Manabe, S., J. Smagorinsky, and R. F. Strickler, 1965: Simulated climatology of a general circulation model with a hydrologic cycle. *Mon. Wea. Rev.*, **93**, 769-798.

Mark A. Miller, A. M., and A. Slingo 2007: The Arm Mobile Facility and Its First International Deployment: Measuring Radiative Flux Divergence in West Africa. *Bul. Amer. Meteor. Soc.*, **88**, 1229-1244.

Masato Shinoda, Takashi Okatani and Mahaman Saloum, 1999: Diurnal variations of rainfall over Niger in the West African Sahel: A comparison between wet and drought years. *Int. J. Climatol*. **19**: 81–94

Mason, S. J. and G. M. Mimmack, 1992: The Use of Bootstrap Confidence Intervals for the Correlation Coefficient in Climatology. *Theor. Appl. Climatol.* **45,** 229-233

Mass, C., 1979: A Linear Primitive Equation Model of African Wave Disturbances. ***J. Atmos. Sci.***, **36**, 2075–2092.

Mathon, V., H. Laurent, and T. Lebel, 2002: Mesoscale Convective System Rainfall in the Sahel. *J. App. Meteo.*, **41**, 1081-1092.

Matthews, A. J., 2004: Intraseasonal Variability over Tropical Africa during Northern Summer. *J. Climate*, **17**, 2427–2440.

McCumber, M., W.-K. Tao, J. Simpson, R. Penc, and S.-T. Soong, 1991: Comparison of ice phase microphysical parameterization schemes using numerical simulations of tropical convection, *J. Appl. Meteor.*, **30**, 985–1004.

McGregor, L. J., 1997: Regional climate modeling. *Meteor. Atmos. Phys.*, **63,** 105–117.

Mekonnen, A., C. D. Thorncroft, and A. R. Aiyyer, 2006: Analysis of Convection and Its Association with African Easterly Waves. *J. Climate*. **19**, 5405-5421

Meinke, H., and R. C. Stone, 2005: Seasonal and inter-annual climate forecasting: The new tool for increasing preparedness to climate variability and change in agricultural planning and operations. *Climatic Change*, **70**, 221-253.

Meynadier, R., O. Bock, F. Guichard, A. Boone, P. Roucou, and J.-L. Redelsperger, 2010: West African Monsoon water cycle: 1. A hybrid water budget data set, *J. Geophys. Res*., **115**, D19106, doi:10.1029/2010JD013917.

Miguel, E., S. Satyanath, and E. Sergenti, 2004: Economic Shocks and Civil Conflict: An Instrumental Variables Approach. *Journal of Political Economy*, **112**, No. 4 725-753. http://www.jstor.org/stable/10.1086/421174

Misra, V., 2005: Simulation of the Intraseasonal Variance of the South American Summer Monsoon. *Mon. Wea. Rev.*, **133**, 663–676.

Mlawer, E. J., S. J. Taubman, P. D. Brown, M. J. Iacono, and S. A. Clough, 1997: Radiative transfer for inhomogeneous atmosphere: RRTM, a validated correlated-k model for the longwave. *J. Geophys. Res*., **102** (D14), 16663–16682.

Mo, K. C., and R. W. Higgins, 1996: Large-scale atmospheric moisture transport as evaluated in the NCEP/NCAR and the NASA/DAO reanalyses. *J. Climate*, **9**, 1531-1545.

Mohino, E., B. Rodríguez-Fonseca, C. R. Mechoso, S. Gervois, P. Ruti, F. Chauvin, 2011: Impacts of the Tropical Pacific/Indian Oceans on the Seasonal Cycle of the West African Monsoon. *J. Climate*, **24**, 3878–3891.

Mooney, P. A., F. J. Mulligan, R. Fealy, 2013: Evaluation of the Sensitivity of the Weather Research and Forecasting Model to Parameterization Schemes for Regional Climates of Europe over the Period 1990–95. *J. Climate*, **26**, 1002–1017.

Moron, V., 1994: Guinean and Sahelian rainfall anomaly indices at annual and monthly scales (1933–1990). *Int. J. Climatol*, **14**: 325–341.

Morrison, H., G. Thompson, and V. Tatarskii, 2009: Impact of cloud micrpohysics on the development of trailing stratiform precipitation in a simulated squall line: Comparison of one- and two-moment schemes. *Mon. Wea. Rev.* **137,** 991-1007.

Morrison, H., J. A. Curry, and V. I. Khvorostyanov, 2005: A new double-moment microphysics parameterization for application in cloud and climate models, Part I: Description. *J. Atmos. Sci.*, 62, 1665–1677.

Morrison, H., and J. O. Pinto, 2006: Intercomparison of bulk microphysics schemes in mesoscale simulations of springtime Arctic mixed-phase stratiform clouds. *Mon. Wea. Rev.*, **134**, 1880–1900.

Moufouma-Okia, W. and D. P. Rowell, 2009: Impact of Soil Moisture Initialisation and Lateral Boundary Conditions on Regional Climate Model Simulations of the West African Monsoon. *Clim. Dyn*. DOI 10.1007/s00382-009-0638-0.

Mounier, F., S. Janicot, and G. N. Kiladis, 2008: The west African monsoon dynamics. Part III: the quasi-biweekly zonal dipole, *J. Climate*, **21**, 1911–1928

Murakami, T., L-X. Chen, A. Xie, and M. L. Shresha, 1986: Eastward propagation of 30–60 day perturbations as revealed from outgoing longwave radiation data. *J. Atmos. Sci*, **43**:961–971.

Navarra A., V. and Simoncini, 2010: A Guide to Empirical Orthogonal Functions for Climate Data Analysis. ISBN: 978-90-481-3701-5 (Print) 978-90-481-3702-2 (Online).

Ndiaye, O., 2010: The predictability of the Sahelian climate: Seasonal Sahel rainfall and onset over Senegal. Ph.D. Dissertation Columbia University

Neelin, J. David, Hui Su, 2005: Moist Teleconnection Mechanisms for the Tropical South American and Atlantic Sector. *J. Climate*, **18**, 3928–3950.

Newell, R. E. and J. W. Kidson, 1984: African mean wind changes between Sahelian wet and dry periods. *J. Climatol.*, **4**:1–7.

Newman, M., G. N. Kiladis, K. M. Weickmann, F. M. Ralph, and P. D. Sardeshmukh, 2012: Relative Contributions of Synoptic and Low-Frequency Eddies to Time-Mean Atmospheric Moisture Transport, Including the Role of Atmospheric Rivers. *J. Climate*, **25**, 7341–7361.

Nicholls, N., 2001: The Insignificance of Significance Testing. *Bul. Ame. Met. Soc.*, **81**, 981-986.

Nicholson, S., 1980: The nature of rainfall fluctuations in subtropical West Africa (Guinea Sahel Soudan), *Mon. Wea. Rev.*, **108**, 473–487.

——,1981: Rainfall and Atmospheric Circulation during Drought Periods and Wetter Years in West Africa. *Mon. Wea. Rev.*, **109**, 2191-2208.

——, D. Entekhabi, 1986: The quasi-periodic behavior of rainfall variability in Africa and its relationship to the Southern Oscillation. *Journal of Climate and Applied Meteorology* **34**: 331–348.

——, 1993: An overview of African rainfall fluctuations in the last decade. *J. Climate* **6**: 1463–1466.

——, and J. Kim, 1997: The relationship of the El Nino–Southern Oscillation to African rainfall. *Inter. J. Climatol* **17**: 117–135.

——, Some, B., Kone, B., 2000: A note on recent rainfall conditions in West Africa, including the rainy season of the 1997 ENSO year. *J. Climate,* **13**, 2628–2640.

——, and J. P. Grist, 2001: A conceptual model for understanding rainfall variability in the West African Sahel on interannual and interdecadal timescales. *Inter. J. Climatol*, **21**, 1733-1757.

——, et al., 2003b: Validation of TRMM and Other Rainfall Estimates with a High-Density Gauge Dataset for West Africa. Part II: Validation of TRMM Rainfall Products. *J. Appl. Meteor*., **42**, 1355–1368.

——, and J. P. Grist, 2003: The seasonal evolution of the atmospheric circulation over West Africa and Equatorial Africa. *J. Climate*, **16**, 1013–1030.

——, 2005: On the question of the ‘‘recovery’’ of the rains in the West African Sahel. *J. Arid Env.*, **63,** 615–641.

——, A. I. Barcilon, M. Challa, J. Baum, 2007: Wave Activity on the Tropical Easterly Jet. *J. Atmos. Sci*., **64**, 2756-2763.

Nieto, R., L. Gimeno, and R. M. Trigo 2006: A Lagrangian identification of major sources of Sahel moisture. *Geophys. Res. Lett.*, **33**, L18707, doi:10.1029/2006GL027232.

Nolan, D. S., C. Zhang, and S. H. Chen, 2007: Dynamics of the shallow meridional circulation around intertropical convergence zones. *J. Atmos. Sci.*, **64,** 2262–2285

Norquist, D. C., E. E. Recker, and R. J. Reed, 1977: The Energetics of African Wave Disturbances as Observed During Phase III of GATE. *Mon. Wea. Rev*., **105**, 334-342.

North, G. R., T. L. Bell, R. F. Cahalan, and F. J. Moeng, 1982: Sampling errors in the estimation of empirical orthogonal functions. *Mon. Wea. Rev*., **110**, 699-706.

Odekunle, T. O., E. E. Balogun, and O. O. Ogunkoya, 2005: on the prediction of rainfall onset and retreat dates in Nigeria, Theor. *Appl. Climatol*., **81**, 101-112.

Okumura, Y., and S-P. Xie, 2004: Interaction of the Atlantic Equatorial Cold Tongue and the African Monsoon. *J. Climate*, **17**, 3589–3602.

Omotosho, J. B., 1985: The separate contributions of squall lines, thunderstorms and the monsoon to the total rainfall in Nigeria. *Int. J. of Climatol.,* **5**, 543–552.

——, 1987: Richardson number, vertical wind shear and storm occurrences at Kano, Nigeria. *Atmos. Res*., **21**, 123-137.

——, 1990: Onset of thunderstorms and precipitation over northern Nigeria. *Int. J. Climatol*., **10**, 849–860.

——, 1992: Long-rang prediction of the onset and end of the rainy season in the West African Sahel. *Int. J. Climatol*., **12**, 369-382.

——, A. A. Balogun, and K. Ogunjobi, 2000: Predicting monthly and seasonal rainfall, onset and cessation of the rainy season in West Africa using only surface data. *Int. J. Climatol*., **20**, 865–880.

——, and B. J. Abiodun, 2007: A numerical study of moisture build-up and rainfall over West Africa. *Meteorol. Appl.* **14**: 209–225.

Opoku-Ankomah, Y., and I. Cordery, 1994: Atlantic sea surface temperatures and rainfall variability in Ghana. *J. Climate* **7**, 551-558.

Osman, O. E., and S. Hastenrath, 1969: On the synoptic climatology of summer rainfall over Central Sudan. *Archiv Meteor. Geophys. Bioklim*., Ser. B., **17**, 297-324.

Payne, S. W., and M. M. McGarry, 1977: The Relationship of the Satellite Inferred Convective Activity to Easterly Waves Over West Africa and the Adjacent Ocean During Phase III of GATE. *Mon.Wea. Rev.*, **105**, 413-420.

Paeth, H., and P. Friederichs, 2004: Seasonality and time scales in the relationship between global SST and African rainfall, *Climate Dynamics*, **23**, 815–837.

Paeth, H., K. Born, R. Podzun, and D. Jacob, 2005: Regional Dynamical Downscaling over West Africa: Model Evaluation and Comparison of Wet and Dry Years. *Meteorologische Zeitschrift*, **14**, 349-367.

Paeth, H., N. M. J. Hall, M. Á. Gaertner, M. Dominguez, S. Moumouni, J. Polcher, P. M. Ruti, A. H. Fink, M. Gosset, T. Lebel, A. T. Gaye, D. P. Rowell, W. Moufouma-Okia, D. Jacob, B. Rockel, F. Giorgi, & M. Rummukainen, 2011: Progress in regional downscaling of West African precipitation. *Atmos. Sc. Lett.*, **12**. 75-82.

Pal, J. S., E. E. Small, and E. A. B. Eltahir, 2000: Simulation of regional-scale water and energy budgets: Representation of subgrid cloud and precipitation processes within RegCM. *J. Geophys. Res.,***105**, 29 579–29 594.

——, F. Giorgi, X. Bi, N. Elguindi, F. Solmon, X. Gao, S.A. Rauscher, R. Francisco, A. Zakey, J. Winter, M. Ashfaq, F.S. Syed, J.L. Bell, N.S. Diffenbaugh, J. Karmacharya, A. Konaré, D. Martinez, R.P. da Rocha, L.C. Sloan, and A.L. Steiner, 2007: Regional Climate Modeling for the Developing World: The ICTP RegCM3 and RegCNET. ***Bull. Amer. Meteor. Soc.***, **88**, 1395–1409.

Palmer, T. N., C. Brankovic, P. Viterbo, and M. J. Miller, 1992: Modeling interannual variations of summer monsoons. *J. Climate,* **5,** 399–417.

Park, C.-K., S. D. Schubert, 1993: Remotely Forced Intraseasonal Oscillations over the Tropical Atlantic. *J. Atmos. Sci.*, **50**, 89–103.

Parker, D. J., R. R. Burton, A. Diongue-Niang, R. J. Ellis, M. Felton, C. M. Taylor, C. D. Thorncroft, P. Bessemoulin and A. M. Tompkins, 2005: The diurnal cycle of the West African monsoon circulation. *Quart. J. Roy. Meteor. Soc.*, **131,** 2839–2860.

Pedgley, D. E. T., and N. Krishnamurti, 1976: Structure and Behavior of a Monsoon Cyclone over West Africa. *Mon. Wea. Rev.*, **104**, 149-167.

Peixoto J. P. and A. H. Oort, 1992: Physics of Climate. Springer- Verlag New York, Inc. 520pp.

Pu, B., and K. H. Cook, 2010: Dynamics of the West African westerly jet. *J. Climate*, **23**, 6263–6276.

Pu, B., and K. H. Cook, 2012: Role of the West African Westerly Jet in Sahel rainfall variations. *J. Climate*, **25**, 2880–2896.

Rakesh, V., Randhir Singh, P. K. Pal, P. C. Joshi, 2009: Impacts of Satellite-Observed Winds and Total Precipitable Water on WRF Short-Range Forecasts over the Indian Region during the 2006 Summer Monsoon. *Wea. Forecasting*, **24**, 1706–1731.

Raicich, F., N. Pinardi, and A. Navara, 2003: Teleconnections between Indian monsoon and Sahel rainfall and the Mediterranean. *Int. J. Climatol.*, **23**, 173-186.

Ramel, R., H. Gallée, and C. Messager, 2006: On the Northward Shift of the West African Monsoon. *Climate Dyn.*, **26**, 429-440.

Ramage, C. S., 1971: Monsoon meteorology. *Intl. Geophys. Ser.* **15**. Academic Press. 296 pp.

Raia, A., and I. F. A. Cavalcanti, 2008: The Life Cycle of the South American Monsoon System. *J. Climate*, **21**, 6227–6246.

Redelsperger, J. L., A. Diongue, A. Diedhiou, J. P. Ceron, M. Diop, J. F. Gueremy, and J. P. Lafore, 2002: Multiscale description of a Sahelian synoptic weather system representative of the West African monsoon. *Quart. J. Roy. Meteor. Soc.*, **128,** 1229–1257.

Redelsperger, J-L, C. D., Thorncroft, A., Diedhiou, T., Lebel, D. J., Parker, J., Polcher, 2006: African Monsoon Multidisciplinary Analysis: An International Research Project and Field Campaign. *Bull. Amer. Meteor. Soc.*, **87**, 1739–1746.

Reed, R. J., D. C. Norquist, and E. E. Recker, 1977: The structure and properties of African wave disturbances as observed during Phase III of GATE. *Mon. Wea. Rev.*, **105,** 317–333.

——, E. Klinker, and A. Hollingsworth, 1988: The structure and characteristics of African easterly wave disturbances determined from ECMWF operational analysis/forecast system. *Meteor. Atmos. Phys.*, **38,** 22–33.

Report on Rural Population, Development and the Environment, 2011: United Nations Population Division, *Department of Economic and Social Affairs*, Sales No. 11.XII.10.

Richman, M. B., 1981: Obliquely Rotated Principal Components: An Improved Meteorological Map Typing Technique? *J. Appl. Meteor.*, **20**, 1145–1159.

Rodwell, M. J., and B. J. Hoskins, 1996: Monsoons and the dynamics of deserts, *Q. J. R. Meteorol. Soc.*, **122**, 1385--1404.

Roja Raman, M., V. V. M. Jagannadha Rao, M. Venkat Ratnam, M. Rajeevan, S. V. B. Rao, D. Narayana Rao, and N. Prabhakara Rao , 2009: Characteristics of the Tropical Easterly Jet: Long-term trends and their features during active and break monsoon phases, *J. Geophysical. Res.*, **114**, D19105, doi:10.1029/2009JD012065.

Roja, R. M., M. Venkat Ratnam, M. Rajeevan, V. V. M. Jagannadha Rao, S. Vijaya Bhaskara Rao, 2011: Intriguing Aspects of the Monsoon Low-Level Jet over Peninsular India Revealed by High-Resolution GPS Radiosonde Observations. *J. Atmos. Sci.*, **68**, 1413–1423.

Ropelewski, C. F., and M. S. Halpert, 1987: Global and regional scale precipitation patterns associated with the El-Nino/Southern oscillation. Mon. Wea. Rev., **115**, 1606-1626.

Rowell, DP, CK Folland, K Maskell, JA Owen, MN Ward, 1992: Modelling the influence of global sea surface temperatures on the variability and predictability of seasonal Sahel rainfall. *Geophysical Res. Lett.* **19***: doi: 10.1029/92GL00939*

_____, 2001: Teleconnections between the tropical Pacific and the Sahel, *Quart. J. Roy. Meteorol. Soc.*, **127**, 1683–1706.

_____, 2003: The Impact of Mediterranean SSTs on the Sahelian Rainfall Season. *J. Climate*, **16**, 849–862.

Roehrig, R., F. Chauvin, J.-P. Lafore, 2011: 10–25-Day Intraseasonal Variability of Convection over the Sahel: A Role of the Saharan Heat Low and Midlatitudes. *J. Climate*, **24**, 5863–5878.

Ropelewski, C.F, M.S. Halpert, 1987: Global and regional scale precipitation associated with El- Ninõ/Southern Oscillation. *Mon. Wea. Re*v. **115**: 985–996.

Rosen, R. D., A. Salstein, and J. P. Peixoto, 1979b: Streamfunction analysis of inter-annual variability in large scale water vapor flux. *Mon. Wea. Rev.,* **107,** 1682–1684.

Hagos, S., C. Zhang, 2010: Diabatic heating, divergent circulation and moisture transport in the African monsoon system. *Quart. J. Roy Met. Soc.* **136**:S1, 411-425

Sardeshmukh, P. D., and B. J. Hoslins, 1988: The generation of global rotational flow by steady idealized tropical divergence. *J. Atmos. Sci*., **45**, 1228-1251.

Schneider, J., and AW. Moore, 1997: A locally Weighted Learning Tutorial Using Vizier 1.0. Available at: http://www.cs.cmu.edu/~schneide/tut5/tut5.html

Schneider, T., P. A. O'Gorman, and X. J. 757 Levine, 2010: Water vapor and the dynamics of climate changes. *Rev. Geophys.*, **48**, RG3001, doi:10.1029/2009RG000302.

Schulza, M., and M. Mudelsee, 2002: REDFIT: estimatingred-noise spectra directly from unevenly spaced paleoclimatic time series. *Computers & Geosciences*, **28**, 421-426.

Segele, Z. T., P. J. Lamb, and L. M. Leslie, 2009: Seasonal-to-interannual variability of Ethiopia/Horn of Africa monsoon. Part I: Associations of wavelet-filtered large-scale atmospheric circulation and global sea surface temperature. *J. Climate*, 22, 3396–3421.

Sellers, et al. 1997: Modeling the exchanges of energy, water, and carbon between continents and the atmosphere. *Science*, **275**, 502-509.

Semazzi, FHM, N.-H. Lin, Y.-L. Lin, and F. Giorgi, 1993: A nested model study of the Sahelian climate response to sea-surface temperature anomalies. *Geophs. Res. Letts*., **20**, 2897-2900.

Seo, H., M. Jochum, R. Murtugudde, A. J. Miller, and J. O. Roads, 2008: Precipitation from African Easterly Waves in a Coupled Model of the Tropical Atlantic. *J. Climate*, **21**, 1417-1431.

Shapiro, L. J., S. B. Goldenberg, 1993: Intraseasonal Oscillations over the Atlantic. *J. Climate*, **6**, 677–699.

Shukla, J. and Y. Mintz, 1982: The influence of land-surface evapotranspiration on the earth's climate. *Science*, **214**, 1498-1501.

Simmonds, I., D. Bi, P. Hope, 1999: Atmospheric Water Vapor Flux and Its Association with Rainfall over China in summer. *J. Climate*, **12**, 1353–1367.

Skamarock, W. C. et al., 2008: A description of the advanced research WRF version 3. NCAR Technical Note, June 2008.

Song-You Hong, Jeong-Ock Jade Lim, 2006: The WRF Single-Moment 6-Class Microphysics Scheme (WSM6). *Journal of the Korean Meteorological Society*, **42**, 129-151.

Stephen Henry Schneider, Terry Louise Root, Michael D. Mastrandrea, 2011: Encyclopedia of Climate and Weather, 2nd ed. Oxford University Press, 2011 483pp. (1488pp)

Steiner, A. L., J. S. Pal, S. A. Rausher, J. L. Bell, N. S. Diffenbaugh, A. Boone, L. C. Sloan, and F. Giorgi, 2009: Land Surface Coupling in Regional Climate Simulations of the West African Monsoon. *Clim. Dyn*., DOI 10.1007/s00382-009-0543-6, 33:869-892.

Sud, Y. C. and W. E. Smith, 1985: The influence of surface roughness of deserts on the July circulation - numerical study *Boundary-layer Meteor*, **33**, 15-49.

Sud, Y. C., K.-M. Lau, 1996: Comments on 'Variability of summer rainfall over tropical north Africa (1906–92): Observations and modelling' by D. P. Rowell, C. K. Folland, K. Maskell and M. N. Ward (April A, 1995, 121, 669–704). *Q. J. R. Meteorol. Soc.*, **122**, 1001-1006.

Sultan, B. and S. Janicot, 2000: Abrupt shift of the ITCZ over West Africa and intraseasonal variability. *Geophys. Res. Lett*, **27**:3353–3356.

Sultan B., S. Janicot, and A. Diedhiou, 2003: The West African Monsoon Dynamics. Part I: Documentation of Intraseasonal Variability**.** *J. Climate,* **16**, No. 21, 3389–3406

Sultan, B., and S. Janicot, 2003: The West African Monsoon Dynamics. Part II: The "Preonset" and "Onset" of the Summer Monsoon. *J. Climate*, **16**, 3407-3427.

Sylla, M. B., A. T. Gaye, J. S. Pal, G. S. Jenkins, X. Bi, 2009a: High-resolution Simulations of West African Climate Using Regional Climate Model (RegCM3) with Different Lateral Boundary Conditions. *Theor.Appl. Climatol*., DOI 10.1007/s00704-009-0110-4, 98:293-314.

Sylla, M. B., E. Coppola, L. Mariotti, F. Giorgi, P. M. Ruti, A. Dell'Aquila, and X. Bi, 2009b: Multiyear Simulation of the African Climate Using a Regional Climate Model (RegCM3) with the High Resolution ERA-interim Reanalysis., *Clim. Dyn*., DOI 10.1007/s00382-009-0613-9

Sylla, M. B., A. Dell'Aquila, P. M. Rutic, and F. Giorgib, 2010: Simulation of the intraseasonal and the interannual variability of rainfall over West Africa with RegCM3 during the monsoon period. *Int. J. Climatol.*, **30**, 1865–1883.

Tarhule, A., 2005: Damaging rainfall and flooding : The other sahel hazards. *Clim. Change*, **72**, 355-377.

Taylor, C. M., E. F. Lambin, N. Stephenne, and R. J. Harding, 2002: The influence of land use change on climate in the Sahel. *J. Climate*, **15**, 3615-3629.

Thompson, R. M., Jr. S. W. Payne, E. E. Recker, and R. J. Reed, 1979: Structure and properties of synoptic-scale wave disturbances in the intertropical convergence zone of the eastern Atlantic. *J. Atmos. Sci*., **36**, 53-72.

Thompson, G., R. M. Rasmussen, and K. Manning, 2004: Explicit forecasts of winter precipitation using an improved bulk microphysics scheme. Part I: Description and sensitivity analysis. *Mon. Wea. Rev.*, **132**, 519–542.

Thorncroft, C. D. and M. Blackburn, 1999: Maintenance of the African easterly jet. *Q. J. R. Meteorol.* SOC. **125,** 763-786.

——, and K. Hodges, 2001: African Easterly Wave Variability and Its Relationship to Atlantic Tropical Cyclone Activity. *J.climate*, **14**, 1166-1179.

——, D. J. Parker, R. R. Burton, M. Diop, J. H. Ayers, H. Barjat, S. Devereau, A. Diongue, R. Dumelow, D. R. Kindred, N. M. Price, M. Saloum, C. M. Tayor, and A. M. Tompkins, 2003: The JET2000 Project: Aircraft Observations of the African Easterly Jet and African Easterly Waves. ***Bull. Amer. Meteor. Soc.***, **84**, 337–351.

——, H. Nguyen, C. Zhang, P. Peyrillé, 2011: Annual cycle of the West African monsoon: regional circulations and associated water vapour transport. *Q. J. R. Meteorol. Soc.* **137**, 129-147. DOI:10.1002/qj.728

Tippett, M. K., A. Giannini, 2006: Potentially Predictable Components of African Summer Rainfall in an SST-Forced GCM Simulation. *J. Climate*, **19**, 3133–3144.

Trewartha, G. T., and L. H. Horn, 1980: An introduction to climate. Fifth Edition. McGraw-Hill, Inc, 416 pp.

Torrence, C., and G. P. Compo, 1998: A Practical Guide to Wavelet Analysis. *Bull. Amer. Meteor. Soc.*, **79**, 61–78.

Vigaud, N., Y. Richard, M. Rouault, and N. Fauchereau, 2007: Water vapour transport from the tropical Atlantic and summer rainfall in tropical southern Africa. *Clim Dyn*., **28**, 113–123.

Vigaud, N., P. Roucou, B. Fountaine, S. Sijikumar, and S. Tyteca, 2011: WRF/ARPEGE-CLIMAT simulated climate trends over West Africa. *Clim Dyn*., **36**:925–944.

Viltard, A., Oubuih, J., de Fé1ice, E, Laurent, H., 1998: Rainfall and the 6-9 day wave-like disturbance in West- Africa during summer 1989. *Meteorol. Atmos. Phys.*, **66**, 229-234.

Vizy, E.K., and K.H. Cook, 2001: Mechanisms by Which Gulf of Guinea and Eastern North Atlantic Sea Surface Temperature Anomalies Can Influence African Rainfall. ***J. Climate***, **14**, 795–821.

Vizy, E.K., and K.H. Cook, 2002: Development and application of a mesoscal climate model for the tropics: Influence of sea surface temperature anomalies on the West African monsoon. *J. Geophys. Res.*, **107** (D3), 10.1029/2001JD000686.

Waliser, D.E., and C. Gautier, 1993: A Satellite-derived Climatology of the ITCZ. ***J. Climate***, **6**, 2162–2174.

Wallace, J. M., P. V. Hobbs, 1977: Atmospheric Science. An Introductory Survey, Elsevier Science, Academic Press. 467pp.

Wang, B., and Z. Fan, 1999: Choice of South Asian Summer Monsoon Indices. *Bull. Amer. Meteor. Soc.*, **80**, 629–638.

Wang, B., and Q. Ding, 2008: The global monsoon: major modes of annual variation in tropical precipitation and circulation. Dyn Atmospheres Oceans **44**,165–183

Wagner, R. G., and A. M. da Silva, 1994: Surface conditions associated with anomalous rainfall in the Guinea coastal region. *Int. J. Climatol.*, **14**, 179–199.

Ward, M. N., 1998: Diagnosis and short-lead time prediction of summer rainfall in tropical North Africa at interannual and multidecadal timescales. *J. Climate*, **11**, 3167–3191.

Webster P. J., 1972: Response of the tropical atmosphere to local steady forcing. *Mon. Wea. Rev.*, **100**, 518-541.

——, 1987: The Elementary Monsoon. In ***Monsoons***, Eds., Fein J. S., and Stephens P. L. John Wiley, New York, pp 3–32.

——, and S. Yang, 1992: Monsoon and Enso: Selectively Interactive Systems. *Q. J . R. Mefeorol. Soc.*, **118,** 877-926

——, 1994: The role of hydrological processes in ocean-atmosphere interactions. *Rev. Geophys.*, **32**, 427-476.

——, V. O. Magaña, T. N. Palmer, J. Shukla, R. A. Tomas, M. Yanai, and T. Yasunari, 1998: Monsoons: Processes, predictability, and the prospects for prediction. *J. Geophys. Res.*, **103**, 14451–14510.

Wheeler, M. and K. M. Weickmann, 2001: Real-time monitoring and prediction of modes of coherent synoptic to intraseasonal tropical variability. *Mon. Wea. Rev.*, **129**:2677–2694.

Weisman, M. L., C. Davis, W. Wang, K. W. Manning, J. B. Klemp, 2008: Experiences with 0–36-h Explicit Convective Forecasts with the WRF-ARW Model. *Wea. Forecasting*, **23**, 407–437.

Wilks D. S., 2006: Statistical Methods in the Atmospheric Sciences (Second Edition), Academic Press, 627p.

World Bank, 2008: The World Development Report, Agriculture for Development.

Wu, M-L., C., O. Reale, S. D. Schubert, M. J. Suarez, R. D. Koster, and P. J. Pegion, 1999: African Easterly Jet: Structure and Maintenance. *J. Climate*, **22**, 4459–4480.

Wu, M-L., C., Siegfried, D. Schubert, Max J. Suarez, and N. E. Huang, 2009: An Analysis of Moisture Fluxes into the Gulf of California. *J. Climate*, **22**, 2216-2239.

Xie, P., and P.A. Arkin, 1997: Global precipitation: A 17-year monthly analysis based on gauge observations, satellite estimates, and numerical model outputs. Bull. Amer. Meteor. Soc., 78, 2539 - 2558.

——, J. E. Janowiak, P. A. Arkin, R. F. Adler, A. Gruber, R. Ferraro, G. J. Huffman, and S. Curtis, 2003: GPCP pentad precipitation analyses: An experimental dataset based on gauge observations and satellite estimates. *J. Climate,* 16, 2197–2214.

Xu, J., S. Rugg, L. Byerle, Z. Liu, 2009: Weather Forecasts by the WRF-ARW Model with the GSI Data Assimilation System in the Complex Terrain Areas of Southwest Asia. *Wea. Forecasting*, **24**, 987–1008.

Xue, Y., and J. Shukla, 1993: The Influence of Land Surface Properties on Sahel Climate. Part 1: Desertification. ***J. Climate***, **6**, 2232–2245.

Xue, Y., and J. Shukla, 1996: The Influence of Land Surface Properties on Sahel Climate. Part II. Afforestation. ***J. Climate***, **9**, 3260–3275.

Xue, Y., 1997: Biophere feedback on regional climate in tropical North Africa. ***Q. J. R. Meteorol. Soc.***, **123**, 1483–1515.

Xue, Y., F. De Sales, W. K.-M. Lau, A. Boone, J. Feng, P. Dirmeyer, Z. Guo, K-M. Kim, A. Kitoh, V. Kumar, I. Poccard-Leclercq, N. Mahowald, W. Moufouma-Okia, P. Pegion, D. P. Rowell, J. Schemm, S. D. Schubert, A. Sealy, W. M. Thiaw, A. Vintzileos S.F. Williams, M-Li C. Wu, 2010: Intercomparison and analyses of the climatology of the West African Monsoon in the West African

Monsoon Modeling and Evaluation project (WAMME) first model intercomparison experiment. *Clim Dyn*., DOI 10.1007/s00382-010-0778-2

Yang, S., X. Ding, D. Zheng, and Q. Li, 2007: Depiction of the variations of Great Plains precipitation and its relationship with tropical central-eastern Pacific SST. *J. Appl. Meteor. Climatol.*, **46,** 136–153.

Yin, X., A. Gruber, and P. Arkin, 2004: Comparison of the GPCP and CMAP merged gauge–satellite monthly precipitation products for the period 1979–2001. *J. Hydrometeor.*, **5,** 1207–1222

Zebiak, S. E., 1993: Air–sea interaction in the equatorial Atlantic region. *J. Climate,* **6,** 1567–1586.

Semazzi, F. H. M., N. Lin, Y. Lin, and F. Giorgi, 1993: A nested model study of the Sahelian climate response to sea-surface temperature anomalies. *Geophys. Res. Lett.,* **20**, 2897-2900.

Zhang, C., D. S. Nolan, C. D. Thorncroft, and H. Nguyen, 2008: Shallow Meridional Circulations in the Tropical Atmosphere. *J. Climate,* **21**, 3453–3470.

Zhang, C., P. Woodworth, and G. Gu, 2006: The seasonal cycle in the lower troposphere over West Africa from sounding observations. *Q. J. R. Meteorol. Soc.*, **132,** 2561–2584.

Zheng, X., 1997: Moist zonally-symmetric models and their applications to West African monsoons. Ph.D. thesis, Massachusetts Institute of Technology, 217 pp.